

Integrated Sediment Yield and Stock Assessment for the Passaúna Reservoir, Brazil

Zur Erlangung des akademischen Grades eines
DOKTORS DER INGENIEURWISSENSCHAFTEN (Dr.-Ing.)

von der KIT Fakultät für
Bauingenieur-, Geo- und Umweltwissenschaften

des Karlsruher Instituts für Technologie (KIT)

genehmigte

DISSERTATION

von

Klajdi Sotiri, Dipl.-Ing., M.Sc.

aus Saranda, Albanien

Tag der mündlichen Prüfung: 11.12.2020

Referent: PD. Dr.-Ing. Stephan Fuchs

Korreferent: Prof. Dr.-Ing. Tobias Bleninger

Karlsruhe (2020)



The contents are available under the terms of an open content license of the type
Creative Commons - Attribution-ShareAlike 4.0 International (CC BY-SA 4.0):
<https://creativecommons.org/licenses/by-sa/4.0/deed.en>

Acknowledgments

I would like to thank extensively the Graduate School for Climate and Environment of the Karlsruhe Institute of Technology for financing the first 20 months of this research through a full scholarship. Secondly, I would like to thank my supervisors PD. Dr.-Ing. Stephan Fuchs and Prof. Tobias Bleninger for the full support and their useful guiding and comments on this work.

Special thanks go to Stephan Hilgert for his unconditioned scientific support and the great time during the multiple Brazil trips of the last four years. A big thank you goes to my PhD colleagues Adrian, Lisa, Jens, Liege, Luziadne, Lais and Lediane for the unforgettable moments during the field campaigns and the memorable happy hours following.

Many thanks to the staff from UFPR, especially Prof. Regina Kishi and Prof. Cristóvão Vicente Scapulatempo Fernandes for the support during the longer stays in Brazil, the DHS laboratory staff for the help during the sediment analyzing, and Prof. Matheus Duraes and Prof. Robson Armindo for the support during the soil sampling campaigns. I am also grateful to Mauricio Bergamini Scheer for the help during the measuring campaigns and for the data support from the SANEPAR side

I am beyond grateful to my family, my father Fredi, my mother Sofika, and my sister Ina for the great support to pursue my passions and interests. Thank you for being always there for me.

Finally and most importantly, to Sara, my best friend and at the same time my fiancé, thank you for being in my corner the whole time. I am very grateful for the love, support, and understanding during these last busy months. Faleminderit nga zemra!

Abstract

Water and energy are the two key aspects driving economic and social development of a region. River impoundments are important structures for providing water, in case of domestic use, irrigation or mining and for providing energy as in the case of hydropower. The human interference in the riverine systems for creating these reservoirs is accompanied with several drawbacks. One and most important: ecosystem disruption. The reservoirs, which cause the disruption of a river continuum, also suffer from it by having a limited lifetime. Rivers are dynamic systems, which transport large amounts of organic and mineral material from the mountains until the sea. When they are impounded, this continuum is divided and the reservoir becomes the first sink of the particles. In order to plan remediation measures, a major scientific and engineering challenge is the assessment of sediment amounts that reach the reservoir in a certain time. The sediment volume/mass can be assessed via either the monitoring and modelling of sediment input from the hydrological catchment or, by measurements of the sediment volume in the reservoir. In the first case the spatial and temporal scale in which sediment mobilization takes place in the watershed, in addition to the episodic nature of sediment formation, make it difficult to derive reliable assessments of sediment input. On the other hand, the underwater environment and the spatial extent of the reservoir contributes also in the lack of reliable results concerning volumetric assessment of sediment.

This study aims at a better assessment of both aspects of sediment input and reservoirs' sediment accumulation. The first part of this thesis deals with the quantification of erosion and sediment input from a watershed via modelling. The rapid population growth in many regions has dictated intense land use and landcover changes. These imply the usage of more dynamic models. Technological advancements in satellite imagery make it possible to improve the spatial and temporal resolution of the models but the overall effects of the integration of this data on the results are still not fully investigated. For assessing the improvement due to the technological advancement, the case of Passaúna catchment, located in southeast Brazil was examined. For this catchment, it was possible to quantify the sediment input and soil loss interannual dynamics in a monthly timestep, and to evaluate to what extent the inclusion of freely available satellite imagery can improve the modelling results. In other words, the integration of freely available Sentinel 2 satellite data made it possible to reduce the time and spatial resolution in comparison to the existing similar approaches.

The second part of the thesis deals with the quantification of the sediment volume in the Passaúna reservoir. In this study, five different remote sensing as well as conventional and proxy sediment sampling techniques are integrated for increasing the accuracy of sediment volume assessment. At the end, an accurate assessment of the sediment volume in the reservoir was

achieved. In addition, a guiding diagram to choose the most suitable sediment detection method, depending on sediment characteristic (sediment magnitude and biochemical activity) was derived.

The results of both sections are closely related as the sediment input from a watershed is also the sediment amount that should be found in a reservoir like Passaúna where the trapping efficiency is ~100%. In this case, there is a difference of almost 50% between the modelled sediment input and the sediment stock in the reservoir. The most important factors contributing in this discrepancy are the non-inclusion of gully-channel erosion in the sediment input model, errors in the calculation process, internal production of the reservoir, and errors in the measuring process.

In overall based on the results of this thesis, the most important findings consist in the successful integration of freely available satellite imagery in a modelling approach to improve the sediment input assessment, and the combination of several methods for an accurate assessment of reservoir siltation. The findings of this thesis can contribute in bridging the gap between the two aspects of sediment budget by initially achieving an accurate reservoirs' sediment stock assessment and secondly by quantifying the discrepancy of each contributing factor for a case study.

Zusammenfassung

Wasser und Energie sind die beiden Schlüsselaspekte der wirtschaftlichen und sozialen Entwicklung einer Region. Stauhaltungen sind wichtige Strukturen für die Wasserversorgung, Bewässerung, Bergbau sowie die Energieversorgung durch Wasserkraft. Die Eingriffe des Menschen in die Flusssysteme durch den Bau von Stauseen sind jedoch mit mehreren Nachteilen verbunden. Grundsätzlich wird hierdurch ein Ökosystem unterbrochen. Die Stauseen, die die Störung eines Flusskontinuums verursachen, leiden auch daran, dass sie eine begrenzte Lebensdauer haben. Flüsse sind dynamische Systeme, die große Mengen organischen und mineralischen Materials von den Bergen bis zum Meer transportieren. Wenn sie aufgestaut werden, wird ein Stausee zur Senke von Partikeln. Eine große wissenschaftliche und ingenieurwissenschaftliche Herausforderung bei der Planung von Sanierungsmaßnahmen ist die Bewertung der Volumina, die das Reservoir in einer bestimmten Zeit erreichen. Das Sedimentvolumen und die entsprechende Masse kann entweder durch Monitoring und Modellierung des Sedimenteintrags aus dem hydrologischen Einzugsgebiet oder durch Messungen des Sediments im Stausee bestimmt werden. Im ersten Fall erschwert die räumliche und zeitliche Skala, in der die Sedimentmobilisierung in dem Einzugsgebiet stattfindet, die Ableitung zuverlässiger Quantifizierung des Sedimenteintrags. Im zweiten Fall trägt die Unterwasserumgebung des Stausees dazu bei, dass oft keine verlässlichen Daten zur Quantifizierung von zurückgehaltenen Sedimenten vorliegen.

Ziel dieser Arbeit ist eine bessere Beurteilung sowohl der Sedimenteinträge als auch der Sedimentablagerungen. Der erste Teil dieser Arbeit beschäftigt sich mit der Quantifizierung von Erosion und Sedimenteintrag aus einem Einzugsgebiet mittels Modellierung. Das rasante Bevölkerungswachstum in vielen Regionen hat intensive Landnutzungs- und Landbedeckungsänderungen zur Folge. Dies impliziert die Verwendung dynamischerer Modelle zur Abbildung der realen Bedingungen. Die technologischen Fortschritte in der Satellitenerkundung ermöglichen es, die räumliche und zeitliche Auflösung der Modelle zu verbessern, wobei die Auswirkungen der Integration dieser Daten auf die Modellergebnisse noch nicht analysiert sind. Um diese Verbesserungen beurteilen zu können, wurden die Einträge aus dem Passaúna Einzugsgebiet im Südosten Brasiliens untersucht. Für dieses Einzugsgebiet war es möglich, die Dynamik des Bodenverlusts und des Sedimenteintrags in einer monatlichen Auflösung zu modellieren und zu bewerten. In andere Worte, durch die Integration von frei verfügbaren Sentinel-2 Satellitendaten konnte die zeitliche und räumliche Auflösung im Vergleich zu den bisherigen Ansätzen reduziert werden.

Neben der Eintragsmodellierung wurde eine Quantifizierung der Sedimente im Passaúna Stausee durchgeführt. Es wurden verschiedene Fernerkundungs- sowie konventionelle und

Proxy-Sediment-Probenahmeverfahren integriert, um die Genauigkeit der Sedimentbestimmung zu optimieren. Am Ende konnte eine genaue Abschätzung des Sedimentvolumens und der -dichte im Reservoir erreicht werden. Darüber hinaus wurde ein Leitdiagramm zur Auswahl der besten Sedimentnachweismethode in Abhängigkeit der Sedimenteigenschaften erarbeitet.

Die Ergebnisse beider Abschnitte sind eng miteinander verbunden, da der Sedimenteintrag aus einem Wassereinzugsgebiet auch die Sedimentmenge ist, die in einem Reservoir wie Passaúna gefunden werden sollte, wo der Sedimentationsvermögen annähernd 100 % beträgt. In diesem Fall unterschätzt die Modellierung um ca. 50 % im Vergleich zum Sedimentbestand im Reservoir. Die wichtigsten Faktoren, die zu dieser Diskrepanz beitragen, sind die Nichtberücksichtigung der Rinnen-Erosion im Sediment-Eingangsmodell, Fehler im Berechnungsprozess, die Eigenproduktion des Reservoirs und Fehler bei der Sedimentquantifizierung.

Die wichtigsten Erkenntnisse, die sich aus den Ergebnissen dieser Arbeit ergeben, sind die erfolgreiche Integration von satelliten-basierten Eingangsparametern in einen Modellierungsansatz zur Verbesserung der Sedimenteintragsabschätzung und die Kombination mehrerer Methoden zur exakten Beurteilung der Stauseeverlandung. Die Ergebnisse dieser Dissertation können dazu beitragen, die Lücke zwischen den beiden Aspekten des Sedimenthaushalts zu schließen, indem zunächst eine exakte Bewertung des Sedimentbestands der Reservoirs vorgenommen wird und zweitens die Diskrepanz der einzelnen beteiligten Faktoren für eine Fallstudie quantifiziert wird.

Përmbledhje

Uji dhe energjia janë dy aspektet kryesore që drejtojnë zhvillimin ekonomik dhe shoqëror të një rajoni. Digat janë struktura të rëndësishme për sigurimin e ujit, për konsum urban, ujitje ose miniera, si dhe për sigurimin e energjisë si në rastin e hidrocentraleve. Sidoqoftë, ndërhyrja njerëzore për krijimin e këtyre rezervuarëve në sistemet lumore, shoqërohet me disa aspekte negative. Një dhe më e rëndësishmja: ndërprerja e rrjedhës së ekosistemit. Rezervuarët, të cilët shkaktojnë ndërprerjen e rrjedhës së një lumi, gjithashtu vuajnë nga ky fakt duke pasur një jetëgjatësi të kufizuar. Lumenjtë janë sisteme dinamike, të cilat transportojnë sasi të madhe të materialit organik dhe mineral nga malet deri në det. Kur sistemet lumore ndëprehen, ky cikël gjithashtu ndahet dhe rezervuari bëhet dekantuesi i parë dhe përfundimtar i grimcave. Për të planifikuar masa riparimi, një sfidë e madhe shkencore dhe inxhinierike është vlerësimi i vëllimeve që arrijnë rezervuarin në një kohë të caktuar. Vëllimi/masa e sedimentit mund të vlerësohet përmes monitorimit dhe modelimit të fluksit të sedimenteve nga pellgu ujëmbledhës ose, përmes matjeve të vëllimit të sedimenteve në rezervuar. Në rastin e parë, shkalla hapësinore dhe kohore në të cilën zhvillohet mobilizimi i sedimenteve, pamundëson një vlerësim të saktë të fluksit të sedimenteve. Nga ana tjetër, mjedisi nënujor i rezervuarit kontribuon gjithashtu në mungesën e rezultateve të besueshme në lidhje me vlerësimin vëllimor të sedimentit.

Ky studim synon një vlerësim më të saktë të fluksit të sedimenteve dhe depozitimit të tyre në rezervuar. Pjesa e parë e kësaj teze ka të bëjë me përcaktimin e sasisë së erozionit dhe fluksit të sedimenteve nga një pellg ujëmbledhës përmes modelimit. Rritja e shpejtë e popullsisë në shumë rajone ka diktuar ndryshime intensive të përdorimit dhe mbulimit të tokës. Përparimet teknologjike në fushën e imazherisë satelitore kanë bërë të mundur përmirësimin e rezolucionit hapësinor dhe kohor të modeleve, por efektet e përgjithshme të integritit të këtyre të dhënave në rezultatet përfundimtare nuk janë hetuar ende plotësisht. Në fund të kësaj pune kërkimore, ishte e mundur përcaktimi i sasisë së sedimenteve dhe prezantimi i dinamikave sezonale të erozionit nga pellgu ujëmbledhës Passaúna në një rezolucion kohor mujor, si dhe të vlerësohet në çfarë mase përfshirja e imazheve satelitore në dispozicion për publikun e gjerë mund të përmirësojë rezultatet e modelimit. Më konkretisht, integrimi i të dhënave satelitore Sentinel 2 në dispozicion për publikun e gjerë bëri të mundur zvogëlimin e rezolucionit kohor dhe hapësinor të modelit në krahasim me qasjet ekzistuese të ngjashme.

Pjesa e dytë e tezës trajton sasinë e vëllimit të sedimentit në rezervuarin e Passaúnas. Teknika më e përdorur për të vlerësuar vëllimin e sedimentit është diferencimi topografik përmes rievimeve të njëpasnjëshme batimetrike. Në këtë studim, pesë teknika gjeohapësinore dhe konvencionale janë integruar për të rritur saktësinë e vlerësimit të vëllimit të sedimenteve që janë depozituar në një rezervuar. Në fund, u bë e mundur të arrihet një vlerësim i saktë i vëllimit të

sedimentit në rezervuarine e Passaúnas. Për më tepër, u krijua një diagram udhëzues për përzgjedhjen e metodës më të përshtatshme të matjes së volumeve të sedimentit, në varësi të karakteristikave të materialit.

Rezultatet e të dy seksioneve janë të lidhura ngushtë pasi sasia e sedimentit nga një pellg ujëmbledhës është edhe sasia e sedimentit që duhet të gjendet në një rezervuar si Passaúna ku efikasiteti i bllokimit është ~ 100%. Në këtë rast, ekziston një ndryshim prej gati 50% midis sasisë së modeluar të sedimentit dhe stokut të sedimentit në rezervuar. Faktorët më të rëndësishëm që kontribuojnë në këtë mospërputhje janë mos përfshirja e erozionit të kanaleve në modelin e fluksit të sedimentit, gabimet në procesin e llogaritjes, prodhimi autokton i rezervuarit dhe gabimet në procesin e matjes.

Në përgjithësi bazuar në rezultatet e kësaj teze, gjetjet më të rëndësishme konsistojnë në integrimin e suksesshëm të imazheve satelitore lirisht të disponueshme në një qasje modeli për të përmirësuar vlerësimin e fluksit të sedimenteve dhe kombinimin e disa metodave për një vlerësim të saktë të sedimentimit të rezervuarit. Gjetjet e kësaj teze mund të kontribuojnë në tejkalimin e hendekut midis dy aspekteve të buxhetit të sedimenteve duke arritur fillimisht një vlerësim të saktë të stokut të rezervuarëve dhe së dyti duke vlerësuar efektet e secilit faktor kontribues për një rast studimi.

Περίληψη

Το νερό και η ενέργεια είναι οι δύο βασικές πτυχές της οικονομικής και κοινωνικής ανάπτυξης μιας περιοχής. Οι κατακρημνίσεις ποταμών είναι σημαντικές δομές για την παροχή νερού, την άρδευση ή την εξόρυξη και για την παροχή ενέργειας, όπως στην περίπτωση της υδροηλεκτρικής ενέργειας. Ωστόσο, η ανθρώπινη παρέμβαση στα ποτάμια συστήματα για τη δημιουργία αυτών των ταμιευτήρων έχει πολλά μειονεκτήματα. Ένα και το πιο σημαντικό: διαταραχή του οικοσυστήματος. Οι ταμιευτήρες που διαταράσσουν ένα συνεχές ποτάμι υποφέρουν επίσης από το γεγονός, διότι έχουν περιορισμένη διάρκεια ζωής. Τα ποτάμια είναι δυναμικά συστήματα που μεταφέρουν μεγάλες ποσότητες οργανικών και ορυκτών υλικών από τα βουνά στη θάλασσα. Όταν διακόπτεται, αυτός ο κύκλος χωρίζεται και ο ταμιευτήρας γίνεται ο τελευταίος σταθμός των ιζημάτων. Μια σημαντική επιστημονική και μηχανική πρόκληση κατά τον προγραμματισμό διορθωτικών μέτρων, είναι η αξιολόγηση των όγκων που φτάνουν στο ταμιευτήρα σε μια δεδομένη χρονική στιγμή. Ο όγκος/μάζα των φερτών μπορεί να προσδιοριστεί είτε με παρακολούθηση και μοντελοποίηση των φερτών από την λεκάνη απορροής είτε με μέτρηση του όγκου των ιζημάτων στο ταμιευτήρα. Στην πρώτη περίπτωση, η χωρική και χρονική κλίμακα στην οποία πραγματοποιείται η κινητοποίηση ιζημάτων στην λεκάνη απορροής καθιστά δύσκολη τον αξιόπιστο ποσοτικό προσδιορισμό των εισερχόμενων φερτών. Από την άλλη πλευρά, το υποβρύχιο περιβάλλον του ταμιευτήρα, συμβάλλει επίσης στην έλλειψη αξιόπιστων αποτελεσμάτων για την ογκομετρική αξιολόγηση των φερτών.

Ο στόχος αυτής της μελέτης είναι η καλύτερη αξιολόγηση τόσο της εισροών φερτών όσο και της κατάθεσης ιζημάτων. Το πρώτο μέρος αυτής της διατριβής ασχολείται με τον ποσοτικό προσδιορισμό της διάβρωσης και εισαγωγής φερτών από μια λεκάνη απορροής χρησιμοποιώντας μοντελοποίηση. Η ταχεία αύξηση του πληθυσμού σε πολλές περιοχές έχει υπαγορεύσει την εντατική αλλαγή της χρήσης και κάλυψης γης. Αυτό συνεπάγεται τη χρήση πιο δυναμικών μοντέλων. Οι τεχνολογικές εξελίξεις στη δορυφορική απεικόνιση κατέστησαν δυνατή τη βελτίωση της χωρικής και χρονικής ανάλυσης των μοντέλων, αλλά οι συνολικές επιπτώσεις της ενσωμάτωσης αυτών των δεδομένων στα αποτελέσματα δεν έχουν ακόμη διερευνηθεί πλήρως. Στο τέλος, ήταν δυνατόν να ποσοτικοποιηθεί η εισαγωγή φερτών και η ετήσια δυναμική απώλειας εδάφους από την περιοχή λεκάνης απορροής του Passaúna σε μηνιαία περίοδο και να εκτιμηθεί σε ποιο βαθμό η συμπερίληψη ελεύθερων διαθέσιμων δορυφορικών εικόνων μπορεί να βελτιώσει τα αποτελέσματα μοντελοποίησης. Πιο συγκεκριμένα, η ενσωμάτωση των ελεύθερα διαθέσιμων δορυφορικών δεδομένων Sentinel 2 κατέστησε δυνατή τη μείωση του χρονική και της χωρική ανάλυση του μοντέλου σε σύγκριση με τις υπάρχουσες παρόμοιες προσεγγίσεις.

Το δεύτερο μέρος της διατριβής ασχολείται με τον ποσοτικό προσδιορισμό του όγκου ιζημάτων στο ταμιευτήρα Passaúna Αυτή η μελέτη ενσωματώνει πέντε διαφορετικές τεχνικές

τηλεπισκόπησης, καθώς και συμβατικές και τεχνικές δειγματοληψίας ιζημάτων, για την αύξηση της ακρίβειας της εκτίμησης όγκου φερτών. Στο τέλος, ήταν δυνατό να επιτευχθεί ακριβής εκτίμηση του όγκου ιζημάτων στο ταμιευτήρα. Επιπλέον, ελήφθη ένα οδηγό διάγραμμα για την επιλογή της καταλληλότερης μεθόδου ανίχνευσης φερτών ανάλογα με τα χαρακτηριστικά του ιζήματος.

Τα αποτελέσματα και των δύο τμημάτων συνδέονται στενά καθώς η είσοδος ιζήματος από μια λεκάνη απορροής είναι επίσης η ποσότητα ιζήματος που πρέπει να βρεθεί σε ένα ταμιευτήρα όπως το Passaúna όπου η απόδοση παγίδευσης είναι ~ 100%. Σε αυτήν την περίπτωση, υπάρχει διαφορά σχεδόν 50% μεταξύ της μοντελοποιημένης εισροής ιζημάτων και του αποθέματος ιζημάτων στο ταμιευτήρα. Οι πιο σημαντικοί παράγοντες που συμβάλλουν των φερτών αυτήν την ασυμφωνία είναι η μη συμπερίληψη της διάβρωσης των μεγαλύτερων καναλιών στο μοντέλο εισαγωγής ιζημάτων, σφάλματα στη διαδικασία υπολογισμού, εσωτερική παραγωγή του ταμιευτήρα και σφάλματα στη διαδικασία μέτρησης.

Σε γενικές γραμμές με βάση τα αποτελέσματα αυτής της διατριβής, τα πιο σημαντικά ευρήματα συνίστανται στην επιτυχή ενσωμάτωση των ελεύθερων διαθέσιμων δορυφορικών εικόνων σε μια προσέγγιση μοντελοποίησης για τη βελτίωση της αξιολόγησης της εισαγωγής ιζημάτων, και ο συνδυασμός πολλών μεθόδων για την ακριβή αξιολόγηση των φερτών σε ένα ταμιευτήρα. Τα ευρήματα αυτής της διατριβής μπορούν να συμβάλουν στη γεφύρωση του χάσματος μεταξύ των δύο πτυχών του προϋπολογισμού φερτών, επιτυγχάνοντας αρχικά μια ακριβή αξιολόγηση αποθεμάτων ιζημάτων στο ταμιευτήρα και, δεύτερον, ποσοτικοποιώντας την ασυμφωνία του κάθε παράγοντα που συμβάλλει σε μια τέτοια μελέτη.

Resumo

Água e energia são dois aspectos principais que impulsionam o desenvolvimento econômico e social de uma região. Os represamentos fluviais são estruturas importantes para o fornecimento de água, no caso para uso doméstico, irrigação ou mineração e para o fornecimento de energia, como no caso das hidrelétricas. No entanto, a interferência humana nos sistemas fluviais para a criação desses reservatórios é acompanhada de várias desvantagens. A primeira e mais importante: ruptura do ecossistema. Os reservatórios, que causam a interrupção de um continuum de rio, também sofrem com uma vida útil limitada. Os rios são sistemas dinâmicos, que transportam grande quantidade de material orgânico e mineral das montanhas até o mar e ao serem represados, esse ciclo é dividido e o reservatório se torna o primeiro coletor de partículas. Para planejar medidas de remediação, um grande desafio científico e de engenharia é a avaliação dos volumes que atingem o reservatório em um determinado período de tempo. O volume/massa de sedimentos pode ser avaliado por meio do monitoramento e modelagem da entrada de sedimentos da bacia hidrológica ou por medições do volume de sedimentos no reservatório. No primeiro caso, a escala espacial e temporal em que a mobilização de sedimentos ocorre na bacia hidrográfica torna difícil obter avaliações confiáveis da carga de sedimentos. Por outro lado, o ambiente subaquático do reservatório contribui também na falta de resultados confiáveis, quanto à avaliação volumétrica do sedimento.

Este estudo objetiva uma melhor avaliação dos aspectos da entrada e deposição de sedimentos. A primeira parte desta tese trata a quantificação de erosão carga dos sedimentos de uma bacia hidrográfica via modelagem. O rápido crescimento populacional em muitas regiões determinou intensas mudanças no uso e cobertura do solo. Isso implica a necessidade de modelos mais dinâmicos. Os avanços tecnológicos nas imagens de satélites tornam possível melhorar a resolução espacial e temporal dos modelos, contudo, os efeitos gerais da integração desses dados nos resultados ainda não são totalmente investigados. Ao final, foi possível quantificar a dinâmica interanual do fluxo de sedimentos e perda de solo da bacia hidrográfica do Passaúna em um intervalo de tempo mensal, e avaliar em que medida a inclusão de imagens de satélite disponíveis gratuitamente pode melhorar os resultados da modelagem. A integração de dados de satélites Sentinel 2 livremente disponíveis permitiu reduzir o tempo e a resolução espacial em comparação com as abordagens semelhantes existentes.

A segunda parte da tese trata da quantificação do volume de sedimentos no reservatório do Passaúna. A técnica mais utilizada para avaliar o volume de sedimentos é a diferenciação topográfica por meio de levantamentos batimétricos subsequentes. Quando a distribuição de profundidade anterior está ausente ou está com uma precisão insuficiente, métodos alternativos precisam ser investigados. Neste estudo, cinco diferentes técnicas de sensoriamento remoto, bem como técnicas de amostragem de sedimentos convencionais e proxy, são integradas para aumentar a precisão da avaliação do volume de sedimentos. Ao final, uma avaliação precisa do

volume de sedimentos no reservatório pode ser alcançada. Além disso, um diagrama de orientação sobre a escolha do método de detecção de sedimentos mais adequado, dependendo da característica do sedimento, foi obtido.

Os resultados de ambas as partes estão diretamente relacionados, uma vez que a entrada de sedimento de uma bacia hidrográfica também é a quantidade de sedimento que deve ser encontrada em um reservatório como no Passaúna, onde a eficiência de retenção é de ~ 100%. Nesse caso, há uma diferença de quase 50% entre a entrada de sedimento modelada e o volume de sedimento acumulado no reservatório. Os fatores mais importantes que contribuem para esta discrepância são a não inclusão da erosão do canal e rios no modelo de entrada de sedimentos, erros no processo de cálculo, produção interna do reservatório e erros no processo de medição.

Em geral, com base nos resultados desta tese, as descobertas mais importantes consistem na integração bem-sucedida de imagens de satélite, disponíveis gratuitamente, em uma abordagem de modelagem para melhorar a avaliação de entrada de sedimentos e a combinação de vários métodos para uma avaliação precisa do assoreamento do reservatório. Os resultados desta tese contribuem para preencher a lacuna entre os dois aspectos do balanço de sedimentos, inicialmente alcançando uma avaliação precisa do estoque de sedimentos dos reservatórios e, em seguida, quantificando a discrepância de cada fator contribuinte para um estudo.

Table of Contents

LIST OF FIGURES	XVII
LIST OF TABLES	XXIII
LIST OF ABBREVIATIONS	XXV
1. RESERVOIRS AND SEDIMENT	1
2. FRAMEWORK OF THE THESIS	3
2.1. RESEARCH QUESTIONS AND CHALLENGES OF THE THESIS	3
2.2. OVERVIEW OF THESIS	6
2.3 STRUCTURE OF THE THESIS	6
3. EROSION AND SEDIMENT INPUT	9
3.1. EROSION AND SEDIMENT FORMATION PROCESSES	10
3.1.1. <i>Detachment by splash</i>	11
3.1.2. <i>Inter-rill and rill erosion</i>	12
3.1.3. <i>Gully erosion</i>	12
3.1.4. <i>Channel erosion</i>	13
3.2. FACTORS INFLUENCING EROSION	14
3.3. SOIL EROSION AND SEDIMENT YIELD QUANTIFICATION	16
3.4. USLE/RUSLE	19
3.4.1. <i>Topographic factor LS</i>	20
3.4.2. <i>Rainfall erosivity factor R</i>	21
3.4.3. <i>Cover and management factor C</i>	22
3.4.4. <i>Soil erodibility Factor K</i>	23
3.4.5. <i>Support practice factor P</i>	25
3.5. SEDIMENT YIELD	25
3.6. SUMMARY AND RESEARCH GAPS	28
4. RESERVOIR SILTATION	29
4.1. SEDIMENTATION PATTERNS IN RESERVOIRS	30
4.2. METHODS FOR MEASURING THE SEDIMENT VOLUME IN RESERVOIRS	32
4.2.1. <i>Hydroacoustic applications for sediment detection and characterization</i>	33
4.2.2. <i>Sediment coring</i>	42
4.2.3. <i>Dynamic freefall penetrometer</i>	44
4.3. TRAP EFFICIENCY OF RESERVOIRS	45
4.4. SUSTAINABLE MANAGEMENT FOR INCREASING RESERVOIR'S LIFETIME	47

4.4.1. Reducing sediment yield from catchment	48
3.4.2. Sediment routing	49
4.4.3. Sediment removal.....	50
4.4.4. Adaptive strategies.....	52
4.5. SUMMARY AND RESEARCH GAPS	53
5. INVESTIGATION AREA	55
6. METHODS AND MATERIALS	57
6.1. SEDIMENT INPUT FROM THE CATCHMENT (RUSLE)	57
6.1.1. Topographic factor <i>LS</i>	60
6.1.2. Soil erodibility Factor <i>K</i>	61
6.1.3. Rainfall erosivity factor <i>R</i>	62
6.1.4. Cover and management factor <i>C</i>	65
6.1.5. Support practice factor <i>P</i>	69
6.1.6. Sediment delivery ratio.....	69
6.2. SEDIMENT VOLUME AND DISTRIBUTION IN THE RESERVOIR.....	71
6.3. HYDROACUSTIC SURVEY.....	72
6.3.1. Bathymetry (<i>Multibeam</i>).....	72
6.3.2. Sediment magnitude measurements.....	72
6.3.3. Sediment classification (<i>EA400</i>)	75
6.4. SEDIMENT SAMPLING AND ANALYZING	80
6.5. DYNAMIC FREEFALL PENETROMETER (<i>GRAVIPROBE</i>)	82
7. RESULTS AND INTERPRETATION	83
7.1. SEDIMENT INPUT FROM THE CATCHMENT (RUSLE)	83
7.1.1. Soil erodibility factor <i>K</i>	83
7.1.2. Rainfall erosivity factor <i>R</i>	85
7.1.3. Cover and management factor <i>C</i>	85
7.1.4. Sediment delivery ratio.....	87
7.1.5. Soil loss and sediment input	88
7.2. SEDIMENT VOLUME AND DISTRIBUTION IN THE RESERVOIR.....	93
7.2.1. Sediment sampling and analyzing.....	93
7.2.2. Topographic differencing from multibeam data	97
7.2.3. Sediment magnitude (<i>SBP</i> and <i>EA400</i>).....	98
7.2.4. Sediment classification (<i>EA400</i>)	100
7.2.5. Dynamic freefall penetrometer (<i>Graviprobe</i>)	104
7.3. SUMMARY	108
8. DISCUSSION	111
8.1. SEDIMENT INPUT FROM THE PASSAÚNA CATCHMENT	111
8.1.1. Comparison of the sediment yield modelling results to literature.....	111

8.1.2. <i>The importance of spring months for the sediment input</i>	113
8.1.3. <i>Limitations of NDVI based modelling approaches</i>	114
8.1.4. <i>Uncertainties of RUSLE results for Passaúna catchment</i>	115
8.1.5. <i>Benefits from the integration of Sentinel-2 data in erosion modelling</i>	115
8.2. SEDIMENT STOCK IN THE PASSAÚNA RESERVOIR	116
8.2.1. <i>Comparison between measurement methods</i>	116
8.2.2. <i>Summary of measurement techniques</i>	123
8.2.3. <i>Comparison between acoustic sediment classification and sediment properties</i>	124
8.2.4. <i>Reservoir lifetime assessment</i>	127
8.3. RESERVOIR SEDIMENT STOCK VS. SEDIMENT INPUT FROM CATCHMENT	131
9. CONCLUSION	137
9.1. HOW CAN THE DEVELOPMENTS IN FREE AVAILABLE SATELLITE IMAGERY CONTRIBUTE TO IMPROVE THE SEDIMENT INPUT MODELLING?	137
9.2. HOW CAN THE ACCURACY OF SEDIMENT VOLUME ASSESSMENT AND SEDIMENT DISTRIBUTION MAPPING BE IMPROVED? ..	137
9.3. CAN THE PASSAÚNA RESERVOIR BE USED AS VALIDATION POINT FOR THE RUSLE BASED SEDIMENT INPUT MODEL?	139
PUBLICATION BIBLIOGRAPHY	141
APPENDIX	167

List of Figures

CHAPTER 1

FIGURE 1—1 MAIN PURPOSES OF THE EXISTING RESERVOIRS (ADAPTED FROM INTERNATIONAL COMMISSION ON LARGE DAMS (2019)). . 1

CHAPTER 2

FIGURE 2—1 SCHEMATIC EXPLANATION OF THE HYPOTHESIS OF THE THESIS (ICONS IN THE FIGURE ARE ADAPTED FROM ICOGRAMS). 5

CHAPTER 3

FIGURE 3—1 GRAPHICAL EXPLANATION OF EROSION AND SEDIMENT FORMATION. 11

FIGURE 3—2 COMPARISON BETWEEN MODELLED AND OBSERVED K FACTOR FOR DIFFERENT SOILS (RENARD 1997). 24

FIGURE 3—3 EMPIRICAL RELATIONS BASED ON THE CATCHMENT AREA DERIVED FROM DIFFERENT LOCATIONS FOR QUANTIFYING THE SDR (WALLING 1983). 27

CHAPTER 4

FIGURE 4—1 SEDIMENTATION STAGES OF A RESERVOIR (ADAPTED FROM MORRIS AND FAN (2010)). 31

FIGURE 4—2 GENERALIZED LONGITUDINAL DEPOSITION PATTERNS OF SEDIMENT (ADAPTED FROM MORRIS AND FAN (2010)). 32

FIGURE 4—3 SCHEMATIC VIEW OF AN ECHO-SOUNDER. 34

FIGURE 4—4 ILLUSTRATION OF GEOMETRICAL SPREADING DURING SOUND PROPAGATION. 35

FIGURE 4—5 SCHEMATIC VIEW OF ECHO SIGNAL DERIVATION. 36

FIGURE 4—6 A. LINEAR SINGLE-BEAM SYSTEM. B. MULTIBEAM SYSTEM. C. PARAMETRIC SUB-BOTTOM PROFILER. 37

FIGURE 4—7 DEFINITION OF SEDIMENT THICKNESS FROM TOPOGRAPHIC DIFFERENCING VIA SUBSEQUENT BATHYMETRIES. 38

FIGURE 4—8 DEFINITION OF SEDIMENT THICKNESS VIA THE DUAL FREQUENCY APPROACH. 39

FIGURE 4—9 SOUND REFLECTION FROM THE SEDIMENT. 40

FIGURE 4—10 ACOUSTIC WAVE PROPAGATION OF PARAMETRIC SYSTEMS (ADAPTED FROM LURTON X. (2002)). 41

FIGURE 4—11 EXAMPLE ECHOGRAM FROM SES2000 COMPACT (PHOTO FROM INNOMAR TECHNOLOGIES GMBH). 42

FIGURE 4—12 A. SCHEMATIC VIEW OF A UWITEC GRAVITY CORER. B. SCHEMATIC VIEW OF A PISTON CORER. 43

FIGURE 4—13 PROPERTIES DERIVED FROM THE DEPLOYMENT OF GP. THE SPIKES IN THE SEDIMENT REPRESENT LAYERS WITH MORE CONSOLIDATED MATERIAL. 45

FIGURE 4—14 CHURCHILL’S CURVE FOR DERIVING THE TRAP EFFICIENCY OF THE RESERVOIRS (MORRIS AND FAN 2010). 46

FIGURE 4—15 BRUNE’S CURVE FOR DERIVING THE TRAP EFFICIENCY OF A RESERVOIR (MORRIS AND FAN 2010). 46

FIGURE 4—16 MANAGEMENT STRATEGIES FOR EXTENDING A RESERVOIR’S LIFETIME (MORRIS 2020). 48

FIGURE 4—17 A. SEDIMENT BYPASSING. B. BYPASS RESERVOIR. 49

FIGURE 4—18 STAGES OF EMPTY FLUSHING (MORRIS 2020). 51

FIGURE 4—19 GENERAL GUIDELINE FOR CHOOSING THE MOST FEASIBLE MANAGEMENT APPROACH BASED ON THE RESERVOIR LIFETIME AND HYDRAULIC RETENTION TIME OF THE RESERVOIR (ANNANDALE ET AL. 2016). 53

CHAPTER 5

FIGURE 5—1 A. LOCATION AND LULC OF PASSAÚNA CATCHMENT. B. PASSAÚNA RESERVOIR AND ITS MOST IMPORTANT FEATURES.	56
--	----

CHAPTER 6

FIGURE 6—1 SCHEMATIC VIEW OF RUSLE APPLICATION FOR PASSAÚNA.	58
FIGURE 6—2 SCHEMATIC VIEW OF THE APPROACHES USED FOR EACH FACTOR IN THE PROCESS SEDIMENT INPUT QUANTIFICATION.....	59
FIGURE 6—3 A. DIGITAL ELEVATION MODEL. B. SPATIAL DISTRIBUTION OF LS-FACTOR.	60
FIGURE 6—4 EROSIVITY IN PASSAÚNA AND PARANÁ AFTER WALTRICK ET AL. (2015)	63
FIGURE 6—5 LOCATION OF PLUVIOMETRIC STATIONS IN THE PASSAÚNA CATCHMENT.....	64
FIGURE 6—6 MONTHLY PRECIPITATION FOR THE TWO LOCATIONS IN PASSAÚNA CATCHMENT	65
FIGURE 6—7 CORRECTION OF NDVI VALUES FOR URBAN AREAS	68
FIGURE 6—8. CHARACTERISTIC ARABLE LAND IN PASSAÚNA.	69
FIGURE 6—9 SCHEMATIC VIEW OF THE APPROACHES USED FOR SEDIMENT STOCK MEASUREMENT AND SEDIMENT CHARACTERIZATION	71
FIGURE 6—10 SEDIMENT THICKNESS DERIVED WITH THE DUAL FREQUENCY APPROACH.....	73
FIGURE 6—11 SEDIMENT THICKNESS DERIVED FROM THE SUB-BOTTOM PROFILING DATA	74
FIGURE 6—12 PHASES OF WAVE PROPAGATION IN THE SEDIMENT IN REGARD TO ACOUSTIC PROPERTIES (ADAPTED FROM HILGERT (2014)).....	75
FIGURE 6—13 ATTACK AND DECAY PHASE IN AN ECHO ENVELOPE	76
FIGURE 6—14 CLASSIFICATION APPROACH FROM SOTIRI ET AL. (2019A).....	79
FIGURE 6—15 SCHEMATIC VIEW OF CORE SAMPLING PROCESS VIA THE HAMMER ACTION.....	80
FIGURE 6—16 SCHEMATIC VIEW OF WET SIEVING.....	81
FIGURE 6—17 PHOTOS OF GP. LEFT BEFORE DEPLOYMENT. RIGHT AFTER DEPLOYMENT.	82

CHAPTER 7

FIGURE 7—1 A. LOCATION OF SOIL SAMPLES. B. INTERPOLATED MAP OF K-FACTOR.	84
FIGURE 7—2 TEXTURE OF SOIL SAMPLES.....	84
FIGURE 7—3 COMPARISON OF R-FACTOR FROM TWO APPROACHES:	85
FIGURE 7—4 MEAN C-FACTOR FOR EACH LULC CLASS FOR ALL THE MONTHS WHERE NDVI DATA IS AVAILABLE (FIGURE A—2 IN APPENDIX). FOR THE OTHER MONTHS THE C-FACTOR WAS INTERPOLATED.	86
FIGURE 7—5 SPATIAL DISTRIBUTION OF C-FACTOR FOR JANUARY AND JULY.	86
FIGURE 7—6 SDR FOR THE MONTHS OF JULY 2017 AND JANUARY 2018.....	87
FIGURE 7—7 EROSION CLASSES IN THE PASSAÚNA CATCHMENT.	88
FIGURE 7—8 A. CONTRIBUTION OF EACH LULC CLASS TO THE OVERALL SOIL LOSS IN THE PASSAÚNA CATCHMENT. B. CONTRIBUTION OF EACH LULC CLASS TO THE OVERALL SEDIMENT INPUT IN THE PASSAÚNA CATCHMENT.	89
FIGURE 7—9 MONTHLY DISTRIBUTION OF SEDIMENT INPUT FROM THE INITIAL MODEL RUN.	89
FIGURE 7—10 COMPARISON BETWEEN INITIAL MODEL RUN AND LULC.....	90
FIGURE 7—11 COMPARISON OF C-FACTOR TO MAXIMUM AND AVERAGE VALUES FOUND FROM LITERATURE.	91
FIGURE 7—12 FINAL DISTRIBUTION OF SEDIMENT INPUT AFTER C AND R-FACTOR CORRECTION.....	91
FIGURE 7—13 A. COMPARISON OF INTERANNUAL DYNAMICS OF THE SYSTEM. B. COMPARISON OF THE YEARLY SEDIMENT INPUT FROM THREE MODELLING APPROACHES.	92

FIGURE 7—14 A. EROSION CLASSES BEFORE C AND R-FACTOR CORRECTION. B. EROSION CLASSES AFTER C AND R-FACTOR CORRECTION. C. ORIGIN OF SEDIMENT BEFORE C AND R-FACTOR CORRECTION. D. ORIGIN OF SEDIMENT AFTER C AND R-FACTOR CORRECTION.	92
FIGURE 7—15 LOCATION AND LENGTH OF CORE SAMPLES IN THE PASSAÚNA RESERVOIR. L1, L2 AND L3 REFER TO THE LAYERS ENCOUNTERED IN THE CORES.	93
FIGURE 7—16 A. RELATION BETWEEN SILT-CLAY FRACTION AND DENSITY. B. RELATION BETWEEN LOI AND SILT-CLAY FRACTION.	94
FIGURE 7—17 SEDIMENT PROPERTIES IN PASSAÚNA RESERVOIR.	96
FIGURE 7—18 COMPARISON BETWEEN ELEVATION-STORAGE CURVE DERIVED FROM THE WASSP MULTIBEAM SYSTEM, AND THE EXISTING CURVE.	97
FIGURE 7—19 LACK OF PENETRATION AND ACOUSTIC TURBIDITY DUE TO GAS PRESENCE IN THE SEDIMENT.	98
FIGURE 7—20 A. SEDIMENT THICKNESS DERIVED FROM THE DOUBLE FREQUENCY APPROACH. B. FREQUENCY DISTRIBUTION OF THE SEDIMENT THICKNESS CLASSES FROM THE MAP.	99
FIGURE 7—21 A. SEDIMENT CLASSIFICATION IN PASSAÚNA RESERVOIR, WHERE: A. THICK SEDIMENT LAYER. SOFT NON-GASSY MATERIAL IN THE FIRST 80 CM. B. THICK SEDIMENT LAYER. SOFT GASSY MATERIAL IN BOTH TOP AND BOTTOM LAYER C. COARSE MATERIAL. OFTEN PRE-IMPOUNDMENT SOIL OR SANDY SEDIMENT. D. THIN SEDIMENT LAYER. VERY COMPACTED OR GASSY TOP LAYER. AND B. DIFFERENTIATION BETWEEN AREAS WITH AND WITHOUT SEDIMENT.	100
FIGURE 7—22 A. RELATION BETWEEN ATTDecaySV1 AND SILT-CLAY FRACTION OF THE SAMPLE. B. RELATION BETWEEN ATTSV1 AND LOI OF THE SAMPLE.	101
FIGURE 7—23 A. MAPPING OF LOI BASED ON THE REGRESSION ANALYSIS OF FIGURE 7—22B. AND THE FREQUENCY DISTRIBUTION OF THE CLASSES IN THE MAP. B. MAPPING OF SILT CLAY FRACTION BASED ON THE REGRESSION ANALYSIS OF FIGURE 7—22A. AND THE FREQUENCY DISTRIBUTION OF THE CLASSES IN THE MAP.	103
FIGURE 7—24 DEFINITION OF SEDIMENT THICKNESS BASED ON DCPR RESULTS FROM THE GP. SEVERAL MEASUREMENT LOCATIONS SHOWED THAT APPROXIMATELY 200 KPA IS AN ORIENTATION VALUE FOR THE BOUNDARY BETWEEN SEDIMENT AND PRE-IMPOUNDMENT SOIL IN THE PASSAÚNA RESERVOIR.	104
FIGURE 7—25 A. LOCATIONS OF GP MEASUREMENT AND THE VISUALIZATION OF THE MEASURED VALUE. THE PIE CHART SHOWS THE FREQUENCY DISTRIBUTION OF THE MEASURED VALUES OF SEDIMENT MAGNITUDE B. THE INTERPOLATED MAP OF SEDIMENT THICKNESS BASED ON THE GP MEASUREMENTS WITH DISTRIBUTION FREQUENCY OF THE INTERPOLATED VALUES.	105
FIGURE 7—26 A. CROSS SECTION PROFILE AA' CLOSE TO THE DAM. B. SCHEMATIC VIEW OF SEDIMENT MAGNITUDE (UP) AND THE RESPECTIVE MEASURED VALUE (DOWN) AT EACH POINT FOR THE AA' PROFILE.	106
FIGURE 7—27 A. LONGITUDINAL PROFILE OF THE RESERVOIR. B. SCHEMATIC VIEW OF SEDIMENT MAGNITUDE (UP) AND THE RESPECTIVE MEASURED VALUE (DOWN) AT EACH POINT FOR THE LONGITUDINAL PROFILE.	106
FIGURE 7—28. DIVISION OF THE RESERVOIR IN COMPARTMENTS.	107

CHAPTER 8

FIGURE 8—1 C-FACTOR AND R-FACTOR FOR THREE MONTHS (JANUARY, JULY, OCTOBER).	114
FIGURE 8—2 COMPARISON BETWEEN CORE SAMPLES AND GP RESULTS FOR TWO LOCATIONS C19 AND C9. LEFT IMAGES SHOW THE LAYERS DEFINED FROM CORE SAMPLES. RIGHT IMAGES SHOW THE LAYERS DEFINED FROM GP DATA.	117
FIGURE 8—3 LEFT: SEDIMENT THICKNESS FROM CORE SAMPLES VS. SEDIMENT THICKNESS FROM GP. RIGHT: SEDIMENT THICKNESS FROM CORE SAMPLES VS. SEDIMENT THICKNESS FROM GP WHEN EXCLUDING THE SHADED POINTS.	118
FIGURE 8—4 PHOTO DOCUMENTATION OF SOME OF THE SHADED POINTS IN FIGURE 8—3A. NONE OF THE CORES HAS REACHED THE PRE-IMPOUNDMENT SOIL.	119

FIGURE 8—5 DCPR OF SHADED POINTS FROM GRAPH IN FIGURE 8—3A. AT ALL LOCATIONS, THE GP DOES NOT REACH THE PRE-IMPOUNDMENT SOIL (DCPR SMALLER OR SLIGHTLY GREATER THAN 200 kPA)	120
FIGURE 8—6 COMPARISON OF SES2000 AND DCPR FROM GP AT POINT C19. THE WATER-SEDIMENT INTERFACE IS CLEARLY DEFINED IN THE SAME DEPTH AS GP. THE ESTIMATED FORMER LAKE BOTTOM IS HIGHLIGHTED AND SHOWS A SIMILAR DEPTH AS THE ONE DEFINED BY THE GP THRESHOLD OF 200 kPA. DUE TO THE HIGH GAS CONTENT, ONLY AT SOME LIMITED LOCATIONS IT WAS POSSIBLE TO USE THE SUB-BOTTOM PROFILING DATA FOR COMPARISON. THE DEPTH OF THE MEASUREMENT APPROACH IS NOT OVERLAPPING AS SUB-BOTTOM PROFILER DATA ARE NOT CORRECTED FOR THE TRANSDUCERS DEPTH.	121
FIGURE 8—7 COMPARISON OF GP WITH EA400 VALUE FROM THE INTERPOLATED MAP OF SEDIMENT THICKNESS.	122
FIGURE 8—8 A. COMPARISON BETWEEN MEASURED AND MODELLED SILT-CLAY FRACTION. B. COMPARISON BETWEEN MEASURED AND MODELLED LOI.....	124
FIGURE 8—9. LEFT: DRONE IMAGE OF THE NORTHERN PART OF PASSAÚNA RESERVOIR IN MAY 2020. (PHOTO COURTESY TOBIAS BLENINGER). RIGHT: SEDIMENT CLASSIFICATION IN PASSAÚNA RESERVOIR BASED ON THE CLASSIFICATION APPROACH OF SOTIRI ET AL. (2019A).....	125
FIGURE 8—10 COMPARISON BETWEEN THE HYDROACOUSTIC SEDIMENT CLASSIFICATION WITH THE DRONE IMAGE FOR THE AREA OF THE FERRARIA BRIDGE (PHOTO COURTESY TOBIAS BLENINGER)	126
FIGURE 8—11 CLASSIFICATION OF PASSAÚNA RESERVOIR BASED ON JURACEK (2015) CLASSIFICATION.....	128
FIGURE 8—12 SEDIMENT ACCUMULATION SCENARIOS IN 100, 200 AND 300 YEARS BASED ON THE ACTUAL SEDIMENTATION RATE MEASURED FROM GP	129
FIGURE 8—13 APPLICABILITY OF SEDIMENT MANAGEMENT TECHNIQUES FOR PASSAÚNA BASED ON ANNANDALE ET AL. (2016)	130
FIGURE 8—14 COMPARISON BETWEEN SEDIMENT STOCK IN THE RESERVOIR AND SEDIMENT INPUT FROM THE CATCHMENT.....	131
FIGURE 8—15 A. IMAGE FROM VEGETATION IN THE PASSAÚNA RESERVOIR BOTTOM NEAR THE LOCATION OF CORE 13 (PHOTO COURTESY LEDIANE MARCON) B. SEDIMENT CORE FROM PASSAÚNA.....	133
FIGURE 8—16. STRATIGRAPHY OF THE SEDIMENT AFTER EMPTYING THE VOSSOROCA RESERVOIR (PHOTO COURTESY STEPHAN FUCHS)...	134
CHAPTER 9	
FIGURE 9—1 GUIDING SCHEME FOR CHOOSING THE MOST APPROPRIATE SEDIMENT DETECTION TECHNIQUE	139
APPENDIX	
FIGURE A—1 NOMOGRAPH FOR CALCULATING THE K-FACTOR BASED ON WISCHMEIER AND SMITH (1978).....	167
FIGURE A—2 NDVI SCENES FROM JULY 2017-JUNE 2018 CALCULATED FROM SENTINEL-2 DATA. DELIVERED FROM EFTAS FERNERKUNDUNG TECHNOLOGIETRANSFER GMBH.....	168
FIGURE A—3 DEGREE OF SOIL SEALING CALCULATED FROM SENTINEL-2 DATA. DELIVERED FROM EFTAS FERNERKUNDUNG TECHNOLOGIETRANSFER GMBH.....	169
FIGURE A—4 SEDIMENT INPUT FROM PASSAÚNA CATCHMENT ON A MONTHLY TIMESTEP.....	170
FIGURE A—5 BATHYMETRY IN 20 CM HORIZONTAL RESOLUTION	171
FIGURE A—6 DYNAMIC PROFILES WITH THE SES2000 COMPACT SUB-BOTTOM PROFILER.....	172
FIGURE A—7 DYNAMIC PROFILES WITH THE LINEAR SYSTEM EA400	173
FIGURE A—8 DENSITY OF CORE SAMPLES	174
FIGURE A—9 GRANULOMETRY OF ALL SEDIMENT SAMPLES	174
FIGURE A—10 LOI OF ALL SEDIMENT SAMPLES.....	174

FIGURE A—11 TERRAIN IN THE NORTHERN PART OF THE RESERVOIR.....175
FIGURE A—12 COMPARISON BETWEEN THE SEDIMENT CLASSIFICATION AND THE DRONE IMAGE176
FIGURE A—13 FINAL DISTRIBUTION OF SEDIMENT INPUT AFTER C AND R-FACTOR CORRECTION177

List of Tables

CHAPTER 1

CHAPTER 2

CHAPTER 3

TABLE 3—1 DATA FOR ZANESVILLE OHIO (FOURNIER 1972), ADAPTED FROM MORGAN 1979	14
TABLE 3—2 TYPE OF CONSERVATION PRACTICES FOR REDUCING SOIL LOSS (BAUMHARDT AND BLANCO-CANQUI 2014)	16
TABLE 3—3 ADVANTAGES AND DISADVANTAGES OF THE MOST WIDELY USED TECHNIQUES FOR ASSESSING THE SEDIMENT YIELD FROM A CATCHMENT.....	17
TABLE 3—4 REVIEW OF EXISTING SEDIMENT INPUT MODEL (MERRITT ET AL. 2003).....	18

CHAPTER 4

TABLE 4—1 ADVANTAGES AND DISADVANTAGES OF THE MOST WIDELY USED TECHNIQUES FOR SEDIMENT DETECTION IN RESERVOIRS	33
TABLE 4—2 LIST OF ADAPTIVE STRATEGIES FOR EXTENSION OF RESERVOIR LIFETIME (MORRIS 2020)	52

CHAPTER 5

CHAPTER 6

TABLE 6—1 SUMMARY OF THE METHODS USED FOR ASSESSING THE SEDIMENT INPUT FROM THE CATCHMENT AND THE SEDIMENT STOCK IN THE RESERVOIR	57
TABLE 6—2 VALUES OF THE DIMENSIONLESS PARAMETER M.....	61
TABLE 6—3 TYPICAL VALUES OF K-FACTOR FOR BRAZILIAN SOILS.	61
TABLE 6—4 C-FACTOR VALUES FOR FIVE LULC CLASSES IN BRAZIL FROM A LITERATURE REVIEW FROM DA SILVA SANTOS (2019).....	65
TABLE 6—5 PULSE LENGTH AND ECHO RESOLUTION FOR ALL THE USED CONFIGURATIONS.....	78

CHAPTER 7

CHAPTER 8

TABLE 8—1 COMPARISON OF THE SEDIMENT INPUT RESULTS WITH THE FINDINGS FROM SAUNITTI ET AL. (2004)112

TABLE 8—2 SUMMARY TABLE FOR ALL THE USED METHODS.....123

TABLE 8—3 SUMMARY TABLE OF RESERVOIR LIFETIME ASSESSMENT BASED ON DIFFERENT MEASURING TECHNIQUES127

TABLE 8—4 OVERVIEW OF FACTORS CREATING INCONSISTENCIES BETWEEN MEASURED SEDIMENT STOCK AND MODELLED SEDIMENT INPUT
.....131

TABLE 8—5 SAMPLING FROM THE SEDIMENT TRAPS.....132

APPENDIX

TABLE A—1. ACOUSTIC PARAMETERS FOR ALL CONFIGURATIONS OF THE 200 KHZ.....178

TABLE A—2. ACOUSTIC PARAMETERS FOR ALL CONFIGURATIONS OF THE 38 KHZ.....181

TABLE A—3. CORRELATION MATRIX BETWEEN THE SEDIMENT PHYSICAL PROPERTIES AND ACOUSTIC PARAMETERS FROM CONFIGURATION A
OF THE 38 KHZ.....184

TABLE A—4. CORRELATION MATRIX BETWEEN THE SEDIMENT PHYSICAL PROPERTIES AND ACOUSTIC PARAMETERS FROM CONFIGURATION B
OF THE 38 KHZ.....185

TABLE A—5. CORRELATION MATRIX BETWEEN THE SEDIMENT PHYSICAL PROPERTIES AND ACOUSTIC PARAMETERS FROM CONFIGURATION C
OF THE 38 KHZ.....186

TABLE A—6. CORRELATION MATRIX BETWEEN THE SEDIMENT PHYSICAL PROPERTIES AND ACOUSTIC PARAMETERS FROM CONFIGURATION D
OF THE 38 KHZ.....187

TABLE A—7. CORRELATION MATRIX BETWEEN THE SEDIMENT PHYSICAL PROPERTIES AND ACOUSTIC PARAMETERS FROM CONFIGURATION A
OF THE 200 KHZ.....188

TABLE A—8. CORRELATION MATRIX BETWEEN THE SEDIMENT PHYSICAL PROPERTIES AND ACOUSTIC PARAMETERS FROM CONFIGURATION B
OF THE 200 KHZ.....189

TABLE A—9. CORRELATION MATRIX BETWEEN THE SEDIMENT PHYSICAL PROPERTIES AND ACOUSTIC PARAMETERS FROM CONFIGURATION C
OF THE 200 KHZ.....190

TABLE A—10. CORRELATION MATRIX BETWEEN THE SEDIMENT PHYSICAL PROPERTIES AND ACOUSTIC PARAMETERS FROM CONFIGURATION
D OF THE 200 KHZ.....191

List of Abbreviations

Carbon: (C).....	29
Companhia do Saneamento do Paraná: (SANEPAR).....	55
Cone Penetration Test: (CPT).....	44
Digital Elevation Model: (DEM)	60
Dynamic Cone Penetration resistance: (DCPR)	45
Dynamic Freefall Penetrometer: (DFFP).....	44
Elevation-Storage Curve: (ESC).....	97
Environmental Agency of Paraná: (IAP).....	55
GraviProbe: (GP).....	82
Inverse Distance Weighting: (IDW).....	73
Landuse and Landcover: (LULC).....	15
Loss on Ignition at 550 °C: (LOI).....	62
Mean Absolute Error: (MAE)	99
Nitrogen: (N).....	29
Normalized Difference Vegetation Index: (NDVI).....	23
Normalized Mean Absolute Error: (NMAE)	99
North American Department of Agriculture: (USDA)	62
Phosphorus: (P)	29
Relative Water Depth: (RWD).....	78
Revised Universal Soil Loss Equation: (RUSLE)	6
Root Mean Square Error: (RMSE)	118
Sediment Delivery Ratio: (SDR)	3
Sediment Water Interface: (SWI)	72
Silt-Clay Fraction: (SCF).....	78
Soil Loss Ratio: (SLR)	22
Sub-bottom Profiler: (SBP)	74
Sustainable Development Goals: (SDGs)	1
Undrained Shear Strength: (USS)	82
Universal Soil Loss Equation: (USLE).....	19
Wet Bulk Density: (WBD).....	78

1. Reservoirs and sediment

Assuring water resources for the next generations is one of the most important engineering and environmental challenges of humankind. From the UN summit of New York 2015, Clean Water and Sanitation for the whole earth population was set as one of the 17 *Sustainable Development Goals* (SDGs) for the 2030 Agenda (United Nations 2015).

Reservoirs are the main systems that can achieve a suitable management in terms of quantity of water withdrawal, even though they disrupt severely the riverine ecosystems. Referring to the inventory published by the International Commission on Large Dams, in 1988 there were around 42,000 reservoirs with a dam higher than 15 m (Morris and Fan 2010). Based on the reports of the same commission, in 2019 the number of reservoirs increased to 58,000. The trend for the future remains similar. Reservoirs are used for various purposes (Figure 1—1). Hydropower, drinking water supply, and irrigation are the most common. However, there is a large number of reservoirs created for industrial process water, tailing or even recreation. Due to the ability of a reservoir to regulate the downstream flow, almost all the reservoirs have as a byproduct also flood protection (International Commission on Large Dams 2019).

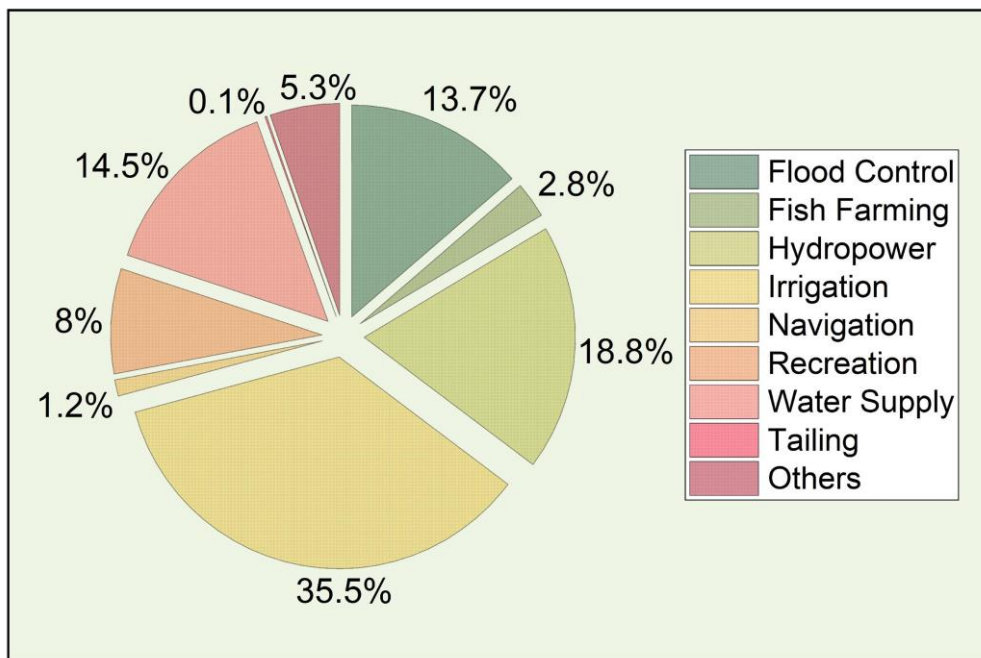


Figure 1—1 Main purposes of the existing reservoirs (adapted from International Commission on Large Dams (2019)).

Because of the increased demand for energy and water in the BRICS countries, most of the new planned reservoirs are located there. Based on the status report of International Hydropower Association in the year 2020, the two countries with the highest increase in hydropower capacity are Brazil (4.92 GW) and China (4.2 GW), while the regions which added the highest capacities were East Asia and the Pacific, followed by South America and then South and Central Asia (International Hydropower Association 2020).

With the actual rates of population growth and natural resources depletion, a real threat is posed to the aquatic ecosystems, thus the reservoirs, from the amount of sediments, nutrients, heavy metals or toxic substances that are emitted into the water bodies (Annandale 2014). Serious attempts should be made in building the capacities for assuring the quantity of water, but also in assuring the quality of the existing water sources as freshwater is an essential natural resource for humans, but also more essential for the aquatic organisms (McCartney et al. 2001; Bednarek 2001).

Sediment formation is a process that originates from the hydrological catchment. The most important sources of sediment in a watershed are the uncovered arable lands with significant slopes. The whole process from particle suspension until settlement is rather dynamic. Most of the particles, which are relocated due to erosive forces, usually do not reach the water bodies but are deposited in depression areas in the catchment. Even the particles that reach the river stretches might be deposited in floodplains, while other particles in the channel bank might be eroded, ending up in impoundments. The high uncertainty that characterizes the sediment formation and transport makes it therefore challenging to have accurate estimations and predictions of sediment fluxes and volumes.

One of the consequences of sediment formation is reservoir siltation. Solids play a crucial role for the lifetime of a reservoir. First, as they are the main factor which reduces reservoir's storage capacity by accumulating in the lakebed, and secondly as they are one of the most important factors that cause water quality deterioration. Annually it is estimated that there is a volume loss of 0.5-1% due to sedimentation (Schleiss et al. 2016). Sumi (2004) reports similar numbers with a volume loss rate of 0.52% yearly. Basson (2009) states that in Asia 70% of the volume used for irrigation will be lost by 2025, while the volume used for hydropower will be reduced to 20% by 2035 (Schleiss et al. 2016). Vörösmarty et al. (2003) estimated that more than 53% of the global sediment flux in regulated basins is trapped in reservoirs (Kondolf et al. 2014). While finally, Annandale (2014) claims that the world net storage capacity has been declining since 1995 due to the overcoming of storage loss on new storage construction.

With such statistics, the need for immediate action in terms of sediment management in reservoirs becomes crucial. This thesis is a contribution to the further understanding of the sediment problematic with focus on both the source and sink of particles.

2. Framework of the thesis

The framework of this study follows the introductory part about reservoirs and sediment. Initially, the challenges that are encountered from the present state of the art solutions are presented, followed by the research questions that this thesis is aiming to provide answers for. In the subsequent section, an overview of the thesis is given. In the overview section, the methods and their aim are briefly described. In the final section of this chapter, the structure of the thesis is presented.

2.1. Research questions and challenges of the thesis

This thesis aims at providing answers both for fundamental and applied research questions regarding the whole process of sediment input from a specific watershed until reservoir sedimentation. There are two important aspects of this dissertation. First, to contribute in closing the knowledge gap between erosion and sedimentation by having a holistic approach of sediment input evaluation-reservoir sedimentation assessment by applying several techniques like, modelling, long-term measurements, and through single campaign measurements of remote sensing and groundtruthing. Secondly, in applied terms, by providing a reliable model, which can describe and document the actual situation of sediment budget. The last is of importance to the reservoir operator in terms of present managing issues and future planning measures.

Extensive research work can be found regarding sedimentation. Yet, there is still a knowledge gap and no long-term solution applicable for resolving this issue. The challenges are not trivial. Assessing the amount of eroded soil is the initial problem as erosion is characterized by high spatial (dependent on terrain, soil type or land cover) and temporal variability (dependent on rain seasonality and interannual variations in land cover) (Wischmeier and Smith 1978; Renard 1997). The results of modelling often are not reliable, mainly due to the uncertainties in the calculation of the contributing coefficients, so a high effort is needed in terms of validation (Merritt et al. 2003). In experimental or monitoring approaches on the other hand, the difficulty consists in extrapolating the findings to the large spatial coverage of the watershed. Even when the erosion is properly estimated, the issue of quantifying the amount of sediment that reaches the water body still needs to be solved. There are many standardized methods for calculating the sediment reaching the river stretches and many different applications already exist. These approaches mostly rely on the calculation of *Sediment Delivery Ratio* (SDR) based on the physical properties of the

investigated watershed (land use classes, slope or distance from river stretch). Still most of these approaches are not reproducible as they are specific for the area where they were derived.

As a validation measure for sediment input modelling, the most widely used approaches for quantifying sediment input at a catchment scale are the long-term (automatic or conventional) monitoring of suspended solids and bed-load transport in river stretches. The derived data are used for both assessing the sediment yield from the investigated catchment and also to calibrate or validate the sediment input models. Monitoring has also major disadvantages. Such measurements are often highly time consuming and produce high costs because of the transport to the monitoring station, sample processing and station maintenance. Secondly, due to the limited monitoring duration, often the rating curves derived from this monitoring approach underestimate the sediment yield from a catchment, as they do not include extremely high or catastrophic flood events. Finally, rivers are highly dynamic systems. The high and sudden fluctuation of river discharge can lead to important errors as the sampling moment in flood events (flood uprising, flood descending or flood peak) is important for the sediment concentration (Wagner et al. 2019).

Reservoirs can be of great importance in this regard, as they represent robust systems which collect the overall eroded material leaving the catchment and reaching the water body during the reservoirs entire lifetime (in case of 100% trapping efficiency) (Figure 2—1). For this reason, the use of reservoirs as an alternative to river monitoring avoids problems associated with insufficient monitoring, inaccurate rating curves or errors due to sudden fluctuation of river discharge. In addition, the duration of a monitoring campaign for reservoir sediment stock is significantly shorter than the duration of river stretch monitoring. Based on the above-mentioned advantages, this thesis follows the hypothesis that in case of an impoundment existence ***the reservoir can be used as a reliable validation/calibration point for reduced complexity sediment input modelling***. As most of the existing modelling approaches have as output the long-term sediment yield from a catchment, the sediment stock can be directly used for comparing the approaches.

An accurate assessment of the sediment input from the watershed and reservoir stock can be a first and crucial step in closing the sediment balance of the investigated catchment. Regarding the state of the art methodological development, this thesis aims at providing answers to the following research questions.

First, in the last years, a significant increase in freely available, sufficient temporal and spatial resolution satellite imagery has been recorded. The effects of the inclusion of such data in sediment input modelling is still not fully investigated. Therefore, the first research question of this study is to investigate ***how the developments in free available satellite imagery can contribute in improving the sediment input modelling in a hydrological catchment***.

Secondly, the challenge consists in the quantification of the sediment volume in the reservoir lakebed. The reservoirs often have a spatial coverage of several square kilometers, so the assessment of sediment magnitude to each single position is rather complicated. Due to its time effectivity, hydroacoustics has turned to be an important development in terms of sediment volume assessment and also sediment classification (Bruk 1985). Regarding the *state of the art* problematic, the challenges are encountered mainly in having a reliable assessment of sediment volume in the cases where the previous depth distribution is not available, or it is available in an insufficient accuracy. Lately more advanced hydroacoustic and penetrometer systems have been developed. Considering these actual developments, the second research question that this thesis aims to answer is: ***How can the combination of several techniques improve the quality of sediment volume assessment and sediment distribution mapping?***

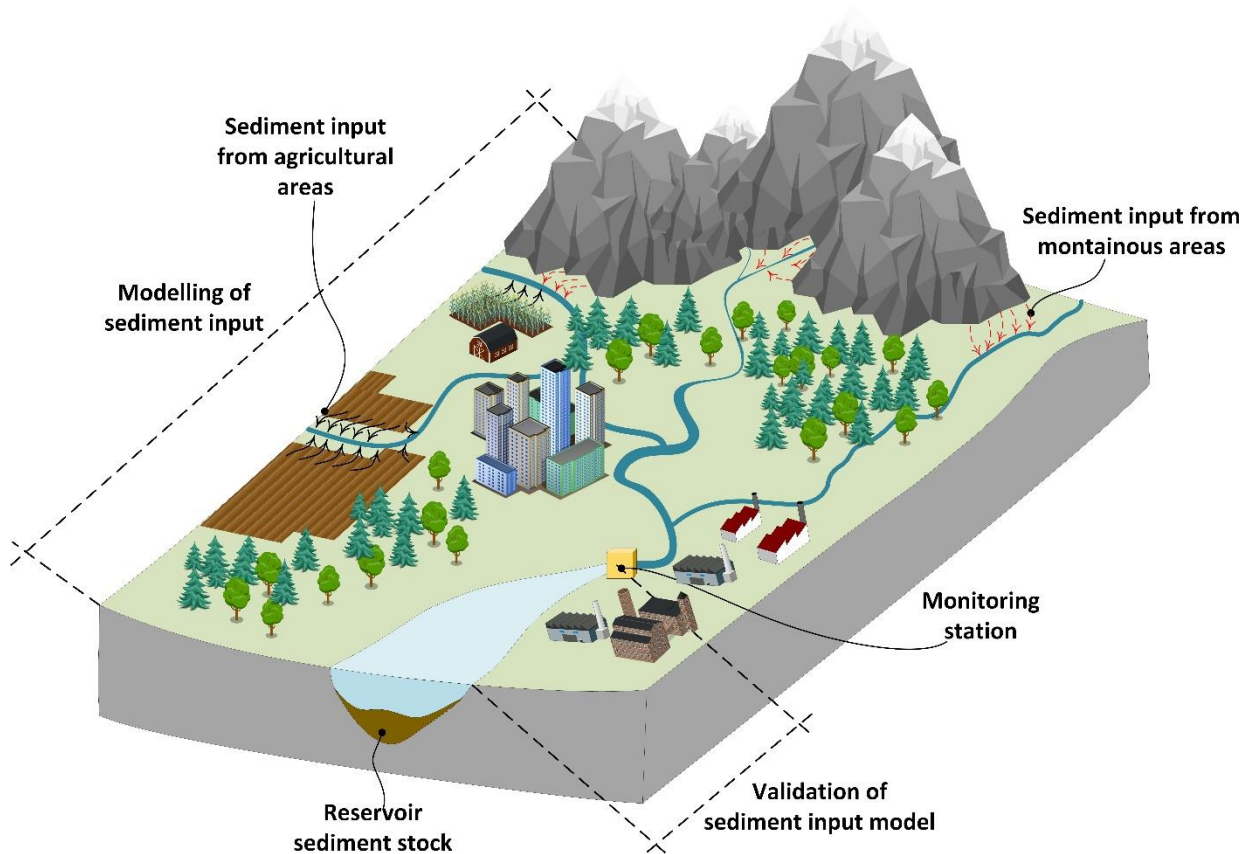


Figure 2—1 Schematic explanation of the hypothesis of the thesis (Icons in the figure are adapted from IcoGrams).

2.2. Overview of thesis

For this thesis, important was not only to derive methodologies but also to combine the findings in 'ready to use' results and techniques for the managing authorities. The first methodological development consists in the combination of existing methodologies for sediment input calculation. The applied methodology is based on the *Revised Universal Soil Loss Equation* (RUSLE). The calculation of some of the parameters was executed with empirical approaches especially for C-Factor, which represents the factor with the higher uncertainties (Estrada-Carmona et al. 2017; Karydas et al. 2020). Of great importance is to assess the spatial distribution of sediment input. Special focus is also given in understanding and reproducing the temporal dynamics of sediment input on a monthly basis, as RUSLE typically evaluates long-term trends rather than specific short term estimations (Lu et al. 2004; Galdino et al. 2016).

Secondly, a sediment magnitude assessment and sediment characterization methodology with the use of multiple techniques and tools was implemented. An integrative approach of hydro-acoustics, sediment sampling and dynamic penetrometer was applied for quantification of the sediment volume and sediment thickness distribution in the investigated reservoir. As single techniques each of them are useful in evaluating the sediment situation, however each of them embraces certain limitations. Echo-sounders are restrained by the gas presence in the sediments, while traditional groundtruthing requires time and high analyses costs. Finally, the penetrometers present proxy parameters for the geotechnical properties of the sediment but no real overview about the real sediment material. By integrating the three techniques, the constraints are minimized and the evaluation becomes more reliable. For the investigated reservoir, until now there was no reliable assessment of sedimentation volume. Therefore, the derived results represent a direct indication about the reservoir lifetime.

2.3 Structure of the thesis

The theses is structured in nine major chapters. In Chapter 1, the basic information about the reservoir situation and a brief overview of the sediment issue is introduced. In Chapter 2 the research objectives, the overview and the structure of this thesis are presented. Chapter 3 and 4 are an extended introduction in the theoretical and scientific background of the present research work. Chapter 3 deals with the issue of soil loss and sediment input processes. This Chapter focuses on explaining the physical processes behind erosion. It presents the main factors that affect soil loss and a short historical summary about erosion research. Furthermore, special focus is given also to the modeling approaches. A broad literature review was conducted to understand which models already exist and which are the factors that cause the highest uncertainties in the results. Chapter 4 concerns reservoir siltation. This chapter presents a documentation of the until

now work about reservoir sedimentation. A section of this chapter are also the fundamentals of hydroacoustic, as for assessing reservoir siltation and characterizing the bottom sediment, extensive echo-sounding activities were conducted.

Chapter 5 describes shortly the investigation area. Here information about population, geology, climate and landuse information of the investigated catchment are included, aside with technical information about the existing reservoir.

Chapter 6 describes extensively the methodology followed for answering each research questions. Here it is explained in detail how the erosion rate and sediment input were calculated, and the main methodology followed for assessing the sedimentation in the reservoir.

Chapter 7 presents the main results with focus to each methodology separately.

Chapter 8 discusses the results of the previous chapter and presents the main differences and overlapping areas with similar studies and relevant literature. In this chapter, special focus is given in comparing the findings among the different methodologies.

Chapter 9, which is the also the final chapter, summarizes the major outcomes and the main findings of this dissertation in concrete answers to the research questions.

3. Erosion and sediment input

Soil is a dynamic system that is highly dependent on the variations of the surrounding environment. Erosion induced changes are the dominant processes in terms of landscape and terrain shaping (Montgomery 2012). Soil erosion is a natural process, defined as the relocation of Earth's surface material by erosive agents (USDA 1954; Werner 1980; Morgan 1979; Fournier 2011; Gericke 2013). According to Quinton et al. (2010), water is the main natural erosive agent as it is responsible for 80% of soil erosion worldwide.

Erosion has multiple environmental and economic impacts. First and most obvious impact is the **degradation and productivity loss of fertile soils**. The long history of anthropogenic activity had significant implications on environmental change at different scales. With the increase in population, there is subsequent growth in food demand. The removal of the natural vegetation, deforestation and the densification of crop cultivation increased the vulnerability of soil towards erosion (Dotterweich 2013; Reusser et al. 2015). Based on the results of Hooke (2000), only during the last century, the per capita removed earth has increased by around 400%. In comparison to 2000 years ago, the per capita removed earth today is around 2000% higher. The results indicate a direct linkage to the rate of population growth and food demand. Soil formation is extremely slow. Under tropical and temperate agricultural conditions, 200 to 1000 years are needed for the creation of 340 t ha⁻¹ of soil. The yearly renewal rate is around 0.2-2 t ha⁻¹ a⁻¹, while the soil loss in agricultural regions fluctuates between 10-100 t ha⁻¹ a⁻¹ (Pimentel et al. 1987). With such high differences in soil erosion-renewal rates, soil conservation practices become a necessity concerning world food economy.

Apart from affecting soil quality in terms of physical properties, erosion is responsible for the biogeochemical degradation of the soil. Around 60% of fertile soil by mass is such 0.25–10-millimetre particles (Banwart 2011). The highest part of the organic material is found in the smaller granulometric fraction of the soil matrix and often in the first centimeters of the soil surface. This physical property makes fine soil, thus organic matter, vulnerable to relocation, as together with the soil particles, nutrients and chemical compounds of the soil are also washed out. The eroded soil is up to three times richer in nutrients than the remaining soil (Young 1989; Pimentel 2006). As stated in Quinton et al. (2010) for arable land mobilization and deposition of soil particles, erosion processes have the same impact on nutrient cycles as the application of fertilizing agents and crop removal. For the total system, including here also other types of landcover and water bodies, erosion is the driving force that shapes the geochemical cycle of many crucial elements. Despite the advancements in understanding during the last decades, still many question

regarding the C:N:P cycles remain unanswered. The uncertainties for the future are enhanced when taking in consideration the change of climatic conditions and the increase of river impoundment structures (Berhe et al. 2018).

Secondly, erosion has severe impacts in the aquatic ecosystems and water budget. Sediment input due to erosion is the main factor **deteriorating water quality, threatening the aquatic biodiversity and reducing river impoundments lifetime**. This issue will be analyzed in details in the next chapter.

All the above-mentioned effects produce an important economic cost. In USA, direct and indirect annual effects of soil erosion are estimated between US\$30 billion and US\$44 billion (Morgan 1979; Pimentel et al. 1987; Uri and Lewis 1998). Pimentel et al. (1995) assessed that in USA it would take an investment of US\$ 6.4 billion per year to reduce soil erosion rates from 17 Mg ha⁻¹ a⁻¹ to 1 Mg ha⁻¹ a⁻¹ only in the cropland and an additional US\$ 2 billion for reducing the soil loss in the pasture land. In a global basis, the soil loss due to water erosion for the year 2012 was estimated 35.9 Pg a⁻¹ (10¹⁵ g) (Borrelli et al. 2017). According to Panagos et al. (2015c) and Borrelli et al. (2018) in Europe the erosion is in the range of 1 Pg a⁻¹. The continents that are more affected are South America, Africa and Asia. All of the latest mentioned have severe erosion on more than 7% of their territory (respectively 8.3%, 7.7% and 7.6%) while Europe has 1.6% (Borrelli et al. 2017).

Brazil is one of the countries that lately has suffered an extensive deforestation and land use change due to cropping and cattle grazing. The area under grain cultivation increased by 80% between 1996 and 2006, particularly in areas such as the Cerrado (Brazilian Savannah). On the other hand, there was a decrease in cattle grazing area in almost all Brazilian states except for Amazon, where it increased by 34% (Merten and Minella 2013). Brazil is estimated to lose around 600-800 million Mg of soil to water erosion (Bahia et al. 1992; Hernani 2002; Manzatto et al. 2002; Miranda et al. 2015). The worst case scenarios for the next 10 years indicate that could be an increase of 20% of eroded mass (Merten and Minella 2013).

3.1. Erosion and sediment formation processes

When water is the erosive agent, erosion is characterized by three main phases. The first phase is the detachment of soil particles. In this phase, the potential energy of the raindrop due to its absolute elevation, is transformed in kinetic energy. The free fall of the raindrops due to gravity, causes remobilization of soil particles when the drops reach the soil surface. The second phase is the transport of the detached material from the accumulated flow and the final phase of erosion is deposition, which occurs when the transport forces are depleted (Wischmeier and Smith 1978; Morgan 1979; Werner 1980). In this regard, erosion is divided in two subcategories:

loss of topsoil (rainsplash and sheet erosion) and terrain deformation (rill, gully and channel erosion) (Figure 3—1) (Bridges and Oldeman 1999).

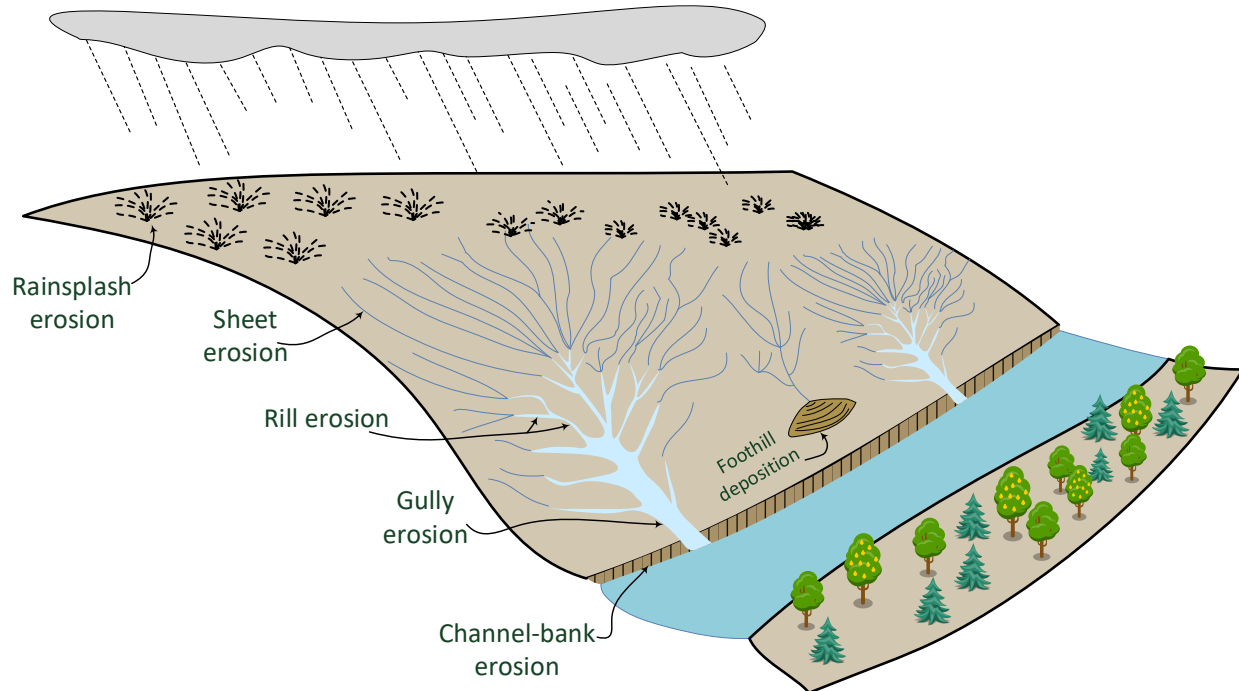


Figure 3—1 Graphical explanation of erosion and sediment formation.

3.1.1. Detachment by splash

The importance of rainsplash energy has been confirmed by many empirical studies (Bryan 1999; Fernández-Raga et al. 2017; Fernández-Raga et al. 2019). Yariv (1976) explains splash processes of erosive rains in three stages. The first stage is the expenditure of the kinetic energy of the raindrop on the dry soil. The depletion of kinetic energy is followed by the increase of the soil water content. Due to this effect, the internal shear stress of the overall matrix is reduced. The third phase starts with the creation of ponds in the soil surface and raindrops interact with the overland flow (Yariv 1976; Bryan 1999).

The relocation of particles due to splash erosion creates also side effects in the runoff processes. In fine grained soils, especially loams and sandy loams, the result of rainsplash is often the formation of surface deposition crusts, which reduce infiltration resulting in higher runoff (Morgan 1979; Werner 1980; Boiffin 1986; Boiffin and Monnier 1986). The crust formation is highly dependent on the slope of the location, as steeper slopes prevent the sealing due to high soil loss rates, while on a flat surface, the fine particles may clog up pores and facilitate ponding (Poesen 1984; Fernández-Raga et al. 2019).

3.1.2. Inter-rill and rill erosion

Baur (1952) defined sheet erosion as the removal of fairly uniform layer of soil or material from the land surface by the action of rainfall and runoff. Sheet erosion is often defined also as *inter-rill* erosion. During the overland movement of the water, the flow is often fully turbulent and has developed significant velocity. The detachment of the particles from the soil mass occurs when the shear stress caused by the flow velocity, exceeds the critical shear stress of the soil matrix (Shields A. 1936). Due to the nonuniformity and the roughness of the soil, the flow creates preferential flows by eroding random pathways, which direct afterwards the overland flow. These random pathways are called *rills*. Together with particles removed as rill and inter-rill erosion, also the particles detached due to rainsplash, remain in suspension and are transported through the created overland flow. The concentrated linear flow is deeper and faster than the dispersed overland flow and, thus, improves the total sediment transport efficiency (Bruno et al. 2008; Carollo et al. 2015).

Several authors have tried to explain the development of rills (Merritt 1984; Sun et al. 2013). Wang (1998) described rill formation in four stages. 1) downward incision and horizontal development along the wetted perimeter of a rill; 2) local erosion by the scarps in a rill; 3) collapsing of rill walls; and 4) lateral migrations of rills (Sun et al. 2013). Merritt (1984) also defined four stages of rill formation, even though he focused more in the triggering point of rill formation and not so much in the widening of the rills. The location of rills and their pattern are determined by microtopography of the soil surface on the hillslope (Carollo et al. 2015). A rill can expand to a maximum width of 30 cm (Carollo et al. 2015; Shit et al. 2016).

3.1.3. Gully erosion

According to Poesen et al. (2003) when the cross-sections of a rill becomes greater than 1 m², they are transformed in gullies. Gullies have similar shapes to river channels; however, they are characterized by a headcut and several knick-points during their course. Gullies can reach a variety of depth, starting from 0.5 up to 30 m. Initially it was believed that gullies are developed exclusively as rill expansion but according to Morgan (1979) there are two additional mechanisms of gully development. Depending on the type of soil and land cover, subsurface flow can be developed. This subsurface flow creates structures such as pipes and tunnels within the soil. These structures expand until they all merge together creating tunnels which act as gullies. The tunnel erosion can contribute up to 25-30% of the catchment sediment input (Zhu 2003). The other mechanism from which the gullies are initiated are the tracks left from landslides. This deep and step scars are occupied and expanded by storm water in erosive rainfalls creating so the gully structure (Fredén and Furuholm 1978).

In comparison to sheet and rill erosion, gully erosion is less investigated. However, recent studies (Wallbrink et al. 1998; Walling 2005; Wilkinson et al. 2009) showed that gullies contribute substantially in the sediment budget at a catchment scale. They do not only contribute as a sediment source but they also increase the efficiency of sediment transport from uplands to valley bottom and river channels as most of the sediments generated from rill and inter-rill erosion, that are not connected to gully structures, are deposited at the foot of the hillslopes (Poesen et al. 2003).

According to Poesen et al. (2006) and Poesen et al. (2003) gully erosion can contribute up to 94% of the total sediment yield from a catchment. Many factors can affect the formation of gullies and their contribution to the overall sediment yield from a hydrological basin. Soil type, terrain slope, land use weather conditions and conservation practices are the most relevant.

3.1.4. Channel erosion

Channel bank erosion can be a significant source of sediment input in a river system (Fox et al. 2016). According to Walling (2005), channel or bank erosion commonly accounts for between ca. 4 and 40% of the suspended sediment loads of UK rivers, with typical values between 5–15%. In the United States, some studies have reported that up to 90% of the sediment yield from certain catchments can originate from streambank erosion (Fox et al. 2016). The rates of channel bank erosion are influenced by *natural factors* such as bank material of river bed, bank geometry, discharge magnitude, riparian vegetation and *anthropogenic factors* such as removal of bank vegetation, trampling and poaching by livestock, flood control structures and reinforcement of river bed and bank with concrete or boulders (Janes et al. 2017).

According to Simon and Rinaldi (2006), the stages in which the stream bank erosion develops are the following:

1. Pre-disturbed channel characterized by hydrological and solids equilibrium
2. Change in the hydrological conditions of the catchment or in the geometrical properties of the channel
3. Degrading river bed but stable lateral banks
4. Lost stability and collapse of lateral banks due to increased slope created by the further river bed degradation
5. Aggradation of the streambed due to accumulation of sediment from upstream reaches
6. The system reaches stability and equilibrium due to the deposition of the sediment

Changing the geometry of a channel can have impacts that are more significant on the sediment budget of the riverine system than the change of the hydrological conditions. A representative example is the Wildhorse Creek in Oklahoma, which is partly feeding the

downstream Lake Texoma. The deepening of the stream in the years 1922–1933, lead to an increase in channel bank erosion. Since the “channel improvements” were completed, a total of 38 million m³ originating from the streambanks of Wildhorse Creek has been deposited in the lake (Fox et al. 2016).

3.2. Factors influencing erosion

A combination of climatic, topographic physical and anthropogenic factors control erosion. As in this thesis erosion is referred only to water erosion, one of the main factors affecting soil loss is **rainfall**. As explained previously, the shape of raindrop and the amount of runoff generated in a rainfall event are crucial. Both factors are directly connected to the rainfall intensity, which together with duration are the most important characteristics in regard to erosion initiation. Fournier (1972) showed the direct connection between rainfall intensity and soil loss for 183 events at Zanesville Ohio (Table 3—1). Depending on the previous conditions of the soil, the intensity of rain that can produce erosion is different (Fournier 1972; Morgan 1979)

Table 3—1 Data for Zanesville Ohio (Fournier 1972), adapted from Morgan 1979

Maximum 5-min intensity (mm h ⁻¹)	Number of events	Average soil loss per rainfall (t ha ⁻¹)
0 – 25.4	40	3.7
25.5– 50.8	61	6.0
50.9 – 76.2	40	11.8
76.3 – 101.6	19	11.4
101.7 – 127.0	13	34.2
127.1 – 152.4	4	36.3
152.5 – 177.8	5	38.7
177.9 – 254.0	1	47.9

Type of soil is another factor that strongly affects the erosion. Various parameters of soil like, structure, organic matter content, soil texture or infiltration capacity are directly interconnected with soil loss. The relation between fine sand-silt-clay is determining in a way also the erodibility of the soil. Richter and Negendank (1977), for the area of Moselle River, discovered that silty and sandy loams are more prone to erosion that soils with higher clay content, because

of the low infiltration capacity and weak cohesion. The proportion between mineral and organic material of the soil is directly related to the aggregate stability. Generally, soils with higher organic matter are more exposed to erosion than the mineral soils, where the mineral fractions increases the stability through chemical bonding of aggregates. Aggregate stability also depends on the type of clay mineral present. Soils containing kaolinite, halloysite, chlorite or finegrained micas, all of which are resistant to expansion on wetting, have a low level of erodibility, whereas soils with smectite or vermiculite swell on wetting and therefore have a high erodibility; soils with illite are in an intermediate position (Morgan 1979).

Natural and human-induced **land use and land cover change** (LULC) have a significant impact on soil erosion. In recent years, many researchers have highlighted the importance of LULC in erosion and sediment formation patterns (Favis-Mortlock and Boardman 1995; Dunj3 et al. 2004; Nearing et al. 2005; Bakker et al. 2008; Cebecauer and Hofierka 2008; Sharma et al. 2011; McGrane 2016). Plant cover is a factor that is widely investigated, concerning its effects on soil protection. Vegetation absorbs the energy of the falling raindrops and acts as a first protective layer for the soil. The protective effectivity of the vegetation layer depends on several components such as, height, coverage factor and density of the canopy. Apart from reducing the kinetic energy of the falling raindrops, the plant cover is also responsible for dissipating the energy of the runoff by increasing the bottom roughness. Greatest reductions in velocity occur with dense, spatially uniform, vegetation covers (Morgan 1979). The runoff energy dissipation is however, more effective in plants with low canopy such as wheat or cotton than in trees whose main advantage is protection to rainsplash erosion.

The **terrain slope** is also an important factor for erosion formation, as the main force that drives water flow is gravity. With increasing slope steepness, the flow velocity of the surface runoff also increases. Higher flow velocities, mean thus higher erodible force of water and larger amount of soil detachment. Likewise slope steepness, slope length is an important factor that controls erosion as soil loss increases with a decreasing slope length (Stomph et al. 2002; van de Giesen et al. 2005; Han et al. 2019)

Land conservation practices are farming operations and management strategies conducted with the goal to control soil erosion by preventing or limiting soil particle detachment and transport in water. Controlling soil erosion by management is generally directed at decreasing the energy of wind or water by limiting their velocity through decreased soil slope for runoff and through barriers for intercepting wind and raindrop impact (Baumhardt and Blanco-Canqui 2014). A proper combination of conservation practices (Table 3—2) can reduce the soil loss up to 10 times (Smith and Wischmeier 1957; Werner 1980).

Table 3—2 Type of conservation practices for reducing soil loss (Baumhardt and Blanco-Canqui 2014)

Mechanical structures	Agronomical practices	Conservation buffers
Terracing	Conservation tillage	Vegetative filter strips
Drop structures	Residue mulching	Grass barriers
Spillways	Cover cropping	Grass waterways
Culverts		Riparian buffers
Gabions		
Ripraps		
Ditches		

The produced soil loss on a specific site is a product of the unique combination of the above-mentioned anthropogenic and natural-physical factors in that specific timeframe. Erosion has distinguishing temporal patterns dependent on the climatic condition and vegetation cover, and particular spatial patterns due to the diversity of terrain, soil type or LULC. When examined in a global or continental scale, soil loss rates and sediment input are highly variable depending on anthropogenic activity and environmental conditions (Panagos et al. 2015c; Borrelli et al. 2017; Borrelli et al. 2018).

3.3. Soil erosion and sediment yield quantification

The techniques used for soil loss/sediment input monitoring can vary depending on the scale and the duration of the monitoring (Table 3—3). The monitoring activities for quantifying soil loss at plot scale are either direct plot soil loss measurements or indirect assessment by using fallout radionuclides as tracers for soil erosion (Alewell et al. 2019). Long term monitoring of suspended solids and bed-load transport in river stretches, depending on the scale and the duration of the monitoring, are also common activities for monitoring sediment input at a catchment scale (Wagner et al. 2019). The main disadvantage of river suspended solids monitoring is often the duration of the monitoring. Most of the soil loss, thus sediment yield, in a hydrological basin can occur in extreme events where in one event the sediment input of several years can be reached. To “catch” such a catastrophic event is often a case of luck as they happen rarely. The sediment rating curves derived without including these events are often misleading and underestimating the actual sediment input in the river stretches. Fallout radionuclides are also used for deriving the sediment yield from a catchment (Walling et al. 1996; Walling et al. 2014). Caesium-137 is the most used material for these applications. The fallout radionuclides can achieve with high accuracy the dating of the sediment. However, they have also restrictions like high analytical costs

or extrapolating of the results from plot-scale measurement to a catchment scale. Finally, river impoundments can be used as a long-term validation point of sediment input in aquatic ecosystems (Elçi et al. 2009; Schleiss et al. 2016; Krasa et al. 2019). Many large reservoirs have a high trapping efficiency. Therefore, the measured sediment stock is the sediment input from the catchment for all the years that the river was impounded, multiplied with the trapping efficiency of the reservoir.

Table 3—3 Advantages and disadvantages of the most widely used techniques for assessing the sediment yield from a catchment

	Method	Advantage	Disadvantage
In river techniques	Rating curves from river monitoring and bedload traps	<ul style="list-style-type: none"> • Ability to capture the temporal dynamics of the sediment input 	<ul style="list-style-type: none"> • Complicated to achieve and often underestimating (lack of isokinetic sampling, exclusion of rare extreme events...)
In catchment	Erosion modelling	<ul style="list-style-type: none"> • Cost effective • Applied before dam commissioning 	<ul style="list-style-type: none"> • Lack of validation data often leads to non-reliable results • Accurate modelling requires also accurate input data which might be expensive or time consuming
	Erosion monitoring plots	<ul style="list-style-type: none"> • Accurate estimation. • Ability to capture the temporal dynamics of sediment input 	<ul style="list-style-type: none"> • Time consuming activity • Need for long term monitoring • Not suitable for large catchments
	Fallout radionuclides as tracers	<ul style="list-style-type: none"> • Accurate estimation of soil loss 	<ul style="list-style-type: none"> • High analytic costs • Extrapolation and upscaling of results at the catchment scale is not easily achievable

Due to the rather large spatial scale which erosion takes place and the high temporal variability, quantification of erosion by monitoring programs can result in high costs. Hence, alternatives like modelling are often included for the quantification of soil loss and localization of hotspots.

According to Morgan (1979), models can be of three types:

a. *Physically based*

Based on mathematical equations to describe the processes involved in the model, taking account of the laws of conservation of mass and energy.

b. *Stochastic*

Based on generating synthetic sequences of data from the statistical characteristics of existing sample data; useful for generating input sequences to physically based and empirical models where data are only available for short periods of observation.

c. *Empirical*

Based on identifying statistically significant relationships between assumed important variables where a reasonable database exists.

Merritt et al. (2003) did an extended review of the existing status for erosion modelling (Table 3—4). His classification approach of models differed slightly from Morgan (1979), where apart from physically based and empirical models, Merritt et al. (2003) introduces additionally conceptual based models.

Table 3—4 Review of existing sediment input model (Merritt et al. 2003)

Model	Type	Scale
AGNPS	Conceptual	Catchment
ANSWERS	Physical	Catchment
Creams	Physical	Field
EMSS	Conceptual	Catchment
HSPF	Conceptual	Catchment
IHACRES-WQ	Empirical/Conceptual	Catchment
IQQM	Conceptual	Catchment
LASCAM	Conceptual	Catchment
SWRRB	Conceptual	Catchment
GUEST	Physical	Plot
LISEM	Physical	Catchment
PERFECT	Physical/Conceptual	Field
SEDNET	Empirical/Conceptual	Catchment
TOPOG	Physical	Hillslope
USLE	Empirical	Hillslope
WEPP	Physical	Hillslope/Catchment
MIKE-11	Physical	Catchment

Nevertheless, most models have no sharp boundaries whether they are physical, conceptual or empirical as many of them contain at least one module derived with a different approach (e.g. in case of physical models they might include conceptual or empirical derived algorithms) (Merritt et al. 2003).

Alewell et al. (2019) did another extensive review of erosion modelling, but this time with focus only on the Universal Soil Loss Equation (USLE). As stated in Alewell et al. (2019), “USLE and its most important modification, RUSLE are by far the most widely used applications of erosion modelling globally”. According to the authors, a query with the Science Direct tool for the last 40 years resulted in 1556 studies using USLE or RUSLE with an average citation rate of cited publications of 18.8. Due to its simplicity and the large number of reference studies, this thesis focuses exclusively on the USLE/RUSLE approach and its applications while the other mentioned models are not considered for assessing erosion and sediment yield.

3.4. USLE/RUSLE

The USLE was originated by Smith and Wischmeier (1957) for assessing the soil erosion in the US agricultural land. The research for quantifying the soil erosion started in 1940 in the Corn Belt and ended with final publication of Wischmeier and Smith (1978), where figures and relations were added to calculate each of the parameters. Since then USLE has revolutionized the way of arable land management in terms of erosion. The USLE defines mathematical equations and constant parameters for calculating the influence of all the above-mentioned human and environmental factors that affect erosion. The equation was derived from 10,000 plot-years of basic runoff and soil loss data in 49 locations in USA. The USLE is an erosion model designed to predict the **longtime average soil losses** in runoff from specific field areas in specified cropping and management systems, and is not appropriate for short term or single events modelling.

The next development in USLE happened in 1997, when Renard et al. (1997) published the Revised form of the Universal Soil Loss Equation. In the new version of RUSLE the core philosophy of USLE was retained, even though significant changes in the calculation of the single parameters were included. RUSLE also included a user interface to facilitate calculations (Renard et al. 1997).

A goal of the equation in both cases was to represent each factor affecting soil erosion with a single coefficient. The soil loss based on USLE/RUSLE is calculated with the following formula:

$$A = L \cdot S \cdot R \cdot C \cdot K \cdot P \quad (1)$$

Where:

A is the soil loss at the investigated area ($ton \times ha^{-1} \times a^{-1}$)

L is the slope length factor (-)

S is the slope steepness factor (-)

R is the rainfall-runoff erosivity factor ($MJ \times mm \times ha^{-1} \times h^{-1} \times yr^{-1}$)

C is the cover management factor (-)

K is the soil erodibility factor ($ton \times h \times MJ^{-1} \times mm^{-1}$)

P is the support practice factor (-)

3.4.1. Topographic factor LS

Plot geometry or terrain has a significant impact on the amount of soil loss. Two aspects of geometry that correlate with soil loss are slope steepness and slope length of a plot. In the USLE they are integrated in the topographic factor LS. LS expresses the expected ratio of soil loss per unit area from a field slope to that from a 72.6 ft (22.13 m) length of uniform 9-percent slope under otherwise identical conditions (Wischmeier and Smith 1978). L is the slope length factor while S is the slope steepness factor. The topographic factor is calculated via the following formula:

$$LS = \left(\frac{\lambda}{22.13}\right)^m \cdot (65.41 \cdot \sin^2 \theta + 4.56 \cdot \sin \theta + 0.065) \quad (2)$$

Where

λ is slope length (m) defined as the distance from the point of origin of overland flow to the point where either the slope gradient decreases enough that deposition begins, or the runoff water enters a well-defined channel that may be part of a drainage network or a constructed channel (Smith and Wischmeier 1957)

θ is angle of slope

m is 0.5 if the percent slope is 5 or more, 0.4 on slopes of 3.5 to 4.5 percent, 0.3 on slopes of 1 to 3 percent, and 0.2 on uniform gradients of less than 1 percent (Wischmeier and Smith 1978).

The first part of the equation refers to the slope length and the second to the slope steepness. The equations were derived separately from cropland plots under natural rainfall conditions on slopes ranging from 3 to 18° in steepness and from 30–300 ft. (0.91–91.44 m) in length.

The slope steepness has a higher influence on the soil erosion than the slope length. Regarding the effects of slope length on erosion at a plot scale, despite Wischmeier and Smith (1958) stating that the slope length has no significant influence in the soil loss, the effects of increasing slope length remain still ambiguous (Alewell et al. 2019). Different researchers

observed that an increase in slope length can produce both an increase (Zingg 1940; Rejman and Brodowski 2005) or decrease (Joel et al. 2002; van de Giesen et al. 2005) in the soil loss.

The development in remote sensing technology and in the accuracy improvement of the digital elevation models and of the geospatial data in general, has boosted also the research for derivation of new approaches for the assessment of the topographic factor. As RUSLE became a tool applied at landscape scale and not only at field scale, new approaches for the calculation of topographic factor were needed. At landscape scale the slope length is substituted by the upslope contributing area (Desmet and Govers 1996). The biggest challenge in this regard is to define and calculate the upslope contributing area of a point. Currently, four flow algorithms exist for the calculation of the upslope contributing area (Alewell et al. 2019):

- a. single-direction flow algorithm (D8)
- b. the multiple flow direction algorithm (MD8)
- c. infinite possible single-direction flow pathways (D^∞)
- d. triangular multiple flow direction algorithm (MD^∞).

But as stated in Alewell et al. (2019), the rapid advancement in the remote sensing technology and the general improvement in the geospatial data availability and accuracy have outpaced the development in flow algorithms. Therefore, effort is needed in adapting the existing algorithms to the availability of the input data.

3.4.2. Rainfall erosivity factor R

Wischmeier and Smith (1958) detected that the soil loss by all of its compartments (rainsplash, rill and sheet) had a direct relation to *Rainfall Erosion Index* (EI_{30}), which is the *kinetic energy* (E) of the rain combined with the *maximum 30-minute intensity* of the same event (I_{30}). Rain showers of less than one-half inch (12.7 mm) and separated from other rain periods by more than 6 hours were omitted from the erosion index computations, unless as much as 0.25 inch (6.35 mm) of rain fell in 15 min (Wischmeier and Smith 1978). For calculating the *unit rainfall kinetic energy* (E_r) in the first edition of USLE the logarithmic function of eq.3 was used.

$$E_r = 0.0119 + 0.0873 \cdot \log_{10} I \quad (3)$$

Where I is the rainfall intensity in mm h^{-1} .

One of the most important evolutions in RUSLE consisted in the use of the exponential relationship for estimating the unit rainfall energy proposed by Brown and Foster (1987).

$$E_r = 0.29 \cdot (1 - 0.72e^{-\frac{I}{20}}) \quad (4)$$

The calculation of the rainfall erosion index EI_{30} is based on the following equation.

$$EI_{30} = \left(\sum_{r=1}^n [E_r \cdot V_r] \right) \cdot I_{30} \quad (5)$$

Where V_r is the rainfall height in (mm) in the r^{th} time period. The final rain erosivity factor R is calculated by dividing the sum of the rainfall erosivity index EI_{30} for a certain period of time with the numbers of years.

Using a universal formula for calculating the unit rainfall energy of a storm can lead to implausible results. The characteristics of a storm are extremely dependent on the geographical location. Therefore, the usage of a certain equation for the calculation of E_r should be properly discussed. To improve the accuracy of the regional USLE/RUSLE models, many studies derived local rainfall energy relations, which take in consideration the characteristic of the rainfall (e.g. duration, raindrop size or maximum intensity) in that specific area (Zanchi and Torri 1980; Onaga et al. 1988; Cerro et al. 1998; Shamshad et al. 2008).

3.4.3. Cover and management factor C

C-Factor in the soil loss equation is the ratio of soil loss from land cropped under specified conditions to the corresponding loss from clean-tilled, continuous fallow land (eq. 6). This factor measures the combined effect of all the interrelated cover and management variables (Wischmeier and Smith 1978).

$$C = \frac{A_{crop}}{A_{fallow}} \quad (6)$$

The C-Factor takes values between 0 and 1 where $C=1$ corresponds to no cover protection from vegetation while $C=0.0001$ corresponds to strong cover due to vegetation. For the initial applications of USLE at plot scale, tables with values of C-Factor (in form of annual average C-Factor) were provide for different crop types and crop periods.

In the RUSLE the C-Factor was calculated from the adopted approach of Laflen et al. (1985) and Wertz et al. (1987) where the C-Factor was derived as a product of *Soil Loss Ratio* (SLR) and rainfall erosion index:

$$C = \sum_{i=1}^n \frac{(SLR_i \cdot EI_i)}{EI_t} \quad (7)$$

Where:

SLR_i is the soil loss ratio for the investigated rainfall event i

EI_i is the rainfall erosivity index for the rainfall event i

EI_t is the sum of rainfall erosivity index for the n rainfall events

n is the number of rainfall events for the modelling time unit

The SLR is the multiplication product of five sub-factors associated with the canopy cover, soil surface conditions and land use. Based on the geographical location and the climatic conditions, different approaches exist for the calculation of each of the subfactors (Renard et al. 1997). The SLR is calculated as follows:

$$SLR = PLU \cdot CC \cdot SC \cdot SR \cdot SM \quad (8)$$

Where:

PLU is the prior-land-use sub-factor

CC is the canopy cover sub-factor

SC is the soil cover sub-factor

SR is the soil roughness sub-factor

SM is the soil moisture sub-factor

Apart from the traditional approaches (ratio between vegetated area and fallow land or the empirical approaches used by RUSLE), either due to lack of data or due to advancement in the earth observation systems, different approaches have been developed for calculating the C-Factor (Zhang et al. 2011). In case of data gaps, several researchers have used the inversed USLE for calculating the C-Factor in case of existing erosion monitoring data (Zhang et al. 1992; Yu et al. 1998). On the other hand, the advancements in satellite imagery have contributed substantially in deriving new approaches for the C-Factor assessment. The improved algorithms for land cover classification have made the application of C-Factors from literature tables possible at catchment or even larger scales. Another newly developed satellite approach, is the derivation of empirical relationships for relating the C-Factor with vegetation indexes like the *Normalized Difference Vegetation Index* (NDVI) (Durigon et al. 2014; Almagro et al. 2019; Karydas et al. 2020). Several such empirical relationships have been developed for different regions worldwide and they show promising results (van der Knijff et al. 1999; Almagro et al. 2019). However, despite its advancements, the application of remote sensing approaches in this area are still not perfect and need to be optimized. The main restriction remain the lack of validation data for these empirically derived C-Factors.

3.4.4. Soil erodibility Factor K

According to Wischmeier and Smith (1978), the soil erodibility is the rate of soil loss per erosion index unit as measured in standard conditions, and it is determined experimentally. The standard condition is the unit plot, 22.6 m long with a 9% gradient, maintained in continuous fallow (tillage and vegetation free for 2 years), tilled up and down the hill slope (Ganasri and Ramesh

2016). Furthermore, the plot is plowed and placed in conventional corn seedbed condition and is prevented from crusting or vegetative growth. In such way the other factors (L,S,P and C) are equal to one and the K-Factor can be determined from the following formula:

$$K = \frac{A}{EI} \quad (9)$$

The soil erodibility values are highly related to the characteristics of the soil as its susceptibility to erosion depends on its physical, mineralogical or chemical properties. For soils containing less than 70% silt and very fine sand, Wischmeier and Smith (1978) derived the following formula for calculating the K-Factor:

$$K = 2.77 \cdot m^{1.14} \cdot 10^{-8} \cdot (12 - a) + 0.0043 \cdot (b - 2) + 0.0033 \cdot (c - 3) \quad (10)$$

Where:

$$m = \text{silt (\%)} + \text{very fine sand (\%)} \cdot (100 - \text{clay (\%)}) \quad (11)$$

a is organic matter (%)

b is structure code in which (1) is very fine granular, (2) is fine granular, (3) is med or coarse granular, and (4) is blocky, platy or massive

c is profile permeability in which (1) is rapid, (2) is moderate to rapid, (3) is moderate, (4) is moderate to slow, (5) is slow, and (6) is very slow

For facilitating the calculation of the K-Factor, a nomograph (Figure A—1 in Appendix) was initially created. The nomograph approach was later approximated in eq. 10. Based on this equation, the soil erodibility can be calculated by combining some mechanical parameters of the soil like texture, structure, permeability and organic matter. These parameters or the interconnection found by Wischmeier and Smith (1978) are not to be applied for every soil type. As for R-Factor, the characteristic of the soils can be specific to the geographical location or to its land cover. The graph presented by Renard (1997) (Figure 3—2) shows the K-Factor from measured values plotted against K-Factor values calculated using the nomograph. It can be observed that K values calculated for soils in the continental part of USA, and especially those provided by Wischmeier and Smith (1978) (black filled dots) are almost

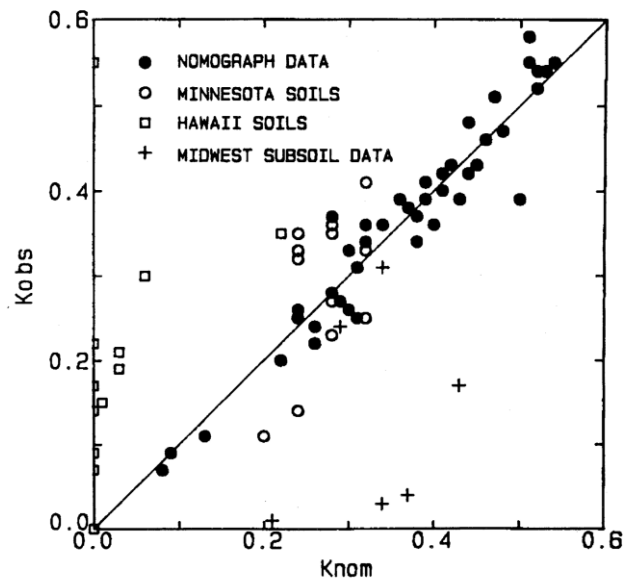


Figure 3—2 Comparison between modelled and observed K factor for different soils (Renard 1997).

equal to the actual measured values of K-Factor. However, soils in Hawaii have completely different soil erodibility compared to the K-Factor values when calculated with the nomograph method. As for the R-Factor also the soil erodibility should be optimally measured locally or calculated with locally derived approaches.

Extensive research has been done in this regard. In their publication Renard (1997) include six approaches for calculating the K-Factor while in a review study, Song et al. 2005, present 10 different approaches. Both studies include calculation approaches derived from various locations of the world and including different soil characteristics (exact granulometry, saturation of soil, bulk density or percentage of certain soil minerals).

3.4.5. Support practice factor P

By definition, factor P in the USLE is the ratio of soil loss with a specific support practice to the corresponding loss with up-and-down-slope culture. The most widely used support practices are contour tillage, strip-cropping on the contour, subsurface drainage and terracing (Wischmeier and Smith 1978). Unlike all the other factors, the P-Factor is a human induced factor and it can decrease the soil loss significantly when applied. P values can range from 0.2 for excellent support practices to 1.0 where erosion control measures are absent. Wischmeier and Smith (1978) provided tables with empirical values of P-Factor for different support practice activities, depending on the slopes of the plots and the spatial coverage of the support practices. However, researchers advice that before using such values, further expert judgment should be required, especially if evident rills or small gully structures are visible (Alewell et al. 2019).

Nowadays for larger than plot scales USLE/RUSLE applications, P-Factor values can be derived from image classifications in combination with expert knowledge (Karydas et al. 2009). Recently also modelling approaches are considered for assessing the P-Factor. Panagos et al. (2015b) modelled the P-Factor in a pan European scale. In their approach, they manage to estimate the P-factor values for arable lands in Europe based on the Common Agricultural Policy implementation by including also other support practices like stonewalls and grass margins.

3.5. Sediment yield

The sediment yield or sediment input is that part of the eroded material which reaches the water body. It is well known that only a small part of this material will be eventually transported into the catchment outlet. Most of the eroded material is temporarily or permanently deposited in the areas where the gradient decreases, at the base of the slope and in floodplains. The magnitude of the sediment yield is highly dependent on the geomorphological and environmental characteristics of the catchment like slope, catchment area, distance of the removed material from

channel or gully, land cover, and soil texture (Walling 1983). The ratio of the overall transported material to the catchment outlet to the gross erosion of the catchment is the *sediment delivery ratio*. At a grid cell but also at a basin's outlet, the SDR is calculated as following.

$$SDR = \frac{SI}{A} \quad (12)$$

Where:

SI is the measured sediment input ($mass \times area^{-1} \times time^{-1}$)

A is the measured eroded material ($mass \times area^{-1} \times time^{-1}$)

Combined with the USLE/RUSLE technique, the SDR is helpful in defining not only the overall sediment yield from the catchment but also its spatial distribution. A large number of studies have been conducted for deriving empirical based approaches for the calculation of the SDR. In a review study Wu et al. (2018) listed 39 different approaches for the quantification of the SDR. The SDR has values ranging from 0 to 1. Most simple approaches use only the area of the hydrological basin in combination with certain empirical factors (eq. 13). However, recent studies have shown that when quantifying the SDR, the geomorphological characteristics (topography, soil texture and land use) and the hydrological regime of the catchment should be considered (Verstraeten and Poesen 2001; Lu et al. 2005; Vente et al. 2007).

$$SDR = \alpha \cdot S^\beta \quad (13)$$

Where:

α is an empirical constant

S is the surface area of the drainage basin

β is an empirical coefficient that contains information about basins characteristics and sediment transport processes (Vente et al. 2007)

Walling (1983) in a review of the until then SDR quantification approaches, based on the area of a hydrological basin, found a great variety of methodologies depending on the geographical location (Figure 3—3). Walling (1983) argues that all these methodologies are a black box, as they do not include in any form any of the characteristics of the catchment or the sediment formation and transport processes. He also states that the problem of not having a generally applicable predictive technique can be related to the spatial and temporal lumping problems of erosion. The values of SDR are not only dependent on the spatial variations of the erosion but also on the temporal scale as a measured SDR is representative only for the time period from which it is derived (Lu et al. 2005). On the scale of a single storm Piest et al. (1975) demonstrated the importance of antecedent soil moisture conditions for the SDR (with SDR values ranging from

1% to 554%). On the longer timescale, deposition and remobilization of the sediment within a basin can be the dominant processes for determining the SDR (Walling 1983). Trimble (1975) demonstrated the importance of these phenomena by showing that even when conservation practices were implemented for reducing the sediment yield from slope erosion, the sediment yield, thus the SDR did not change on short term because the previously deposited material in slope bases and floodplains was remobilized and transported to the outlet of the catchment. To reestablish the normal erosion-sediment yield balance on the temporal scale, all the previously deposited material should be transported in the river and the freshly eroded material should be transported to the water body without discontinuity.

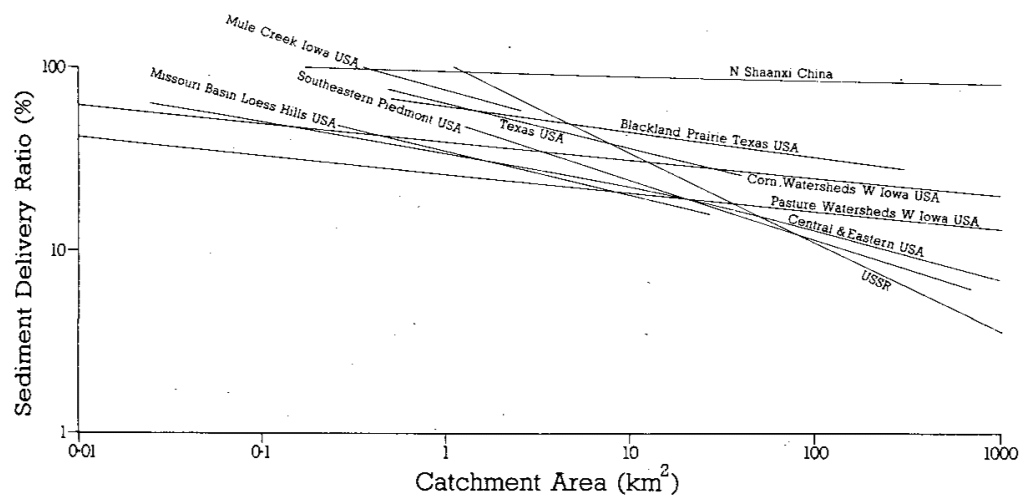


Figure 3—3 Empirical relations based on the catchment area derived from different locations for quantifying the SDR (Walling 1983).

The sediment yield is highly dependent on the terrain and land use of a hydrological catchment. An effective connection of hillslopes with the channel network results in highly efficient sediment transfer processes (Cavalli et al. 2013). Recently, approaches using the catchment connectivity are being applied. Connectivity is defined as the transfer of energy and matter between two landscape compartments or within a system as a whole (Chorley and Kennedy 1971), while hydrological connectivity is a term often used to describe the linkages between runoff and sediment generation in upper parts of catchments and the receiving waters (Croke et al. 2005). The integration of the connectivity approaches in the GIS environment has led to satisfying results in SDR modelling. The main advantage of this method is the non-restricted geographical applicability, as several studies suggest that the usage of the connectivity index as an input parameter for SDR produce satisfying results globally (Cavalli et al. 2013; Hamel et al. 2015; Rosa et al. 2016; Grauso et al. 2018a).

3.6. Summary and research gaps

In this chapter, the most important aspects of erosion and sediment input from a watershed were discussed and several techniques for the assessment of the sediment yield were discussed. Accurate quantification of the sediment input at a catchment scale is a difficult task that can be performed with several approaches, which require high costs and time. The spatial and temporal components of the sediment formation processes make it impossible to implement holistic monitoring programs at a catchment scale. Monitoring is focused mostly on representative points of the catchment and for a certain period of time. Hence, it is not rare that this monitoring techniques cannot capture the dynamics of the system, as major sediment input events, that can account for the largest part of the sediment input in decades maybe, are rare and often not included in the databases. Concerning the spatial distribution of the sediment input, it highly depends on the morphologic, climatic and anthropogenic conditions of the area (slope, LULC, precipitation, soil properties and conservation practices). As a result, it is highly variable throughout a catchment.

The most widely used technique in regard to erosion and sediment input quantification is modelling, and among others the RUSLE based models. Models are able to deliver both the overall sediment input from the catchment and its spatial distribution. The major drawbacks of RUSLE models are the lack of calibration and validation of the outcomes. As these approaches deliver mostly long term mean values of soil loss and afterwards sediment input (by multiplication with SDR), the monitoring of the river stretch for such long periods is often impossible. Therefore, alternative methods need to be explored. Large river impoundments represent the perfect opportunity, as they collect almost the entire material incoming from a hydrological catchment. However, important research gaps exist in this area. Initially, the accuracy of sediment volume measurements is not sufficient for performing validation and calibration of the model, and secondly the processes from sediment formation at a plot scale until deposition in the reservoir (channel deposition, gully and channel erosion, trap efficiency) are relevant for the comparison between the two values. If all the previously mentioned issues are properly addressed, the usage of reservoirs as validation points can contribute in having more accurate sediment input models, and consequently a sustainable management of the hydrological catchment and protection of water resources.

4. Reservoir siltation

River impoundments are important structures for the development of certain areas as they enable the storage and reuse of large volumes of water. As such, the proper maintenance of these systems becomes a necessity. Independently from their function, reservoirs suffer from the same problems but at a different extent. When their lifetime is not threatened from certain catastrophic events (Kilburn and Petley 2003; Duffaut 2013), siltation rate is the factor that defines the lifetime of a reservoir.

Sediment trapping in reservoirs, causes a chain of negative reactions in the downstream areas (Maavara et al. 2020). Initially the ecosystems continuity is disrupted by forbidding the upstream or downstream migration of all the living organisms in the river. Apart from the living organisms, the sediment is also prevented from moving downstream of the dam. Due to the lack of sediment supply, the downstream areas are expected to have severe channel bank erosion and costal erosion (Gaillot and Piegay 1999; Draut et al. 2011; Ma et al. 2012; Kondolf et al. 2014). Dams have significant effects also in the nutrient's cycle of the system. *Carbon (C)*, *Nitrogen (N)* and *Phosphorus (P)* are trapped in the reservoir causing the nutrient starvation of the downstream areas. Trapping of P in stagnant water bodies like reservoirs, which are in the worst case stratified for a long period of the year, can boost significantly the eutrophication process. Trapping carbon in anoxic environment on the other hand, can trigger intense methanogenesis in the sediment and methane ebullition from the reservoirs (Maavara et al. 2020).

The problems associated with sedimentation are not only of an ecological prospective but also technical and economical (Palmieri et al. 2001; Schleiss et al. 2016). Sediments have several negative effects on the operation of the reservoir and its structures. Most common problems related to sedimentation include the loss of storage volume. Storage volume loss directly affects the water withdrawal from a reservoir, as less water is available. When sediment is deposited in the active storage area of a reservoir, studies show that the water use efficiency of the reservoir declines (Okumura and Sumi 2012). In case of hydropower the water-use efficiency is defined as the ratio between overall turbinated amount of water and the overall inflow volume.

For hydropower, the abrasion of hydraulic machinery is another problem of sediment-laden water. Abrasion occurs when the water passing through the turbines contains mineral particles, which are harder than the material from which the turbines were manufactured. No coarse grained material is needed for causing abrasion. As showed in the Nathpa Jhakri hydropower plant in

India, it is enough that the silt clay fraction contains a high share of minerals like quartz, feldspar or tourmaline for causing significant problems (Annandale et al. 2016). When the coarse material in the reservoir reaches the impoundment or the intake structure, apart from severe abrasion of the turbines, clogging of outlets can occur (Auel et al. 2010).

4.1. Sedimentation patterns in reservoirs

According to Morris and Fan (2010), when no sediment remediation measures are implemented and no dam decommissioning is taken in consideration, from dam commissioning until reaching a stable sediment balance the reservoir passes in three stages (Figure 4—1):

1. **Continuous sediment trapping.** When the impoundment is installed, there is a holistic change in the hydrodynamic conditions of the system. From a free flowing river characterized by high velocities, the system has changed to a stagnant waterbody with minimal velocities. The lack of turbulence and high velocities enables the coarse material, which in normal conditions would travel through the impoundment structure, to remain in the riverine zone of the reservoir. The fine material on the other hand, apart from being partly directly deposited together with the coarse material, will be transported by either stratified or non-stratified flow to the deeper part of the reservoir in form of suspended matter.
2. **Growing floodplain.** When the reservoir storage capacity is depleted, the actual sediment deposition is as well diminished. In this phase, the reservoir has a mixed regime of deposition and scour. A sediment floodplain will be created and the reservoir itself will act mostly as a river stretch as soon as the sediment will reach the spillway. A main channel will be created while both sides of embankments of the new channel will consist of fine sediment. The creation of a channel is often a characteristic of large reservoirs as in narrow reservoirs the overland flow can cover the entire surface.
3. **Full sediment balance.** The final stage is when the sediment entering the system upstream is the same with the sediment leaving the system. It is not enough that only the amount of material is in balance but also the grain size distribution. For this to happen, the coarse material should be transported near the dam and in case of large flooding events to be transported to the downstream reach.

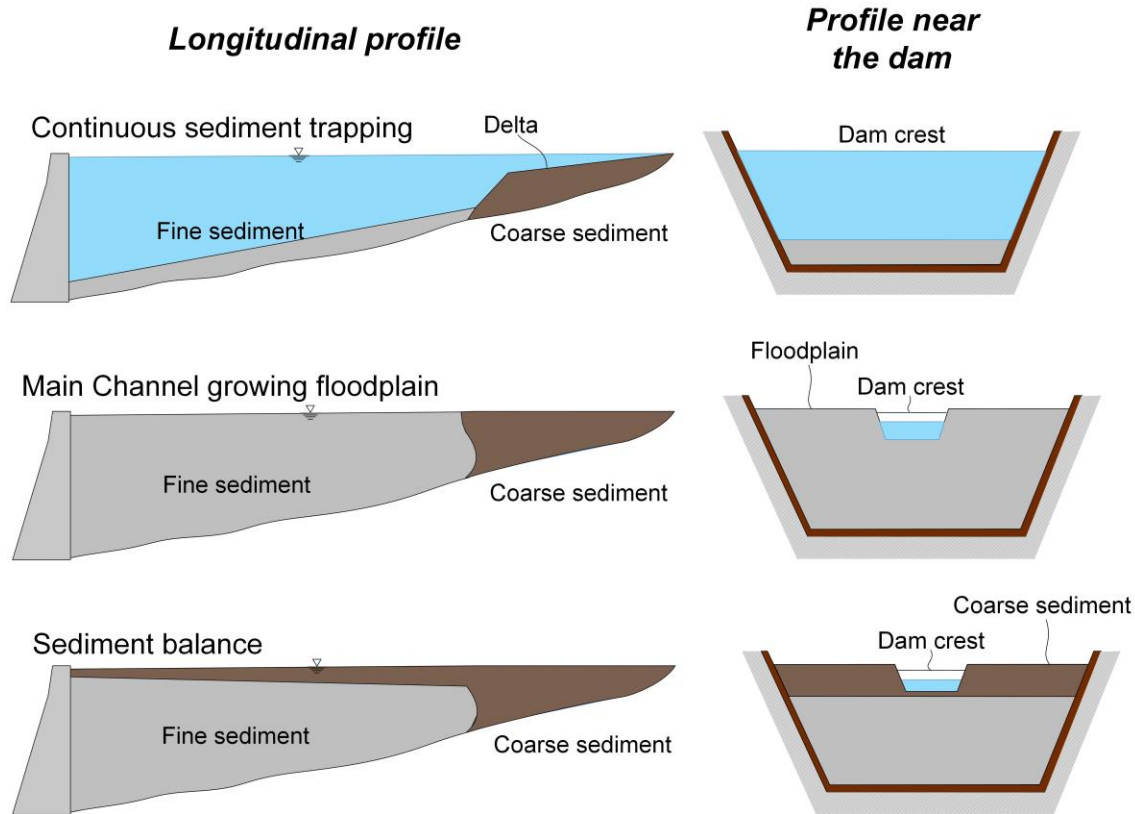


Figure 4—1 Sedimentation stages of a reservoir (adapted from Morris and Fan (2010)).

When planning the long term operation of a reservoir and the sediment remediation strategies, important is not only to know the sediment stock but also the spatial deposition patterns of the investigated water body. The deposition patterns of the reservoir can deliver important information about the operation restrictions that can occur and afterwards facilitate the process of choosing the most effective remediation measure. Based on the shape of the reservoir and the geomorphological and climatic characteristics of its hydrologic basin, the longitudinal deposition patterns of a reservoir can vary widely. In general, most of the reservoirs follow one or many of the four basic deposition patterns illustrated in Figure 4—2.

1. **Delta** deposits occur mostly in reservoirs where sediment is dominated by coarse material. The existence of a delta does not mean necessarily that no fine-grained material can be also deposited. In reality, the deltas are a mixture of fine and coarse-grained material.
2. **Wedge** type deposits occur mainly in reservoirs with low residence time. This includes small reservoirs or impoundments, which are fed by high discharge rivers. Reservoirs that are operated in low water level during flood events show also the same deposition pattern.
3. **Uniform** type deposits are observed mostly in narrow reservoirs with high water level fluctuations and low sediment input.

4. **Tapering** deposits are common in large reservoirs with constant pool elevation. The distance to the dam is rather large therefore, the sediment loads transported via stratified or unstratified flow are not able to reach until the dam and settle in the middle of the reservoir.

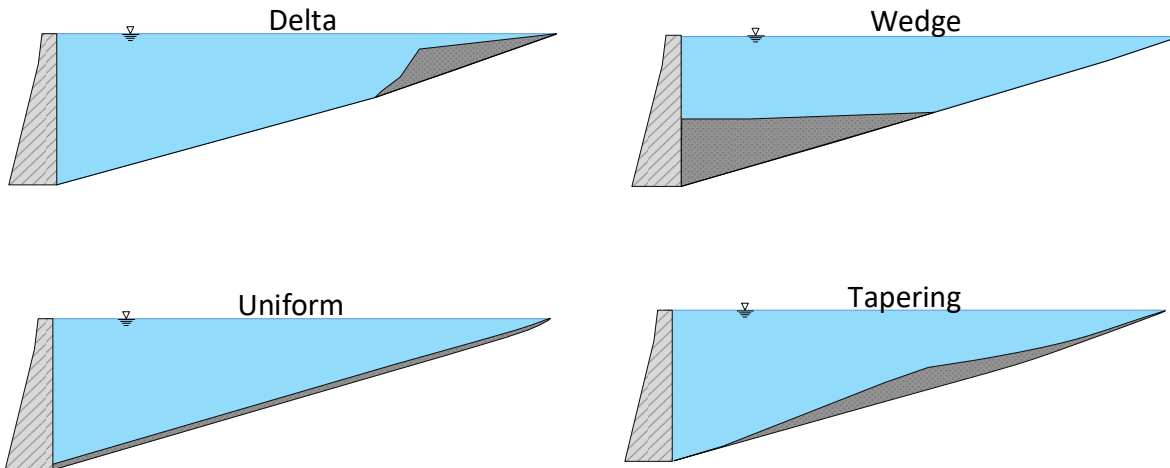


Figure 4—2 Generalized longitudinal deposition patterns of sediment (adapted from Morris and Fan (2010)).

4.2. Methods for measuring the sediment volume in reservoirs

Measuring the sediment volume in a reservoir is not trivial. The oldest approach for doing so is by measuring changes in water depth at the same location and deriving the sediment thickness. The measurements were executed in various locations in a reservoir, afterwards interpolated and finally the volume of the deposited sediment was calculated. In the 19th and 20th century, before the technological advancement in remote sensing, the measurements were executed manually from the side of a boat with a sounding line and lead weight. This method was not as efficient, as an insufficient number of points could be measured during a survey and also the inaccuracy in positioning and in the vertical direction was large. With the developments in the echo-sounding technology, the task of topographic differencing became significantly easier as the equipment was able to record multiple points in a second and the positioning accuracy was better. The developments in defining the sediment volume continued and several other techniques were developed for investigating also the sub-bottom environment of a lake. As shown in Table 4—1, these developments included the further transformation of the hydroacoustic systems for more accurate topographic differencing (multibeam systems) but also for sub-bottom mapping, like in the case of parametric echo-sounders. Apart from acoustic systems, other conventional systems were developed for sampling the sediment up to a certain depth. The latest developments are recorded in the area of penetrometers where information about sediment thickness and sediment

properties can be recorded simultaneously. In the following sections, all the methods presented in Table 4—1 are described in more details.

Table 4—1 Advantages and disadvantages of the most widely used techniques for sediment detection in reservoirs

	Advantages	Disadvantages
Subsequent bathymetric surveys	<ul style="list-style-type: none"> • Accurate sedimentation rate if the sedimentation is higher than the margin of error of the used device • Additionally delivers accurately the actual available water storage 	<ul style="list-style-type: none"> • Not suitable for low sedimentation rates • Often expensive and complex systems
Sub-bottom profiling	<ul style="list-style-type: none"> • Can achieve penetration depths up to hundreds of meters • Can detect layers in the sediment 	<ul style="list-style-type: none"> • Sensitive to gas presence in the sediment • Expensive and complex systems
Sediment coring	<ul style="list-style-type: none"> • Accurate sediment thickness • Cost effective equipment • Can define also the sediment properties 	<ul style="list-style-type: none"> • Time consuming • Limited penetration depth (normally up to 2 m in deep reservoirs)
Penetrometer	<ul style="list-style-type: none"> • Easy to operate • Time efficient compared to coring 	<ul style="list-style-type: none"> • Limited penetration depth depending on sediment type • Proxy values which need groundtruthing validation

4.2.1. Hydroacoustic applications for sediment detection and characterization

Hydroacoustics is an indispensable tool for mapping the underwater environment. It is the most effective way to probe the lakebed or seabed, as no other energy can propagate in that range. Electromagnetic waves are of limited use, as the water is a highly conductive medium, while traditional single point groundtruthing techniques are subject to constraints regarding the time and costs required for sampling and analysis processes (Lurton X. 2002; Caiti A. et al. 2006).

Initially, acoustics was mainly used in seawater applications. With the increasing number of human-made water bodies, it is increasingly applied also in shallow waters (lakes and reservoirs).

Principles of hydroacoustics

Echo-sounders, which work on the principle of underwater acoustic wave propagation, are active systems used widely in several applications. Apart from sedimentation, they are also included in applications such as military, fishing or navigation. The echo-sounder consists normally of an electric pulse generating unit (transceiver) and another unit which transforms the emitted electric pulses in acoustic waves and vice versa (transducer). The whole system is connected to a power source, to a positioning system and is controlled via a computer unit (Figure 4—3). The echo-sounders send an acoustic pulse and are able to receive the reflection of the sound from a certain target (fish, vessel or ground). From this response, the travel time of the wave can be measured and therefore by multiplying with the sound velocity, the distance can be calculated.

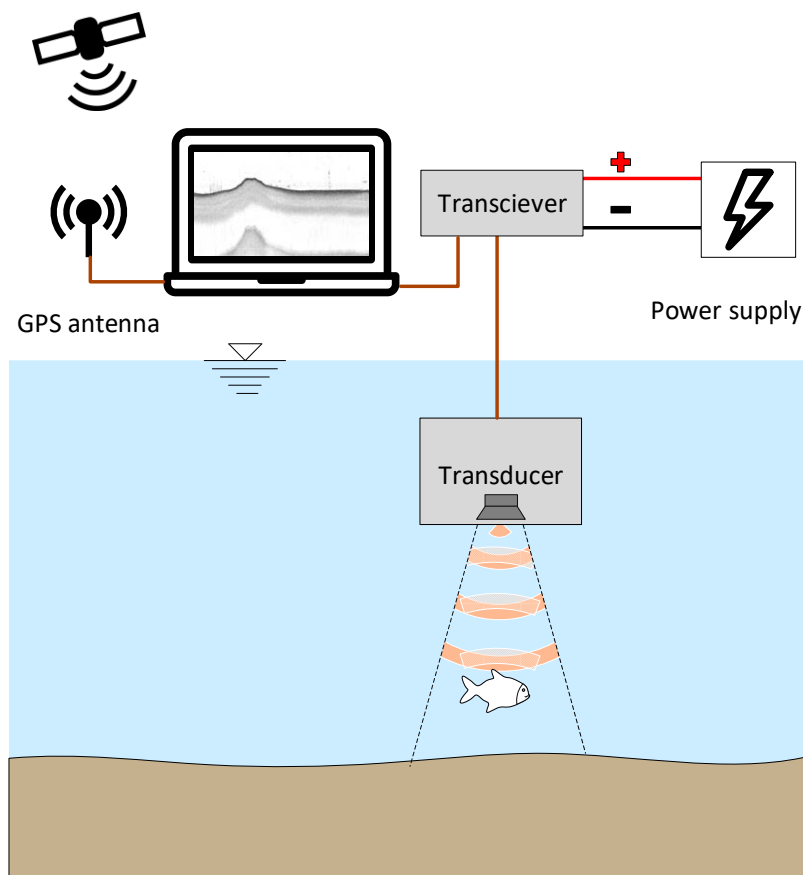


Figure 4—3 Schematic view of an echo-sounder.

The transformation of an electrical pulse in an acoustic pulse in most transducers is based on the piezoelectricity principle. When electricity field is applied to certain types of natural or

synthetic crystals (ceramic), a deformation of these materials is observed. These deformations are highly dependent on the electrical excitation and cause acoustic wave. The above-mentioned process is reversible and can be used for turning the acoustic waves in electric signal. In a single frequency transducer, these pizoceramic elements are grouped into one array, and are covered with a sonic permeable structure for protection from any impact.

During propagation, acoustic waves lose their intensity due to *geometric spreading* and *absorption*. The sum of geometric spreading and absorption is also called *transmission loss*.

The geometrical spreading can be either spherical or cylindrical. The geometrical spreading in this section refers only to the spherical expansion of the sound wave. During the geometric spreading the same acoustic energy has a higher intensity near the sound source and a lower intensity near the target (Figure 4—4 $I_{1m} > I_r$). To express the transmission losses due to geometrical spreading (TL_{GS}) in a decibel scale, the power at 1 m distance from the acoustic source is used as reference (Figure 4—4).

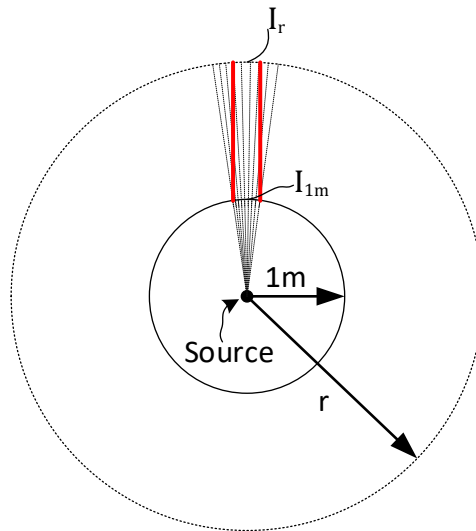


Figure 4—4 Illustration of geometrical spreading during sound propagation.

$$P_{1m} = P_r \quad (14)$$

$$4 \pi 1^2 I_{1m} = 4 \cdot \pi \cdot r^2 \cdot I_r \quad (15)$$

$$\frac{I_r}{I_{1m}} = \frac{1^2}{r^2} \quad (16)$$

$$TL_{GS} = 10 \log \frac{I_{1m}}{I_r} = 10 \log \frac{r^2}{1^2} = 10 \log(r^2) \quad (17)$$

$$TL_{GS} = 20 \log(r) \quad (18)$$

Where P is the power respectively at 1 m distance from the source and at r distance from the source and I (W m^{-2}) is the intensity of the sound.

A part of the transmission losses are attributed also to the absorption of energy from the propagation medium. During the wave attenuation, a part of the energy is lost due to the frictional dissipation and is transformed into heat. Each propagating medium has an attenuation coefficient α (db m^{-1}) which expresses the absorption properties of the environment and is directly related to the viscosity of the material. The transmission losses due to absorption (TL_{ABS}) at r distance from the source are calculated with the following formula:

$$TL_{ABS} = \alpha \cdot r \quad (19)$$

For receiving the emitted echo, the transmission losses of a wave are included twice in the travel time of the pulse, thus once for the emitted pulse and once for the reflected pulse from the target. As shown in the below scheme (Figure 4—5) the *echo level* (EL) in decibel of a received signal can be calculated with the following formula:

$$EL = SL - 2TL + TS \quad (20)$$

Where SL is the source level in db, TL are the geometrical spreading and absorption losses and TS is the target strength. The target strength (TS) is determined as the intensity of the reflected sound one meter from the target, related to the intensity of the sound hitting the target. This is the general sonar equation and can be applied independently from the target type as the sound propagation and reflection follows the same principles whether it hits a stone, a school fish, a submarine, or bulky sediment.

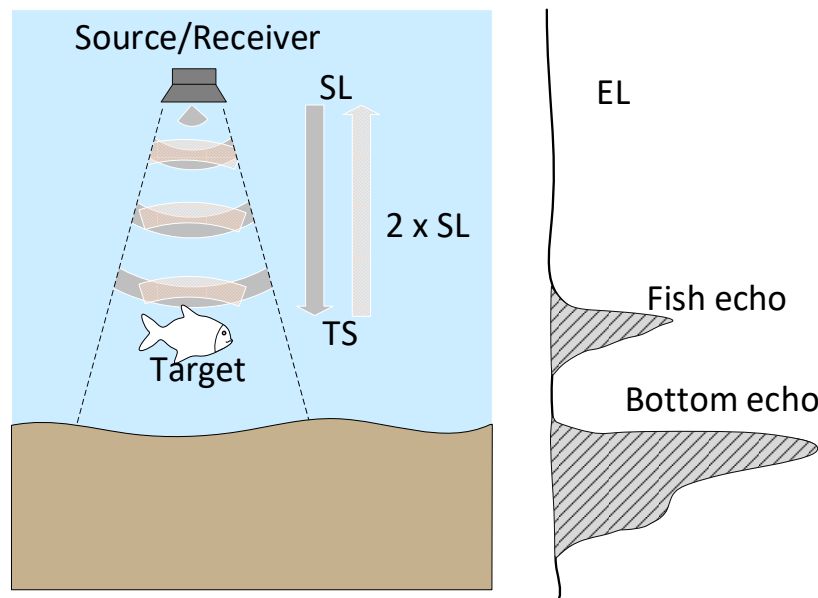


Figure 4—5 Schematic view of echo signal derivation.

Subsequent bathymetric surveys for sediment detection (topographic differencing)

The echo-sounding technology has a vast usage in detection and volumetric measurements of sediment. The most widely used applications concern the subsequent measurements of a reservoir bottom for defining the storage loss and therefore the siltation rate (Cross and Moore 2014; Yan et al. 2018). For performing an accurate bathymetry, normally frequencies in the range of 200 kHz are chosen (Jakubauskas and deNoyelles 2008; Morris and Fan 2010). Usually single beam echo-sounders are used for performing this task (Figure 4—6a). The single beam systems are easier to operate and cheaper to acquire compared to other systems (multi-beam) (Odhiambo and Boss 2004; Furnans and Austin 2008). The data processing requires less time, and the sensors are not as sensitive and complex as the multibeam systems.

The introduction of multibeam technology has increased the accuracy of bottom detection up to a cm level (Ernstsen et al. 2006). While for single beam echo-sounders it is possible to have only one integrated value for an area (Figure 4—6a), the advantages of the multibeam systems consist in the possibility of recording multiple depth points by emitting multiple sound beams at the same time (Figure 4—6b.). In comparison to single beam systems, the multibeam systems are more complicated in both operation and data processing. The multibeam systems integrate also a sensor for pitch, heave and roll correction while for single beams that is usually not the case. As the single beam relies in interpolation methods for having the overall depth distribution in the reservoir, the errors associated to this process can be large. For multibeam systems, the inaccuracies from interpolation are low due to the high density of the measured points.

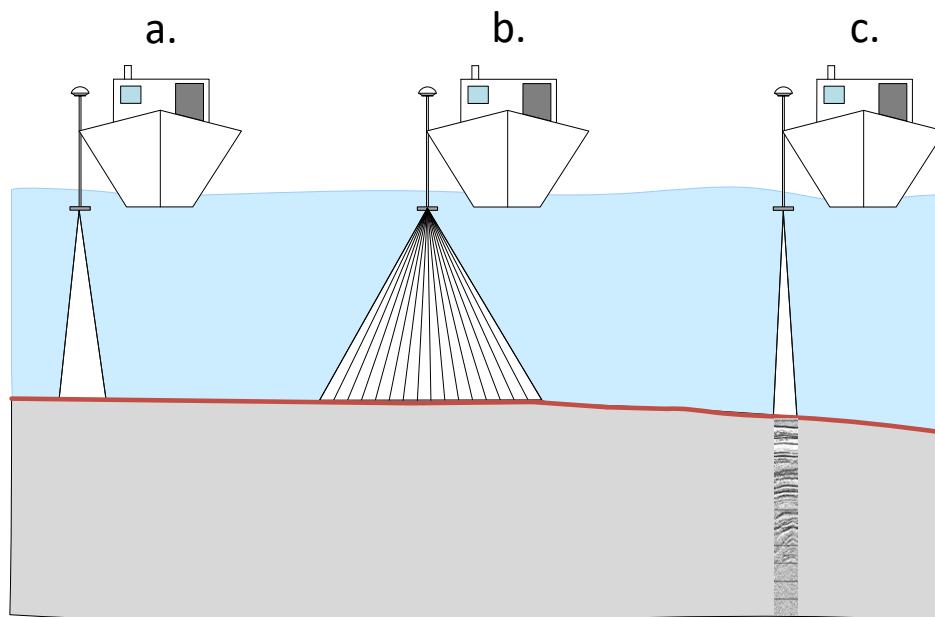


Figure 4—6 a. Linear single-beam system. b. Multibeam system. c. Parametric sub-bottom profiler.

When it comes to detecting the sediment thickness via subsequent bathymetries, both systems work on the same principle (Figure 4—7). The sediment thickness is calculated via the following relation:

$$d_{sediment} = d_{pre-impoundment} - d_{actual} \quad (21)$$

$$d_{actual} = d_{measured} + d_{transducer} \quad (22)$$

Where $d_{sediment}$ is the sediment thickness at the investigated location, $d_{pre-impoundment}$ is the depth at the investigated location before flooding the area, d_{actual} is the actual water depth while $d_{measured}$ and $d_{transducer}$ are respectively the depth measured from the hydroacoustic system and the submersion depth of the transducer. Performing a bathymetric survey for finding the sediment thickness includes also advantageous byproducts for the reservoir management. The bathymetry gives the opportunity to measure the actual storage volume of the reservoir and to plan the short term and midterm management of the water resource accordingly.

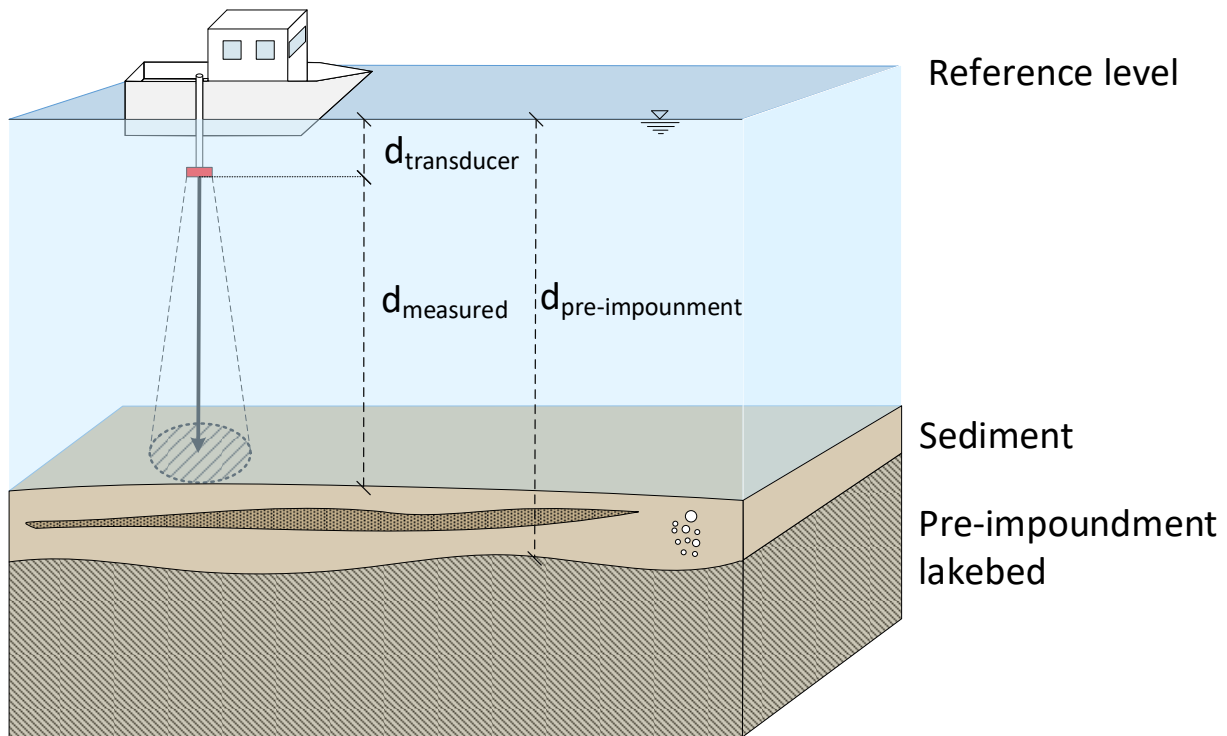


Figure 4—7 Definition of sediment thickness from topographic differencing via subsequent bathymetries.

Multi frequency echo-sounders for sediment detection

Multi frequency echo-sounders are systems that can emit simultaneous or alternating waves of different frequencies. They often emit one high frequency, which is very sensitive to the density changes in the sediment water interface (in the range of 200 kHz) and one wave with low frequency (<38 kHz) that can penetrate the sediment to a certain extent (Jakubauskas and

deNoyelles 2008). These systems are widely used for sediment detection in lakes and reservoirs (Dunbar et al. 1999; Odhiambo and Boss 2004; Jakubauskas and deNoyelles 2008; Clark et al. 2015; Iradukunda et al. 2020). The high frequency is used for finding the actual water sediment interface, while the low frequency is used to detect the pre-impoundment bottom as showed in Figure 4—8. The actual sediment thickness is calculated by subtracting the former from the later. However, such methodologies are confined to non-gassy sediments as gas represents an important barrier for sound penetration. When gas voids are present, a so-called acoustic turbidity layer can be detected in the echogram. The acoustic turbidity layer creates a strong bias in the sediment magnitude calculations and without groundtruthing it can generate misleading results.

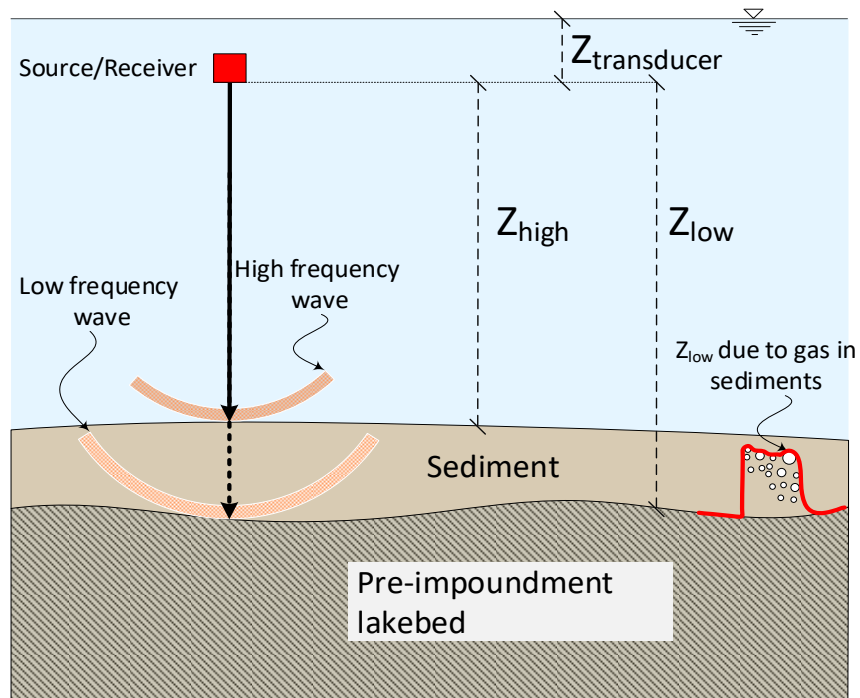


Figure 4—8 Definition of sediment thickness via the dual frequency approach.

Hydroacoustic sediment classification

Lakebed classification is an important decision support tool that improves reservoir lifetime assessment as well as management and personnel cost efficiency of operators. It provides solutions for engineering applications by differentiating between fine and coarse material in dredging activities or for environmental use by defining the greenhouse gas patterns and quantifying ebullition from water bodies (Ostrovsky et al. 2008). There is extensive literature dating back to the 1980s about seabed classification with linear hydroacoustic systems. Until recently, major developments were made in this area (Orlowski 1984; Chivers 1990; Anderson and Pacheco 2011). Today, most systems used for seabed mapping include multi-frequency transducers with a high and a low acoustic frequency as explained above, though both linear

single-beam (Orlowski 1984; Chivers 1990; Heald and Pace 1996; Siwabessy et al. 1999; Anderson et al. 2008; Brouwer 2008) and multibeam systems (Clarke, J. Hughes, E et al. 1997; Preston et al. 2004) are commonly applied in sediment classification.

For lakebed classification, two techniques can be used based on the physical phenomena: one that relies on the coherent reflection of the sound wave at the water sediment interface, and the other, which is based on the backscattering effect inside the sediment (Le Gac et al. 2006). *Coherent* reflection or specular reflection is the part of the sound wave which is reflected symmetrically (in the specular direction) with the incident wave. It depends on the impedance contrast between water and sediment and also from the grazing angle at the interface. A part of the incident wave is refracted and penetrates the sediment. Due to the irregularities in the sediment matrix, the wave is reflected in all angular directions. This phenomena is called *backscatter* (Le Gac et al. 2006) (Figure 4—9).

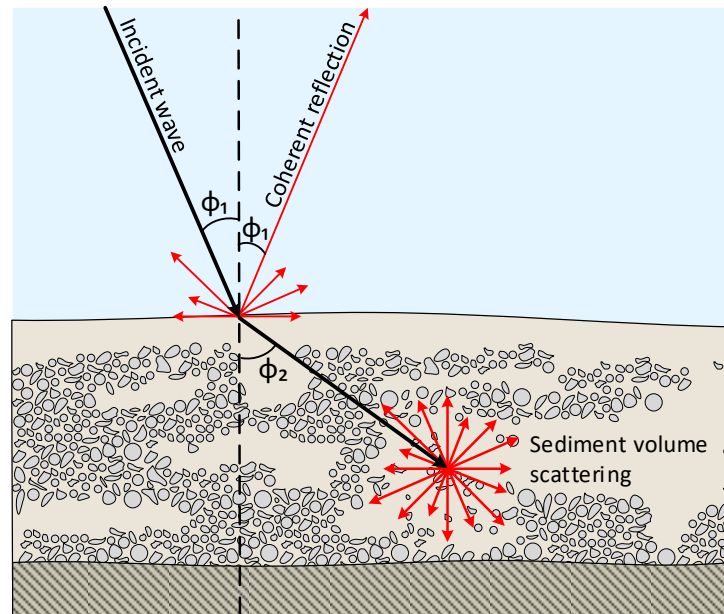


Figure 4—9 Sound reflection from the sediment.

For single beam echo-sounders, the vast majority of the classification approaches are based on the determination of both coherent and backscatter strength of the soundwave. One of the most widely used approaches is the *First echo division method* where acoustic parameters are calculated for both the coherent and backscatter part of the reflection (Orlowski 1984). Other approaches do not investigate only the backscatter and coherent part of the reflection but various statistical or energetic parameters of the echo envelope. Tęgowski et al. managed to calculate a total number of 83 parameters including here spectral, fractal, wavelet statistical and energetic parameters from the reflection curve of the sediment (Tęgowski and Łubniewski 2000, 2002; Tęgowski 2005).

During the last period, an increase has been observed in the usage of multibeam echo-sounders for habitat mapping and bottom classification especially in the marine environment (Wilson et al. 2007; Diesing et al. 2014; Janowski et al. 2018). The multi-beam echo-sounders, due to their high operating frequencies, have limited penetration depth in the sediment. Therefore, researchers rely mostly on the backscatter reflection of the sound from the surface layer of the sediment for performing sea-bottom classification (Lamarche and Lurton 2018). Due to the inability of these systems to deliver information about the deep sediment layers, their usage for inland water applications is still restricted.

Sub-bottom profilers for sediment detection

Sub-bottom profilers are echo-sounders designed to explore the first layers of sediment below the seafloor over a thickness that often reaches tens of meters (Lurton X. 2002). Most of the new systems use principles of non-linear acoustics for generating the sound waves.

When a wave is transmitted at high pressure, during its propagation it is distorted. The pulse maxima travels slightly faster while the pulse minima slightly slower (Figure 4—10). Parametric echo sounders work on this principle. They transmit two signals of slightly different high frequencies at high sound pressure (primary frequencies, e.g. 100 and 110 kHz). Due to nonlinearities in sound propagation at high pressures, both signals interact and new frequencies arise. One of the frequencies arising is the sum of two frequencies (e.g. 210) and the other is the difference of the transmitted frequencies (e.g. 10 kHz). These are called secondary frequencies and the later one is of great importance. This generated secondary frequency is low and, hence, can deeply penetrate into the lakebed (Urlick 1982; Wunderlich and Müller 2003; Wunderlich et al. 2005; Saleh and Rabah 2016). The most significant advantage of this new frequency is that it 'inherits' the directivity of the high frequencies from which it is generated, thus a narrow sound beam and short pulse length. A narrow beam and a short pulse length means better horizontal and vertical resolution and consequently, better data quality.

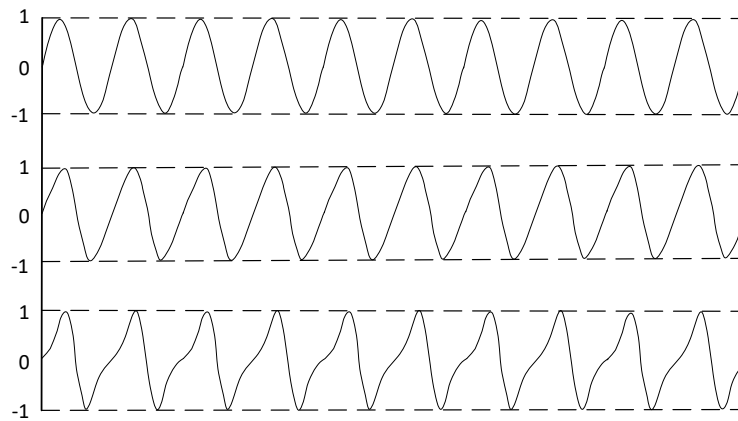


Figure 4—10 Acoustic wave propagation of parametric systems (adapted from Lurton X. (2002)).

The parametric echo-sounders operate on frequencies 1-15 kHz. Their operation is different from the linear systems. Linear systems focus on catching the backscattered part of the reflection while the sub-bottom profilers on the coherent part of the reflection. The echograms of the sub-bottom profilers present the acoustic impedance discontinuities so the reflection comes from the interfaces between the layers. That makes it possible for the sediment layers to be clearly distinguished (Figure 4—6c.).

In linear acoustics, the transducers can generate the sound pulse with the desired frequency directly. For generating low frequency waves with small opening beam angles, large transducers are required (due to the directivity pattern). With the use of non-linear acoustics this low frequency and small opening angle waves, can be achieved with transducers of small size. Another advantage of the parametric systems are the high vertical resolution (Figure 4—11). They can achieve resolutions at centimeter scale while achieving also penetrations up to some tens of meters (Innomar Technologies GmbH). By having such specifications, the parametric echo-sounders are helpful in detecting the sediment layers and computing the sediment stock in reservoirs (Yutsis et al. 2014).

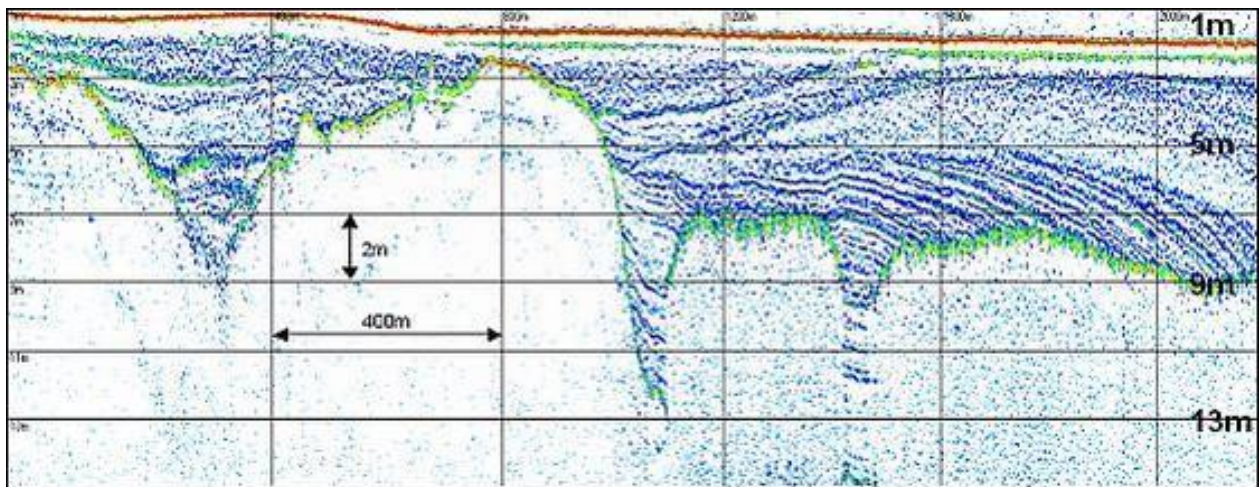


Figure 4—11 Example echogram from SES2000 compact (Photo from Innomar Technologies GmbH).

4.2.2. Sediment coring

Apart from sediment thickness, sediment coring shows also the sediment material deposited in the lake bottom. The first meters of the sediment can be sampled with relative simplicity. Two of the most widely used coring techniques for freshwater sediment, are *gravity coring* (Figure 4—12a) and *vibrocoring* (Figure 4—12b.). Both of these techniques are applicable from small vessels and do not need special transporting or operating platforms. The limitations of both methods consist in the limited sampling length and the high time effort needed for sampling and analyzing when compared to hydroacoustics.

The gravity corer is released from the vessel and penetrates the sediment through its momentum, developed from falling. Afterwards it is pulled in the vessel where the core is removed from the liner and analyzed for the parameters of interest. It needs no external power supply and it is the easiest way for taking core samples. When long cores are sampled, the weight of the corer is rather large and it can be physically demanding when the winch is operated manually. For soft sediment, the gravity corer can penetrate the sediment in the range of 1.5 m, but the penetrating depth varies based on the sediment compactness, density or grainsize distribution. Most of the gravity corers include additional weights as hammers for increasing the penetration depth.

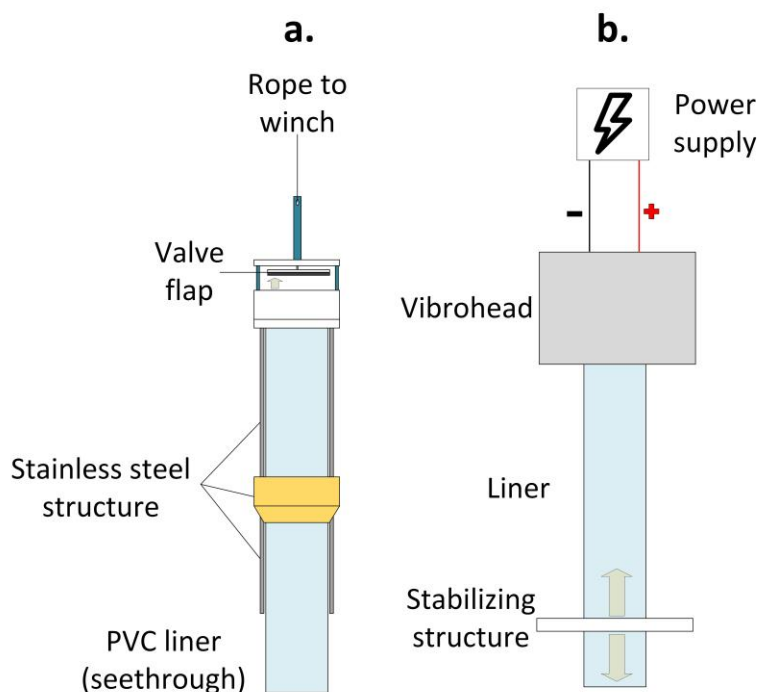


Figure 4—12 a. schematic view of a Uwitec gravity corer. b. Schematic view of a piston corer.

The vibrocorer on the other hand, apart from gravity, uses external power for increasing the penetration depth. In the upper part of the structure, there is a vibrating mechanism, which is called vibrohead. Through induced vibrations, the vibrohead facilitates the penetration of the corer in the sediment. When it touches the sediment, the movable stabilizing structure creates a basement area for the corer and makes the core sampling process easier. In unconsolidated silt/clay layers, the device can extrude samples up to 3 m of length (Annandale et al. 2016). In comparison to the gravity corer the vibrocorer can achieve deeper penetration but due to vibrations it can alter the sediment physical properties (void ratio or density).

Longer sediment cores require high effort and costs. They need large vessels or large working platforms, adapted coring devices, long sampling time and extensive experience (Uwitec 2014).

4.2.3. Dynamic freefall penetrometer

Penetrometers are widely used for determining the geotechnical parameters of soils. Their first applications in underwater environment dates back in the 1970s (Dayal and Allen 1973; Lunne 2012). For both soil and sediment applications penetrometers are divided in two major groups: *Quasi static or static penetrometers* and *dynamic or impact penetrometers*

In quasi-static penetrometer applications, a cone-tipped rod is mounted in large and heavy reaction frames from where it is pushed mechanically into the ground at a rate of 0.02 m s^{-1} up to 100 m, for what is called the *Cone Penetration Test (CPT)* (Lunne et al. 2002; Dorvinen 2016). The CPT is a widely used test for determining geotechnical characteristics of materials. The major drawback of these penetrometers is the difficulty in deployment in underwater environment. Due to their large weight, they require large vessels, which can increase substantially the costs of surveys.

Another type of penetration, is when the probe is allowed to impact the target material with a certain velocity dictated by deployment conditions, penetrometers mass and geometry (Mulukutla 2009). This type is called dynamic penetration. The *Dynamic Freefall Penetrometers (DFFPs)* originally measure the deceleration of the probe due to the impact and friction with sediment. The calculated deceleration is used for deriving basic geotechnical parameters such as cone penetration resistance, shear strength or bearing capacity of the sediment (Figure 4—13). Dynamic penetrometers have distinct advantages to the quasi-static penetrometers. They are more compacted and do not need external power for penetrating the sediment. They have also smaller dimensions and mass. Therefore, their deployment is possible from small vessels. As they operate on a freefall principle, their penetration is restricted to some meters in case of soft muddy sediments and to a couple of decimeters in the case of sandy bottom, in contrary to the quasi static penetrometers, which can reach penetrations of up to some hundreds meters (Dorvinen 2016).

Most common applications of dynamic free fall penetrometers for underwater environment, are geotechnical characterization of *marine* (Osler et al. 2006; Stark et al. 2014; Albatal and Stark 2017; Stark et al. 2017), *harbor* (Kirichek and Rutgers 2019; Kirichek et al. 2020) or *freshwater* (Corella et al. 2013; Stark et al. 2013; Corella et al. 2016) sediments. Based on the visualized curves, important information can be derived about the consistence of the bottom material and also for the layering effect inside the sediment. For example, the spikes in Figure 4—13 (Dynamic Cone Penetration Resistance graph) are indicating the presence of more compacted material

between the soft mud layers. The presence of spikes in the curves is not the only method for determining sediment layers. An abrupt change of slope in the *Dynamic Cone Penetration resistance* (DCPR) curve can also indicate the initiation of a new layer (Hakanson 1986; Stark et al. 2009; Stark et al. 2013). This is a promising technique for sediment detection, as it can be applied for detecting the sediment thickness when the DFFP reaches until the pre-impoundment soil. The new DFFP systems include extremely powerful loggers that can achieve data acquisition at a sample rate of some kHz (up to 5 kHz) and consequently, provide accuracy of $\pm 1\text{cm}$ when the impact point is correctly defined (Seifert and Kopf 2012).

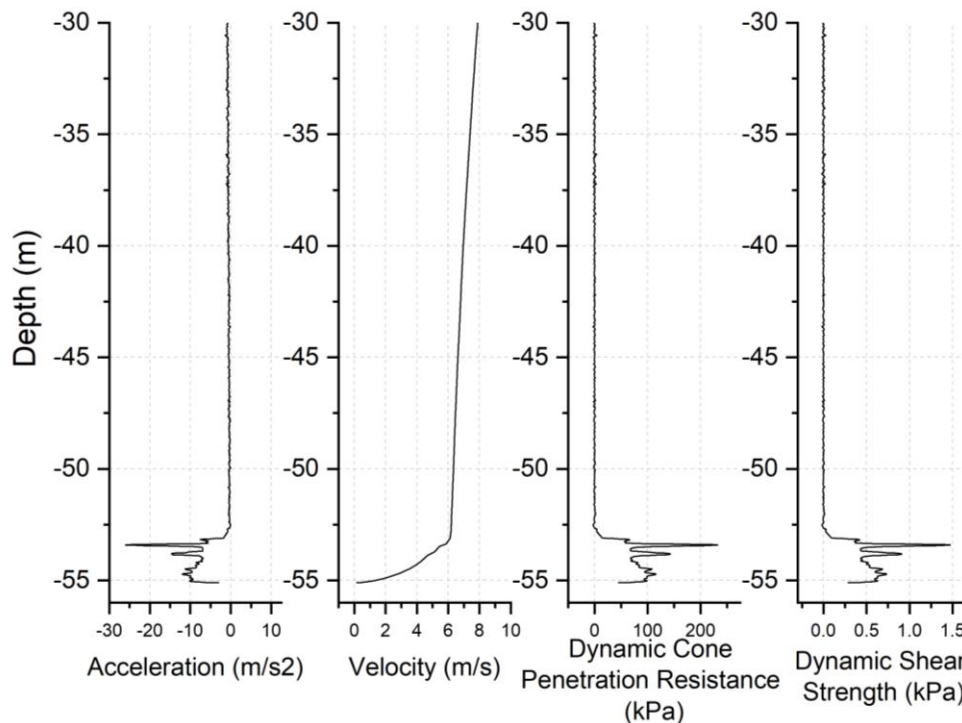


Figure 4—13 Properties derived from the deployment of GP. The spikes in the sediment represent layers with more consolidated material.

4.3. Trap efficiency of reservoirs

The trap efficiency of a reservoir is the ratio between the sediment deposited in the reservoir to the total amount of sediment incoming from the river. Churchill (1948) was one of the firsts to develop a method to quantify the trap efficiency for settling basins, small reservoirs, flood retarding structures, semidry reservoirs and frequently sluiced reservoirs, all operated from the Tennessee Valley Authority (Figure 4—14). Churchill (1948) based his empirical relation on the relationship between the sediment release and the sedimentation index of a reservoir, which is the ratio of the retention period in seconds (capacity divided by inflow rate) to the mean velocity in the reservoir in m s^{-1} (inflow divided by the average cross section area).

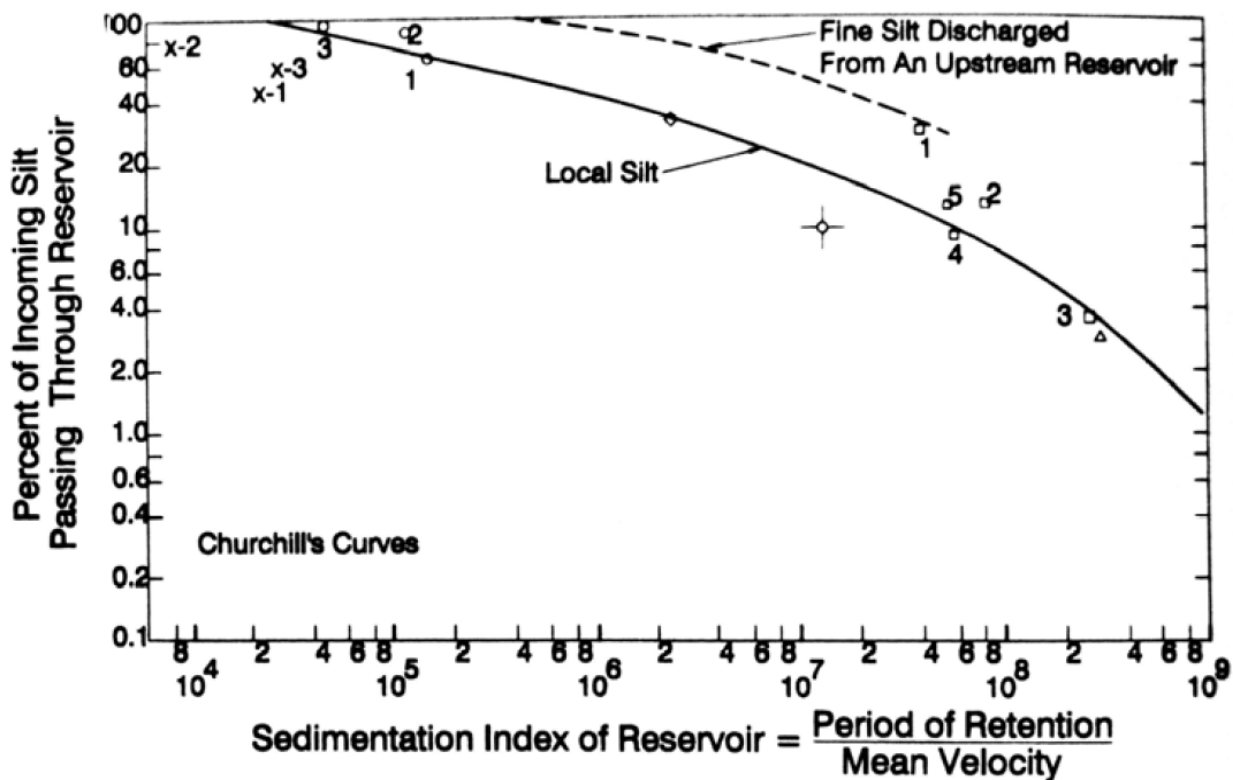


Figure 4—14 Churchill's curve for deriving the trap efficiency of the reservoirs (Morris and Fan 2010).

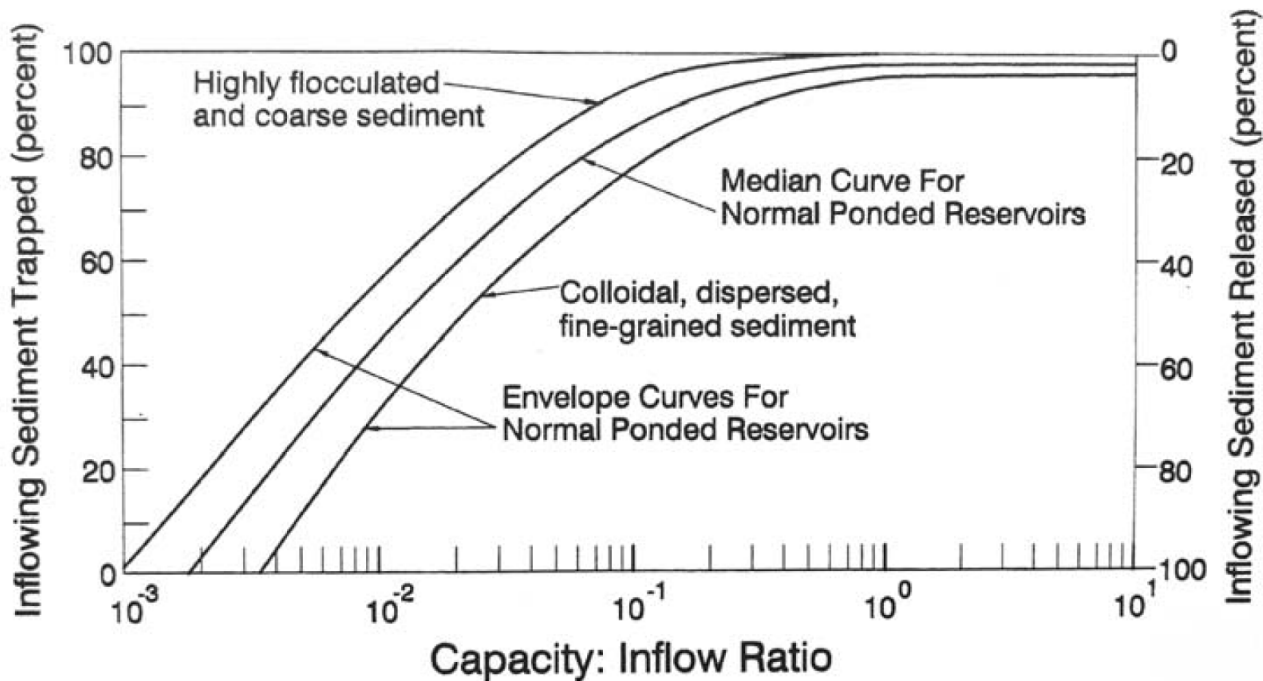


Figure 4—15 Brune's curve for deriving the trap efficiency of a reservoir (Morris and Fan 2010).

Brune (1953) developed another empirical method for the quantification of long term trap efficiency. In contradiction to Churchill (1948), Brune (1953) developed an empirical relation between the capacity inflow ratio and trap efficiency based on data from 44 reservoirs operated from the Tennessee Valley Authority (Figure 4—15). U.S. Department of the Interior, Bureau of Reclamation (2006) suggests that a general guideline is to use the Brune method for large storage or normal ponded reservoirs and the Churchill curve for settling basins, small reservoirs, flood retarding structures, semi-dry reservoirs, or reservoirs that are continuously sluiced.

The two above mentioned approaches are the most widely used methodologies for assessing the trap efficiency of a reservoir. They are both general relations derived from a certain number of reservoirs and can carry within them certain disadvantages. One drawback of this method consists in the fact that they do not take in consideration the type of sediment. When comparing reservoirs with similar hydro-morphological characteristics, in areas where sediment is dominated from sand or gravel material, the trap efficiency is expected to be higher compared to reservoirs where the sediment is dominated from silt-clay material. Another disadvantage is the absence of information about the existing storage level in case of floods. The trap efficiency for a reservoir that is operated in constant water level is higher than for a reservoir with similar hydro-morphological characteristics, which has large fluctuations of water level. In case of flood events for reservoirs operating in drawdown conditions, a larger amount of sediment will pass in the reservoir outlet due to the shorter residence time. In maximum level conditions, the reservoir residence time will be longer and therefore more sediment will be trapped. Finally, the above mentioned approaches do not take in consideration the geometry of the reservoir providing similar results for wide-short reservoirs and long-narrow reservoirs with similar volumes. Based on the previously mentioned disadvantages, other trapping efficiency relations are developed by adapting the existing curves of Churchill and Brune for local sediment conditions (Dendy 1974; Gill 1979; Heinemarm 1981; Garg and Jothiprakash 2008; Mulu and Dwarakish 2015).

4.4. Sustainable management for increasing reservoir's lifetime

Sustainable sediment management seeks to achieve a balance between sediment inflow and outflow, restoring sediment delivery to the downstream channel, maximizing long-term storage, hydropower and other benefits, while minimizing environmental harm (Morris 2020). According to Morris (2020), the management strategies for extending the reservoir lifetime are grouped in four categories: 1. *reducing sediment yield from the catchment*, 2. *sediment routing*, 3. *removing of deposited sediment* and 4. *adaptive strategies* (Figure 4—16). The first two management strategies focus on reducing the incoming sediment yield from the drainage while the last two categories focus on the sediment problematic after the sediment has been deposited.

The four major categories and their sub-categories, as explained in Morris (2020) are shown in the below graph.

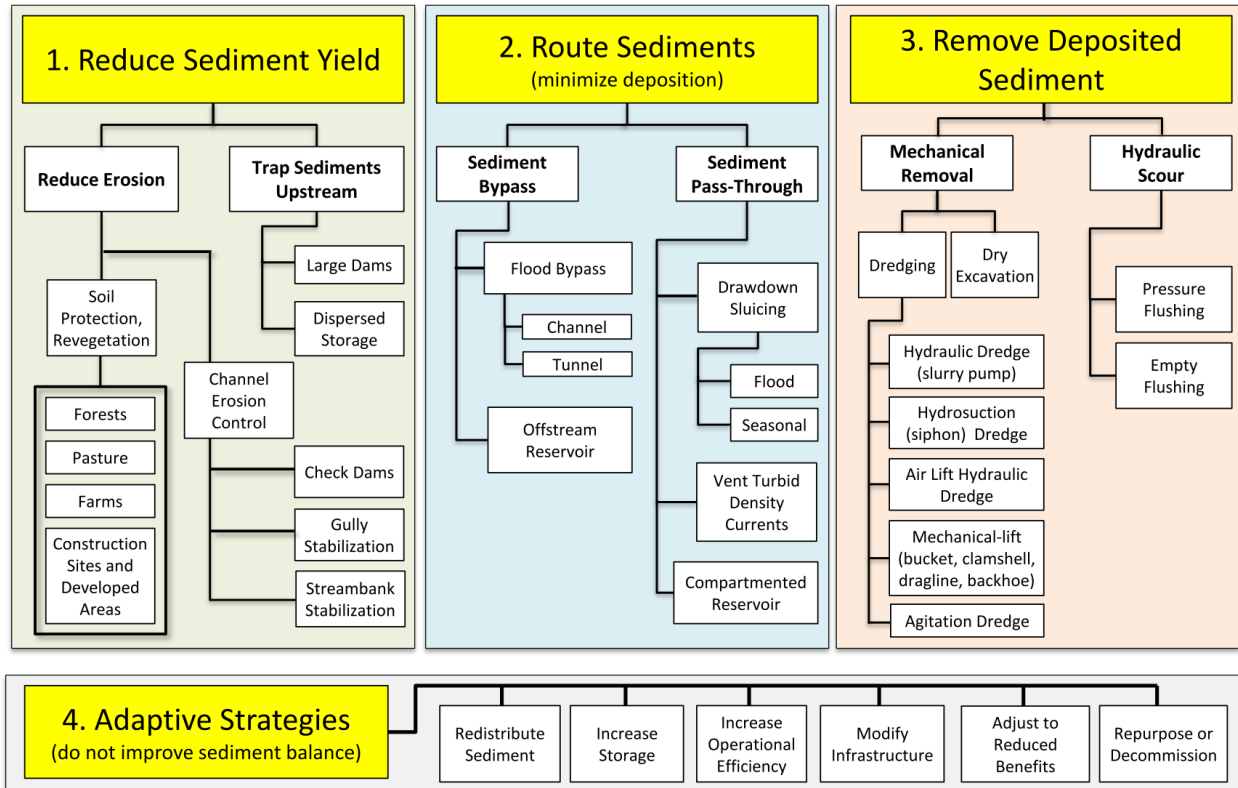


Figure 4— 16 Management strategies for extending a reservoir’s lifetime (Morris 2020).

4.4.1. Reducing sediment yield from catchment

Erosion and sediment input from a catchment are two processes whose lifetime is much longer than the reservoirs. For longer reservoir’s lifetime, significant effort should be made in either selecting an area, which is not suffering significantly from erosion, or erosion remediation measurements should be included parallel with the dam commissioning or during the reservoir operation. Several approaches can be followed for reducing the sediment input from a hydrological basin. They can include afforestation, sustainable farming practices, no-till agriculture or soil protection. The erosion hotspots in a watershed can be determined via monitoring, modelling or a combination of the previous two. To sustain long-term reduction in erosion rates in the agricultural sector, technology packages that produce direct benefits to the farmers through better soil management, need to be implemented, by reducing also the downstream sediment yield as a secondary benefit (Morris 2020).

The other method used for reducing the sediment yield in a reservoir are check dams in gullies, gully stabilization, or streambank stabilization. In China for example, until 2004 there were more than 110,000 warping dams in the gullies and more than 30 million ha of new farming land

have been gained in the plateau. Because of it, 210×10^9 tons of silt has been detained (International Hydrological Programme et al. 2004). Another measure for minimizing the sediment input is the commissioning of large dams upstream the major dam. Hydropower cascades as an example, apart from exploiting the full hydro-energetic potential of the river, they have as a byproduct also sediment yield minimization. However, the installation of large dams with the aim to protect a downstream structure is rear as the project are rarely economically feasible (Morris 2020).

3.4.2. Sediment routing

Sediment bypassing and sediment passing through a reservoir are the two strategies widely used for directly diverting the sediment. Sediment bypassing as it is shown in (Figure 4—17) can be achieved by a sediment bypass channel or tunnel or by the construction of off-stream reservoirs. Bypassing deviates the sediment-loaded water directly downstream the dam. In the case of off-stream reservoirs, the aim is to deviate the clear water in the reservoir and not the water during flood periods as during the flood periods the river brings the highest sediment loads. Another advantage of the bypass tunnels and off-stream reservoirs is that the sediment continuity is not interrupted. Most of the sediment in the system reaches the downstream area preventing the sediments starvation of the river below the dam (Auel and Boes 2011). Japan is one of the countries that has implemented sediment-bypassing measures since 1908 (in the Asahi Dam). The use of bypass structures for sediment rerouting has shown satisfying results in Japan. However, the use of this approach is still limited due to the high economic cost associated with the construction or with the topographic and hydrologic conditions of the catchment-reservoir area (Sumi 2004).

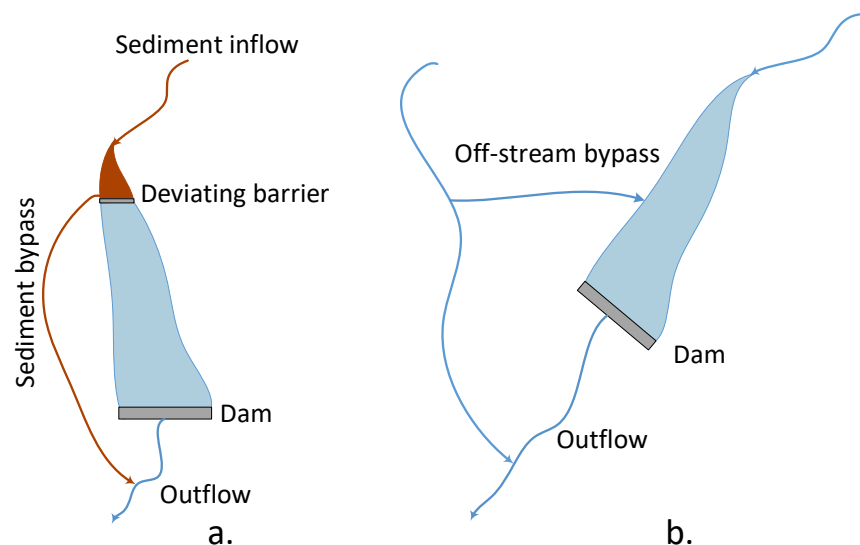


Figure 4—17 a. Sediment bypassing. b. Bypass reservoir.

Other sediment routing methods are those who focus on routing of the sediment through the reservoir. This can be achieved via sluicing, turbidity currents venting or reservoir compartmentation. Drawdown routing or sluicing is achieved by emptying the reservoir before flooding events (Kondolf et al. 2014). In this way, the sediment-laden flow passes directly through the reservoir with a minimum deposition. Sluicing is most effective in narrow reservoirs and in hydrologically small reservoirs which capture only a fraction of annual runoff volume and have a deep high-capacity low-level outlet (Morris 2020). Sluicing is a cost effective method for preventing future cost ineffective methods of sediment removal.

Turbidity currents are formed due to the higher density of the sediment-laden flows. The density currents can travel long distances in the longitudinal direction of the reservoir reaching until the pre-impoundment structure or the outlet structure. They are known as a main mechanism for distant sediment transport within lakes and reservoirs and in Alpine areas they are the main mechanism of sedimentation (Schleiss et al. 2016). The turbidity currents have in general high concentration of fine silt clay material which does not have any significant effect. In the long term, the release of turbidity currents is beneficial as sediment that would be deposited in the lakebed is released downstream with minimal effects on the infrastructure. If they are not released through the outlet structures, when the turbidity current reaches the dam, it will rise up against the face of the impoundment and mix in the vertical direction. The effect of this impact will make the turbidity current to return or promote sediment settling by creating a muddy lake in the foot of the dam (Schleiss et al. 2016).

Another way of routing the sediment is by manipulating the reservoir shape and installing internal barriers (Morris 2020). The technique can achieve significant impacts as shown by Jayadi et al. (2018). However, the reservoir compartment is a technique that is not widely used as the geometry of most reservoirs, does not allow the installation of such structures.

4.4.3. Sediment removal

Sediment removal can be achieved either mechanically or by hydraulic scouring by using the eroding potential of flowing water. Dredging and dry excavation are the two methods used for mechanical sediment removal. Dry excavation is typically used for the cleanout of debris basins, which are normally empty and contain coarse sediments that dewater quickly. However, it has been used for removing also large amount of silt from the Congswell Reservoir near Los Angeles (Morris and Fan 2010). Dredging on the contrary, is used for increasing substantially the reservoirs storage volume by removing the silt clay fraction and a fraction of sand. Elzinga (2017) lists the dredging devices in suction dredger, cutter suction dredger, grab dredger, backhoe dredger, submersible dredge pump, water injection dredger and siphon dredger. Dredging has certain advantages compared to other measures. Initially, during dredging the reservoir can continue its normal operation. Secondly, the removal of the material can occur topically where it

is needed and with high accuracy (near the outlets or dam). Lastly, compared to other measures like sluicing or flushing the water losses are relatively small. Along with the advantages, dredging has also some disadvantages. Among others, the most important are the high costs and the challenges encountered in finding a suitable solution for depositing the material.

The second method used for sediment removal is by using the kinetic energy of the water for flushing the sediment. Flushing can occur either under pressure or in drawdown conditions (empty). Pressure flushing occurs when a low-level outlet or an intake is opened to release sediment while the reservoir level is high. The effect of flushing is local as only limited part of the sediment at a certain distance upstream of the outlet will be remobilized and removed (Morris and Fan 2010; Morris 2020). Empty flushing is used for increasing partly the active storage capacity of a reservoir. As explained in Morris (2020) the flushing happens in three stages (Figure 4—18):

1. **Drawdown** from which a relatively low amount of sediment is released as explained above but the sediment upstream is remobilized and is distributed uniformly in the longitudinal direction

2. **Emptying**. During this phase the fine sediment is remobilized from the free-flowing river and it is directed through the outlets

3. **Refilling** is the final phase where the water level is brought to the initial conditions.

In the manual of U.S. Department of the Interior, Bureau of Reclamation (2006) about sedimentation and erosion, it is discussed that flushing is mostly successful in middle or small reservoirs. Kondolf et al. (2014) while referring to data from Sumi (2008), also states that for flushing to be successful, the ratio of reservoir storage to mean annual flow should not exceed 4%, because with larger storage the reservoir cannot be easily drawn down. The effects of flushing can also be hard to mitigate. If the flushing causes a concentration of suspended solids that exceeds certain thresholds, severe oxygen depletion, leading to massive death of the organisms in the river can happen (Vaoligao et al. 2012; Vaoligao et al. 2016; Quadroni et al. 2016). Apart from the effects that are associated with the suspended solids,

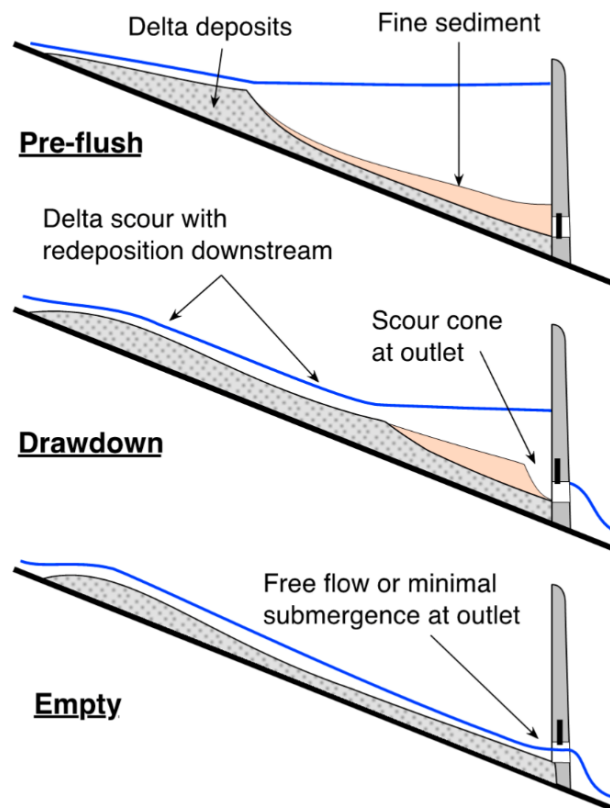


Figure 4—18 Stages of empty flushing (Morris 2020).

the effects of flushing can also be hard to mitigate. If the flushing causes a concentration of suspended solids that exceeds certain thresholds, severe oxygen depletion, leading to massive death of the organisms in the river can happen (Vaoligao et al. 2012; Vaoligao et al. 2016; Quadroni et al. 2016). Apart from the effects that are associated with the suspended solids,

Kondolf et al. (2014) argues that, in case of flushing in non-flood periods, the sediment deposited on the river bed can severely destroy the habitat needed by the aquatic invertebrates and for fishes to lay their eggs.

4.4.4. Adaptive strategies

When no sediment reduction can occur, alternative strategies have to be taken in consideration. These adapted strategies for the extension of a reservoir’s lifetime focus neither on sediment removal, nor on reducing the sediment deposition and the sediment input in the reservoir. When the approaches explained in the previous sections are not applicable (economically not feasible or no proper engineering solution) the extension of a reservoirs lifetime can occur via the increase of storage capacity by dam heightening, decrease the yield of a reservoir or redistribution of sediments. The existing adaptive strategies are grouped in Table 4—2 as suggested from Morris (2020).

Table 4—2 List of adaptive strategies for extension of reservoir lifetime (Morris 2020)

Adaptive Strategy	Description
Redistribution of Sediments	Operate pool levels to manipulate the geometry of delta deposits, especially to retard movement of the delta toward intakes.
Increase of storage	Raise dam or build new storage or supply project elsewhere.
Improvement of operational efficiency	Optimize operation to maximize benefits from declining storage volume. May involve pool re-allocation, operational optimization, conjunctive use with groundwater and similar strategies.
Modification of infrastructure	Modify sediment-sensitive infrastructure to accommodate increasing sediment loads or encroachment by sediment deposits.
Decreased delivery of benefits	Users adapt to reduced water supply or other benefits through conservation, abandoning low-value water-intensive activities, etc.
Repurpose or decommission	Reservoir no longer serves intended purposes and is permanently removed from operation. Dam may be removed. Reservoir area may be repurposed (e.g., aggregate mining, wildlife sanctuary).

4.5. Summary and research gaps

Sediments have several negative effects on the operation of the reservoir and its structures. Most common problems related to sedimentation include the loss of storage volume, the abrasion of hydraulic machinery, clogging of outlets or even the danger of dam damaging when the sediment has reached the impoundment structure. Several techniques can be applied for tackling the reservoir sedimentation (Boes and Müller-Hagmann 2015). In Figure 4—19, Annandale et al. (2016) present a general guideline for choosing the most feasible management approach based on the reservoir lifetime and hydraulic retention time of the reservoir.

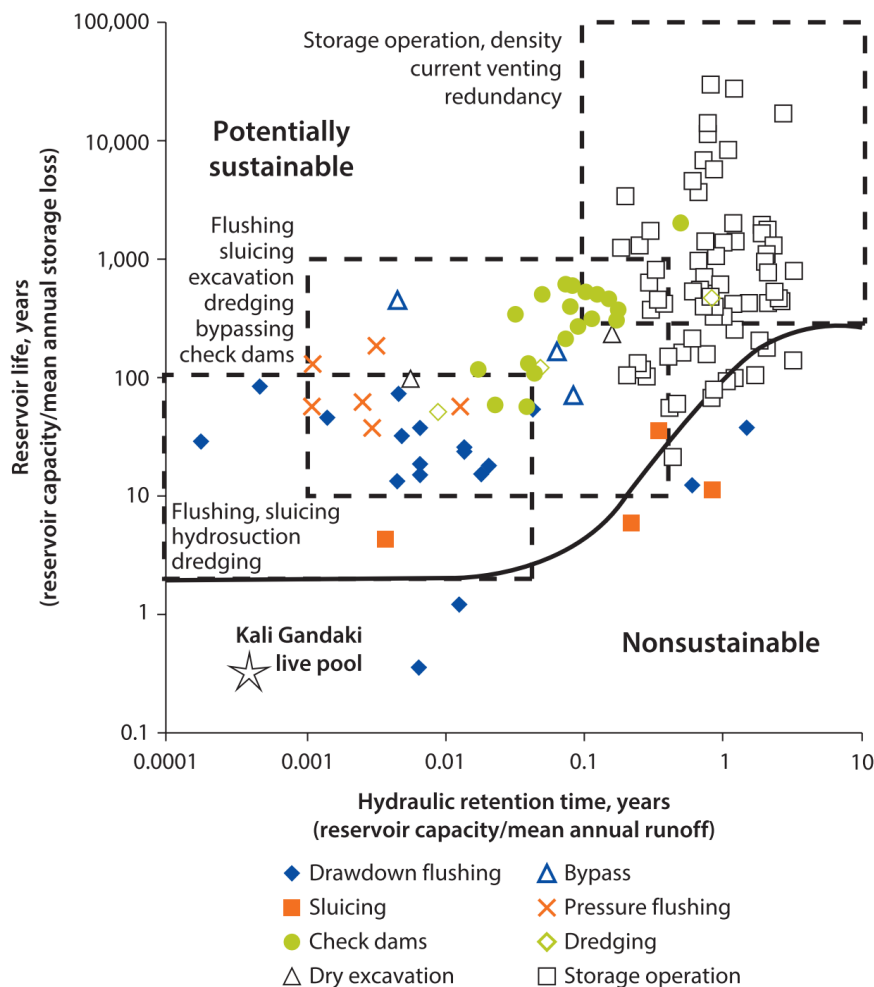


Figure 4—19 General guideline for choosing the most feasible management approach based on the reservoir lifetime and hydraulic retention time of the reservoir (Annandale et al. 2016).

However, Annandale et al. (2016) argue that the graph should be used exclusively as a guideline and not as a design tool as no proper conclusion can be derived based only on reservoir lifetime and hydraulic retention time. The information about sediment type, sediment volume and spatial

distribution is critical for choosing and implementing the sediment management actions. The sedimentation patterns are highly dependent on the reservoir morphological and hydrodynamical characteristics but also on the hydrological conditions of the inflows and their respective catchments. The physical-chemical characteristics of the sediment are strongly connected with the geomorphological characteristics of the reservoir drainage area and with the biochemical conditions of the reservoir itself in case of autochthonous sediment. Sedimentation in reservoirs is an unsteady and non-uniform process, driven by several physical processes, which are difficult to measure or to model. There are extreme inflow events with short duration, but significant sediment loads, there are density and/or turbidity currents, transporting the sediment over large distances, there are complex sedimentation and resuspension processes related to lake mixing, and finally all processes associated to sediment characteristics, such as flocculation, liquification or remobilization. Thus, usually only the consequences of reservoir sedimentation, such as sediment accumulation, is measured in practice. Most of the existing guidelines suggest that the most accurate way for assessing the sedimentation of the existing reservoirs is topographic differencing through subsequent bathymetric surveys (Bruk 1985; Carvalho et al. 2000; U.S. Department of the Interior, Bureau of Reclamation 2006; Morris and Fan 2010; Annandale et al. 2016; Central Water Commission and Central Dam Safety Organisation 2019). However, for the oldest reservoirs, the depth distribution maps are usually in an insufficient accuracy or does not even exist. Hence, alternative methods need to be examined for an accurate sediment stock and distribution assessment, in reservoirs where no previous bathymetric studies exist. As explained in section 4.2., several other methods can be applied for sediment detection. A combined utilization of remote sensing and conventional sediment assessment methods can improve significantly the accuracy of the siltation rate assessment. The execution of each of the above-mentioned detection methods requires also significant efforts and it is not suitable for each of the reservoirs. Therefore, a guideline, explaining which is the most appropriate technique for sediment detection, would be rather helpful in reducing the survey costs and improving the planning of sediment remediation measures. Moreover, an accurate sediment distribution pattern, apart for assisting in a sustainable management of the reservoir, can contribute also in answering fundamental scientific questions concerning the deposition, resuspension and transport dynamics in a reservoir, as the outcomes of sediment surveys can act as validation measurements for numerical modelling approaches.

5. Investigation area

The Passaúna Reservoir is located in the southeastern part of Brazil in the Paraná State (Figure 5—1a). The hydrological catchment of the Passaúna River is located in the Primeiro Planalto Paranaense, between parallels 25 ° 15 ' - 25 ° 35' South and meridians 49 ° 25 ' - 49 ° 20' West. The hydrological catchment covers partly the municipalities of Curitiba, Araucaria, Campo Largo, Campo Magro and Admiral Tamandaré and it is a sub-basin of the Iguaçu River. It has a surface area of approximately 150 km² and creates an average yearly river flow of 2 m³ s⁻¹. Most of the catchment is covered by forest (43%) and agricultural area (26%) (Figure 5—1a). Despite being an Environmentally Protected Area since 1994, a yearly increase of 2.25% (adapted from Instituto Brasileiro de Geografia e Estatística 2011) has been recorded in the population of the catchment (actual population 66,000). The sanitation facilities through the catchment are mostly available but still a part of the untreated sewage enters the river system from the semi-formal urban areas.

The Passaúna Reservoir is created from a 1200 m long and 17 m high rock-fill dam with internal clay core. The intake is located approximately 3 km from the dam. The reservoir has a surface area of 8.5 km² (Figure 5—1b). It started its operation in 1989 and it is used for providing 30% of the drinking water for the metropolitan region of Curitiba. The Passaúna river composes 65.6% of the contribution area to the intake located into the reservoir, followed by incremental summation of small sub basins < 1 km² (8.4%), the Ferraria river (6.9%), the own reservoir area (5.9%), the runoff lands around the reservoir (4.0%), the Eneas river (3.6%), and two other unnamed sub basins with 3.2% and 2.6% respectively (Carneiro et al. 2016). The reservoir was constructed and is operated from the *Companhia do Saneamento do Paraná* (SANEPAR). For the years 2009-2013 the *Environmental Agency of Paraná* (IAP) classified Passaúna as *Oligotrophic* and *Moderately Degraded* water body (due to the long and frequent occurrence of oxygen deficit periods in the hypolimnion) (Instituto Ambiental do Paraná 2017).

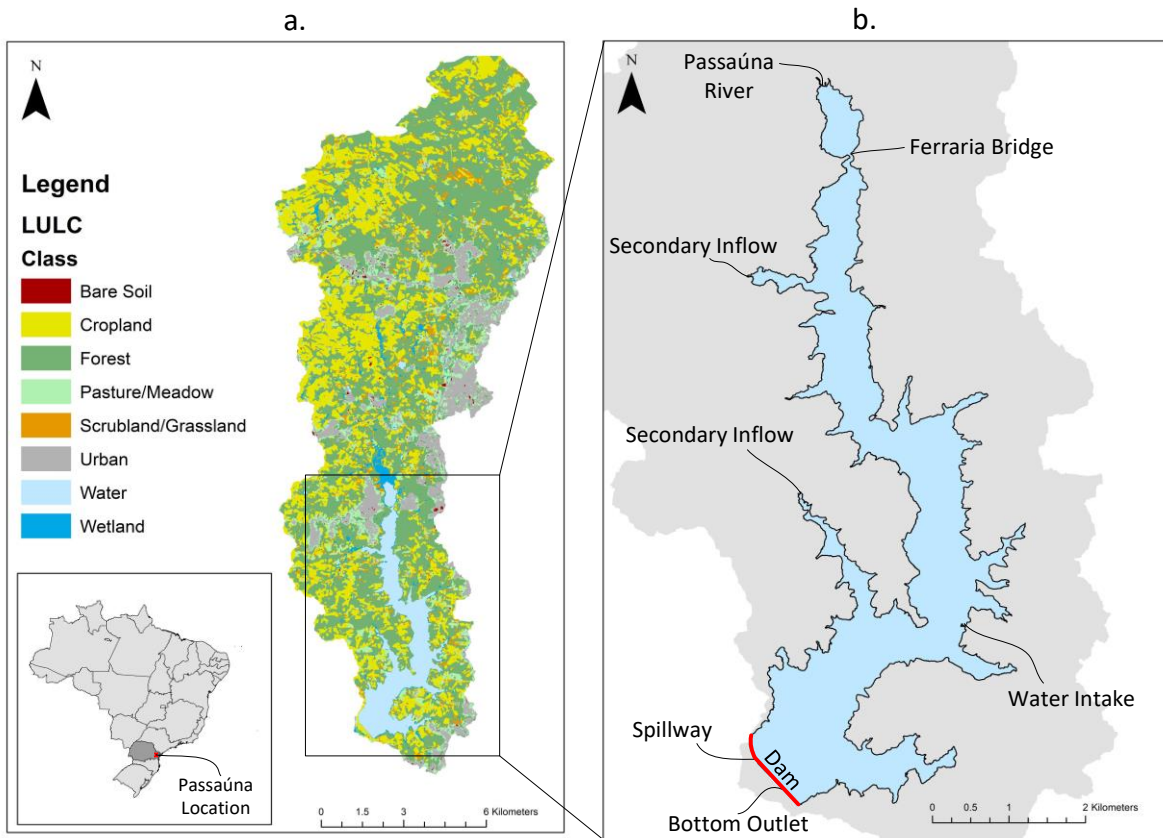


Figure 5—1 a. Location and LULC of Passaúna catchment. b. Passaúna reservoir and its most important features.

6. Methods and materials

In this chapter, the main methodologies for the quantification of the sediment input and sediment stock are described. Initially the model implemented for the quantification of sediment input from the catchment is explained and afterwards several techniques for measuring the sediment volume and sediment thickness in the Passaúna reservoir are described in detail. All the methods used are summarized also in the below table (Table 6—1).

Table 6—1 Summary of the methods used for assessing the sediment input from the catchment and the sediment stock in the reservoir

	Category	Equipment or approach used
In catchment	Sediment input modelling	RUSLE based model
		Subsequent bathymetry (Multibeam system WASSP F3Xi)
In reservoir	Hydroacustics	Sub-bottom profiling (Parametric system SES2000 compact)
		Single beam, dual frequency echo-sounder (Linear system EA400)
	Penetrometer	Dynamic freefall penetrometer (GraviProbe)
	Sediment sampling	Gravity corer with hammer action (Uwitec) and sediment grab sampling

6.1. Sediment input from the catchment (RUSLE)

For this study, the use of reduced complexity modeling approaches was aimed. An adapted RUSLE based model was used for calculating the sediment input from Passaúna catchment (Figure 6—2). A literature review was performed former to any modelling activities for defining the best possible approach for calculating each of the single coefficients. Each of the RUSLE factors represents one of the natural and anthropogenic phenomena as shown in Figure 6—1. The

integration of freely available satellite imagery in a high spatial and temporal resolution from the satellite platform Sentinel-2 and the existing precipitation data, made it possible to reduce the temporal resolution of the model to a monthly time step. For the calculation of the K-Factor, two soil sampling campaigns were conducted. From the collected soil samples, the soil properties were defined and subsequently the K-Factor was calculated based on a regional empirical relation. For the C-Factor, NDVI data from Sentinel-2 satellite platform was used. In addition, a locally derived empirical relation between the vegetation index NDVI and the C-Factor was used. For the R-Factor assessment, this study relies on two different approaches, one on literature values of R-Factor and another one by using precipitation data recorded from the local authorities. In general, no land conservation practices were observed. Therefore, the P-Factor was set to maximum value of one.

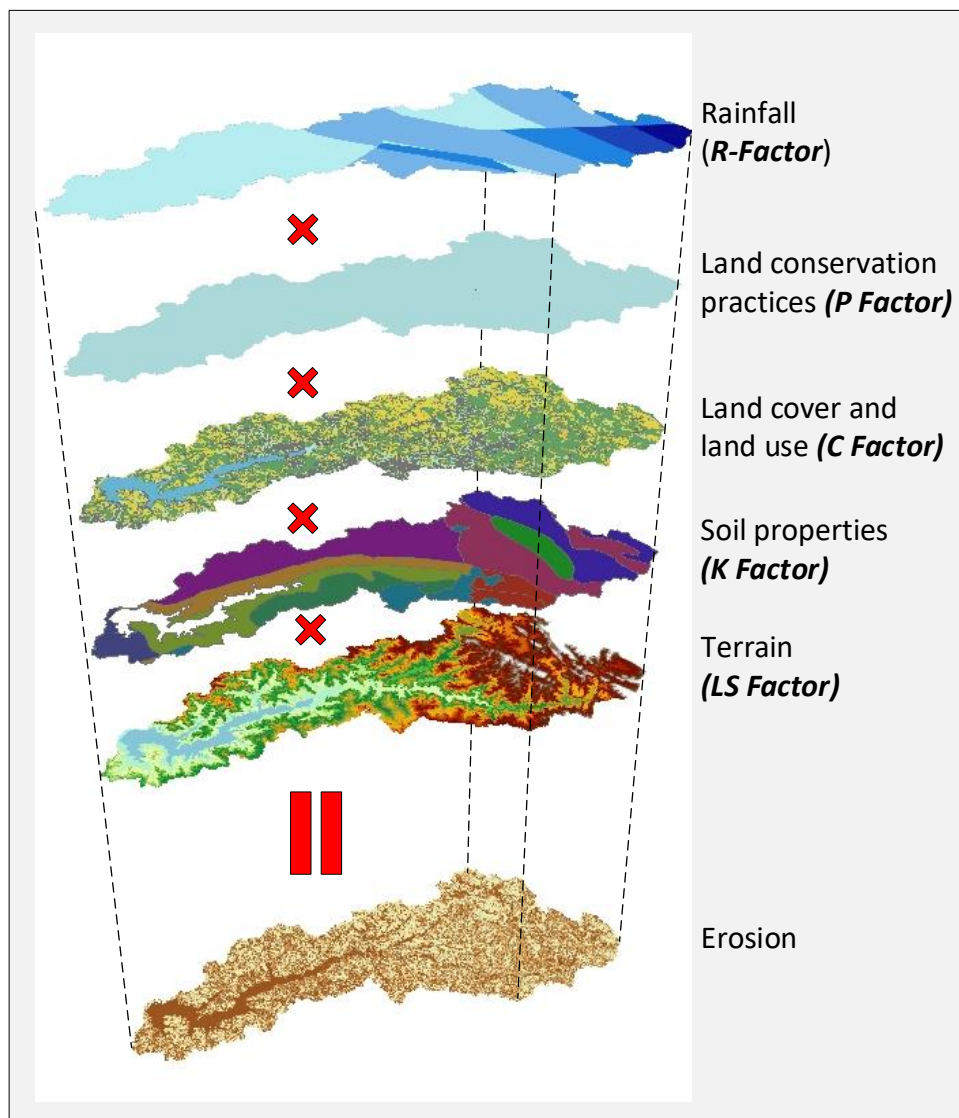


Figure 6—1 Schematic view of RUSLE application for Passaúna.

For calculating finally the sediment input, the soil loss calculated from the RUSLE is multiplied with the SDR. The SDR calculation is based on the connectivity index approach of Vigiak et al. (2012), where coefficients integrating information about terrain and land cover are included in the equation. The sediment yield calculation was executed as the below diagram (Figure 6—2) is showing. The quantification approach of each factor is described in detail in the below sections.

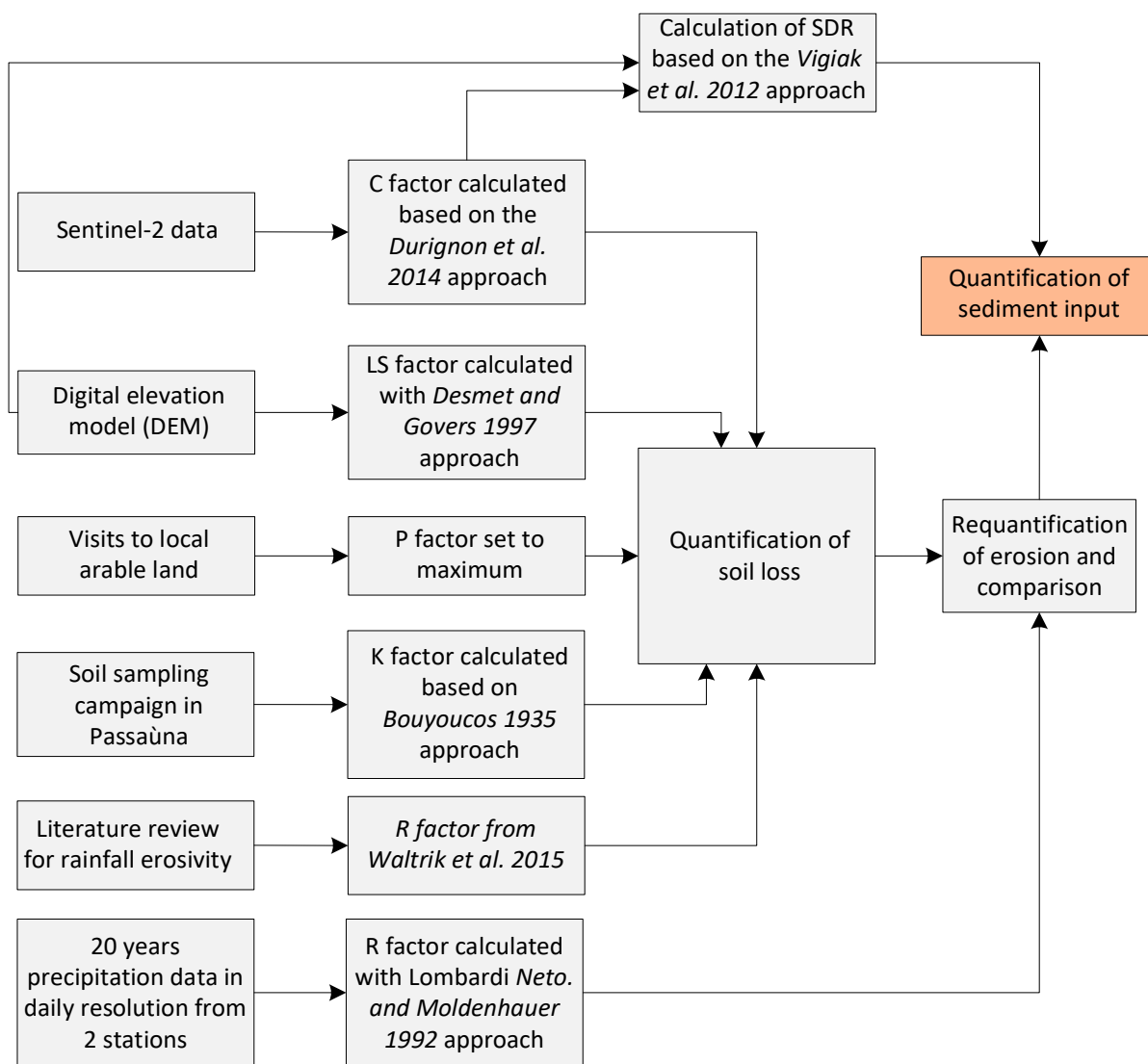


Figure 6—2 Schematic view of the approaches used for each factor in the process sediment input quantification

6.1.1. Topographic factor LS

The initial relation derived by Wischmeier and Smith 1978 for calculating the topographic factor was later adapted by Desmet and Govers (1997), especially for the L-Factor. The basis for the calculation of the pixel based topographic factor was a *Digital Elevation Model* (DEM) of an accuracy of 10 m available from TanDEM-X service (Figure 6—3a).

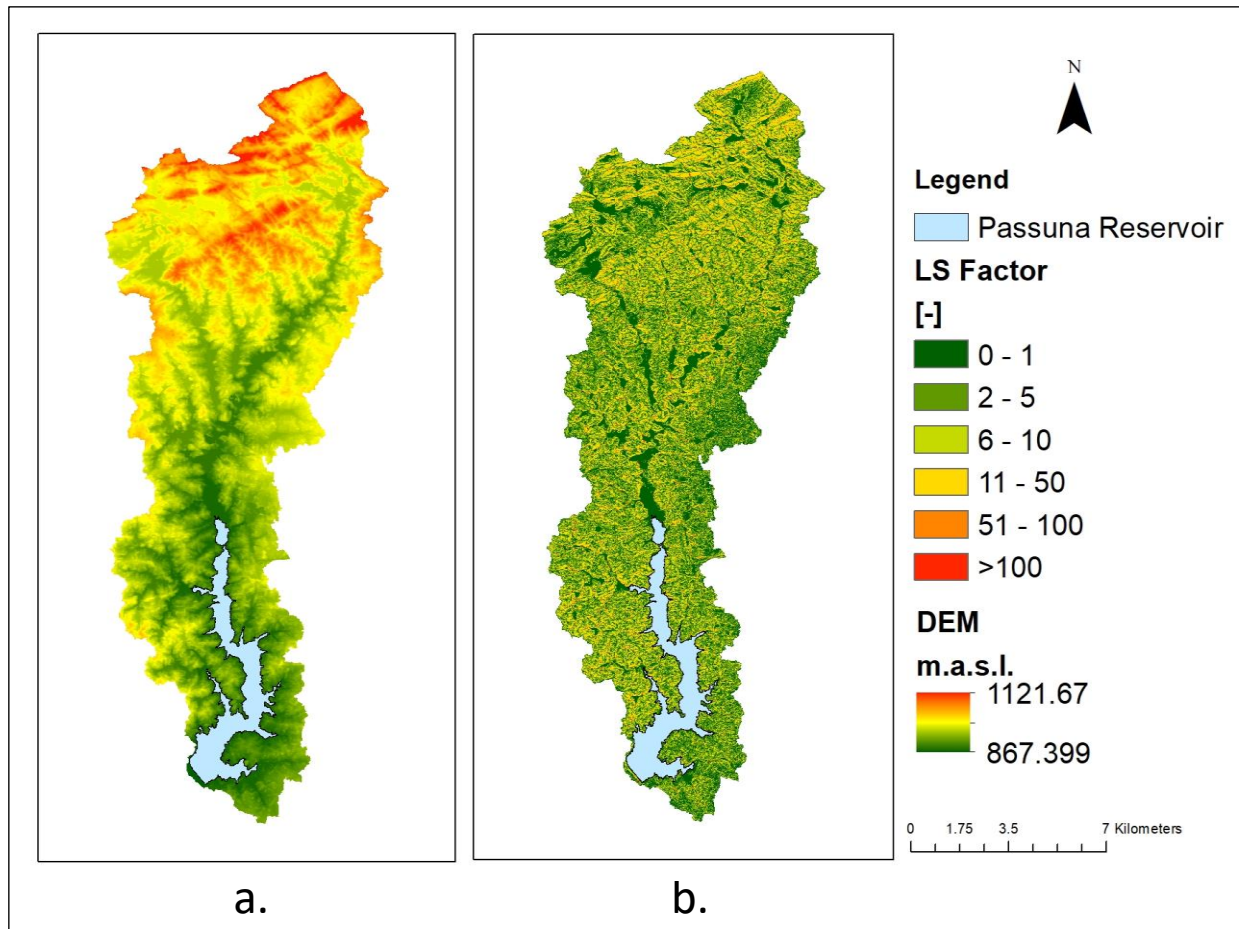


Figure 6—3 a. Digital elevation model. b. Spatial distribution of LS-Factor.

For the calculation of LS-Factor, the open source platform inVEST (inVEST- Natural Capital Project) was used. The LS-Factor was calculated as follows:

$$LS_i = \frac{(A_{i-in} + D^2)^{m+1} - A_{i-in}^{m+1}}{D^{m+2} \cdot x_i^m \cdot 22.13^m} \cdot S_i \quad (23)$$

Where:

S_i slope factor calculated from terrain slope θ in radians

$$S = 10.8 \sin \theta + 0.03 \quad \text{when } \theta < 9\% \quad (24)$$

$$S = 16.8 \sin \theta - 0.50 \quad \text{when } \theta > 9\% \quad (25)$$

- D grid cell dimension
 A_{i-in} contributing area (m^2) at the inlet of a grid cell which is computed from the d-infinity flow direction method
 $x_i = |\sin \alpha_i| + |\cos \alpha_i|$ when $\theta > 9\%$ (26)
 α_i is the aspect direction for grid cell i
 m length exponent factor (Table 6—2)

Table 6—2 Values of the dimensionless parameter m .

Slope % [s]	M
$s < 1$	0.2
$1 < s < 3.5$	0.3
$3.5 < s < 5$	0.4
$5 < s < 9$	0.5
$s > 9$	$m = \beta / (1 + \beta)$

Where: $\beta = \left(\frac{\sin \theta}{0.0986} \right) / (3 \cdot \sin \theta^{0.8} + 0.56)$ (27)

The LS-Factor is presented directly in Figure 6—3b.

6.1.2. Soil erodibility Factor K

The K-Factor corresponds to the soil erodibility or the soil susceptibility to erosion, which reflects the spatial variability of possible soil erosion depending on its structural and compositional characteristics (Abdo and Salloum 2017). This factor can be determined through experiments, carried out in field plots by using of a specific measurement setup (Marques et al. 2019). Alternatively, it may be obtained from predefined estimates based on the soil classes documented in the published literature reporting soil erodibility values for soil classes observed in different regions of Brazil (Table 6—3).

Table 6—3 Typical values of K-Factor for Brazilian soils.

Soil Class	K-value ($t \ h \ MJ^{-1} \ mm^{-1}$)	Source
Haplic Inceptisol	0.03	(Clemente et al. 2017)
Humic Inceptisol	0.0175	(Schick et al. 2014)
Oxisol	0.018	(Silva et al. 1997)

In order to determine the K-Factor, two soil sampling campaigns were organized in the Passaúna catchment with a total of 22 soil samples (Figure 7—1a). The texture (silt, clay and

sand fractions) and Loss on Ignition at 550 °C (LOI) were defined for each sample. For each point location, three subsamples were taken as replicates within a radius of 5 m. Disturbed material was dried and sieved in 2 mm mesh and the texture analysis was done by the Bouyoucos hydrometer method (Gee and Or 2002) based on the classification of the *North American Department of Agriculture* (USDA), which addresses that the particle sizes between 0.05-2 mm are sand, between 0.002-0.05 mm are silt, and smaller than 0.002 mm clay. For the samples of the first campaign, also some physical parameters of the soil were measured. The sampling and analysis of the soil samples were performed from the Department of Soil and Agricultural Engineering of the Federal University of Parana in context of the research project MuDak-WRM (www.mudak-wrm.kit.edu/). All the soil samples were used for calculating the K-Factor at each location. For this study we applied the equation (eq. 28) proposed by Bouyoucos (1935) for the sample points collected covering Ultisol, Red Oxisol and Typic Eutraqox classes.

$$K = \frac{SAN + SIL}{CLA} \cdot \frac{1}{100} \quad (28)$$

Where SAN, SIL and CLA are sand, silt and clay fraction in percentage, respectively.

Afterwards the values were interpolated by using the Inverse Distance Weighting technique for having the information in the full coverage of the watershed.

6.1.3. Rainfall erosivity factor R

Based on the availability of data we investigated two approaches for calculating the R-Factor.

a. Based on literature findings

Rufino et al. (1993) studied extensively the relations between the rain erosivity calculated from pluviographic (disdrometric) and pluviometric data. Optimally, the rain erosivity is calculated by using long-term pluviographic data even though this type of data is mostly unavailable. The pluviometric data is often more easy to access but has a major disadvantage as it gives no information about the duration of the rain. Rufino et al. (1993) derived three different equations for three different locations in Parana for relating the erosivity calculated from the pluviometric data (R_{pm}) with the erosivity calculated from the pluviographic data (R_{pg}).

For the calculation of R_{pm} the approach from Lombardi Neto. F. and Moldenhauer (1992) was implemented. For the calculation of erosivity index EI , the rain coefficient C_c from Fournier (1961) was used (eq. 29–30).

$$EI = 68.730 \cdot (C_c)^{0.841} \quad (29)$$

$$C_c = \frac{p^2}{P} \quad (30)$$

Where:

- p average monthly precipitation in mm
- P yearly average precipitation in mm

The R_{pm} -Factor for each month is equal to the EI value of each month as discussed by Lombardi Neto. F. and Moldenhauer (1992).

While for the calculation of R_{pg} the approach from Castro Filho et al. (1982) was applied

$$EI = [28.814 \cdot (10.8 + 7.896 \cdot \log I_{30})] \cdot P \cdot I_{30} \cdot 10^{-3} \quad (31)$$

Where:

- I_{30} maximum rain that occurs in 30 min. interval in $mm \cdot h^{-1}$
- P monthly total precipitation in mm

The monthly erosivity factor was calculated as a mean value of EI from all the erosive events in the specific month.

$$R = \frac{\sum_1^n EI}{n} \quad (32)$$

Where:

- n number of erosive events

Based on the above mentioned research, Waltrick et al. (2015) calculated the erosivity factor for the whole state of Paraná in a monthly resolution (Figure 6—4). In their research Waltrick et al. (2015) integrated data from 114 pluviometric and pluviographic stations with more than 20 years of data (1986-2008).

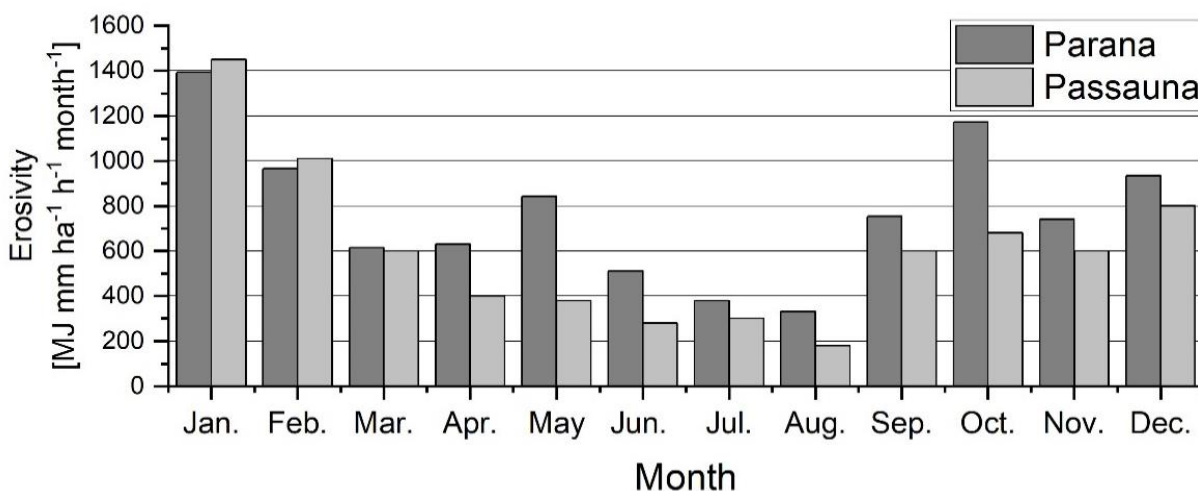


Figure 6—4 Erosivity in Passaúna and Paraná after Waltrick et al. (2015)

Waltrick et al. (2015) delivered also the spatial distribution of erosivity through the entire state of Parana. The values used for this study were extracted from the monthly erosivity maps for the area of Curitiba. As the spatial coverage of Passaúna catchment is 150 km, for the whole catchment a constant value of R was used for each month.

b. Based on pluviometric data of daily frequency

For the calculation of the R-Factor with the second approach, the data of two pluviometric stations in the catchment were used. The stations are a part of the hydrological information system of Instituto das Águas do Paraná. The station of Colonia Dom Pedro is located in the central part of the catchment while the other station Barragem Sanepar (Dam), is located in the south part of the catchment near the dam (Figure 6—5). For both of the stations, precipitation data from 2000 until 2018 were available on a daily basis.

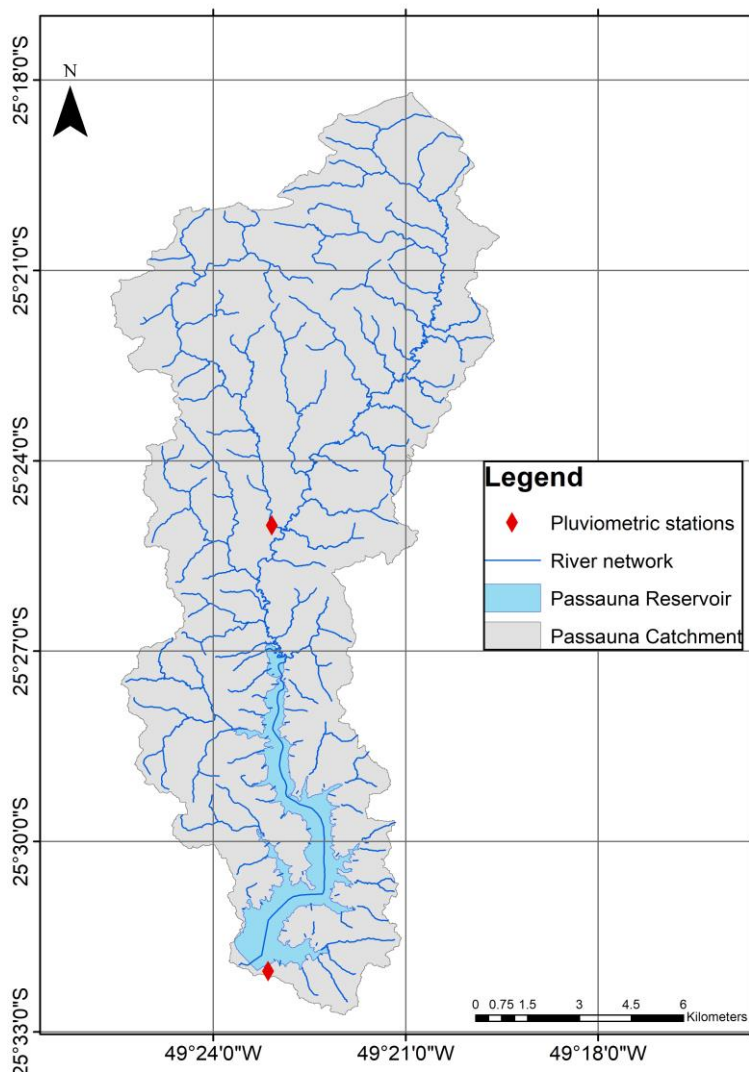


Figure 6—5 Location of Pluviometric stations in the Passaúna catchment

For the calculation of the R-Factor, the approach from Lombardi Neto, F. and Moldenhauer (1992) (eq. 29—30) was applied. The precipitation patterns at both locations are similar, therefore only one value of erosivity factor was used for the whole catchment (Figure 6—6).

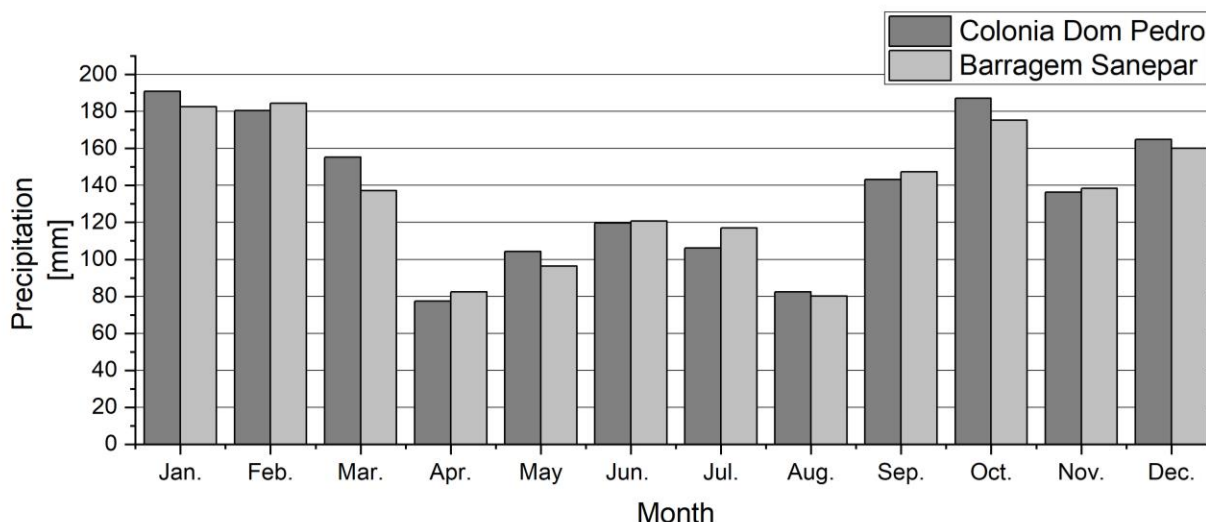


Figure 6—6 Monthly precipitation for the two locations in Passaúna catchment

6.1.4. Cover and management factor C

The landcover factor C is one of the most important factors when it comes to what is causing the highest inconsistencies in the outputs of a RUSLE based model (Risse et al. 1993; Ferreira et al. 1995; Estrada-Carmona et al. 2017). Optimally, the C-Factor is determined from experimental soil erosion plots under natural rainfall conditions (Nearing et al. 2000; Almagro et al. 2019). This type of data is expensive to produce and most of the models use literature values for the C-Factor. One of the most important drawbacks for the use of constant C-Factors is the high variability of values for the same landcover class among different literature sources. A literature review from da Silva Santos (2019) showed that the C-Factors among the same class could differ up to thousand times (Table 6—4).

Table 6—4 C-Factor values for five LULC classes in Brazil from a literature review from da Silva Santos (2019)

Land use	C_{max}	$C_{average}$	C_{min}
Bare soil	1.00000	0.69649	0.10000
Impervious areas	1.00000	0.25748	0.00000
High vegetation	0.09000	0.00774	0.00004
Low vegetation	0.63000	0.09934	0.00750
Water	0.00000	0.00000	0.00000

Another major disadvantage of constant C-Factor values is the inability to capture the spatial and temporal variability of the C-Factor among the same LULC class. With the developments in the satellite-based earth observation systems and the increase of data availability during the last decade, more scientists base their approaches on remote sensing data (Durigon et al. 2014; Panagos et al. 2015; Borrelli, et al. 2017).

For the calculation of the C-Factor in this study, the Sentinel-2 data was processed and spatial information about LULC, urban soil sealing and NDVI was derived.

The availability of valid image data for land cover applications is limited by cloud cover varying to local climate conditions. Sudmanns et al. (2019) provide statistics on the spatiotemporal distribution of cloud cover at the time of the satellites overpass. In the case of the Passaúna study area, an average cloud cover percentage of 56% is reported. Hence, the temporal frequency of usable data reduces from five days to an average of ~11 days.

For generation of the LULC maps the Random Forest algorithm was used for pixel-wise labeling of a Sentinel-2 time series raster stack (Breiman 2001). The scenes have been selected based on image quality criteria and with the aim to represent different phenological phases. Train and test sample data was collected through visual interpretation of aerial images as well as fieldwork. The estimate of overall accuracy based on a hold-out test set is 84%.

NDVI was the core parameter derived from the Sentinel-2 dataset. The NDVI is related to vegetation density, biomass and productivity (Tucker and P. J. Sellers. 1986). It was calculated based on the 10 m red (Band 4) and near-infrared (NIR) (Band 8) bands of Sentinel-2 (eq.33). An automated processing chain was established comprising the download, preprocessing (atmospheric correction), optimized cloud masking, scene selection and processing of land surface variables. The automated processing was not focused only on NDVI but also on other variables like degree of soil sealing or LULC. The use of NDVI values for the calculation of the C-Factors enabled a model set up with a monthly temporal resolution.

$$NDVI = \frac{NIR - RED}{NIR + RED} \quad (33)$$

Imperviousness is defined as the fractional coverage of artificially sealed ground, which impedes water from infiltration into the ground. The calculation of imperviousness is based on a strong inverse relationship between vegetation cover and impervious surface as well as the idea that an urban landscape can be linearly decomposed into vegetation, impervious and soil (Ridd 1995; Kaspersen et al. 2015). The imperviousness layer was calculated based on a min-max-rescaling of the NDVI derived from a satellite acquisitions between the maturity and senescence onsets. The rescaling was guided by visual comparison of results with submeter resolution aerial

images as well as findings Kaspersen et al. (2015), who studied the linear relationship between NDVI and imperviousness across several European cities. The calculation of the NDVI and imperviousness maps in monthly resolution was executed from EFTAS Fernerkundung Technologietransfer GmbH. The maps were delivered in the framework of the research project MuDak-WRM (www.mudak-wrm.kit.edu/). Two NDVI based approaches were considered for the calculation of the C-Factor in this study: Durigon et al. (2014) and van der Knijff et al. (1999). As shown in Almagro et al. (2019), for Brazilian conditions the methodology derived from Durigon et al. (2014) (eq. 34) produces more reliable results therefore this approach was used for the calculation of the C-Factor.

$$C = \frac{-NDVI + 1}{2} \quad (34)$$

The previous mentioned satellite derived data was used for calculating the C-Factor also in non-sealed urban areas (Figure A—3 in Appendix). As it can be seen from Figure 6—7, in the urban areas the NDVI is in the range 0.25 which would result in a C-Factor of 0.35-0.40, which corresponds to C-Factor values from arable land. Therefore, a filter was applied to the data with the simple logical condition that if a pixel in the urban areas had more than 60% soil sealing, the NDVI at the same location should be 0.999 as it was assumed that no or very little sediment can occur from sealed areas.

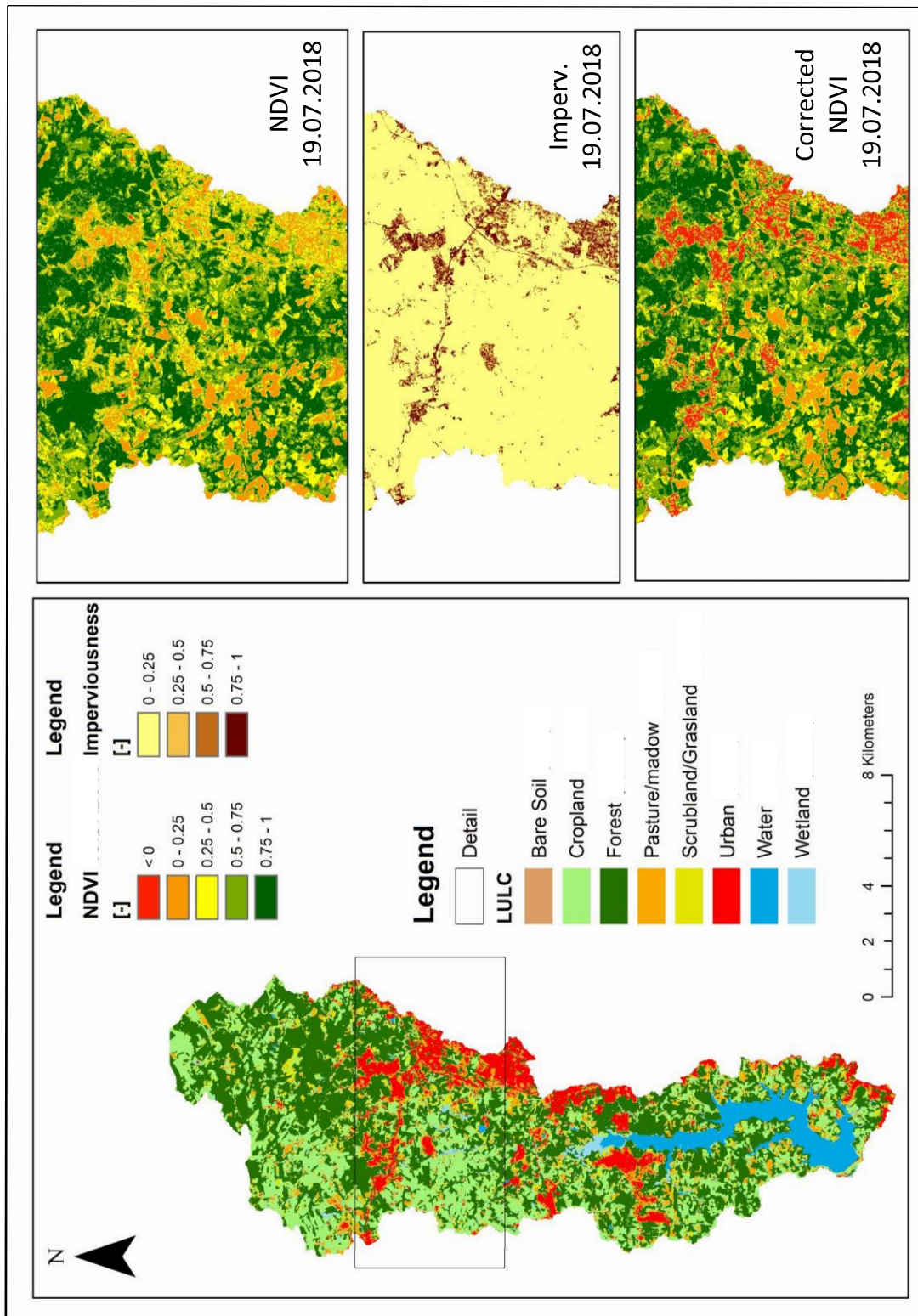


Figure 6—7 Correction of NDVI values for urban areas

6.1.5. Support practice factor P

During the several field trips in Passaúna catchment, many agricultural properties were visited and at almost all of them, no support practice was observed (Figure 6—8). Therefore, the P-Factor was set to a constant value of 0.



Figure 6—8. Characteristic arable land in Passaúna.

6.1.6. Sediment delivery ratio

Sediment delivery ratio plays a crucial role on the discrepancies of the results as it is directly related to a large number of factors (amount of soil displacement, geometry of the transporting paths, land cover of the surrounding area or amount of surface runoff) (Walling 1983). For this study, the SDR was calculated based on the Flow Connectivity Approach by Vigiak et al. (2012). The calculation of the connectivity index, and subsequently SDR, was implemented in ArcMap 10.5 as described in Borselli et al. (2008).

The index of connectivity (IC_k) at a certain point is calculated with the following formula:

$$IC_k = \log_{10} \left(\frac{D_{up,k}}{D_{dn,k}} \right) \quad (35)$$

Where:

D_{dn} downslope component of k^{th} cell

D_{up} upslope component of k^{th} cell

$$D_{dn} = \sum_k \frac{d_k}{W_k \cdot S_k} \quad (36)$$

Where:

d_k length of the of k^{th} cell along the downslope path (m)

W_k weight of the k^{th} cell dependent of the local conditions (land use, hydrological conditions or soil type), in this case only the land cover was accounted for, so $W_k = C_k$ (-)

S_k slope of the k^{th} cell (-)

$$D_{up} = \bar{W} \cdot \bar{S} \cdot \sqrt{A} \quad (37)$$

Where:

\bar{W} averaged weight of upslope contributing area dependent of the local conditions (land use, hydrological conditions or soil type), in this case only the land cover was accounted for so $\bar{W} = \bar{C}$ (-)

\bar{S} average slope of the upstream contributing area (-)

A area of the upstream contributing area

Finally the sediment delivery ratio was calculated on a pixel basis by using the approach developed from (Vigiak et al. 2012):

$$SDR_k = \frac{SDR_{max}}{\left(1 + \exp\left(\frac{IC_{0,k} - IC_k}{K_{IC,k}}\right)\right)} \quad (38)$$

Where:

SDR_{max} is the maximum attainable SDR coefficient at k^{th} cell, set to 1 as soil in the Passaúna catchment has a very high percentage of silt, clay and fine sand

IC_k is the index of connectivity at the cell k

$IC_{0,k}$ is a calibration parameter with a value of 0.5 (Vigiak et al. 2012; Jamshidi et al. 2014)

$K_{IC,k}$ is a calibration parameter with a value of 2.0 (Vigiak et al. 2012; Jamshidi et al. 2014)

6.2. Sediment volume and distribution in the reservoir

Five different approaches were followed for assessing the sediment volume and its spatial distribution in the reservoir. The methods included the application of three hydroacoustic systems, the use of grab and core sampling devices for groundtruthing and the addition of a dynamic free fall penetrometer (Figure 6—9). The methods were compared among each other for finding the most suitable method to use in systems like Passaúna. The overall sediment volume in the reservoir was used as a validation value for sediment input modelling explained in the above section. The general procedure followed for sediment characterization follows the below schematic graph.

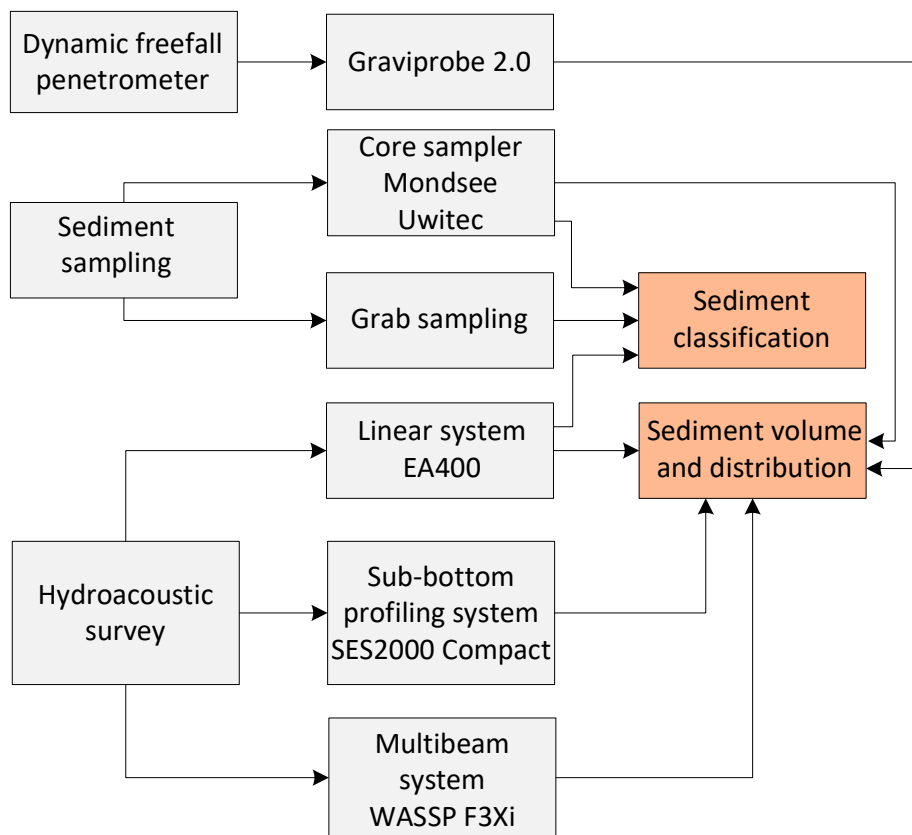


Figure 6—9 Schematic view of the approaches used for sediment stock measurement and sediment characterization

6.3. Hydroacoustic survey

Three different acoustic systems were used to obtain the sediment accumulation in the Passaúna reservoir. The systems included a multibeam system, a dual frequency single beam echo sounder and a parametric sub-bottom profiler. The multibeam was used to obtain a high resolution bathymetric map as a basis for volume comparison with pre-impoundment maps. The two single beam echo-sounders were used to detect the sediment thickness and to perform an acoustic sediment classification.

6.3.1. Bathymetry (Multibeam)

Initially a high resolution bathymetric survey was conducted using a WASSP F3Xi multibeam echo sounder with 160 kHz, 224 single beams and an opening angle of 120°, resulting in a swath width of ca. 3 times the water depth. The multibeam was combined with a Hemisphere V123 Compass for location and heading information and with a WSP-038 IMU unit for Roll/Pitch (0.25° accuracy) and heave (5 cm accuracy) correction. The system allowed for a vertical resolution of ± 2 cm and an average horizontal resolution of 20 cm. Since the outer beams of each multibeam system tend to produce more errors than the inner beams, large parts of the survey were conducted with 50% beam overlap. The survey duration was ~50 hours (ca. 300 km of boat tracks) and created 1000 GB of data. The recorded data was imported in the Autoclean software (BeamworX), where all the errors in measurements were erased. Afterwards a less dense number of points was exported as ascii file for interpolation in ArcGIS10.6.

There was no previous bathymetric survey or topographic map of the reservoir bottom for comparing our results in terms of sediment. However, from the reservoir operator SANEPAR, the depth-volume curve used for the management of the water resources was provided for comparison.

6.3.2. Sediment magnitude measurements

The second acoustic system that was used, was the EA400 (Kongsberg Inc. 2006). The EA400 is a single beam dual frequency linear echo-sounder, which emits primary frequencies of 200 and 38 kHz. The EA400 survey aimed on the investigation of the difference between the actual *Sediment Water Interface* (SWI) from the 200 kHz and the depth of the strongest reflectance layer, obtained by the 38 kHz.

The transducer was installed in an aluminum vessel with an incidence angle of 0°. The transducers depth was set 45 cm. CTD-profiles (CastAway®-CTD) were taken for sound speed corrections. The measured profiles included (stable) static and (moving) dynamic profiles (Figure A—7 in Appendix). During the static profiles, the boat was stabilized with three anchors and the

water column and sediment was ensouified for a minimum period of 40 seconds (ca. 400 pings). The static profiles were recorded at each groundtruthing position before of the sediment sampling process, to obtain an undisturbed acoustic response from the sediment layers. During driving, the EA 400 was set to an input power of 100 W, a pulse length of 0.256 ms for the 200 kHz frequency and 0.512 ms for the 38 kHz frequency. By increasing the pulse length, the sound wave penetration in the sediments increases. However, increasing the pulse length is not always the better solution as the echogram resolution is decreasing significantly. The best configuration is a tradeoff between best penetration possible and minimal information loss due to the reduced vertical resolution. The driving speed was in the range of 4–5 m s⁻¹ in order to minimize the noise caused from the engine of the boat. For real time data recording, the EA400 software was used and the stored data was later processed in Sonar5Pro (Balk and Lindem 2014).

Several findings suggest that sound waves with frequencies in the range of 20–40 kHz are able to detect the actual sediment thickness (Dunbar et al. 1999; Odhiambo and Boss 2004; Jakubauskas and deNoyelles 2008; Elçi et al. 2009; Clark et al. 2015; Patton 2016; Iradukunda et al. 2020). In order to calculate the sediment thickness, we used the difference between the SWI and the penetration of the 38 kHz from the linear echo-sounder.

The recorded data was split in two channels (200 and 38 kHz) and then visualized in the Sonar5Pro software (Balk and Lindem 2014). The bottom line (SWI), which was captured by the 200 kHz (Z200) was detected automatically by the software while the penetration depth line of the 38 kHz (Z38) was drawn manually for each line (Figure 6—10). The X, Y, Z coordinates of each point were then extracted and imported in ArcMap where an interpolation using the *Inverse Distance Weighting* (IDW) technique was performed, and the final sediment magnitude distribution in the reservoir was visualized.

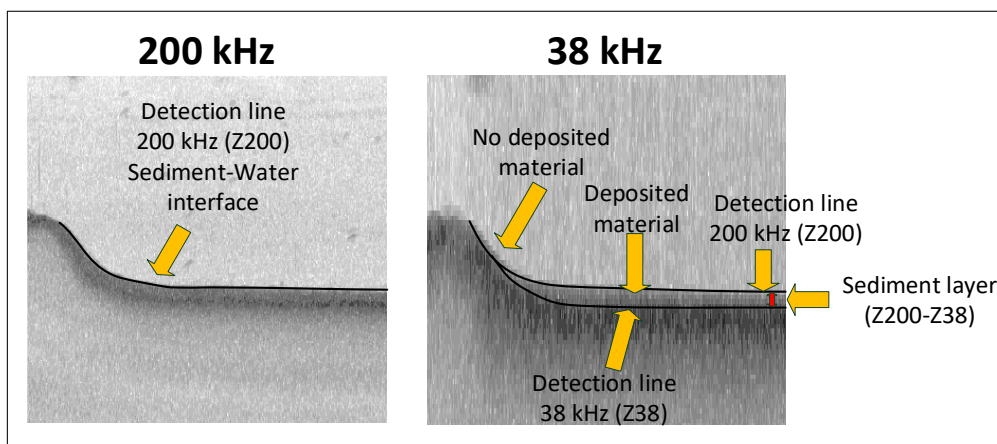


Figure 6—10 Sediment thickness derived with the dual frequency approach

The third acoustic system used in this study was the SES2000 Compact produced by (Innomar Technologies GmbH). The SES2000 Compact is a parametric multi frequency single

beam echo sounder, which can cover a water depth range from 0.5-400 m. Depending on the sediment type and noise, it penetrates the sediment up to 40 m. Its layer resolution varies from 1–5 cm. It has a primary frequency band of 85–115 kHz for the acquisition of the bottom track and a secondary low frequency band of 4-15 kHz for the sub-bottom data. The echo sounder can emit up to 40 pings s^{-1} (Innomar Technologies GmbH 2016).

In order to cover a wide range of frequencies, during the survey soundwaves with 4, 6, 10, 12, 15 kHz frequencies were used. Compared to the linear systems, *Sub-bottom Profilers* (SBP) have the advantage of high penetration with high resolution. In reservoirs such as Passaúna, where the sedimentation rate is in the range of some $cm a^{-1}$, high resolution systems are needed to precisely monitor the reservoir (Missiaen et al. 2008; Yutsis et al. 2014). The acoustic system was connected to a Leica 1200 DGPS system to reach a positioning precision in the cm range. Also here, CTD-profiles (CastAway®-CTD) were used for sound speed corrections. The measured profiles included (stable) static and (moving) dynamic profiles following the same procedure as with the linear echo-sounder. The survey was planned in such a way that a cross section of the reservoir could be recorded each 50–100 m (Figure A—6 in Appendix). Apart from the cross sections also a number of longitudinal transects were recorded.

The recorded data was visualized and processed in ISE2 software (Innomar Technologies GmbH 2016). The sediment layers when present, were drawn manually while for the water sediment interface the automatic bottom detection algorithm of the software was applied. The bottom detection line was afterwards manually corrected when errors were observed. The sediment thickness was derived as shown in Figure 6—11. From the depth of present water sediment interface the depth of the former lake bottom was subtracted and the sediment thickness was calculated.

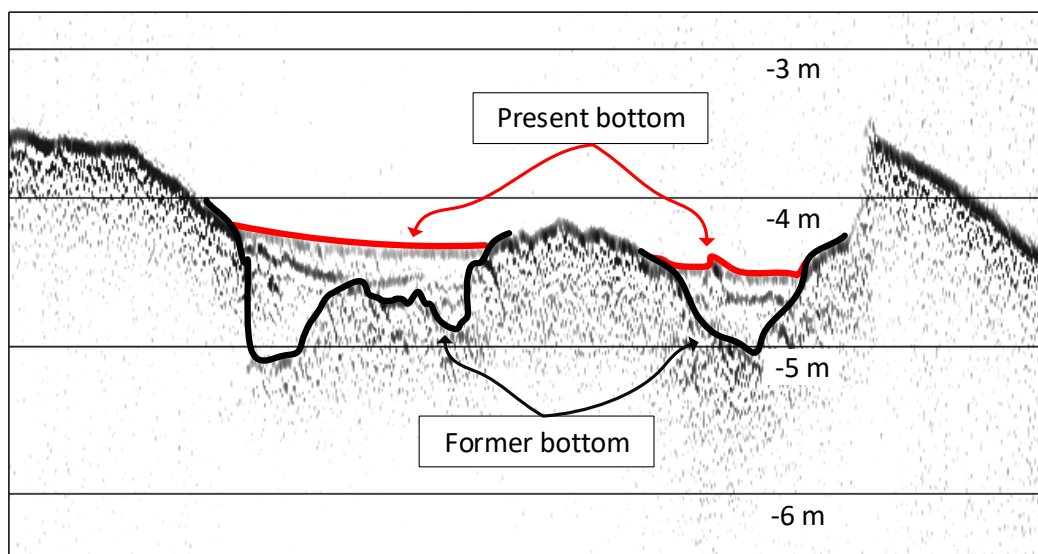


Figure 6—11 Sediment thickness derived from the sub-bottom profiling data

6.3.3. Sediment classification (EA400)

The second application of the linear system was the sediment classification. In case of sediment removal preparations, like dredging costs assessment or modelling for resuspension or flushing activities, the information of lakebed material is rather helpful. The application of hydroacoustic techniques has proven to be extremely valuable as large areas can be covered in short time when compared to the traditional sediment sampling (Orlowski 1984; Chivers 1990; Clarke, J. Hughes, E et al. 1997; Anderson et al. 2008; Ostrovsky and Tęgowski 2010; Anderson and Pacheco 2011). Hydroacoustics is widely used not only for sediment classification, but also for gas detection in the sediment or underwater habitat mapping (Siwabessy et al. 1999; Kloser et al. 2002; BioSonics Inc. 2008; Ostrovsky et al. 2008; Hilgert et al. 2019b)

The two classification approach applied for this study are based on the *First Echo Division* classification approach of Orlowski (1984) and Burczynski (1999) where the echo envelope is divided in three parts or acoustic parameters as shown in Figure 6—12.

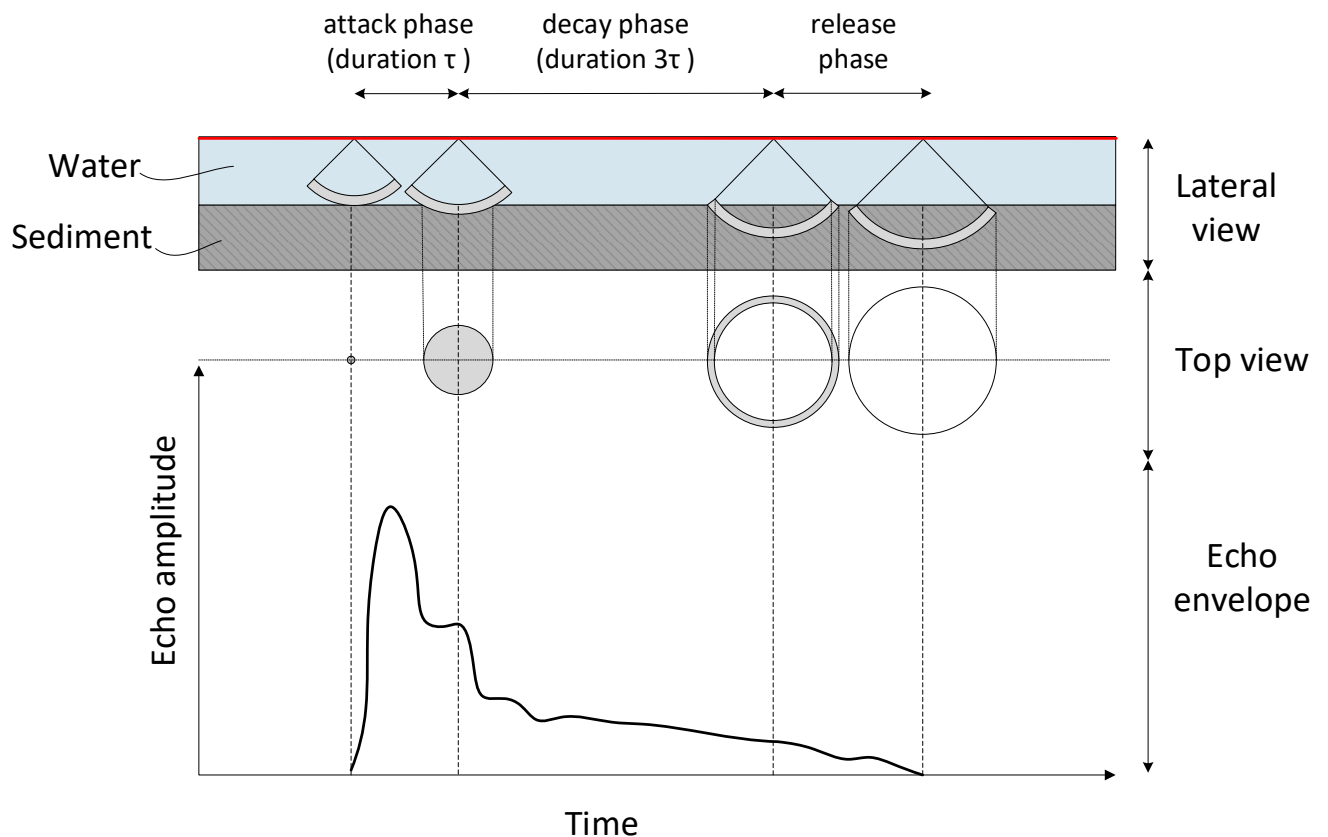


Figure 6—12 Phases of wave propagation in the sediment in regard to acoustic properties (adapted from Hilgert (2014)).

The three acoustic parameters include:

Attack phase, which is associated with the hardness of the lake bottom and accounts for the coherent part of the sound reflection. It starts from the sediment water interface and has a duration of one pulse length

Decay phase, which is associated with the roughness of the sediment bottom and accounts for the volume backscatter part of sound reflection. It starts from the end of the attack phase, a distance of one pulse length from water sediment interface, and lasts until the time when the front of the pulse reaches the boundary of the ideal beam pattern (approximately 3 pulse lengths).

Release phase, lasting until the time when the pulse completely enters the bottom. In this study is not included as the calculated algebraic values are irrelevant.

Each of the above mentioned acoustic parameters was calculated automatically in Sonar5Pro. The terms attack and decay can be found often in literature as *Hardness* and *Roughness* respectively. They were initially introduced from Chivers (1990). The first part of the echo describes generally the surface of the sediments while the second part or decay phase depends more on the backscattering effect taking place in the sediments. As the backscattering effect is related mainly with the physical roughness of the sediment, it is also called acoustical roughness. The attack phase is estimated by calculating the integral of the echo envelope of the first part of bottom echo ($E1'$) and the decay phase is estimated by calculating the integral of the second part of first bottom echo ($E1$) (Figure 6—13) (Orlowski 1984).

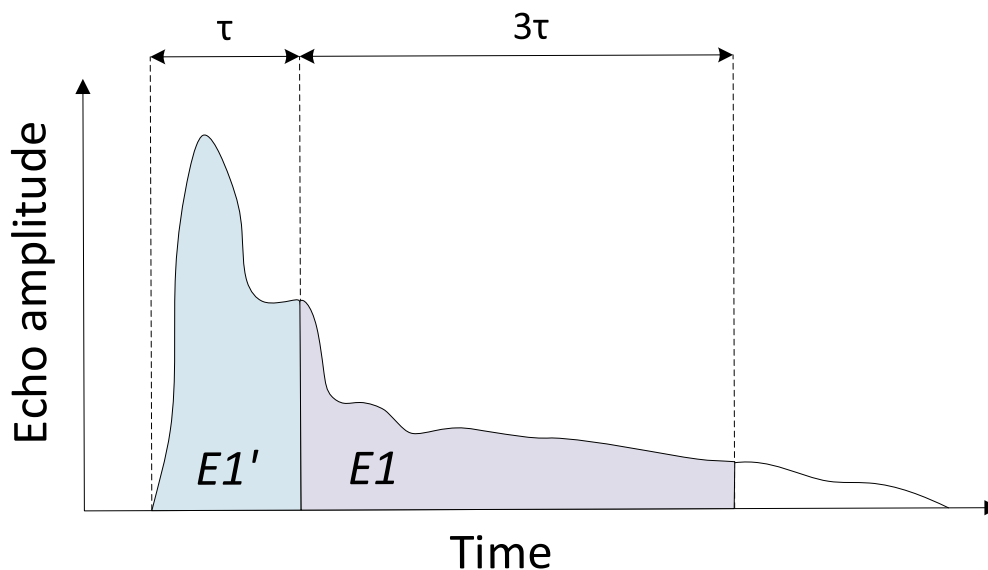


Figure 6—13 Attack and Decay phase in an echo envelope

To transform in mathematical values the average volume backscattering strength during both attack and decay phase, the echo strengths ($Sv1_i$) of each single sample belonging to that phase are converted into intensities, summarized, divided by the number of samples, and converted back into a dB value (Balk and Lindem 2014; Hilgert and Fuchs 2015; Hilgert et al. 2016). The values $attackdecaySv1$ and $attSv1/decSv1$ were also calculated. As explained in Tęgowski (2005) these values can include important information of the lakebed composition.

$$attackSv1 (E1') = 10 \log \left[\frac{1}{N_A} \sum_{i=AI_1}^{AI_2} \left(10^{\frac{Sv1_i}{10}} \right) \right] [dB] \quad (39)$$

$$decaySv1 (E1) = 10 \log \left[\frac{1}{N_D} \sum_{i=DI_1}^{DI_2} \left(10^{\frac{Sv1_i}{10}} \right) \right] [dB] \quad (40)$$

$$attackdecay Sv1 = 10 \log \left[\frac{1}{N_A + N_D} (N_A \cdot 10^{attackSv1/10} + N_D \cdot 10^{decaySv1/10}) \right] [dB] \quad (41)$$

Where

N_A is the number of attack samples and N_D is the number of decay samples calculated as following:

$$Number\ of\ Attack\ samples\ N_A = \left[\frac{1\ pulse \cdot \tau c}{Sample\ interval} \right] = \left[\frac{\tau c}{\frac{\tau c}{8}} \right] = 8 \quad (42)$$

as the wave of the EA400 system is composed by eight samples (pulses)

$$Sample\ interval = \frac{\tau c}{8} \left[\frac{m}{sample} \right] \quad (43)$$

$$Number\ of\ Decay\ Samples\ N_D = 3 N_A = 3 \cdot 8 = 24 \quad (44)$$

as the attack phase has a duration of one pulse and the decay phase of three pulses

AI_1 is the first sample taken during attack phase or rather the one which is detected as bottom.

AI_2 is the last sample taken during the attack phase.

DI_1 is the first sample taken during decay phase.

DI_2 is the last sample taken during the decay phase

For the static profiles, the above-mentioned parameters were calculated for four different configurations of the system as shown in Table 6—5, where the changing parameter was the pulse length.

Table 6—5 Pulse length and echo resolution for all the used configurations.

Configuration	200 kHz			38 kHz		
	Pulse length [ms]	Pulse length [m]	Echo resolution [m]	Pulse length [ms]	Pulse length [m]	Echo resolution [m]
A	0.064	0.096	0.012	0.256	0.384	0.048
B	0.128	0.192	0.024	0.512	0.768	0.096
C	0.256	0.384	0.048	1.024	1.536	0.192
D	0.512	0.768	0.096	2.048	3.072	0.384

In the case of Sonar5 software, the calculation of the $E1'$ (attackSv1) and $E1$ (decaySv1) is executed automatically in the Seabed classification option for each ping. Initially, the process was implemented to the static lines. For each profile, the calculated acoustic parameters were exported as ascii files. Apart from the first bottom echo, the program was calculating also the acoustic parameters from second bottom at some points that the second bottom was available. The second bottom values even though calculated, were not used for the seabed classification as at most locations they were not recorded. After being exported, each ascii file was processed with Matlab. All unnecessary and extreme values were deleted and the file was containing only positioning data and $E1$, $E1'$, attackdecaySv1 and attSv1/decSv1 values. For each profile, a mean value of the former mentioned parameters was calculated. The data was used to investigate the correlation of acoustic parameters with the sediment characteristics retrieved from groundtruthing e.g. grain size, density and LOI. Parts of the echograms where other objects like, fishes or bubbles had a strong reflection, were not included. The minimum number of pings for each profile was 300. However, in most of the profiles the number of pings which was analyzed was between 500–1000.

The derived equations from the regression analysis between acoustic and physical parameters of the sediment were applied to the acoustic parameters calculated from the dynamic profiles. The dynamic profiles were afterwards visualized and interpolated for assessing the sediment characteristics throughout the entire area of the reservoir

The other approach used for this study is the one developed from Sotiri et al. (2019a). While analyzing more 100 sediment core samples from six different reservoirs, Sotiri et al. (2019a) developed a clustering approach where the sediment acoustic response (above mentioned acoustic parameters) was set into a relation with the physical properties of the material such as, *Wet Bulk Density* (WBD), *Silt-Clay Fraction* (SCF), LOI and *Relative Water Depth* at the location

(RWD) (Figure 6—14). When plotting attackSv1 against decaySv1, clusters could be observed. This clusters as shown in Sotiri et al. (2019a) had distinguished physical parameters and therefore could be used for defining the sediment type

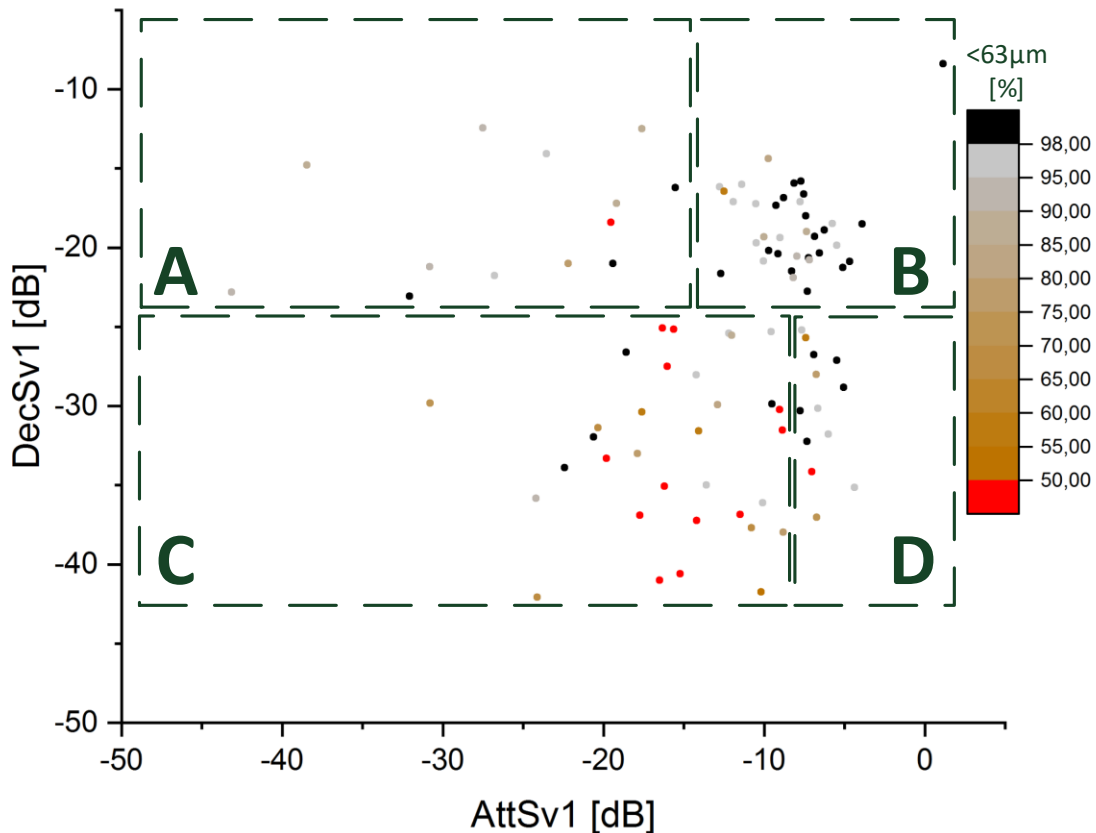


Figure 6—14 Classification approach from Sotiri et al. (2019a)

The classification approach resulted in four different lake bottom classes

- A. Thick sediment layer. Soft non-gassy material in the first 80 cm.
- B. Thick sediment layer. Soft gassy material in both top and bottom layer.
- C. Coarse material. Often Pre-impoundment soil or sandy sediment.
- D. Thin sediment layer. Very compacted or gassy top layer.

The Attack and Decay parameters were calculated for each of the recorded envelopes from the dynamic profiles in the Passaúna reservoir. The classification algorithm was applied to these points in order to assign one of the above classes to each of them. Finally, the classes were visualized and interpolated by using the inverse distance weighting technique as in the case of the first classification approach

6.4. Sediment sampling and analyzing

Sediment core sampling is a method that can help in documentation of the sediment thickness when the cores are undisturbed and the sampling device penetrates until the pre-impoundment soil. For this study, a “Niderreiter 90” corer manufactured by Uwitec was used. The corer consists of a metallic stainless steel structure and replaceable 86 mm diameter PVC tube. If operated only by gravity, the corer has a weight of 8 kg. In order to have a deeper sediment penetration, we incorporated an additional 7 kg weight, which can be operated also as a hammer to penetrate harder sediments (Figure 6—15). The corer is easy to transport. It is connected to a portable manual winch, which can be installed in any type of survey vessel and operation at water depth of up to 100 m.

For this study, 23 sediment cores were sampled in the Passaúna reservoir. In some cases, the “hammer action” was used for a better sediment penetration, especially at the positions where the sediment was compact or water depth did not allow for a sufficient penetration of the corer. In addition to core sampling, grab samples were taken.

Grab sampling generally is less accurate than core sampling, since the sediment structure is disturbed and sampling depth is not clear. During transport to the surface even with closed jars, the fine material may be washed out. The core sample is more reliable in this context, as the material is sealed and no material is washed out. For this reason, the gravity corer was used more often than the grab sampler, even though grab sampling is less time consuming. For sediment processing, the cores were cut in a longitudinal profile. The sample length varied from 12 cm in the less sedimented areas to 92 cm in the deep areas. The stratigraphy of each core was

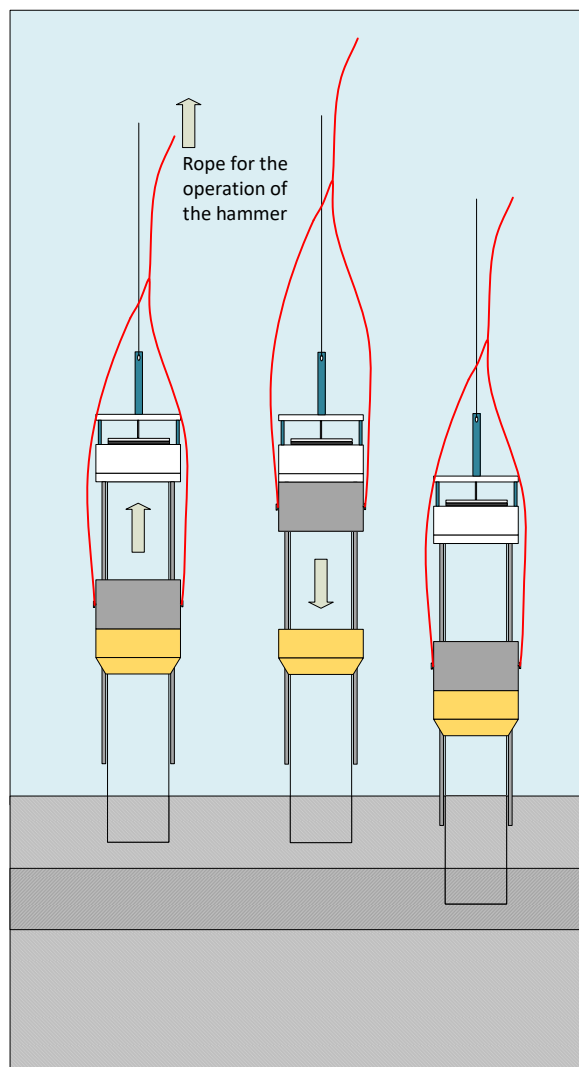


Figure 6—15 Schematic view of core sampling process via the hammer action

described after visual assessment for color, structure, texture, gas voids, and organic macroremains such as vegetation, roots and leaves. The material with similar characteristics was defined as a layer and its thickness was measured. Density samples were taken only from the cores. Visually, it was assessed that the grab samples were highly disturbed and that wet bulk density (WBD) measurements did not reflect the *in situ* density of the sediments before sampling. For WBD analysis, a cylinder with a fixed volume of 43.2 cm^3 (35 mm diameter and 45 mm length) was used for extracting the volume sample. A density sample was extracted from all the consolidated sediments layers, while for sediment samples that had high water content the density was assumed 1 g cm^{-3} . The sampled material was weighted after drying in 105°C for 24 hours and density was calculated. From each layer, 300 g of homogenized material were sampled, if the layer weight was more than 300 g or the entire layer material was sampled, if the layer was less than 300 g in weight. The samples were transported to the laboratory, where they were manually wet-sieved by using distilled water (Figure 6—16). For granulometry, five sieves were used. The sieves had the following mesh sizes: 2 mm; 500 μm ; 250 μm ; 125 μm ; 63 μm . After sieving, the samples were dried in 105°C for 24 hours. Then, the dry mass of each sample was measured and the granulometry was defined. For the core samples, each layer was sieved separately. The final granulometry of each core was determined by summing up the fractions of every layer of the same core and including a weighting factor related to the layer thickness to correct the relative share of each layer. Finally, the LOI was also determined by burning the samples at 550°C for four hours. For each station, also a set of pulse length dependent acoustic parameters was calculated, for creating statistical relations between the physical and acoustic parameters.

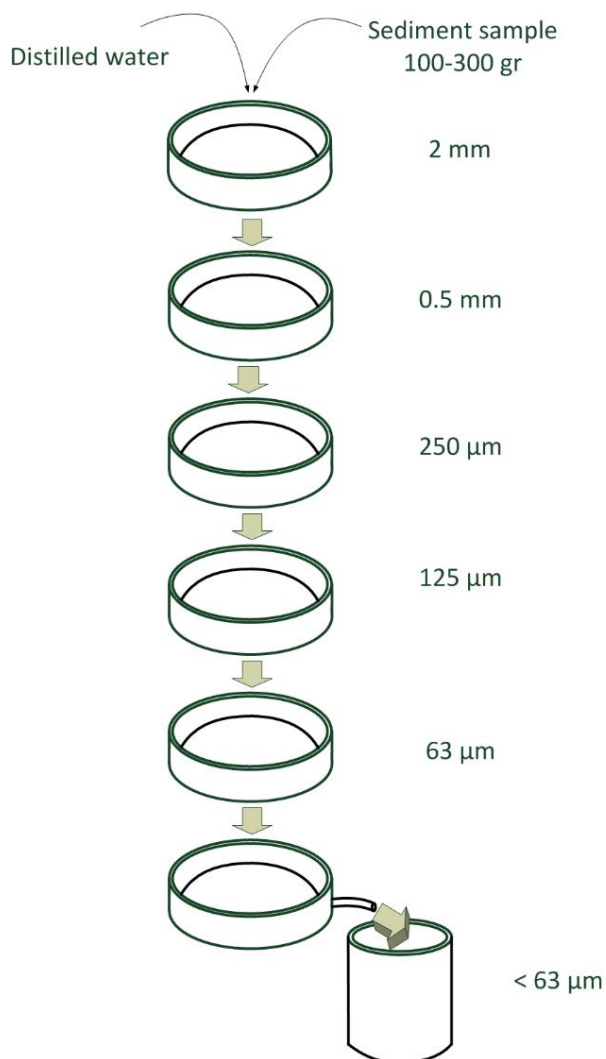


Figure 6—16 Schematic view of wet sieving.

6.5. Dynamic freefall penetrometer (GraviProbe)

For the investigation of the spatial thickness distribution of the unconsolidated sediment layer, the portable DFFP GraviProbe was used in addition to the core samples. The *GraviProbe* (GP) is made of stainless steel and has a weight of 8 kg. It is 960 mm long and has a diameter of 50 mm (Figure 6—17). During deployment, the internal pressure sensors and accelerometers have a sampling rate of 5120 Hz. It accelerates in freefall and penetrates fluid and consolidated sediment layers. The probe communicates via WiFi with an Android device (tablet or mobile phone) from which the data can be downloaded. The data measured by the on-board acceleration, inclination and pressure sensors feed a dynamic model that determines the geotechnical parameters *Dynamic Cone Penetration Resistance* (DCPR) and *Undrained Shear Strength* (USS). The penetration depth into the sediment can be derived from the acceleration curve. For water depths up to 30 m the “Rheo” version with pressure sensors measurement range from 0 to 3 bar is used. The cone penetration resistance is used to detect layers in the sediment. In particular, the differentiation between diverse sediment compositions or sediment types are possible, as the grain size and bulk density directly affect the cone penetration resistance.



Figure 6—17 Photos of GP. Left before deployment. Right after deployment.

With the 134 GP measurements distributed longitudinal as well as transversal, a good spatial coverage of the reservoir was reached (Figure 7—25a). All parts of the reservoir, including points in the main body, sidearms, entrance of the reservoir, near the dam and near the intake were covered. In order to investigate the lateral sediment distribution in high detail, six cross sections were covered with additional measurement points.

7. Results and interpretation

The most important findings of this thesis are presented in this chapter. The section is divided in two major parts. Initially the results from sediment input are described, followed by the main findings from sediment stock and distribution measurements in the reservoir. The aim of this chapter is not only the presentation of the results but also their interpretation. Where needed, correction and calibration of the methods are also implemented. Finally, a summary with the most important messages of this subsection is given.

7.1. Sediment input from the catchment (RUSLE)

In this section, the results of sediment input and erosion are presented. The focus is set initially to the explanation of the results from K-, R-, C-Factors and SDR while LS- and P-Factor values, due to their simplicity, are explained and evaluated directly in the methodology section. Afterwards, the soil loss and sediment input outcomes are presented. The results include the spatial distribution of soil loss and sediment input on a yearly and monthly basis but also the calibration of the models concerning the C-Factor.

7.1.1. Soil erodibility factor K

In general, the soil shows a low erodibility factor ($<0.02 \text{ t ha h ha}^{-1} \text{ MJ}^{-1} \text{ mm}^{-1}$) (Figure 7—1*b*). The most erodible soils are located in the northern part of the catchment, which, according to the soil map created from the Brazilian Agricultural Corporation (EMBRAPA) (Embrapa Solos 2007) is dominated by Distrofic Latossol (Oxisol). The results are also aligned with further literature values in that geographic area, which also assessed that the K-Factor for Latossol (Oxisol) is in the range $0.019\text{--}0.026 \text{ t ha h ha}^{-1} \text{ MJ}^{-1} \text{ mm}^{-1}$ (Mannigel et al. 2002; Silva et al. 2009; Duraes et al. 2016*b*; Duraes et al. 2016*a*). The western part of the catchment, which is also dominated by Oxisol, showed low soil erodibility with values reaching up to $0.013 \text{ t ha h ha}^{-1} \text{ MJ}^{-1} \text{ mm}^{-1}$.

As shown in Figure 7—2 the soil has a similar texture pattern throughout the catchment. The silt-clay content of the samples was always above 50%. The sand content in the soil is also relatively high (reaching up to 50% at some locations). Most of the catchment is covered by sandy clay, which has low to average erodibility.

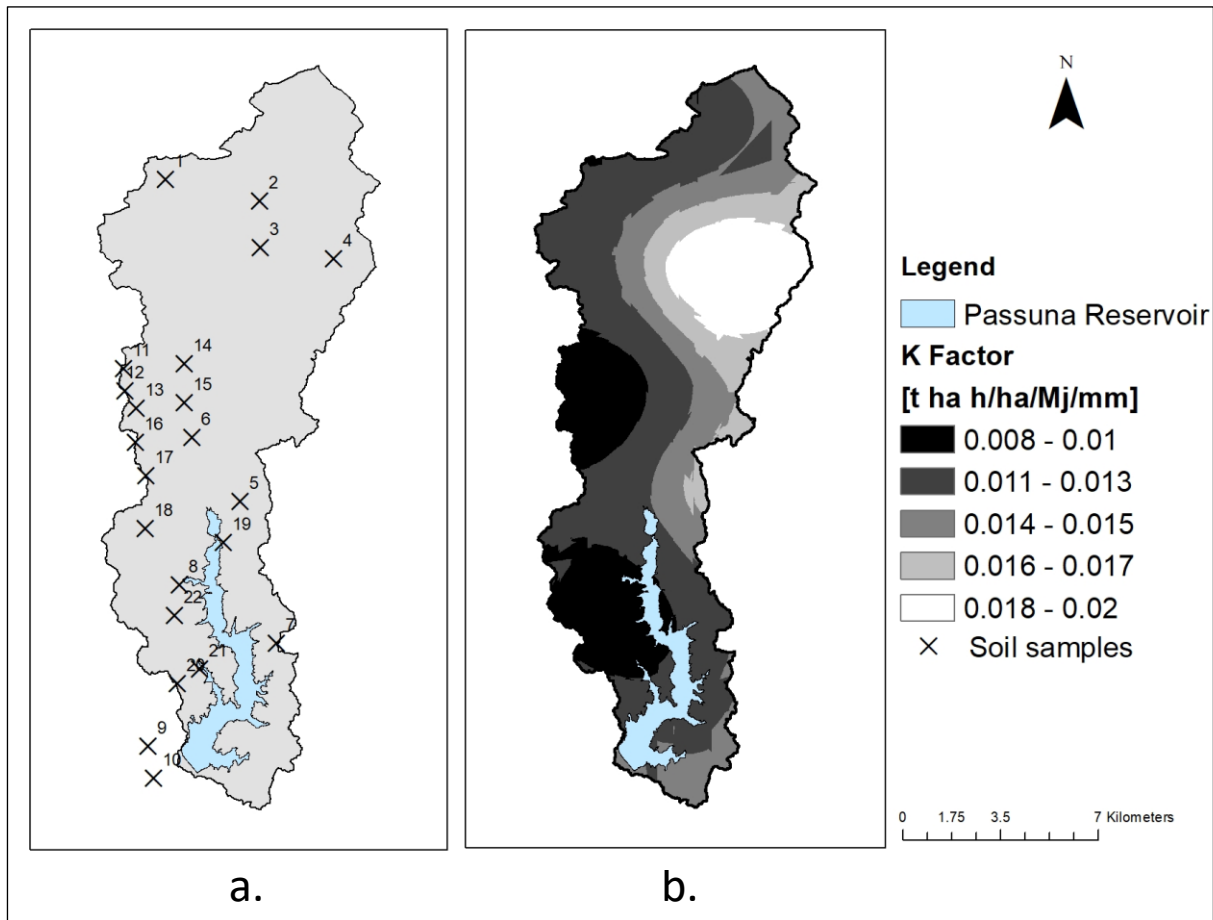


Figure 7—1 a. Location of soil samples. b. Interpolated map of K-Factor.

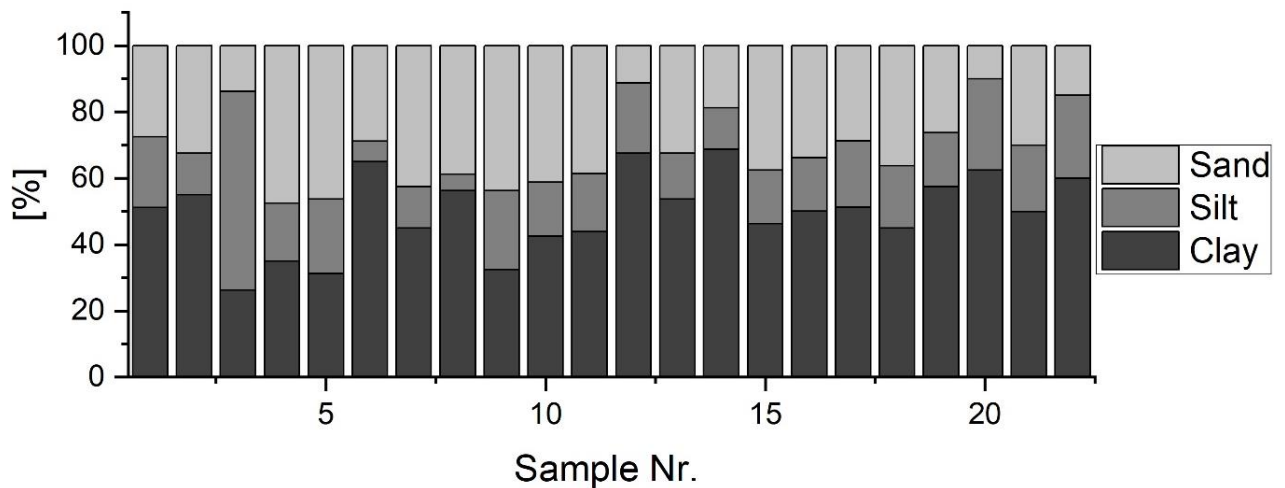


Figure 7—2 Texture of soil samples

7.1.2. Rainfall erosivity factor R

The R-Factor computed based on precipitation data showed different results from the R-Factor calculated by Waltrick et al. (2015). The largest differences are observed in January, April and in October. The data from Waltrick et al. (2015) shows high differences among the months and overestimates substantially for the month of January. The precipitation data from both pluviometric stations show a more uniform distribution from what Waltrick et al. (2015) is suggesting (Figure 7—3). The calculations from Waltrick et al. (2015) include also a margin of error due to the low density of weather stations. In certain regions, these maps cannot represent the rain erosivity when brought in a mesoscale plot. Therefore, for the final calculation of erosion and sediment input the R-Factor calculated from the pluviometric data in the Passaúna catchment was used.

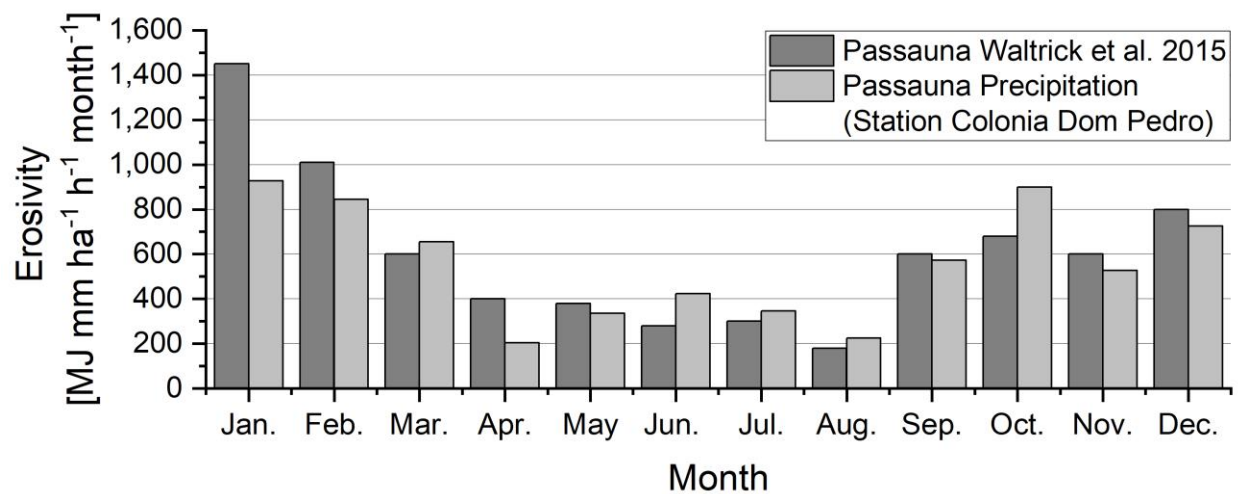


Figure 7—3 Comparison of R-Factor from two approaches:

7.1.3. Cover and management factor C

For each of the available NDVI maps the C-Factor was computed (Figure 7—5). The highest seasonal change in the C-Factor values was observed for cropland (Figure 7—4). Between January and February, which is harvesting time and November, which is seeding time there is a change of almost 100% in the C-Factor. A high interannual change in the C-Factor was also observed in the scrubland/grassland areas. Winter and spring are characterized by a low vegetation coverage while summer and partially autumn by a high vegetation coverage. Forests showed moderate changes mainly because a small percentage of the trees in humid sub-tropic regions lose their leaves during winter. The seasonal change in the forest C-Factors can also be related to the misclassification of certain areas with other LULC into forest class. Pasture and meadow follow a similar land cover pattern. In summer and autumn, the vegetation cover is high while in winter and spring, it diminishes. Bare soil has the smallest changes from all classes.

There is a seasonal change of maximum 0.05 among the months and this can be attributed to the errors of the LULC classification process.

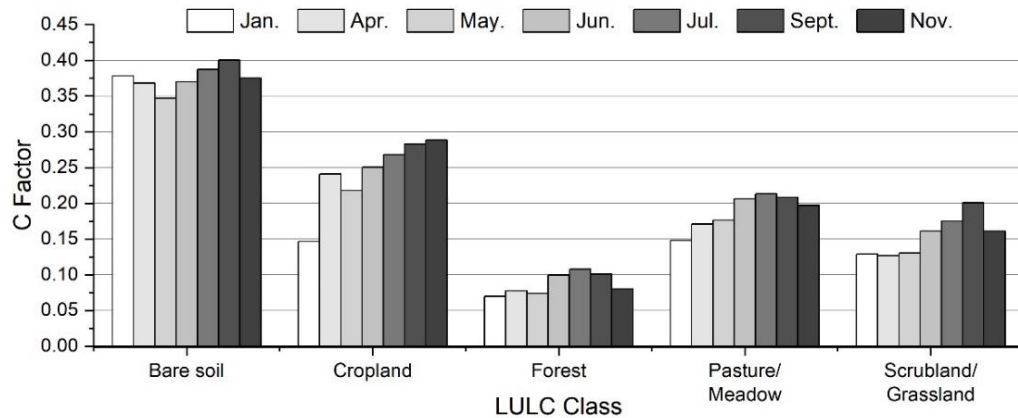


Figure 7—4 Mean C-Factor for each LULC class for all the months where NDVI data is available (Figure A—2 in Appendix). For the other months the C-Factor was interpolated.

The difference among the seasons can be clearly observed also in the spatial distribution of the C-Factor (Figure 7—5). The west area of the catchment, where most of the agriculture activity is located, shows higher values in July than in January. In July, which corresponds to the winter period, the soil is mostly uncovered and has a C-Factor greater than 0.3. In January, which corresponds to summer and wet season, most of the catchment is covered by vegetation. Only sporadic parts of the agricultural areas, which were not planted, have a high C-Factor in January.

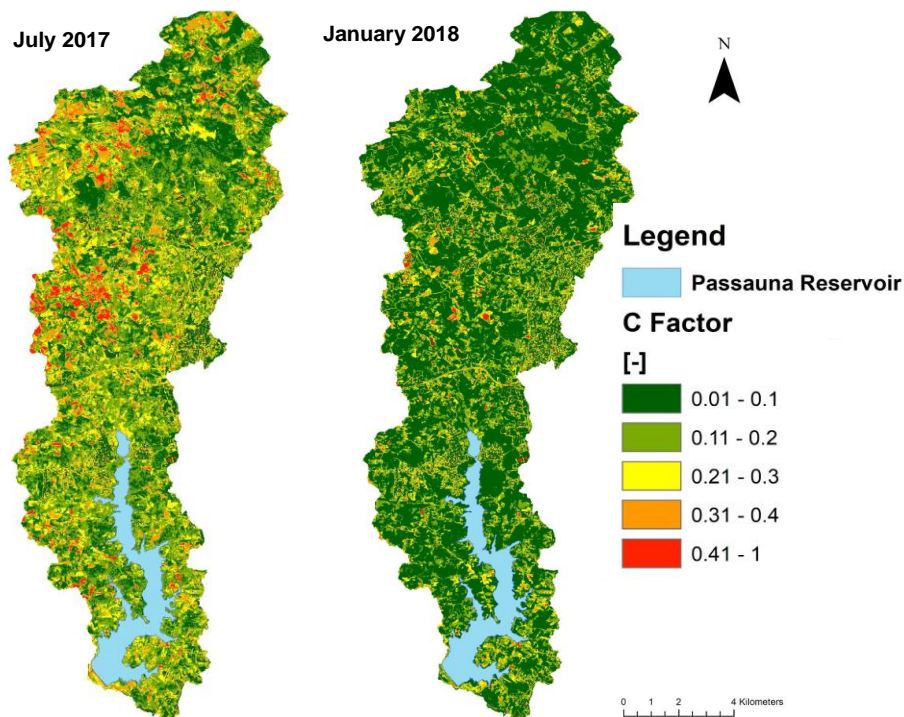


Figure 7—5 Spatial distribution of C-Factor for January and July.

7.1.4. Sediment delivery ratio

Based on the physiographic characteristics of Passaúna catchment the SDR was calculated for each of the investigated months by applying the approach developed by Vigiak et al. (2012) (Figure 7—6). In general, the calculated SDR values could reach values up to 0.15 in the dry months and rarely in some locations above 0.15. The interannual vegetation cover that characterizes the region contributes in having low SDR values throughout the catchment. The highest SDR was observed in unprotected soil areas near the river stretches and in high slopes. The largest part of the catchment has SDR values lower than 7.5% in both dry and wet season. As explained in Borselli et al. (2008) connectivity, thus SDR, vary in both time and space. To define the change in the spatial patterns, the mean SDR was computed from each of the months. The results show low differences between the months. The mean SDR for the dry month July was calculated 6% while for the wet month 5%.

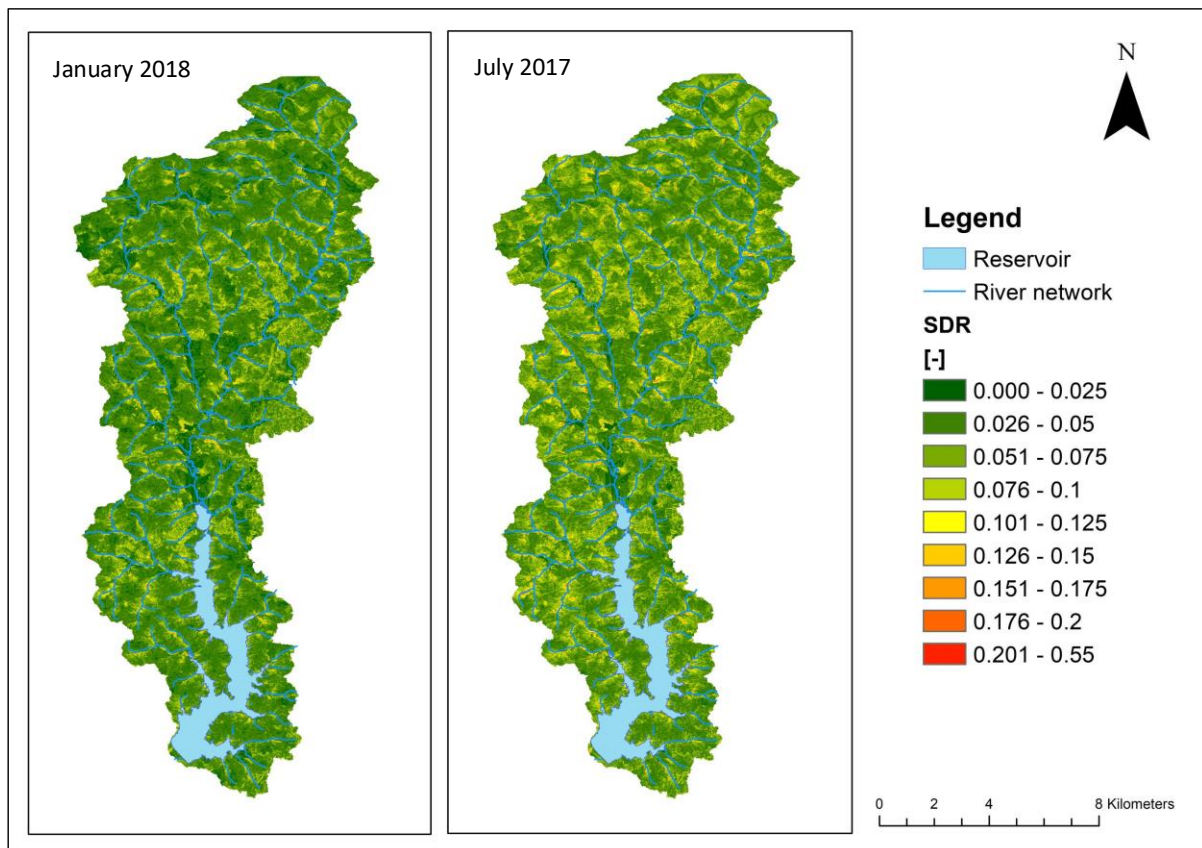


Figure 7—6 SDR for the months of July 2017 and January 2018.

7.1.5. Soil loss and sediment input

The Revised Universal Soil Loss Equation was applied in a monthly time step for the Passaúna catchment for calculating the soil loss. The initial calculation of erosion and sediment input was performed by using the R-Factors derived by Waltrick et al. (2015). The soil loss of all the months was summed to the average yearly long-term soil loss (Figure 7—7). The results show that most of the soil loss is concentrated in the northern part of the catchment, mainly due to the watershed's topography. The largest part of Passaúna catchment (71%) has more than $10 \text{ t ha}^{-1} \cdot \text{a}^{-1}$ of soil loss. Based on the erosion classes defined by Morgan (1979), 35% of the watershed suffers from *High* soil loss, 16% from *Severe*, 18% from *Very Severe* and 2% from *Catastrophic*. Only 16% of the catchment has *Very Slight* erosion, while to the classes *Slight* and *Moderate* correspond respectively only 5% and 7%. A spatial pattern of reduced erosion compared to the other areas can be observed in the urban areas (rectangles in Figure 7—7). Other areas that have very slight erosion, are the floodplains of Passaúna river where due to the flat topography and vegetation cover, minimal soil loss was calculated

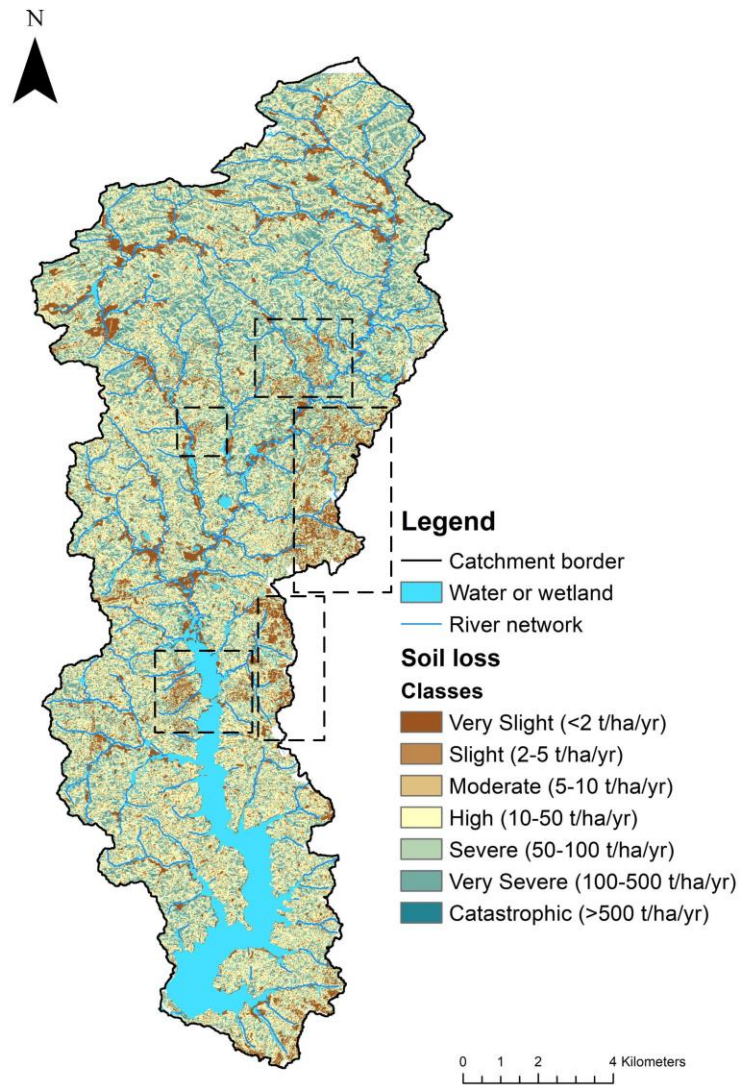


Figure 7—7 Erosion classes in the Passaúna catchment.

reduced erosion compared to the other areas can be observed in the urban areas (rectangles in Figure 7—7). Other areas that have very slight erosion, are the floodplains of Passaúna river where due to the flat topography and vegetation cover, minimal soil loss was calculated

The sediment yield or sediment input from Passaúna watershed was derived by multiplying the soil loss from each month with its respective SDR. When comparing the sediment input source with the LULC specific soil loss (Figure 7—8), it can be observed that they follow a similar pattern. This indicates that the SDR does not play a major role in alternating the spatial patterns of sediment input. By analyzing the origin of sediment in terms of LULC, it can be observed that 75% of the sediment originates from forest and cropland and only 25% comes from pasture/meadow

covered areas, scrubland/grassland or urban areas (Figure 7—8). According to the initial modelling results, the areas, which contribute most in the sediment input, are the forests with 40% of the total sediment input followed by cropland with 35%. The areas that contribute the least in the sediment budget are the urban areas with 7%.

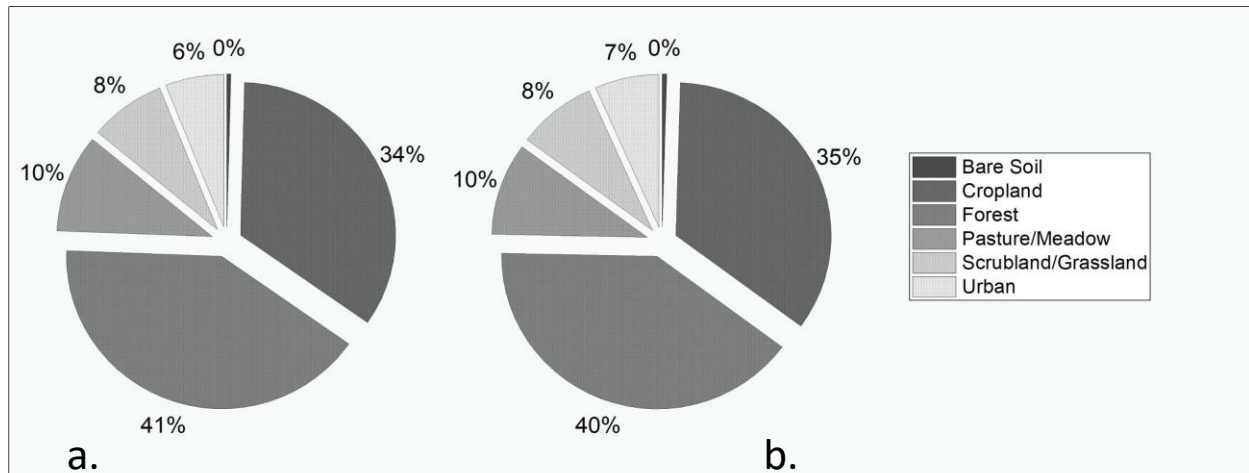


Figure 7—8 a. Contribution of each LULC class to the overall soil loss in the Passaúna catchment. b. Contribution of each LULC class to the overall sediment input in the Passaúna catchment.

Concerning the interannual dynamics of the sediment input, the results show high sediment input in all the wet months (September-March) (Figure 7—9). Most of sediment input occurs in January with 14,000 tons, even though the vegetation cover of the catchment is rather high. In the month of August, despite the low vegetation cover, the overall sediment input from the catchment is the lowest.

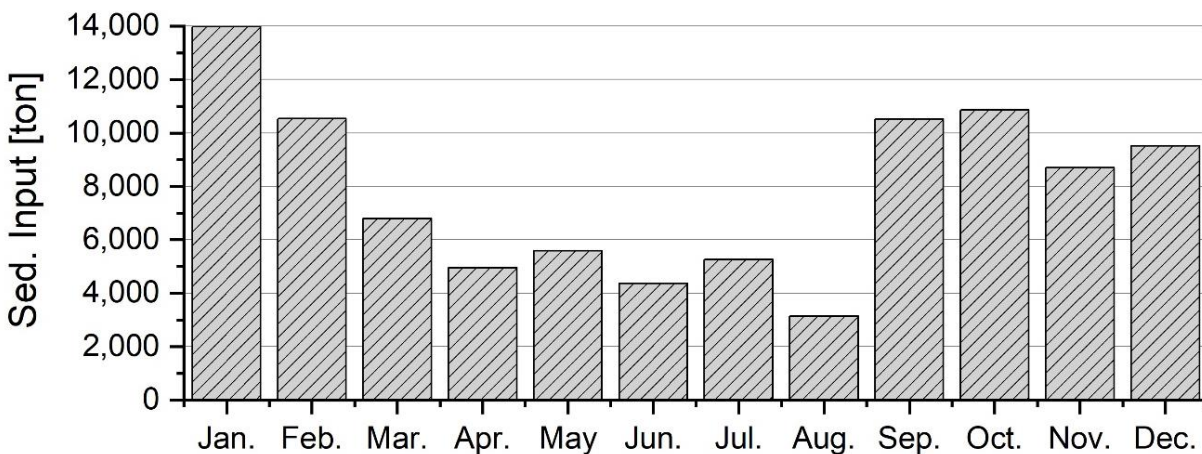


Figure 7—9 Monthly distribution of sediment input from the initial model run.

Based on Figure 7—8 and by comparing the sediment yield distribution to the LULC map (Figure 7—10) it can be observed that high sediment input occurs from the forested areas. The

high share of sediment input from forested areas observed in the above Figure 7—8 cannot be attributed only to the large coverage of forested areas, but also to the actual high specific sediment input calculated from the model. Even in the months of winter, when the precipitation is low, there is significant sediment input from the forested areas. The findings suggest an overestimation of a specific RUSLE factor. By comparing the mean value of the calculated C-Factor for the forest areas in Passaúna catchment with literature values, it can be assessed that the C-Factor is significantly overestimated (Figure 7—11). The average C-Factor found in literature (Table 6—4), is almost 20 times lower than the calculated C-factor values during the months of July and October (Figure 7—11). The values of *Max.* and *Average* in Figure 7—11 refer to the maximum C-Factor found in the extensive literature review by da Silva Santos (2019) (in Figure 7—11 *Min=0*). The approach developed from Durignon et al. (2014) seems to overestimate the C-Factor in forested areas (around 20 times). Therefore, an arbitrary correction factor of 0.05 was applied to the C-Factor by multiplication. This value of 0.05 was chosen as the calculated values of C-Factor were 20 times higher than the average C-Factor of forest areas in that region. Furthermore the new R-Factor, calculated from the pluviometric data was also included in the new equation for giving the final results shown in Figure 7—12 and Figure 7—13 (spatial distribution for all months in Figure A—4 in Appendix).

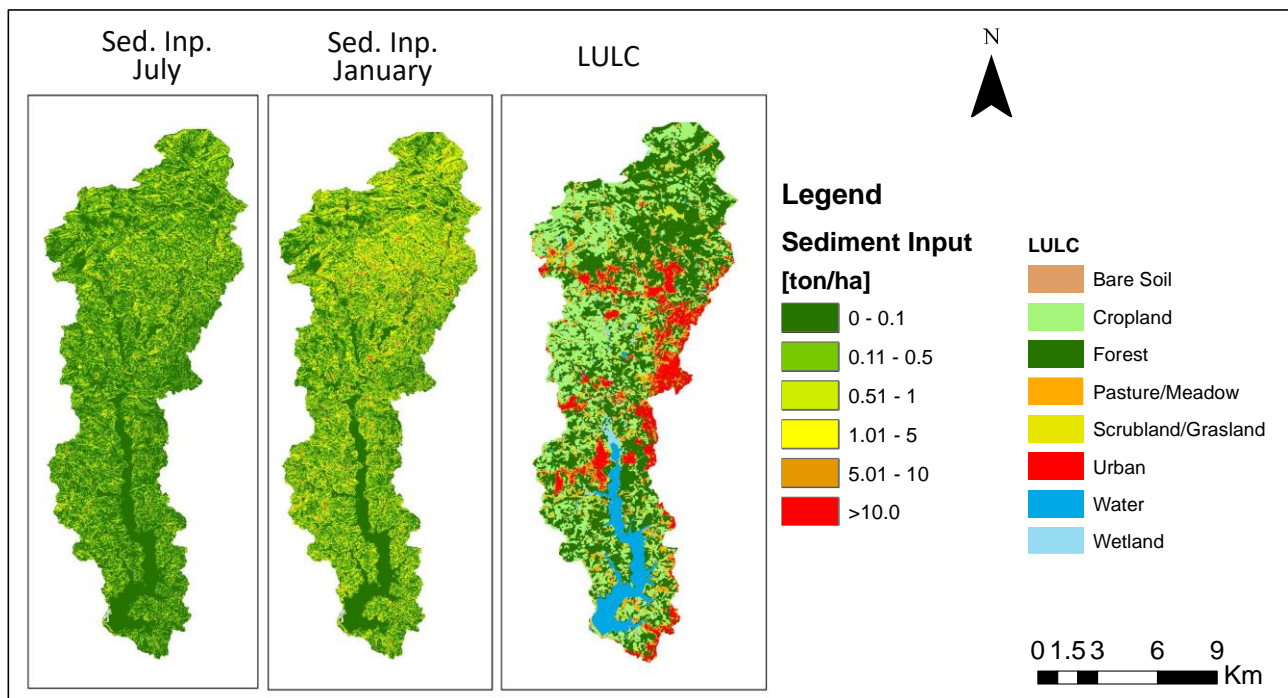


Figure 7—10 Comparison between initial model run and LULC.

The C-Factor correction decreased the overall amount of sediment input in the Passaúna reservoir by 30% from an initial 94,300 ton a⁻¹ to 57,300 ton a⁻¹. After the inclusion of the new R-Factor calculated from the daily precipitation data, the sediment input decreased a further 5% to 54,800 ton a⁻¹ (Figure 7—13b). The use of the new R-Factor shifted also the seasonal dynamics of the sediment input. The final calibrated model indicates that the most important month in terms of sediment yield is not January but October (Figure 7—13a). The month with the lowest input is April and not August, as it was in the initial model results. The spatial distribution of sediment input is changing significantly between the last model run (C&R correction) and the initial model run (Figure 7—12 and Figure A—13). The sediment input from forested areas is reduced substantially in the final model to less than 1000 kg ha⁻¹ a⁻¹. For the overall operational time of Passaúna reservoir (30 years), the accumulated sediment stock should be approximately 1.64 x 10⁶ tons.

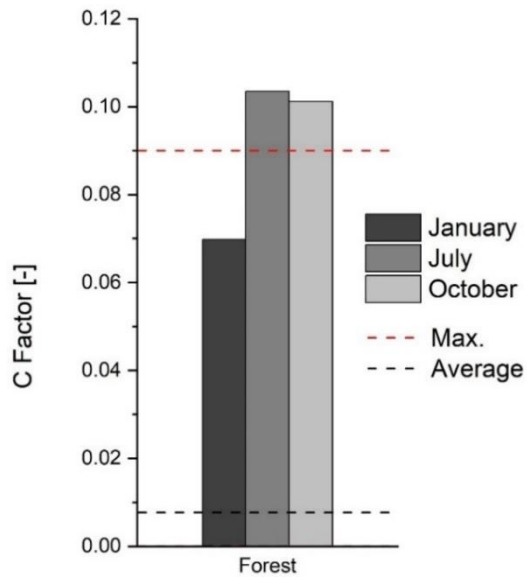


Figure 7—11 Comparison of C-Factor to maximum and average values found from literature.

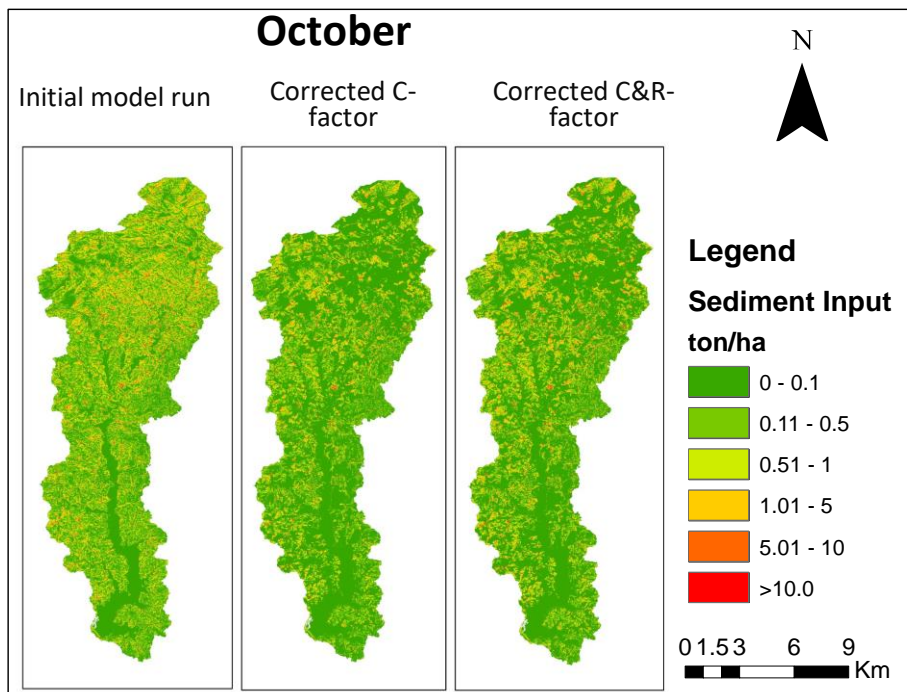


Figure 7—12 Final distribution of sediment input after C and R-Factor correction.

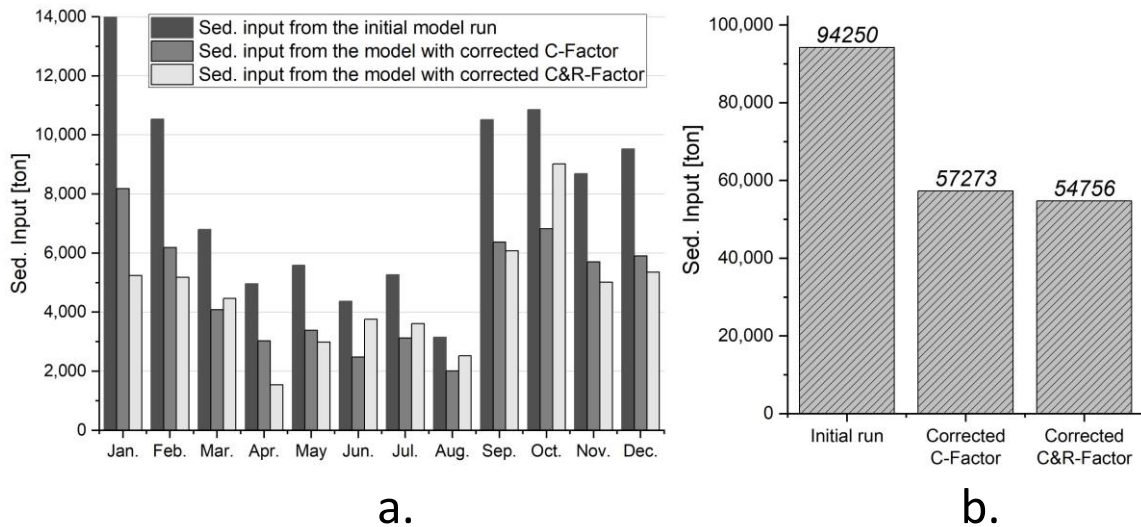


Figure 7—13 a. Comparison of interannual dynamics of the system. b. Comparison of the yearly sediment input from three modelling approaches.

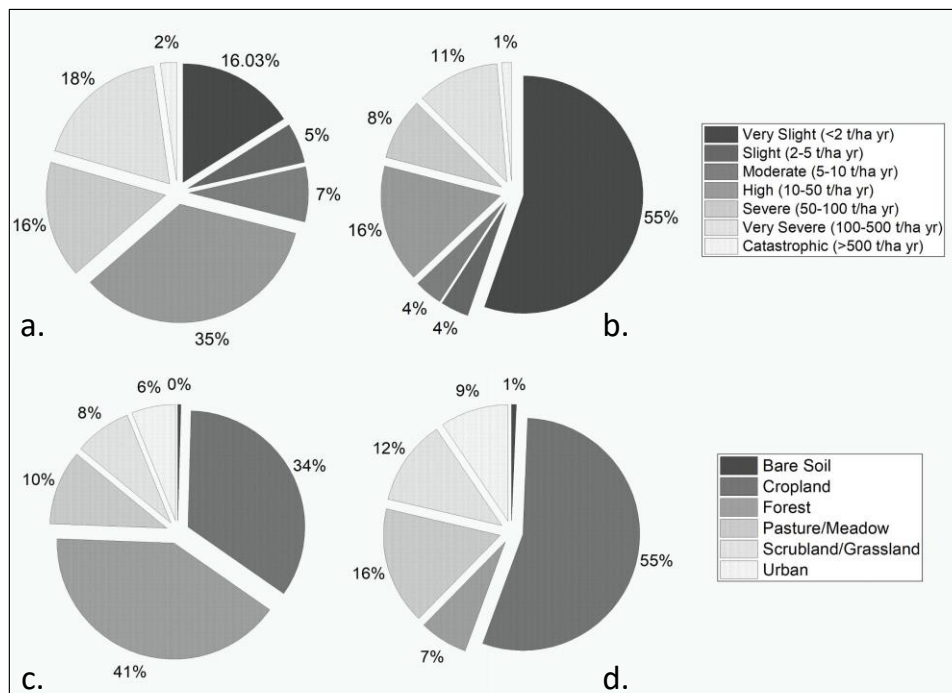


Figure 7—14 a. Erosion classes before C and R-Factor correction. b. Erosion classes after C and R-Factor correction. c. origin of sediment before C and R-Factor correction. d. origin of sediment after C and R-Factor correction.

As it can be observed from Figure 7—14c. and Figure 7—14d., with the final calibration of the model, the cropland is the most important source of sediment (55% of the total sediment input), while sediment input from forest decreased by 34% to a final share of 7%. The final calibration shifted also the erosion classes (Figure 7—14a and Figure 7—14b), where more than half of the catchment (55%) has very slight erosion compared to the 16% in the initial model run.

7.2. Sediment volume and distribution in the reservoir

In this section a synopsis of the most important results from the reservoir surveying is given. The results include the outcomes of the sediment sampling (groundtruthing), hydroacoustic surveying (multibeam, linear system and parametric sub-bottom profiler), and DFFP deployments. The results are not only focused in performing volumetric measurements and calculations but also in defining the physical properties of the lake bottom. The results presented in this section will be used as a validation to the modelling results from the previous section.

7.2.1. Sediment sampling and analyzing

In total, eight grab samples and 23 sediment cores were collected from the inflow to the dam with an average core length of 46 cm (Figure 7—15). The longest core is C14 with 92 cm length, while the shortest core is C2 (12 cm), whose location is characterized by relatively high flow velocities and as a result has little sediment accumulation.

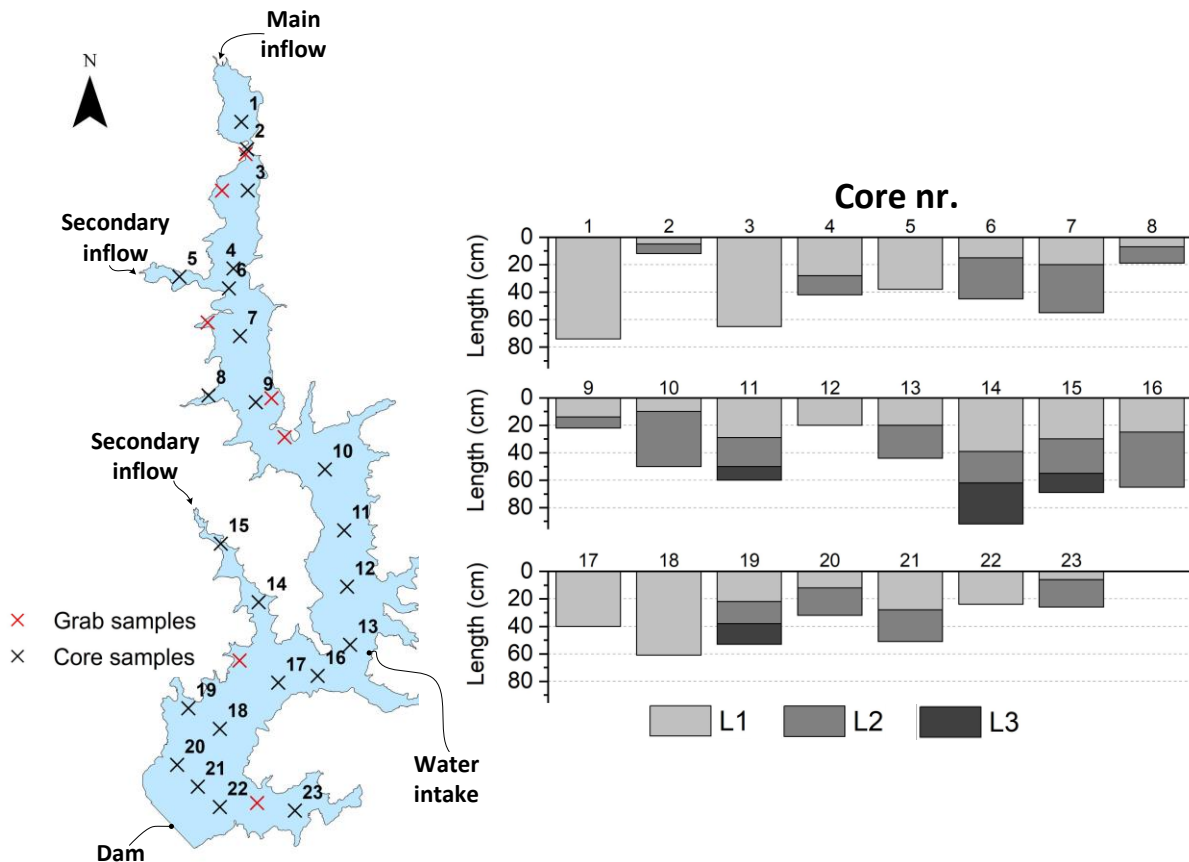


Figure 7—15 Location and length of core samples in the Passaúna reservoir. L1, L2 and L3 refer to the layers encountered in the cores.

The sidarm where C14 was sampled is collecting the water from a hydrological catchment with intense agriculture and potential erosion. Therefore, both C14 and C15 were longer than the average. Most of the cores that are longer than the average (C1, C3, C7, C11, C16, C18 and C21) are located in the center of the thalweg. This fact suggests that most of the sediment is stored in the central part of the reservoir.

Most of the cores consist of unconsolidated, fine-grained low-density material. The deep areas (>8 m) had WBD values lower than 1 g cm^{-3} , due to voids filled with free gas. In the shallow parts, the WBD reaches values up to 1.6 g cm^{-3} (Figure 7—17). The average WBD of all the sediment samples is 1.12 g cm^{-3} . Including also the information from seven grab samples, 19 out of 30 samples consisted in more than 95% of silt-clay material (<63 μm) (Figure 7—17) (Sotiri et al. 2019b). The material includes also a high fraction of organic material with an average of 17%. The maximum LOI was measured in C18 (50.9%) and the lowest for the grab sample G7 located in an area with high flow velocities, at a distance of five meters north of C2 (8.4%). The sediment properties are visualized in Figure A—8, Figure A—9, and Figure A—10 in the Appendix section.

Finally, the relation between the three sediment parameters was investigated. As shown in Figure 7—16a, there is a direct linear relation between granulometry and WBD. Low silt-clay fraction in a sediment core, corresponds also to high density of the sample. Such a fact is to be expected as the granulometric distribution is one of the principal factors affecting density. Sand has a density fluctuating between $1.5\text{--}1.6 \text{ g cm}^{-3}$, while clay and silt in the range of 1.2 g cm^{-3} (Yu et al. 1993).

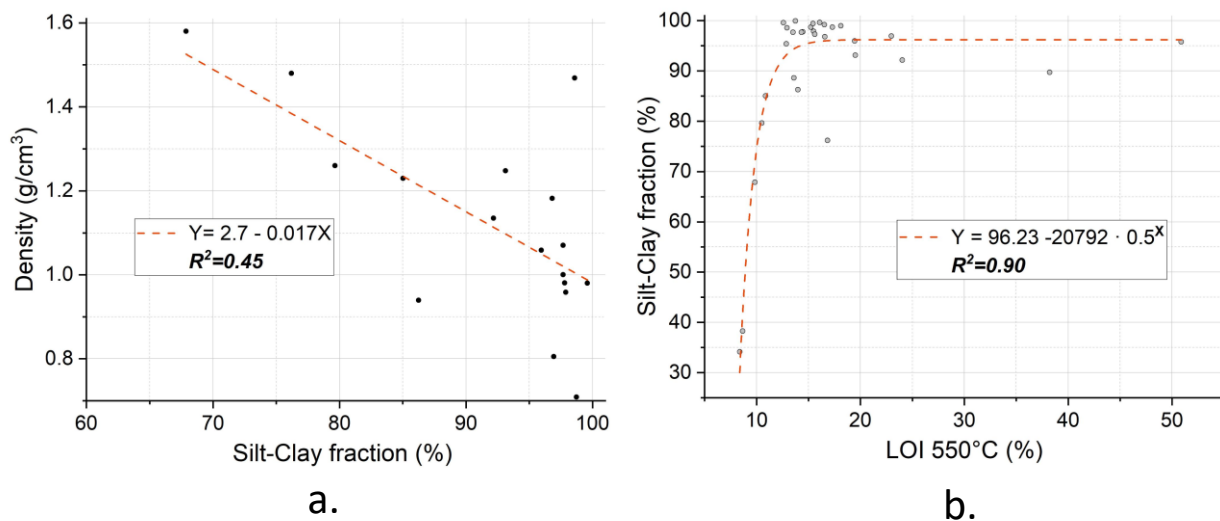


Figure 7—16 a. Relation between silt-clay fraction and density. b. Relation between LOI and silt-clay fraction.

The relation between LOI and silt-clay fraction on the other hand is more complex (Figure 7—16b). A change in LOI does not fully reflect the changes in the grainsize distribution. Until an

LOI of 12–13%, the two parameters follow a direct relation. Afterwards a change in LOI is not reflected in the silt-clay fraction. In the first part of the graph, the silt-clay fraction increases with an increase of LOI. After this point, the silt-clay fraction remains constant. Therefore, for the Passaúna reservoir, an increase in LOI above the 13% threshold will most probably not affect the diffractation between silt-clay fraction and sand. This fact suggests that if in a sample the LOI is expected to be more than 13% then the sample will be dominated by fine grain material, most probably to a fraction of more than 90% and vice versa.

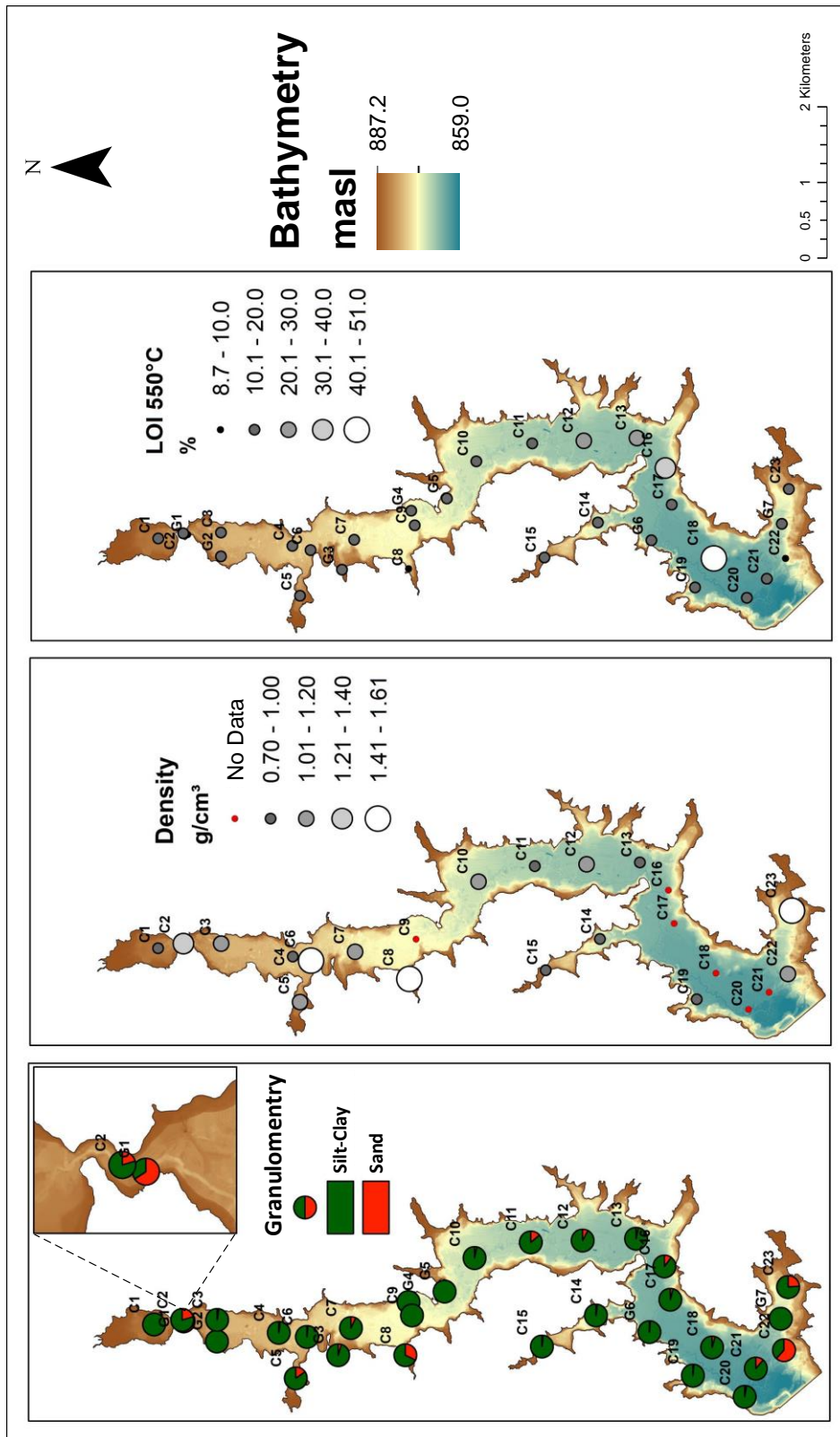


Figure 7—17 Sediment properties in Passaúna reservoir.

7.2.2. Topographic differencing from multibeam data

A bathymetric map with a 20 cm raster resolution and a 3-D model were created after performing the multibeam survey (Figure A—5 in Appendix). Based on the bathymetric data also a new Elevation-Storage Curve (ESC) of the reservoir was derived (Figure 7—18). The dead storage is 19.5 hm³ out of 69.3 hm³, which is the overall storage capacity of the reservoir at normal operational level (887.2 masl). The elevation of the bottom outlet is at 869.1 masl, and for normal operation level, it means a maximum depth of 18.1 m.

The comparison of the actual ESC with the former ESC shows that the actual volume at some depths is larger than at the time of impoundment. Either erosion took place at those locations during 30 years of the Passaúna operation or the accuracy of the older ESC is insufficient for comparison and derivation of sedimentation volumes. Since, the flow velocities in the reservoir are significantly lower than the velocities required for eroding the pre-impoundment soil, erosion can be excluded as the cause of the local sediment deficit.

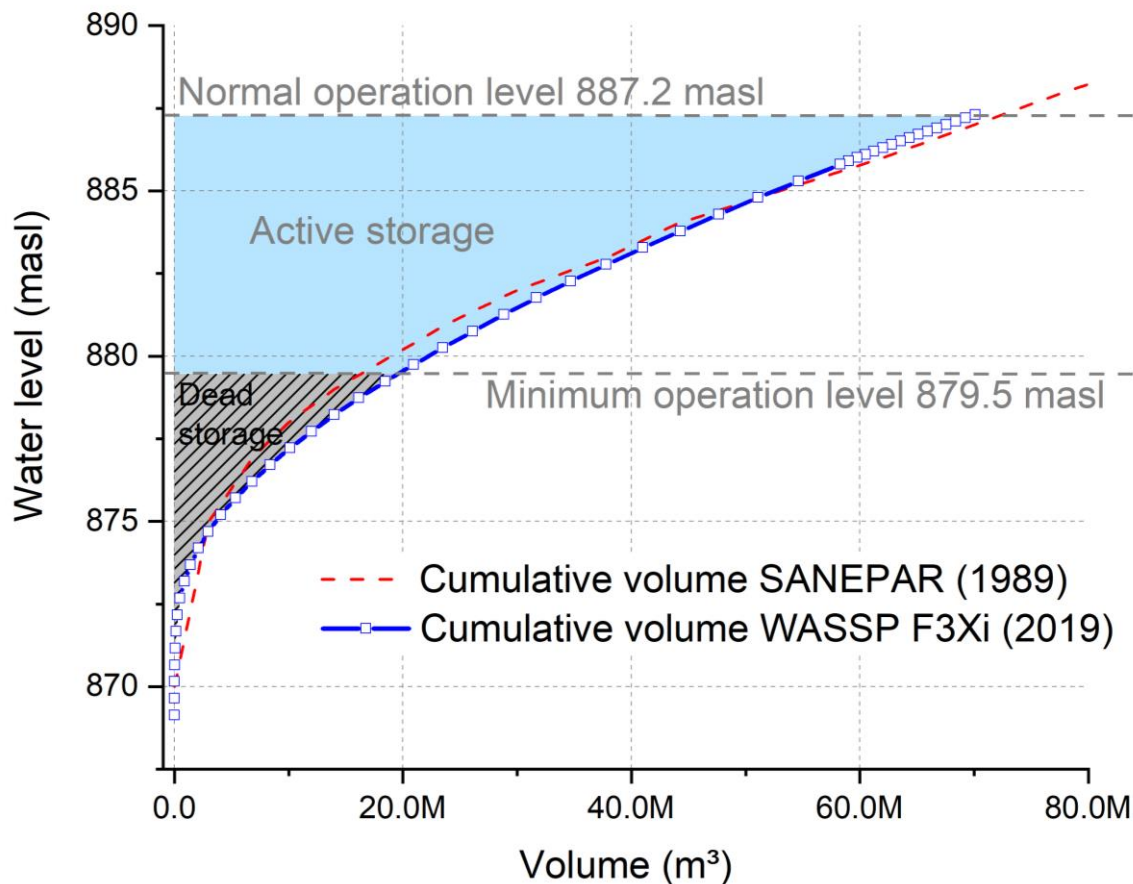


Figure 7—18 Comparison between Elevation-Storage curve derived from the WASSP multibeam system, and the existing curve.

7.2.3. Sediment magnitude (SBP and EA400)

Parametric hydroacoustic system SES2000 Compact

Passaúna catchment has a high anthropogenic influence. This results in a high nutrients input in the Passaúna river and subsequently in the Passaúna reservoir (shown by the high LOI of the sediment in Figure A—10). The high organic matter input and the high temperatures occurring, is a hint that significant gas production can be expected. The presence of high gas contents in the sediment was a major restriction in the application of sub-bottom profiler. As shown in Figure 7—19, the increase of gas concentration in the sediment resulted in a reduced sound penetration. At locations where the gas presence was minimal, the pre-impoundment bottom could be easily detected. When surveying gas-rich areas, the signal to noise ratio decreases and the pre-impoundment bottom becomes undetectable so no usable information could be obtained (Figure 7—19). The lack of sufficient penetration in the presence of gassy material is common for the sub-bottom profilers (Schneider von Deimling et al. 2013; Tóth et al. 2014; Tóth et al. 2015). High gas content in the sediment of Passaúna reservoir is reported from several studies. Marcon et al. (2019) reported gas ebullition events up to $600 \text{ ml m}^{-2} \text{ d}^{-1}$ in certain areas of the Passaúna reservoir while Hilgert et al. (2019c) reported a potential methane production of 17.16 ml d^{-1} for each liter of sediment in some areas. The presence of gas was also frequently visually observed during the survey through the entire area of the reservoir and in most of the retrieved sediment cores (Figure 8—4). Therefore, neither any spatial sediment distribution patterns nor the sediment volume could be derived from the parametric system.

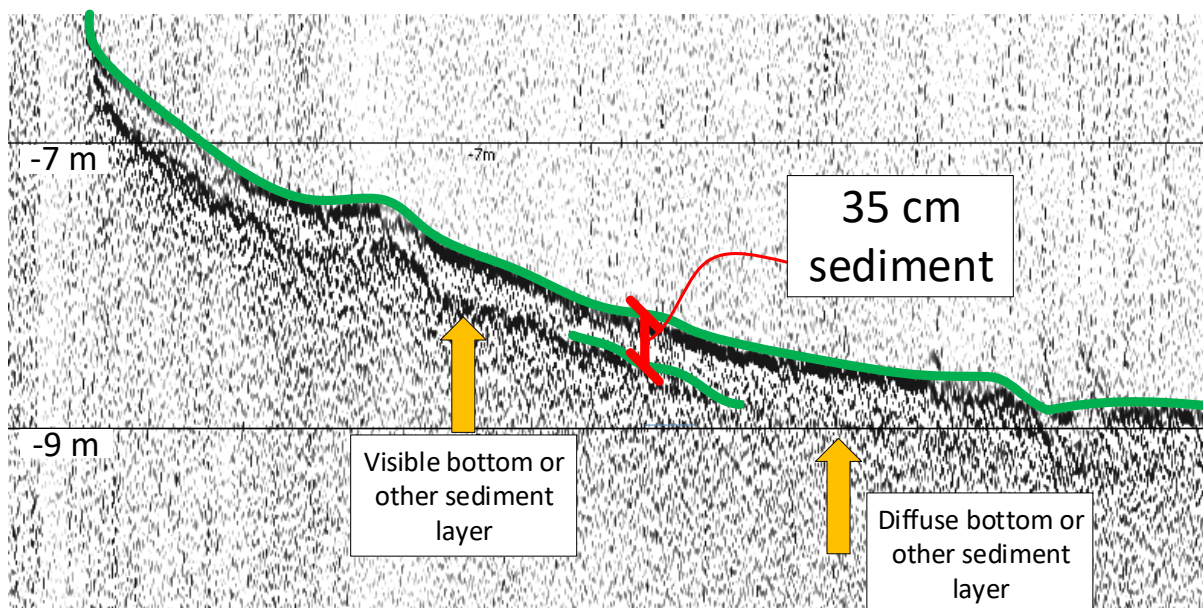


Figure 7—19 Lack of penetration and acoustic turbidity due to gas presence in the sediment.

Linear single-beam hydroacoustic system EA400

As shown in Figure 7—20a-b, most of the reservoir has more than 30 cm of sediment thickness. The calculated average sediment thickness is 36 cm. The highest accumulation is observed in the southern part of the reservoir, closer to the dam. In these areas, the sediment can reach up to 1 m above the pre-impoundment soil. Areas with more than 1 m of sediment are almost inexistent and can be found only in some limited locations.

The total sediment volume accumulated in the reservoir based on the hydroacoustic survey with the EA400 (dual frequency approach) is 2.47 mil. m³. According to this measurement, the Passaúna reservoir has lost 3.4% (0.11% per year) of its total volume during its 30 years of operation.

For the 38 kHz frequency wave, a pulse length of 0.512 ms corresponds to a vertical resolution of the echogram of 9.6 cm. Therefore, errors associated with the accuracy of the device can reach up to 9.6 cm (27% of the mean interpolated value). When comparing the sediment magnitude from the EA400 at the static profiles (core locations) to the interpolated values at the same locations, a mean absolute error (MAE) of 15 cm was calculated (minimum absolute error 2 cm, maximum absolute error 48 cm, normalized mean absolute error (NMAE) of 42%). In this value, the errors associated with the device accuracy are also included.

In most of the points (68%) the interpolated values are lower than the sediment thickness values derived from the static profiles from the same system.

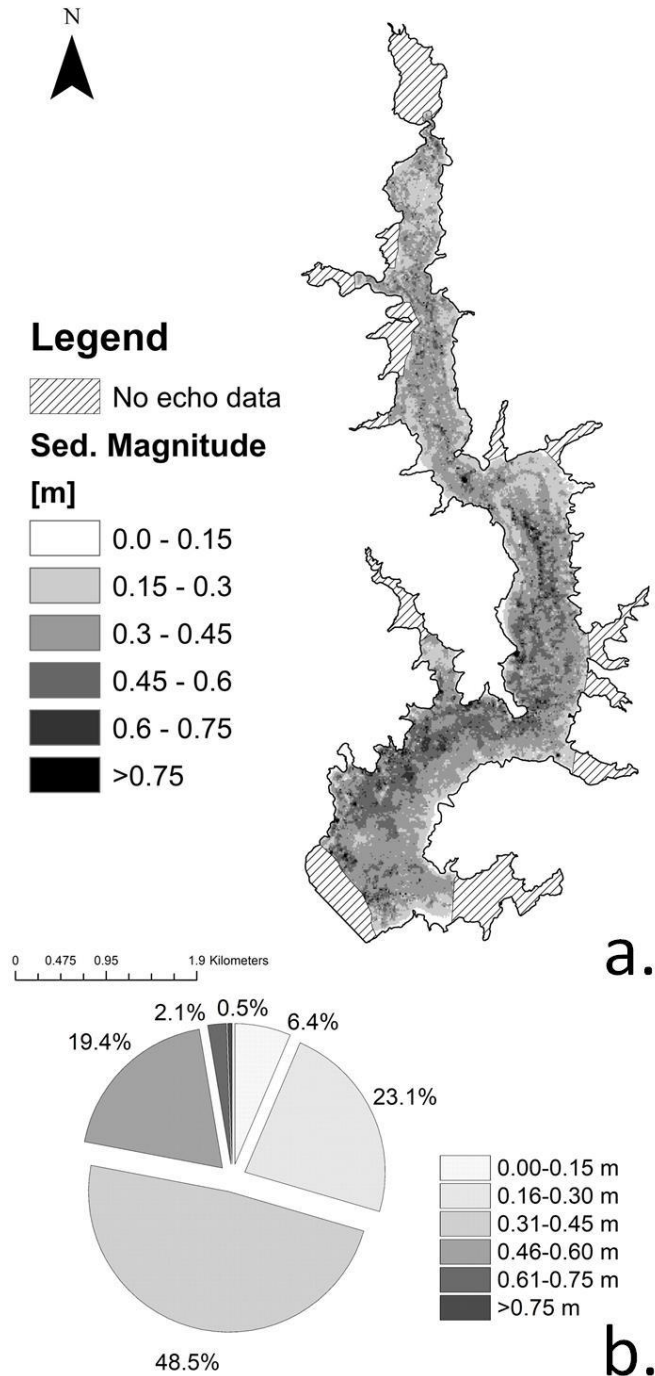


Figure 7—20 a. Sediment thickness derived from the double frequency approach. b. Frequency distribution of the sediment thickness classes from the map

7.2.4. Sediment classification (EA400)

From the results of the classification approach from Sotiri et al. (2019a), classes A, B, and C were the most widely detected in the reservoir (Figure 7—21a). Most of the reservoir is covered with gassy sediment apart from the northern side. The area covered in sediment is both class A and class B. Class A is concentrated more in the deep central parts of the reservoir and near the intake. The presence of class A indicates the presence of soft material on the top layer, which might include either a fluid mud layer or the presence of vegetation. Class B existence implies the existence of thick sediment layers rich in gas and this is the most common class in the reservoir coverage.

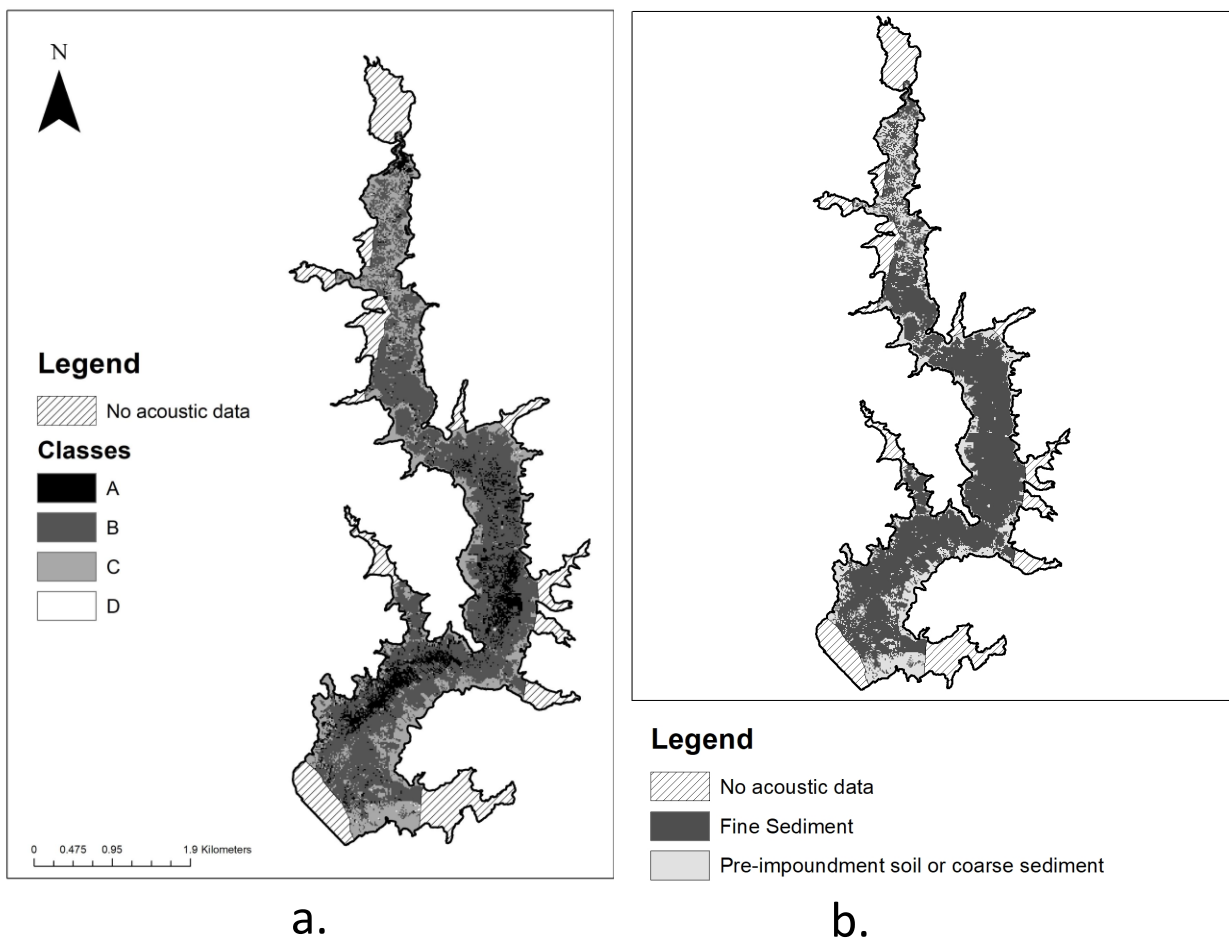


Figure 7—21 a. Sediment classification in Passaúna reservoir, where:
 A. Thick sediment layer. Soft non-gassy material in the first 80 cm.
 B. Thick sediment layer. Soft gassy material in both top and bottom layer
 C. Coarse material. Often Pre-impoundment soil or sandy sediment.
 D. Thin sediment layer. Very compacted or gassy top layer.
 and b. Differentiation between areas with and without sediment.

When approximating the shoreline of the reservoir, C is the dominant class. This is an expected result as near the shore the slope and the elevation of the bottom are increasing. In the northern part of the reservoir prevails also class C even though it is unclear if sandy sediment is present or pre-impoundment soil.

The classes A and B were grouped together in one class while the classes C and D in another one and are visualized in Figure 7—21b creating a map of where sediment is deposited and where not.

The other classification approach used, relied directly on the correlation of single physical parameters with the acoustic properties of the sound wave derived from the First Echo Division Method (Table A—1 and Table A—2 in Appendix). For all the frequencies and configuration a correlation matrix was derived (from Table A—3 to Table A—10 in Appendix). The best correlating configuration was the Configuration B, which was also the configuration of the driven lines. The best two regression analysis are presented in the below graph. For the 200 kHz the best correlating parameters were LOI and AttSv1 while for the 38 kHz the silt-clay fraction of the sediment sample with the AttDecSv1. The former set of parameters performed better than the later with an $R^2=0.66$ compared to the later ($R^2=0.31$)

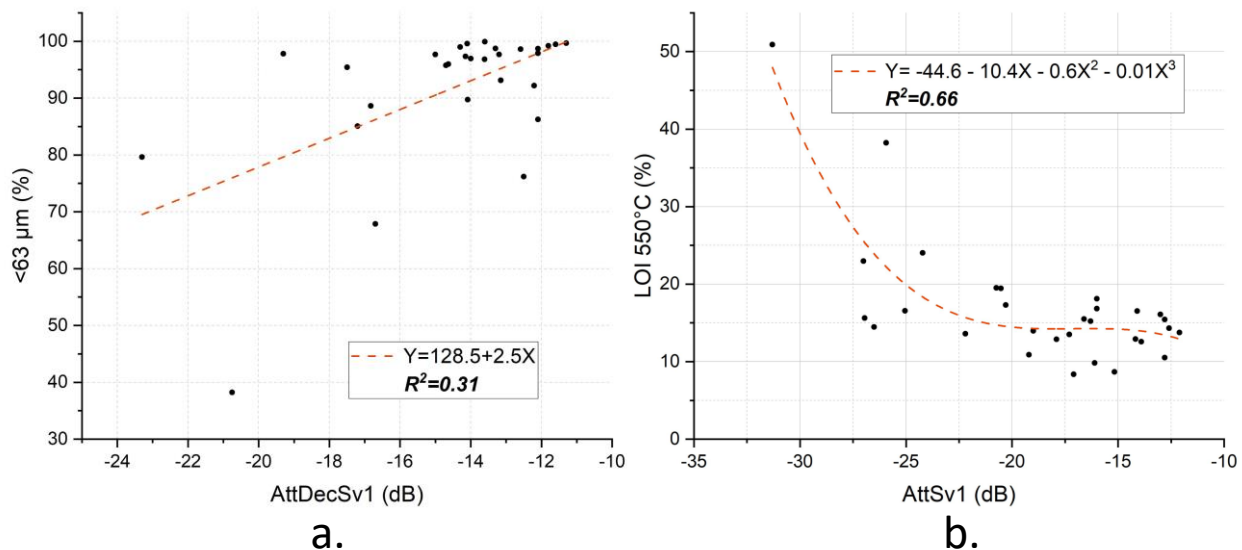


Figure 7—22 a. Relation between AttDecaySv1 and silt-clay fraction of the sample. b. Relation between AttSv1 and Loi of the sample.

Figure 7—22a indicates that a higher value of AttDecSv1 implies also a high silt-clay content, thus bulky sediment. High AttDecSv1 values are found in elongated echo envelopes due to the high volume backscatter from the bulky and relatively thick sediment layer. The bulky sediment in Passaúna reservoir is a mixture of fine-grained material with low WBD as shown in section 7.2.1. The relationship between the acoustic parameter and the silt clay fraction is also a representation

of the above description. With increasing AttDecSv1 from the sediment, also the silt-clay content should be expected to increase, as the sediment should be more bulky.

Figure 7—22*b* on the other hand, indicates a low organic share in the sediment with high acoustic response from the first 19 cm of the sediment. High acoustic response, thus high hardness, is often a characteristic of sediment matrix with large mineral share and less organic content, thus lower LOI. High LOI is often an indicator of gas content, which cause a major interference in the acoustic results. A logical explanation would be the existence of an unconsolidated first layer (fluid mud or vegetation) that does not allow the formation of large void structures due to its consistency or the gas voids are present in the deeper layers of the sediment. The nonlinear polynomial fit suggests that the acoustic response is able to easily capture the changes in LOI in the range 15%–50%, while the changes below the 15% are not easily detectable due to the bias created from the gas content and the low sensitivity of the hydroacoustic system. The equations derived from the linear and nonlinear curves in the above graphs (Figure 7—22) were applied to the acoustic parameters from the driven profiles. The points were interpolated via the IDW technique and the results are presented in Figure 7—23.

The LOI map shows a similar pattern with the map derived from the classification approach in Figure 7—21*a*. The material rich in organic content is concentrated in the areas near the intake and in the southwestern part of the reservoir. Most of the sediment in the reservoir (53.5% of the reservoir coverage) has an organic share between 10% and 20%. Visible is a high LOI in a large part of the reservoir. If compared to the sediment information in Figure 7—17 there is an obvious bias, as the sediment in the areas with LOI more than 50% do not show the same trend. Most of the sediment samples in these areas had a LOI in the range of 10-20%. As seen in Figure 7—22*b*, the AttSv1 values can describe the changes in the LOI up to a value of 50%. Therefore, the equation cannot be extrapolated to AttSv1 values lower than 31.3 dB. For applying the equation also to the areas with more than 50% of LOI, further points AttSv1-LOI need to be generated in order to extend or calibrate the polynomial fit.

The spatial distribution of silt-clay fraction in the sediment presented in Figure 7—23*b*, showed also the considerable limitations of the classification approach. According to the classification results, more than 90% of the reservoir area is covered by sediment with a silt-clay fraction less than 80% and only 4% of the reservoir area is covered by material dominated by fine grainsize. From groundtruthing, only 5 of 30 samples had a silt-clay fraction of less than 80%. In this case, the discrepancies in the result have to be attributed to the low R^2 of the regression analysis between the sediment properties and the acoustic parameters.

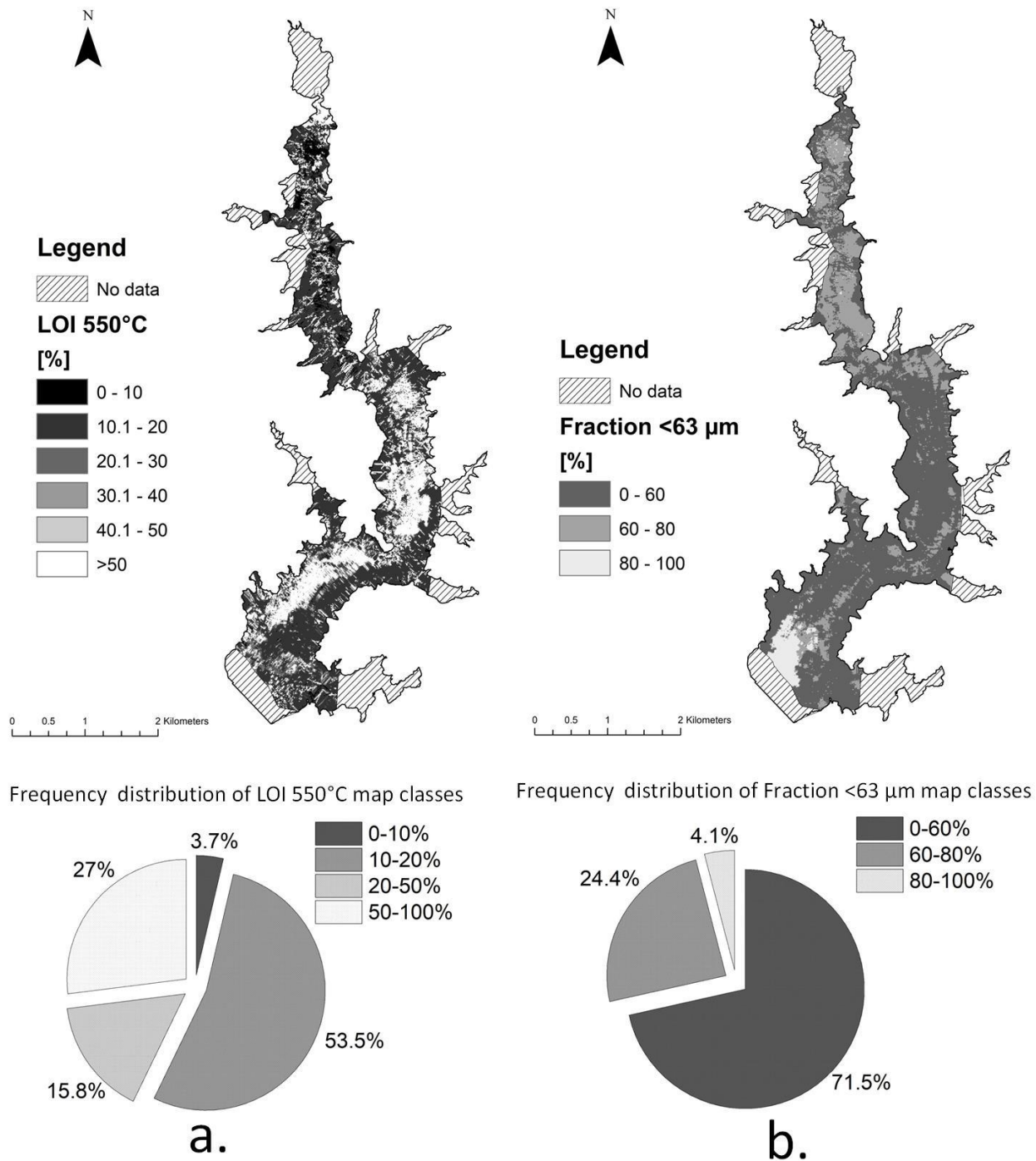


Figure 7—23 a. Mapping of LOI based on the regression analysis of Figure 7—22b. and the frequency distribution of the classes in the map. b. Mapping of Silt clay fraction based on the regression analysis of Figure 7—22a. and the frequency distribution of the classes in the map.

7.2.5. Dynamic freefall penetrometer (Graviprobe)

The GP was deployed at 134 points in the Passaúna reservoir (Figure 7—25a). From the behavior of the dynamic cone penetration resistance, it was defined that a DCPR of 200 kPa is an orientation threshold for discriminating between sediment and pre-impoundment soil. Furthermore, each abrupt change of slope in the curve can be linked to a change in sediment material, thus with a new layer (Figure 7—24). Based on the GP measurements, in the reservoir the sediment thickness ranges from 0 m to 1.8 m, with an average of 0.57 m (Figure 7—25a). As mentioned before, an IDW interpolation technique was applied to the data for having the spatial distribution of sediment thickness. The interpolated values at the measurement locations were compared with the value from the GP measurement. A NMAE of 22.8% (ranging between -97–105%) was calculated due to the interpolation.

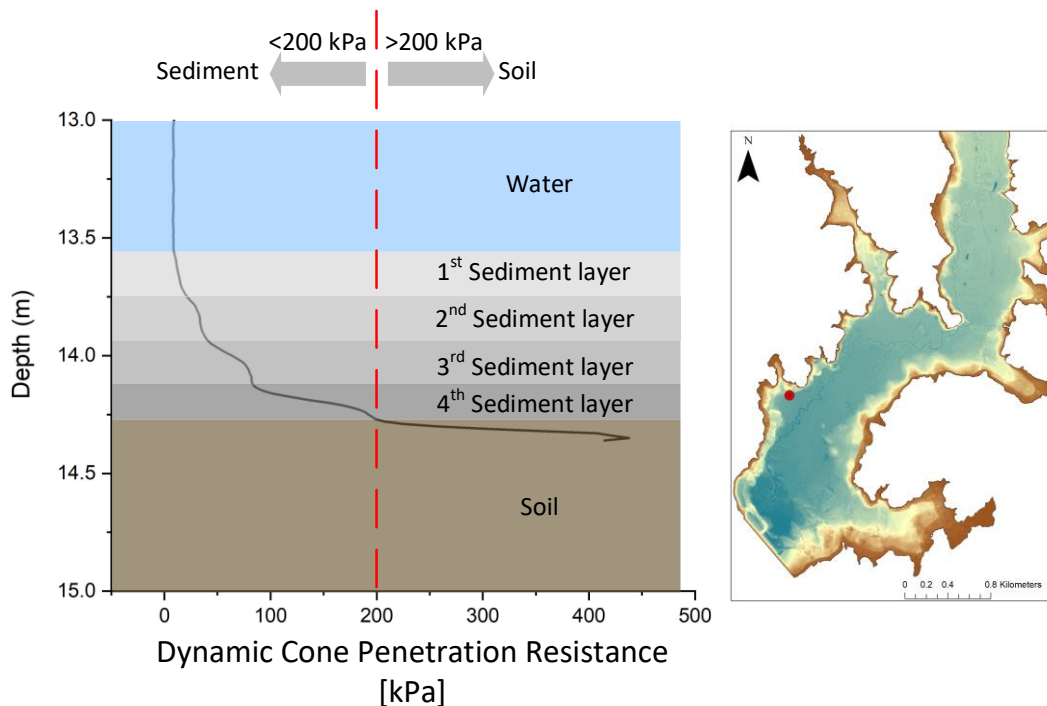


Figure 7—24 Definition of sediment thickness based on DCPR results from the GP. Several measurement locations showed that approximately 200 kPa is an orientation value for the boundary between sediment and pre-impoundment soil in the Passaúna reservoir.

As it can be observed from the cross-section profile (Figure 7—26) the sediment is concentrated more in the thalweg and less at the sides. In the longitudinal direction (Figure 7—27), the sediment accumulated mostly in the deep part near the dam. Another sediment hotspot is the inflow of the reservoir. In the entrance area south of the Ferrara Bridge, the sediment is accumulated up to 1.8 m. In these areas (upstream and downstream the Ferrara Bridge), the high velocities and the incoming turbulence from the river are reduced and the larger particles settle. There are also some sporadic accumulation areas in the central part of the

reservoir, where the sediment can reach up to 1 m thickness. Nevertheless as shown in Figure 7—25b, in most of the reservoir (53% of the reservoir bottom) the magnitude is in the range of 0.3 to 0.7 m. The interpolation results show an overall sediment volume in the reservoir of 3.36 hm³. This volume corresponds to 4.6% of Passaúnas initial volume. According to the GP results, the average siltation rate in the Passaúna reservoir is 0.15% or 112,000 m³ per year. Based on the sediment sampling results the sediment has an average density of 1.12 gr cm⁻³. Therefore, the total mass of sediment in the reservoir is approximately 3.8·10⁶ tons.

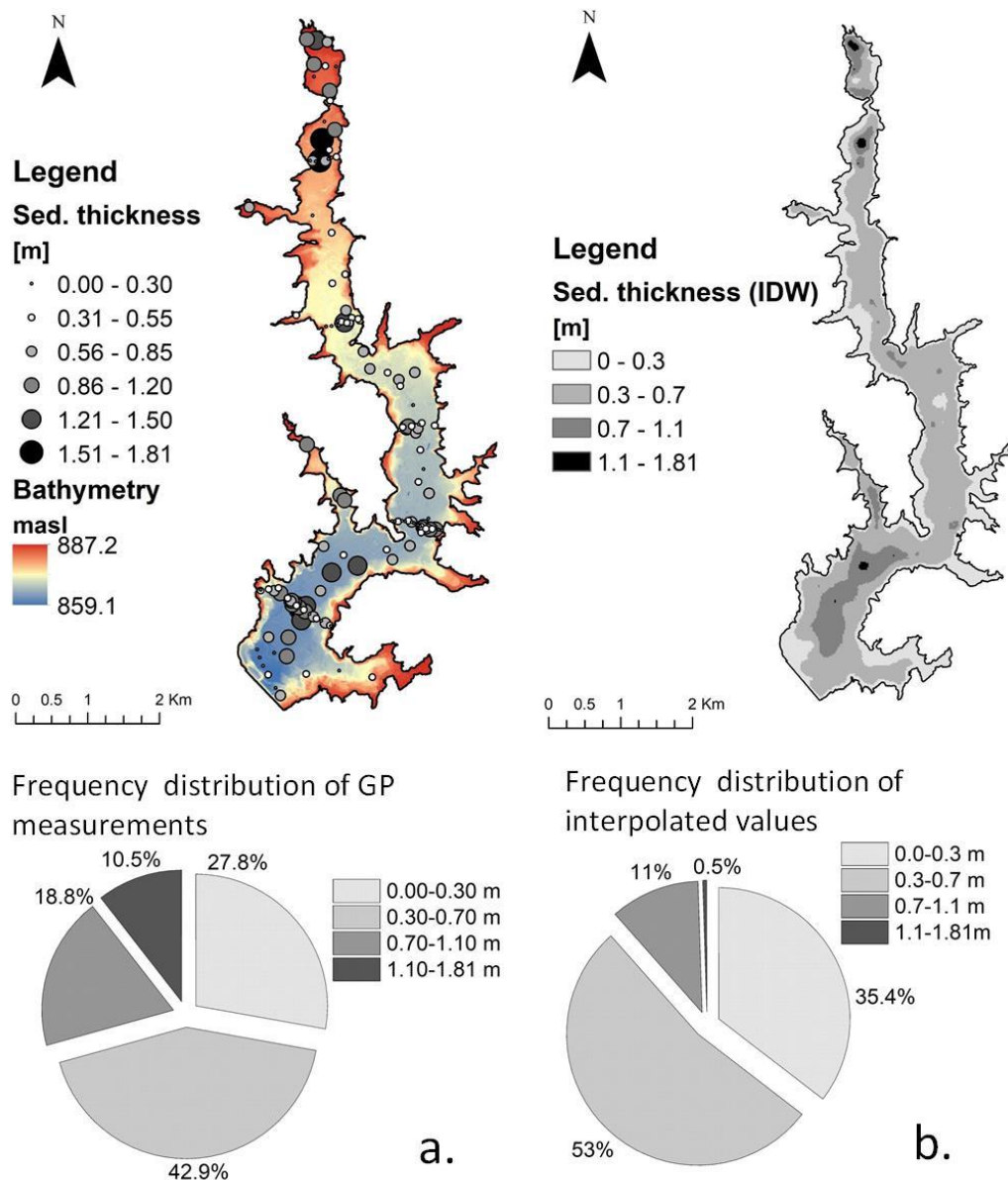


Figure 7—25 a. Locations of GP measurement and the visualization of the measured value. The pie chart shows the frequency distribution of the measured values of sediment magnitude b. The interpolated map of sediment thickness based on the GP measurements with distribution frequency of the interpolated values

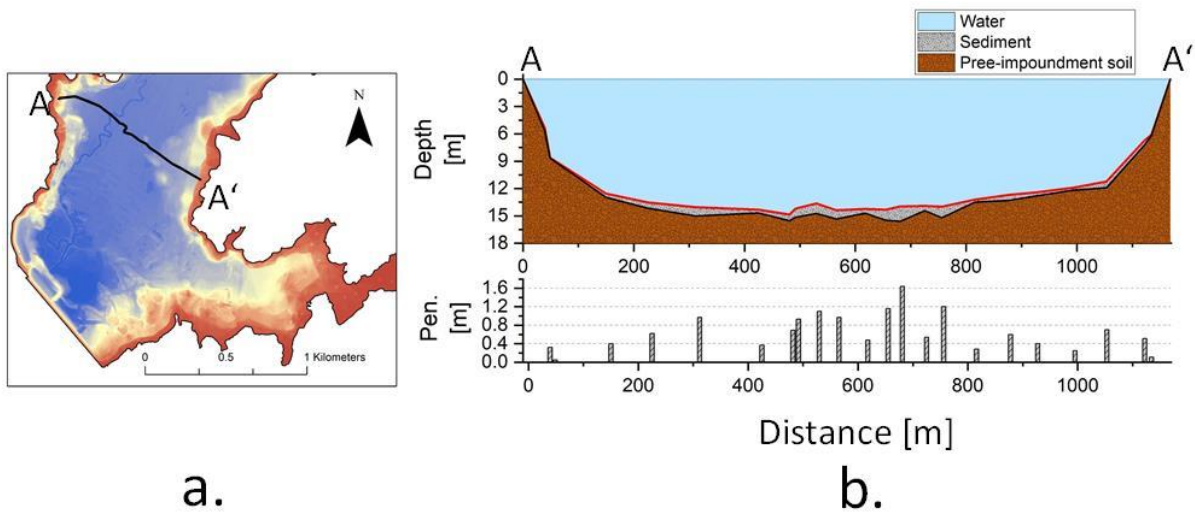


Figure 7—26 a. Cross section profile AA' close to the dam. b. Schematic view of sediment magnitude (up) and the respective measured value (down) at each point for the AA' profile.

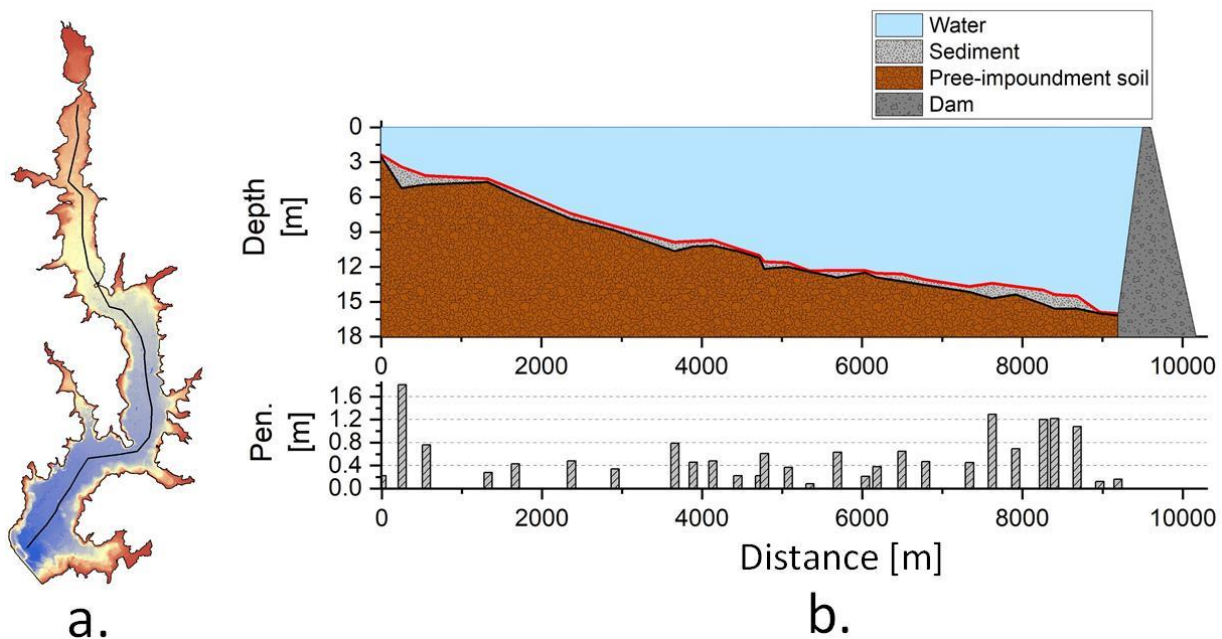


Figure 7—27 a. Longitudinal profile of the reservoir. b. Schematic view of sediment magnitude (up) and the respective measured value (down) at each point for the longitudinal profile.

After the interpolation, the frequency distribution of sediment magnitude values changes significantly as shown in the pie charts of Figure 7—25a and Figure 7—25b. This indicates that the interpolation technique has a significant effect on the overall results. The average sediment magnitude of the raster is 40 cm, which is 30% smaller than the average of all measurements (57 cm). An underestimation of the average value from the interpolation technique shows an underestimation of the calculated sediment volume.

In order to compare properly the interpolated map with the measured values, the spatial component should also be taken in consideration. This means that if most of the measurements are located in the thalweg (disproportionally with its surface compared also to the bank slope areas) the average value for the measurements will be higher than the average from the interpolated values, as most of the accumulation is expected in the thalweg. Therefore, the reservoir was divided in two parts, thalweg and reservoir bank slope as showed in in Figure 7—28. For each of the compartments the average sediment thickness from the GP measurements was calculated. Finally, an overall average value for the whole reservoir was calculated as showed in Eq.45.

$$\bar{M} = \frac{(\bar{M}_t \cdot A_t + \bar{M}_b \cdot A_b)}{A_t + A_b} \quad (45)$$

Where \bar{M}_t and \bar{M}_b are the average of the measurements in the thalweg and reservoir bank respectively, while A_t and A_b are the areas of the above mentioned compartments.

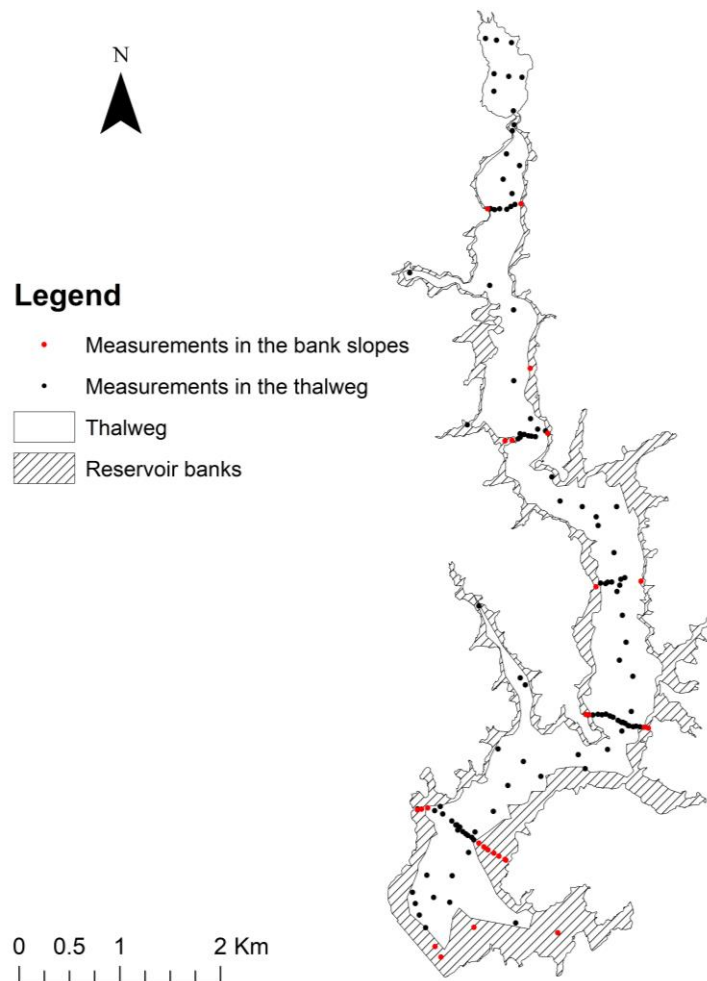


Figure 7—28. Division of the reservoir in compartments

Based on the Eq.45, the average sediment magnitude measured in the reservoir is 62 cm, so 36% higher than the mean raster average (40 cm). Based on the average values the interpolation can lead to an underestimation of up to 36%.

7.3. Summary

In this chapter, the main findings concerning erosion and sediment input from the watershed and the measurement of the reservoir sediment stock are presented. To avoid the discrepancies created from the NDVI based C-Factor, the initial erosion and sediment input models were calibrated, especially for the forested areas. The results showed a specific sediment input of $370 \text{ t km}^{-2} \text{ a}^{-1}$. As expected, most of the sediment originates from the arable land (55%). Most of the catchment (55%) is characterized by very low soil loss ($<2 \text{ t ha}^{-1} \text{ a}^{-1}$), even though a large part of the catchment (36%) suffers from high soil loss ($>10 \text{ t ha}^{-1} \text{ a}^{-1}$) with values that reach more than $500 \text{ t ha}^{-1} \text{ a}^{-1}$. The most important month in terms of sediment input is October, where 26% of the overall yearly sediment input occurs. The yearly-modelled sediment input from sheet and rill erosion is nearly 55,000 tons, which results in 1.64 million tons of sediment in the reservoir for 30 years of operation.

Regarding the reservoir activities, three hydroacoustic systems were used in combination with the GraviProbe and sediment sampling to assess the sediment situation. From the 30 sediment samples in the reservoir, it could be stated that in most of the Passaúna's coverage, unconsolidated, rich in silt clay fraction and high organic share material dominates the sediment. From the multibeam system, it was assessed that the actual storage volume of Passaúna Reservoir is 69.3 hm^3 . Despite the accurate digital elevation model derived from the multibeam system no sediment volume assessment could be performed. The lack of accurate, previous depth distribution information was the factor that prevented the assessment. The sub-bottom profiler was also used for assessing the volume of the deposited material. The high gas contents while approaching the thalweg made it impossible to discriminate between the sediment layer and the pre-impoundment soil. Therefore, no spatial and volumetric information could be derived with this system. The last hydroacoustic system used was the linear system EA400. The device was used for detecting the sediment thickness via the use of dual frequency approach and for performing an acoustic lakebed classification. The dual frequency approach resulted in a sediment volume of 2.47 mil. m^3 , corresponding to a volume loss of 3.4% or 0.11% per year. The results showed that the sediment was distributed rather uniformly in the reservoir where most of the areas did not exceed 0.7 m of sediment thickness. The results of sediment classification based on the Sotiri et al. (2019a) approach showed also that most of the reservoir is covered by fine grained bulky sediment with high gas content while the results from the other approach showed large deviation from the measured values of LOI and silt-clay fraction.

Finally, the GP was deployed at 134 locations for measuring the sediment thickness. The mean sediment thickness derived from the GP measurements was 0.57 m. After interpolating, the overall sediment volume was assessed to be 3.36 hm³, which corresponds to a total volume loss of 4.6% or 0.15% per year (112,000 m³ per year). The GP results as well as the ones from the linear echo-sounder showed that highest sediment thickness was measured in the southern part of the reservoir between the dam and the water intake.

8. Discussion

The main scientific objective of this thesis is to investigate the potential use of the reservoir sediment stock as validation for the sediment input model. In order to do so, the accuracy and limitations of the applied methods need to be discussed, which is also the focus of this chapter. Before discussing the potential use of the sediment stock as validation for the sediment input model, which is practically related to the level of bias created between modelled sediment input and measured sediment stock, a detailed investigation is made to assess the performance of the sediment input modelling and the accuracy of the sediment volume measurements. At the end of this chapter, the major discrepancies between the two outcomes are discussed.

8.1. Sediment input from the Passaúna catchment

In this section, the more important aspects of the sediment input modelling are discussed. At first, the modelling results are compared with literature results from studies in the area of Passaúna and other regional studies as a basic plausibility check. Next, the interannual dynamics of sediment input and their cause are discussed and put in relation to managing strategies. Another topic in focus of this section, are the limitations of the NDVI based approach for the calculation of the C-Factor. Here the causes of the results bias due to the NDVI are discussed fundamentally. Apart from NDVI-caused discrepancies, the RUSLE model itself causes deviations from the real sediment input. These limitations of RUSLE are also discussed in this section. The final issue discussed are the benefits from the inclusion of freely available satellite data in erosion/sediment input modelling.

8.1.1. Comparison of the sediment yield modelling results to literature

Several studies were conducted in the Alto Iguacu area in regard to soil erosion (Saunitti et al. 2004; Duraes et al. 2016a). Saunitti et al. (2004) conducted a similar study in the Passaúna catchment. The methodology followed to calculate erosion was though different. The soil loss and sediment input were calculated in a yearly time step. For the calculation of C-Factor, a LULC map with literature values were integrated. Despite the similarities in the spatial distribution patterns, the findings from this study indicate that the soil loss is lower than what Saunitti et al. (2004) calculated (Table 8—1). Our results show that almost 63% of the catchment had very slight, slight or moderate erosion against the 52% from Saunitti et al. (2004) findings. Major differences were also observed in the areas with very severe and catastrophic erosion. Saunitti et al. (2004)

calculated that 33% of the catchment had more than $100 \text{ t ha}^{-1} \text{ a}^{-1}$ of soil loss while this study showed only 12.7% of the catchment had more than $100 \text{ t ha}^{-1} \text{ a}^{-1}$.

Another study conducted in the Passaúna catchment was the one from da Silva Santos (2019). In his study, da Silva Santos (2019) investigated the effects of different C-Factors found from literature, in the erosion and sediment input from Passaúna catchment. The C-Factors used for the study are specific for Brazilian conditions. The erosion results for the average C-Factor are presented in Table 8—1. Da Silva Santos (2019) found that 85% of the catchment had very slight up to moderate soil loss. Almost 11% of the catchment had high soil erosion and only 4 % had severe to catastrophic soil loss. These results imply a lower soil loss compared to the results of the present study, where around 22% of the catchment have severe to catastrophic soil loss. In terms of sediment, da Silva Santos (2019) for the same model setup found an input of 300% higher than in the present study, which is in contradiction with the erosion findings. By investigating the spatial distribution of soil loss, it seems that an overestimation of erosion occurs for the impervious areas (most of urban areas in da Silva Santos (2019) show high to catastrophic soil loss). As the applied C-Factor was an uncalibrated average of the overall C-Factors found in literature, the used values of C-Factor for impervious areas were significantly high, which most probably created also the discrepancies between the results

Table 8—1 Comparison of the sediment input results with the findings from Saunitti et al. (2004)

Soil erosion classes	% of watershed		
	Present study	Saunitti et al. (2004)	da Silva Santos (2019)
Very Slight ($<2 \text{ t ha}^{-1} \text{ a}^{-1}$)	55.5		
Slight ($2\text{-}5 \text{ t ha}^{-1} \text{ a}^{-1}$)	3.5	52	85.3
Moderate ($5\text{-}10 \text{ t ha}^{-1} \text{ a}^{-1}$)	3.7		
High ($10\text{-}50 \text{ t ha}^{-1} \text{ a}^{-1}$)	15.8	10	10.8
Severe ($50\text{-}100 \text{ t ha}^{-1} \text{ a}^{-1}$)	9.0	5	2.5
Very Severe ($100\text{-}500 \text{ t ha}^{-1} \text{ a}^{-1}$)	11.3	33	1.4
Catastrophic ($>500 \text{ t ha}^{-1} \text{ a}^{-1}$)	1.4		

Wagner (2019) conducted another study in the Passaúna watershed but he focused mostly on continuous monitoring of suspended solids in the Passaúna river before entering the reservoir. In his study, Wagner (2019) collected 33 large volume river samples between February 2018 and July 2019. In his study, also measurements from one intensively measured high-flow event from October 2018 are included. The point where the measurements were conducted, collects water from 55% of the overall Passaúna reservoir catchment. For this case, Wagner (2019) calculated an annual average flux of 10,800 ton a⁻¹. This value is approximately 300% lower than the value calculated for sediment input from 55% of the catchment from this study. Wagner (2019) explains this discrepancies with the importance of episodic high flow events whose dynamic is not properly described by the derived rating curves of suspended solids.

Other regional studies such as the one from Duraes et al. 2016a or the more holistic study from Borrelli et al. 2017 show similar patterns of soil loss in the area of Parana and Alto Iguacu. However the information presented in these studies is too coarse and cannot be directly compared with the findings of this study. As far as the mean specific sediment input is concerned (367 t km⁻² a⁻¹), it is comparable and in the same range with similar regions in Brazil (Araujo and Knight 2005).

8.1.2. The importance of spring months for the sediment input

October and September are the most important months in regard to the sediment input and soil loss (Figure 7—13a). Especially for October, the combination of the RUSLE factors is the most effective for producing the highest amount of sediment. Figure 8—1 shows the combination of C- and R-Factor for the three most characteristic months of the year. In case of the C-Factor, October has similar values with July, which is one of the driest and coldest months of the year and has the lowest vegetation cover. As far as the R-Factor is concerned, the erosivity is as high as the erosivity in the month of January, which is the month with the highest rainfall (together with October and February). In case of October, the worst possible combination is present as the rainfall erosivity is maximal while the vegetation cover is minimal. This above mentioned combination of factors produces the highest soil loss from a system. In case of proper land management strategies, like proper crop rotation, application of crop residues and cover crops in the unprotected soil during winter and spring months (April-October), a significant reduce in sediment input could be achieved (Sullivan 2003b, 2003a; SoCo Project Team 2009)

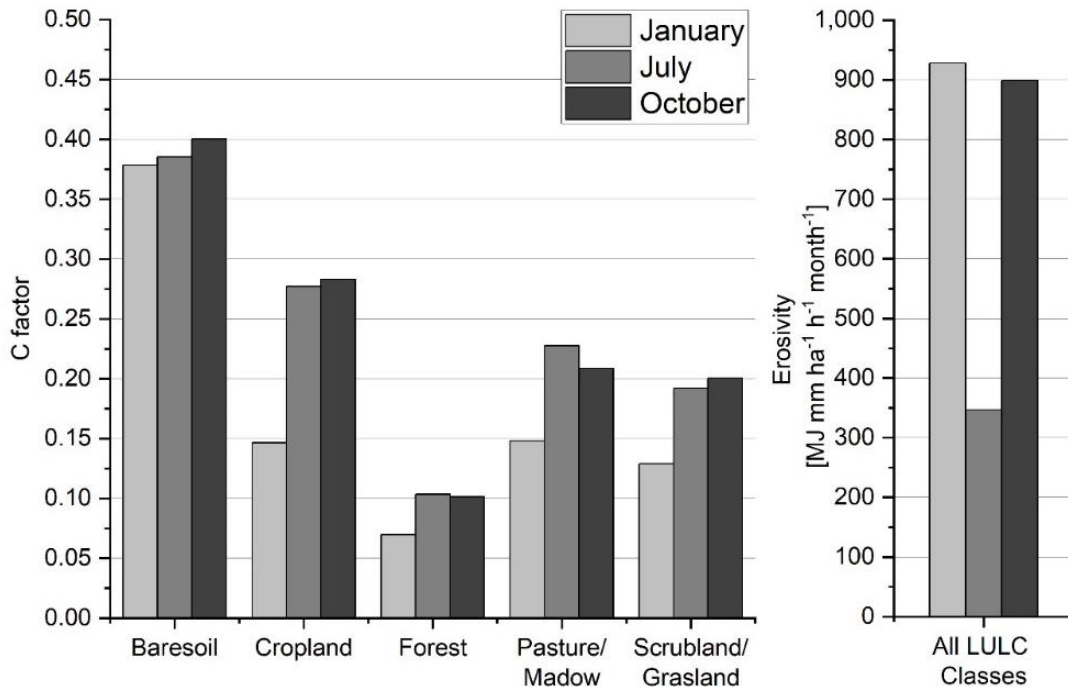


Figure 8—1 C-Factor and R-Factor for three months (January, July, October).

8.1.3. Limitations of NDVI based modelling approaches

In the uncorrected C-Factor results, a similarity in the values of plant covered arable land and forest areas was observed. Despite the similarities in the cover canopy between planted arable land and forest (according to the NDVI values), the topsoil physical properties between these two classes are completely different. While in the erosion component associated with the rainsplash, both LULC classes behave similarly due to the comparable protection from plant canopy, in the component of erosion associated with runoff, forest and arable land have different behavior. The soil surface below the plant cover in the arable land is basically bare and facilitates the detachment of soil particles from surface runoff. On the other hand, in forests, the soil is covered often by low vegetation (grass, leaves or meadows), which creates difficulties in the creation of runoff and in soil particle detachment. In addition, the soil is more compact in forested areas than in arable land, where usually tillage takes place. In its original form, the C-Factor has a direct relation to the soil loss ratio (Renard et al. 1997). The SLR is a product of five sub-factors, which are prior land use, canopy cover, surface cover, surface roughness and soil moisture. All of the former factors, except the canopy cover are associated with the conditions of the soil surface, indicating the importance of the top soil conditions for soil movement initiation. Therefore the C-Factor cannot be calculated only by taking in consideration the vegetation index (canopy cover) but should also include the properties of the soil surface, especially in non-agricultural areas (Wang et al. 2002; Zhang et al. 2002; Zhang et al. 2011; Panagos et al. 2015a).

8.1.4. Uncertainties of RUSLE results for Passaúna catchment

RUSLE was developed as a tool for long-term soil loss calculation at a field scale. By calculating the C-Factor from a certain scene in 2017 or 2018 we assume that the LULC of that specific month has not changed during the last 20 years (rain data available for 20 years). This is to a certain extent not correct. In the Parana state from 1990 there has been an increase of almost 45% in the arable land and 5% yearly increase in urban areas (Zalles et al. 2019). Most of this area that changed in agricultural land used to be forest and this suggests a gradual increase in erosion in the last 20 years.

This is one of the major drawbacks of this method. However, this drawback can also represent an opportunity. In case of existence of precipitation and NDVI data for single months for the entire investigated period, the RUSLE could be adapted from a long-term soil loss calculation tool to a more dynamic tool, to calculate the actual sediment input and soil loss from that certain month of that specific year. In this way, a calibrated model could be used to derive an accurate balance of sediment input for each month and not only a long term average of sediment input as in the until now applications. In case of the reservoir operation, having an exact amount of sediment coming into the reservoir can be crucial for the long-term strategical planning and the day to day operation of the reservoir.

8.1.5. Benefits from the integration of Sentinel-2 data in erosion modelling

The use of vegetation index for the calculation of land cover factor is not new. Several studies were conducted based on this principle. However the spatial accuracy of the images (Landsat or MODIS) in most of the existing literature is relatively low (around 30-250 m) (Zdruli et al. 2016; Pham et al. 2018; Grauso et al. 2018b; Almagro et al. 2019; Chuenchum et al. 2020). With the inclusion of freely available Sentinel-2 data there is an increase in spatial and temporal resolution of the data regarding the vegetation cover. Improved spatial accuracy and temporal frequency in satellite imagery leads to better erosion modelling results (Gianinetto et al. 2019; Karydas et al. 2020).

By application of more advanced processing steps in the Sentinel-2 dataset, more specific information can be derived about the investigated area (ex. the degree of soil sealing). Certain information can be used as in this case for a better mapping of erosion and sediment input.

8.2. Sediment stock in the Passaúna reservoir

In this section, the results from the sediment investigation are discussed. Initially all the measuring approaches are compared among each other to define the accuracy or advantages and disadvantages of each method. The performance of each method was assessed via statistical coefficients, which are also presented in a summarized form in Table 8—2. A proper overview of the methods and of their performance can contribute to define the most accurate and therefore suitable method for assessing the sediment stock in the Passaúna reservoir. Finally, the hydroacoustic sediment classification approach is evaluated by relating the modelled sediment properties with the actual measured values. Here, the focus is put only on the two sediment parameters presented also in the results section (LOI and silt-clay fraction).

8.2.1. Comparison between measurement methods

When comparing the sediment layer information from the core samples with the sediment layers from the GP, especially for C19, a distinct similarity can be observed (Figure 8—2). For C19, layer 1 and layer 2 are accurately detected by both techniques. The layer thickness from C19 is equal to the layer thickness from the GP. Layer 3 is thinner in the sediment core compared to the GP information and no layer 4 could be sampled by the corer. This can be attributed to the compactness of the lower sediment or the friction developed between the sediment and the liner. The sediment corer encounters more difficulties in sampling the sediment layer below the end of layer 3 while the GP due to its shape characteristics can penetrate easily also the other layers.

At location C9, the layers detected from the GP are not similar with the sediment layers as sampled from the gravity corer. The total penetration from GP at location C9 is 30 cm while the length of the core sample is 22 cm. Both methods had a difference of 8 cm. As the core sample and the GP had a position shift between them, most probably, the heterogeneity of sediment thickness between these two locations may create the difference in the outcome. The range of the sediment thickness is also low (20–30 cm). Therefore, the errors associated with deployment and sampling may be also higher (compaction of core sample due to hammering or integration of some cm from former lakebed in the sediment layer discussed in the following paragraphs).

As Figure 8—2 also indicates, an increase in sediment WBD for C9 is observed in accordance to an increase in the DCPR. For the first layer a WBD of 0.92 g cm^{-3} corresponds to an average DCPR of 20 kPa while a WBD of 1.08 g cm^{-3} in the third layer, corresponds to an average DCPR of 80 kPa.

This fact represents an opportunity for the development of a sediment classification techniques via the use of GP as highlighted also in Hilgert et al. 2019a.

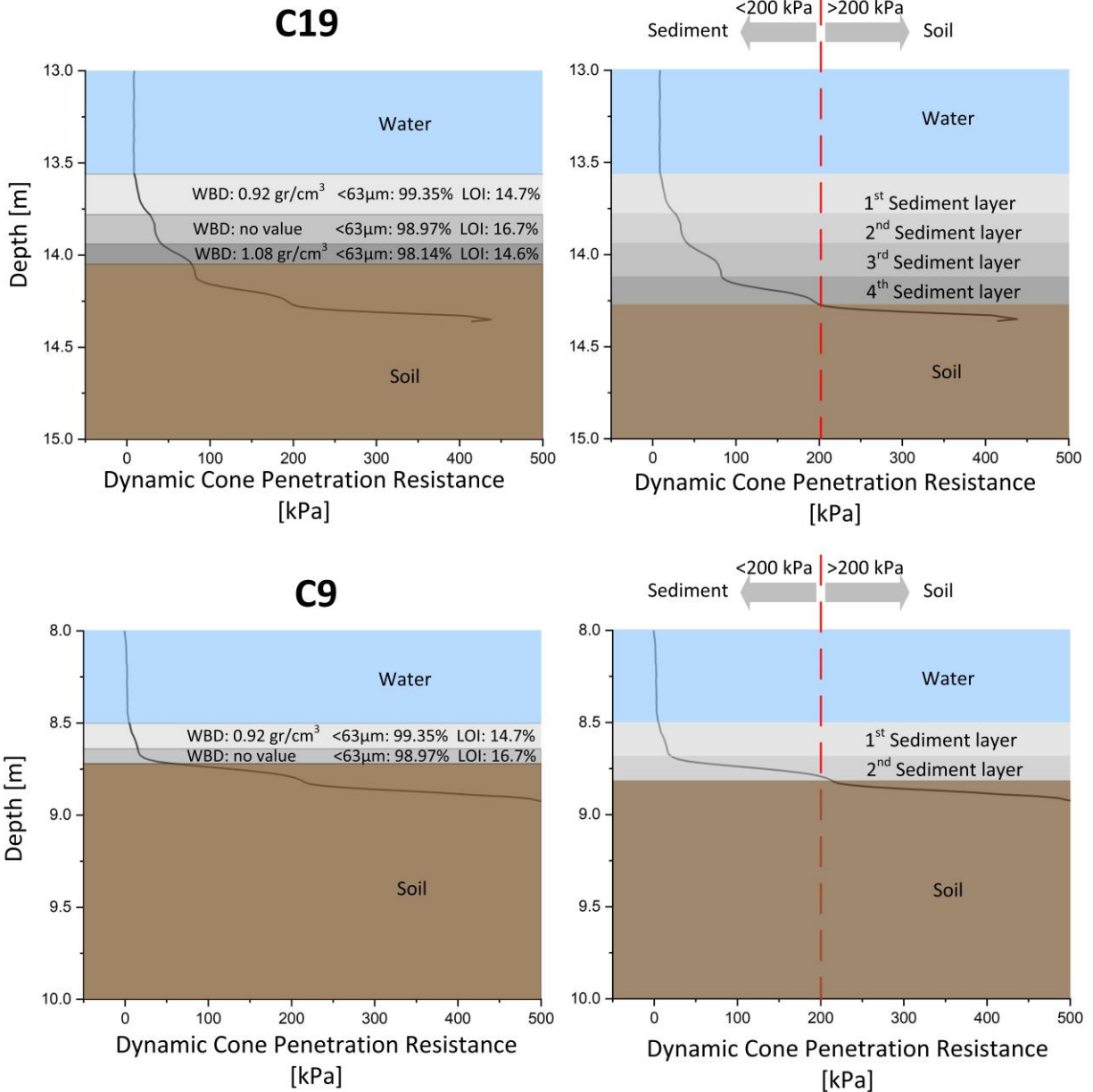


Figure 8—2 Comparison between core samples and GP results for two locations C19 and C9. Left images show the layers defined from core samples. Right images show the layers defined from GP data.

At all the locations where GP and core data are available, the findings from both methods (Figure 8—3) were compared. It can be observed that when plotted against each other, most of the points follow the 1:1 pattern with a 17.5 cm offset (Figure 8—3 right), apart from the six shaded points (C14, C15, C17, C18, C21 and C22) (Figure 8—3 left). These shaded points show a higher and disproportional sediment thickness from GP deployment compared to sediment coring. Due to the limited length of the liners at the locations C18, C14, and C15, no more sediment could be sampled. At location C21, the second layer of the sediment was mostly mineral, sticky silt-clay

material from the dam construction phase, and was hindering any further core penetration. C17 was mostly unconsolidated material and a significant part of the core was lost during the sampling procedure. As far as C22 is concerned, the discrepancies to the GP data might have occurred due to a change in positioning with some meters between the GP deployment and core sampling.

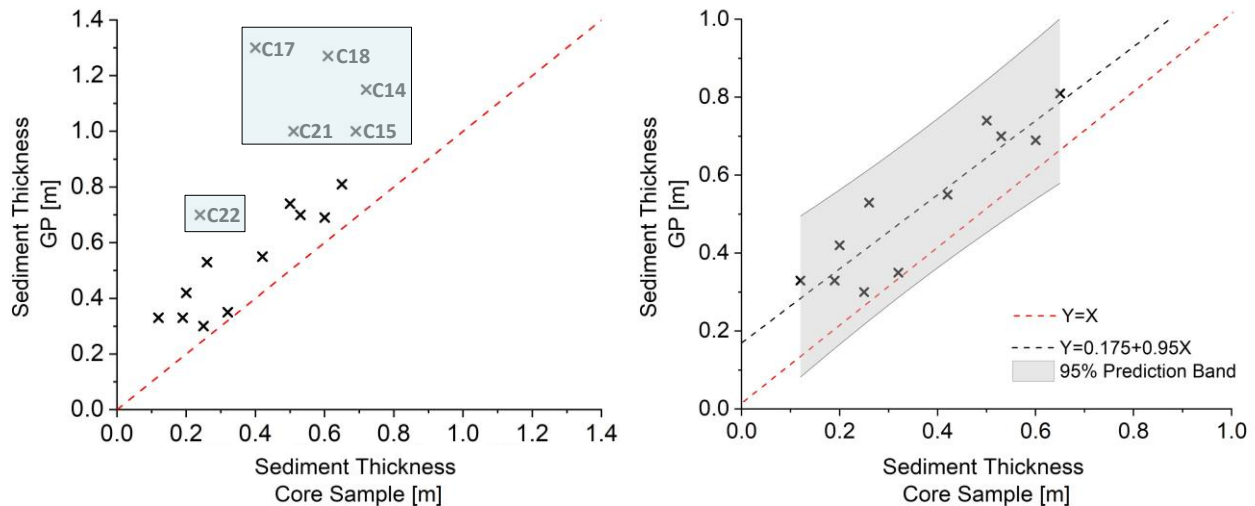


Figure 8—3 Left: sediment thickness from core samples vs. sediment thickness from GP. Right: sediment thickness from core samples vs. sediment thickness from GP when excluding the shaded points.

When analyzing visually the above mentioned sediment cores (C14, C15, C17, C18, C21 and C22), it could be clearly observed that none of these points had reached the pre-impoundment soil and due to the compactness of the deeper sediment layers or friction in the liner, the corer could not penetrate any further (Figure 8—4) (excluding C17 where around 10 cm of the bottom layer were lost during sampling). The photos of the cores demonstrate that the sediment at the corresponding sites is likely to be thicker than the length of the cores, while the GP, due to its shape and weight penetrated presumably until the pre-impoundment soil. When excluding the shaded points from the comparison, the Root Mean Square Error (RMSE) of the GP measurements (in relation to core sample's length) is 17.2 cm, while the mean absolute error is 15.6 cm.

The inability to reach the pre-impoundment soil and the sediment heterogeneity are not the only causes producing discrepancies. Disturbances like shortening, tilting or depressurization of the core can cause significant changes in the core length. As shown in Dück et al. (2019), 30% of the gravity cores (especially the ones with high silt-clay content) from Olsberg and Urft Reservoir in Germany showed shortening. As Passaúna reservoir is covered mostly by silt and clay material the risk of shortening can be significant. Another factor that can affect the sediment thickness from the cores is depressurization and gas release. In Passaúna, volumetric gas content from 2% to 15% was observed (unpublished data). The disturbances due to the initial impact of the corer, the further hammering of the cores and the absence of hydrostatic pressure

in atmospheric conditions, might have an influence on the length of the sediment core by releasing the gas and compacting the sediment. Therefore, the sediment thickness derived from core sampling might be lower than the real sediment thickness on the lake bottom. Moreover, from Figure 8—3b it can be observed that the GP measurements suggest constantly a higher sediment thickness than the core samples. Based on the two previously mentioned indices (core disturbance and graph illustration) it is probable that the GP results are closer to the real situation compared to the coring results.

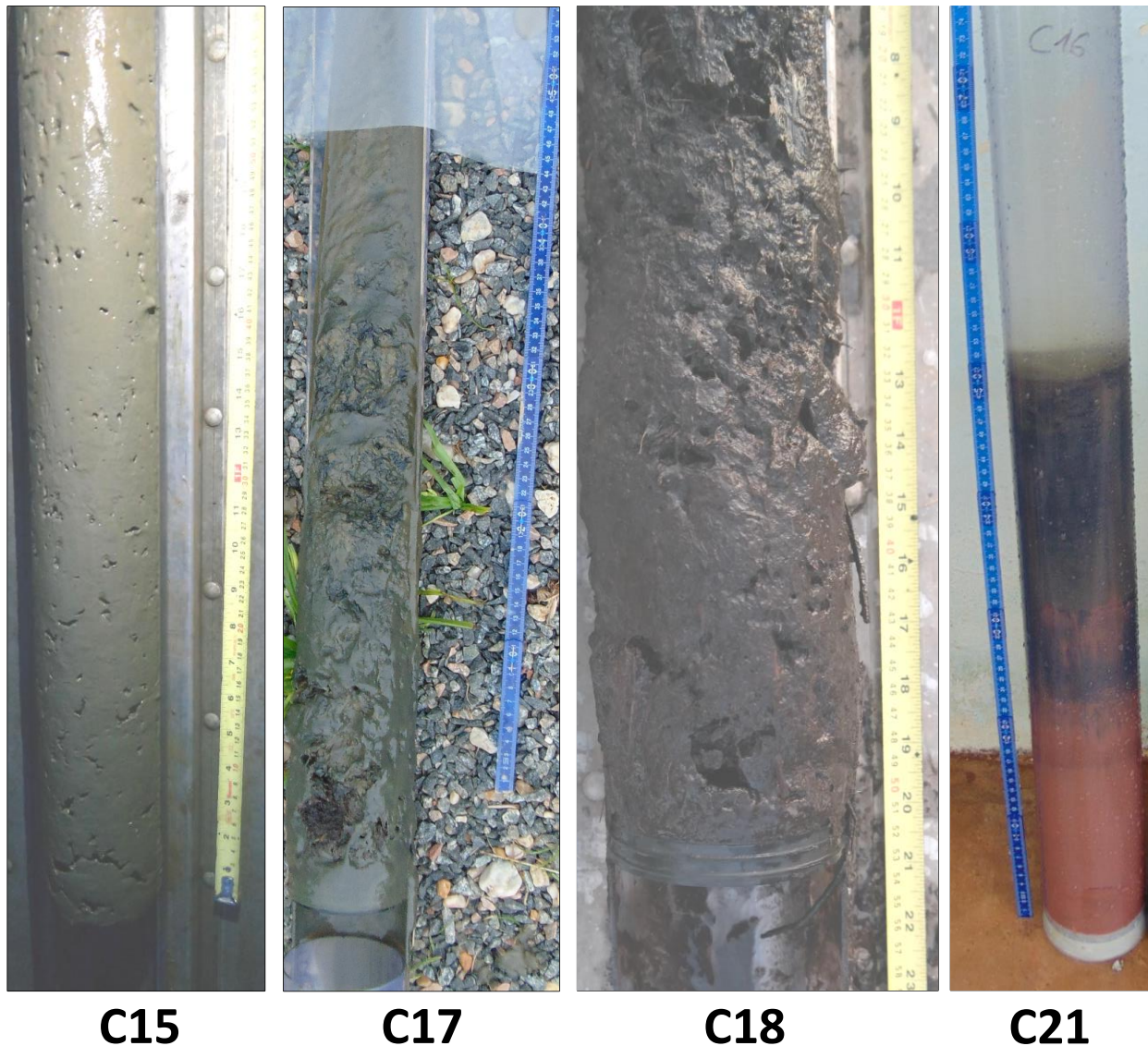


Figure 8—4 Photo documentation of some of the shaded points in Figure 8—3a. None of the cores has reached the pre-impoundment soil.

For the marked group of sampling points the dynamic cone penetration resistance is lower than, or significantly close to 200 kPa, which was defined to be the orientation threshold for differentiating between sediment and pre-impoundment soil (Figure 8—5).

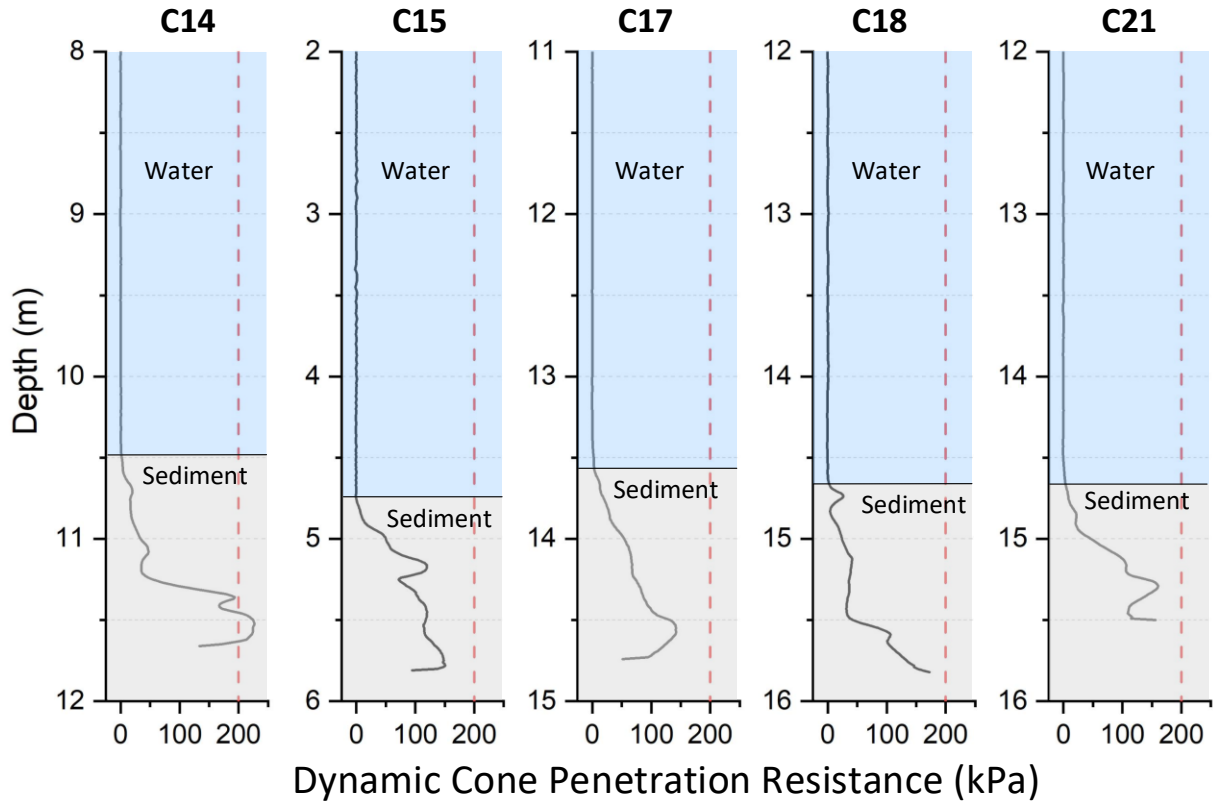


Figure 8—5 DCPR of shaded points from graph in Figure 8—3a. At all locations, the GP does not reach the pre-impoundment soil (DCPR smaller or slightly greater than 200 kPa).

Therefore, the actual sediment thickness could be higher than the one derived from the GP penetration. The sediment thickness results provided by the GP measurement show only the minimum amount of the sediment that can be detected in the reservoir. The results comparison suggest that the actual sediment volume derived for the GP measurements is lower than the actual sediment volume in the reservoir.

The sediment magnitude from the GP measurements was compared also to the information from the static profiles recorded with the sub-bottom profiler with 10 kHz at the same locations (where gas content allowed it). As shown in Figure 8—6, the sediment thickness detected from the GP corresponds to the sediment thickness observed from the sub-bottom profiler. Despite the fitting sediment thickness, no clear overlapping of the in-between sediment layers could be observed. A major role in the differences between the results of the two methods can play the heterogeneity of the sediment matrix. The parametric system is extremely sensitive to any minimal change in the sediment matrix (including here the granulometry, WBD or gas content). The

information of the layer integrates the acoustic response of a 60 cm diameter footprint of the echosounder at 13 m water depth. The information of the layers from the GP is confined to the GP footprint of 50 mm of diameter. Therefore, the small scale variations in the sediment matrix is accompanied with different layering results between the sub-bottom profiler and the GP.

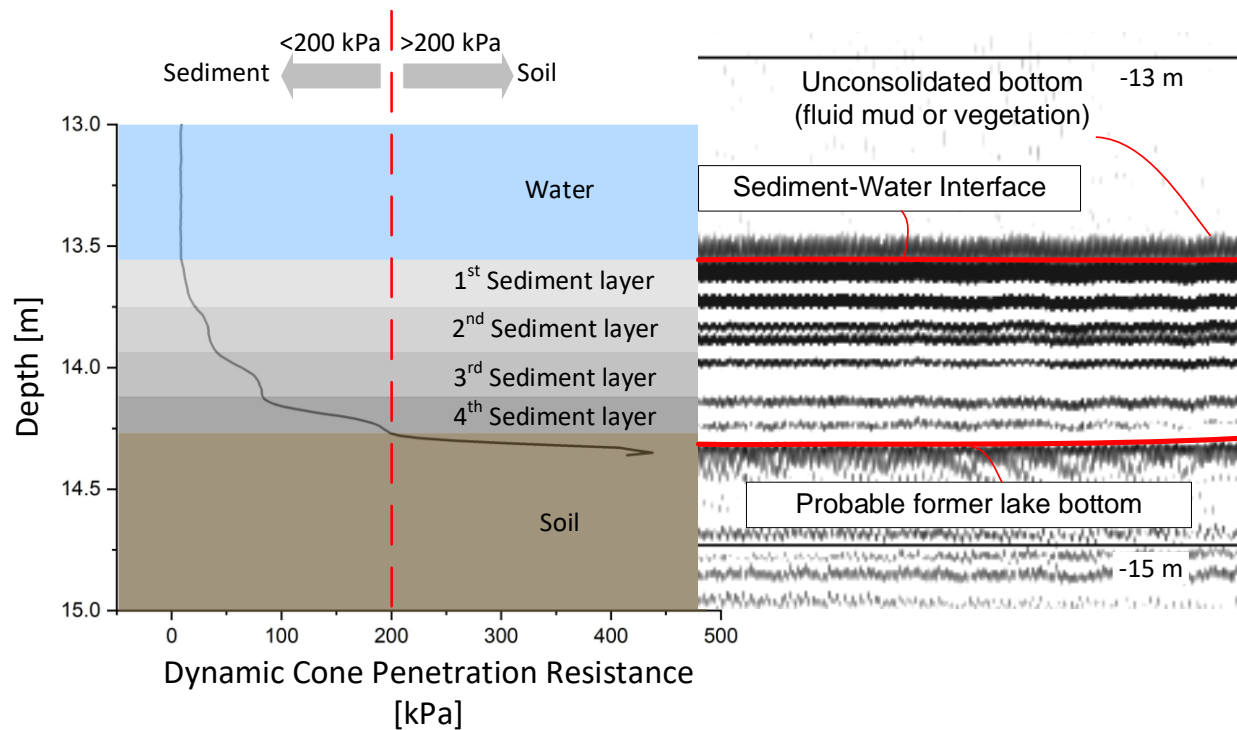


Figure 8—6 Comparison of SES2000 and DCPR from GP at point C19. The water-sediment interface is clearly defined in the same depth as GP. The estimated former lake bottom is highlighted and shows a similar depth as the one defined by the GP threshold of 200 kPa. Due to the high gas content, only at some limited locations it was possible to use the sub-bottom profiling data for comparison. The depth of the measurement approach is not overlapping as sub-bottom profiler data are not corrected for the transducers depth.

From the interpolated map of sediment thickness from the EA400 hydroacoustic system, the sediment thickness at the same location of the GP deployment was extracted. By analyzing the sediment thickness from the two methods, no significant correlation ($Pearson R.=0.086$) could be observed (Figure 8—7). The mean absolute error of the EA400 results is 32 cm compared to the GP measurements (NMAE=56%). Assuming that the GP can deliver the sediment thickness with a certain accuracy, the dual frequency approach seems to underestimate the sediment thickness in the areas where more than 67 cm of sediment is present. The high gas content in the sediment produces significant errors in regard to sediment magnitude calculation as gas represents a barrier to the sound penetration. The effects of free gas on hydroacoustics are well-investigated (Anderson and Hampton 1980; Anderson and Bryant 1990; Abegg and Anderson 1997; Lurton X. 2002). The sediment detection line derived from the 38 kHz (as shown in Figure 6—10) is strongly affected by the high volumetric gas content. With such high values of free gas, the acoustic

impedance of the sediment matrix is expected to be high and the sound penetration extremely low. For this reason, the maximum sediment thickness calculated from the interpolated EA400 data is less than half of the maximum sediment magnitude from the GP (Figure 8—7). In the upper part of the lake bottom, the echo reflection was lower while when the gas became predominant in the sediment matrix, the sediment was reflecting as pre-impoundment bottom, leading to inaccurate sediment thickness determination.

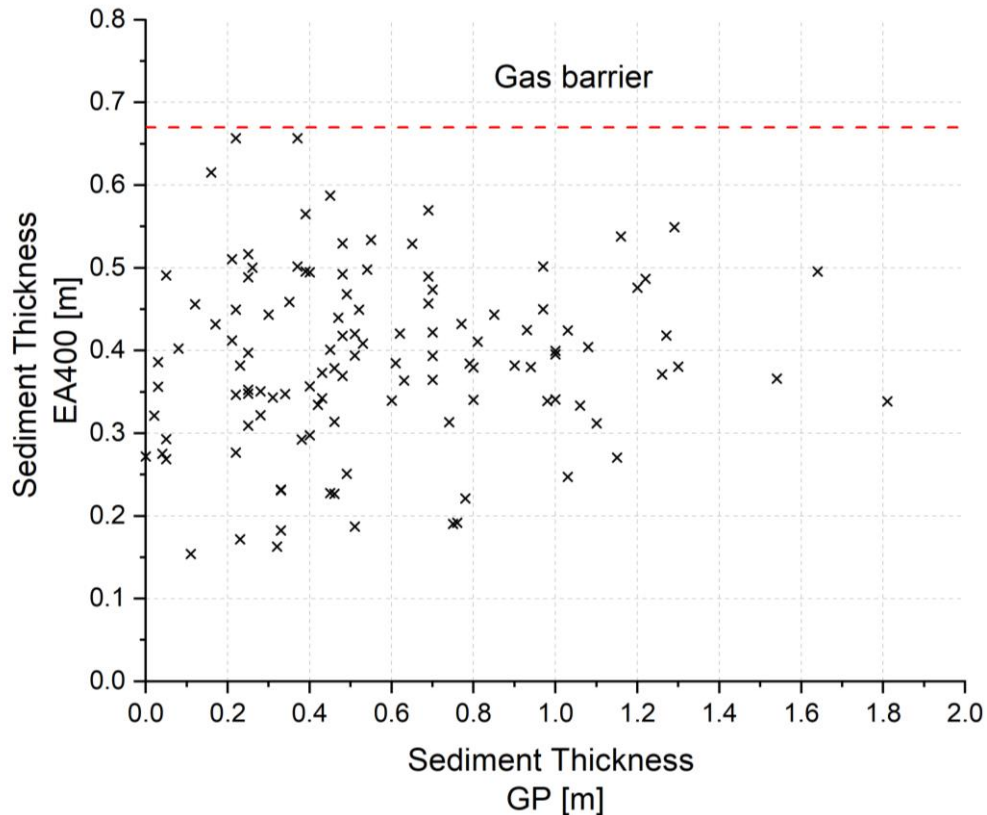


Figure 8—7 Comparison of GP with EA400 value from the interpolated map of sediment thickness.

The sub-bottom profiler had a much higher resolution and a higher gas sensitivity, which enabled to directly detect the gas rich areas by not showing the former lake bottom even when the smallest amount of gas was present. Compared to the sub-bottom profiler results, the echograms of the EA400 showed deeper penetration due to the integration of acoustic response at 9.6 cm resolution (pulse length). The information of the EA400 was more diffuse and it could not be determined whether the information was correct or it was an artifact due to the low accuracy of the system. For the detection of the sediment layer, more powerful sources and lower gas presence might be required.

8.2.2. Summary of measurement techniques

As explained at the respective paragraphs in the results section, all of the approaches carry significant errors (Table 8—2). Those errors are initially associated with the accuracy of the devices. In this regard, the two devices that perform better are the GP and the sub-bottom profiler. The linear single beam system has clear limitations, which can produce errors up to 27% for Passaúna. As far as the overall accuracy of the measurements is concerned, the EA400 showed clear limitation in finding the actual sediment distribution when compared to the GP results with a NMAE of 56%. Interpolation is also a cause of bias in the results. Combined with the results accuracy, the interpolation technique IDW can cause a deviation of 22.8–36% and 42% for the GP and EA400 measurements respectively. However, these values can differ significantly depending on the amount of points, their spatial distribution and the interpolation technique. The other approaches could not be properly evaluated due to the lack of reference data.

Table 8—2 Summary table for all the used methods

Method	Device accuracy (cm [%])	NMAE due to interpolation and device accuracy (%)
Topographic differencing via multi-beam	n. a.	n. a.
Single beam linear system EA400 - spatial information	9.6 [27]	42
Single beam linear system EA400 - point information at core locations	9.6 [27]	n.a.
Parametric sub-bottom profiler SES2000	1–5 [n. a.]	n. a.
Core samples	n. a.	n. a.
DFFP GraviProbe spatial information	1 [2]	22.8–36

n.a. – not assessable

8.2.3. Comparison between acoustic sediment classification and sediment properties

As described in the results section, the performance of the sediment classification model with hydroacoustic properties was not optimal. The statement is reinforced also by the graphs in Figure 8—8a and Figure 8—8b where the $X=Y$ line fits poorly to the measured versus modelled points. Regarding the silt-clay fraction, the modelled values after interpolation are underestimating significantly when the silt-clay fraction of the sediment is above 90%. In overall, the NSE for the silt-clay fraction prediction model is -13.3. The LOI model also did not perform optimally. At some location with LOI in the range of 10–20% the model could predict the LOI of the sediment with satisfactory results. However, in the same range of LOI for some other locations the model results deviated up to 600% from the measured values. For the LOI model, the NSE was lower than the NSE for the silt-clay fraction model but still far from an optimal value (NSE=-3.5).

The low performance of the silt clay-fraction model can be attributed to the high amount of gas. Usually, locations with high sand-gravel fraction reflect similarly with location rich in gas voids. The hydroacoustic system cannot discriminate between these two parameters therefore sometime it misclassifies the areas with high gas content in areas with high sand content as shown in Figure 8—8a. Moreover, this misclassification is more often present in samples with high silt-clay fraction, which are often also richer in gas than sandy sediment. For the LOI the misclassification occurs, as explained also in section 7.2.4, mainly because of the extrapolation of the regression analysis equation to acoustic values lower than the defined interval in Figure 7—22.

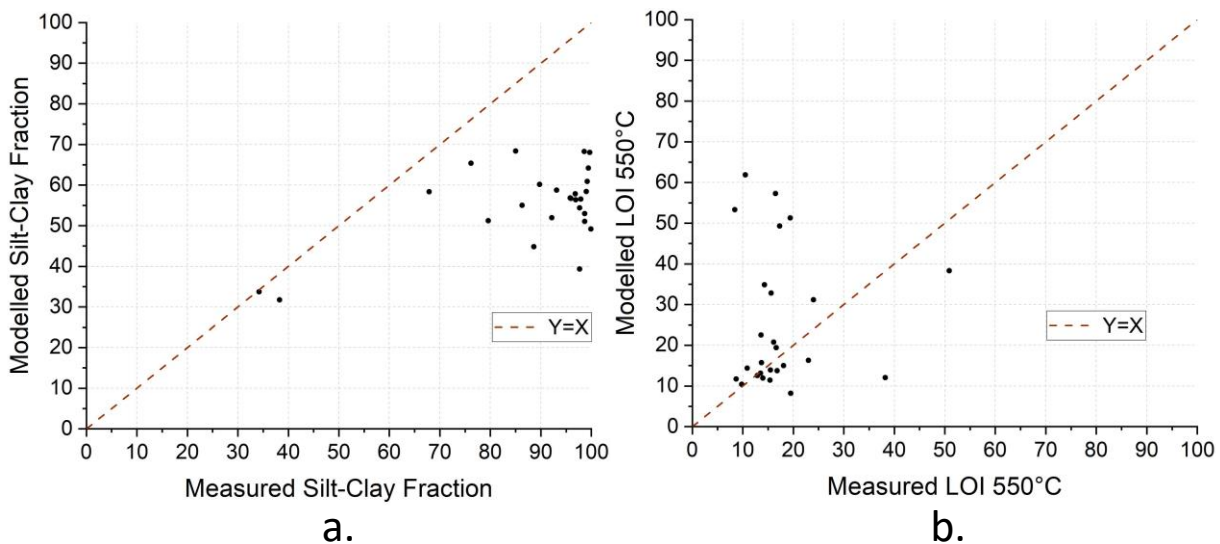


Figure 8—8 a. Comparison between measured and modelled silt-clay fraction. b. Comparison between measured and modelled LOI.

In regard to the second classification technique used, the northern part of Passaúna showed a patchy pattern with alternation of sediment and pre-impoundment soil from the entrance until the Passaúna Park (Figure 7—21). As it can be seen from the below drone footage of May 2020 (Figure 8—9), the alternating pattern has to be attributed to the terrain of the region as shown from the below figure and Figure A—11 in the Appendix section. The terrain is directing the flow in the reservoir entrance and as a result the sediment. Due to the highly changing terrain, the water follows only preferential pathways leading to the sedimentation of the areas located near these preferential pathways. Due to the loss of accuracy created from the interpolation, the patterns between drone image and hydroacoustic classification do not perfectly overlap.

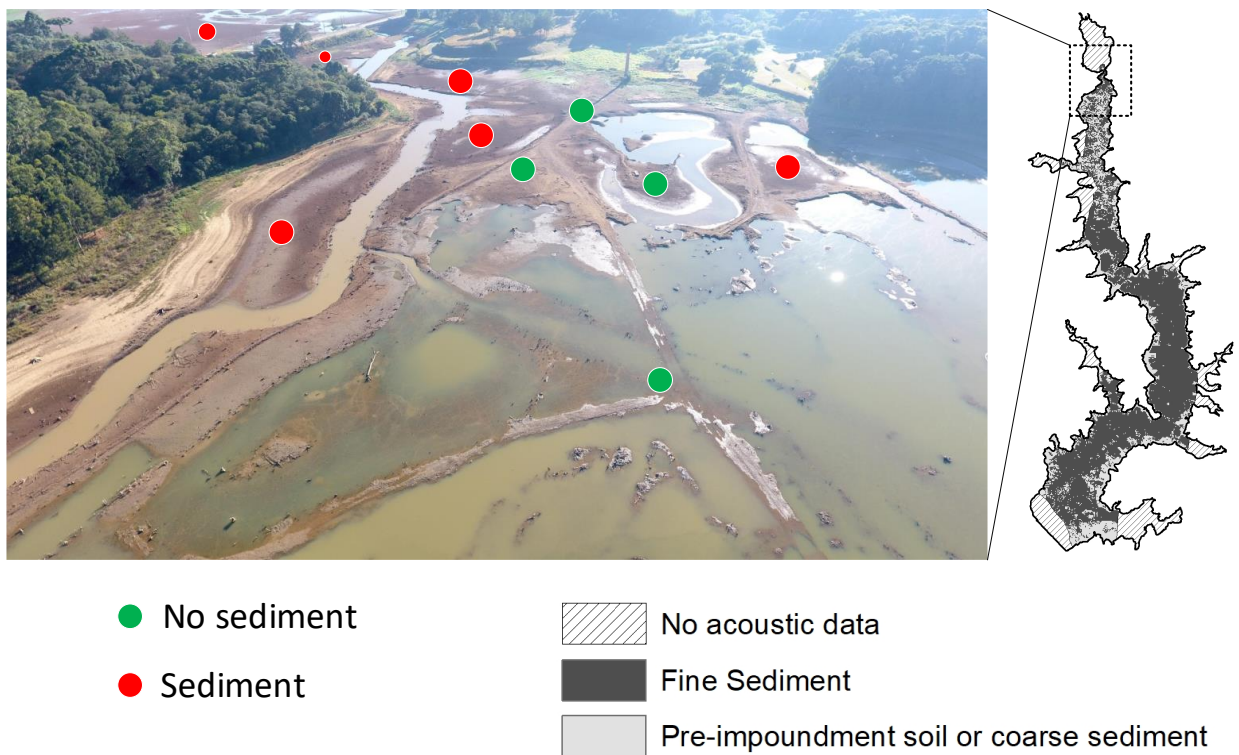


Figure 8—9. Left: drone image of the northern part of Passaúna reservoir in May 2020. (photo courtesy Tobias Bleninger). Right: sediment classification in Passaúna reservoir based on the classification approach of Sotiri et al. (2019a)

When examining the measured single points to the drone image (Figure 8—10), it can be observed that the no sediment area in the river bed is mapped accurately by the classification approach. In addition, the areas with high sediment deposits near the river banks were mapped correctly (red circles). However, some of the locations with visible lack of sediment were misclassified in areas with sediment (yellow circles). This effect was observed in several areas where the comparison was performed (Figure A—12). The misclassification at the locations of the yellow circles can be attributed to the existence of vegetation or fluid mud layer covering the lakebed structures or the consistency of the lake bottom at those locations. To achieve an

accurate assessment the sediment and soil consistency needs to be examined in the areas of interest. Due to the travelling limitations to the area, the comparison was performed based only on the visual assessment of the images.

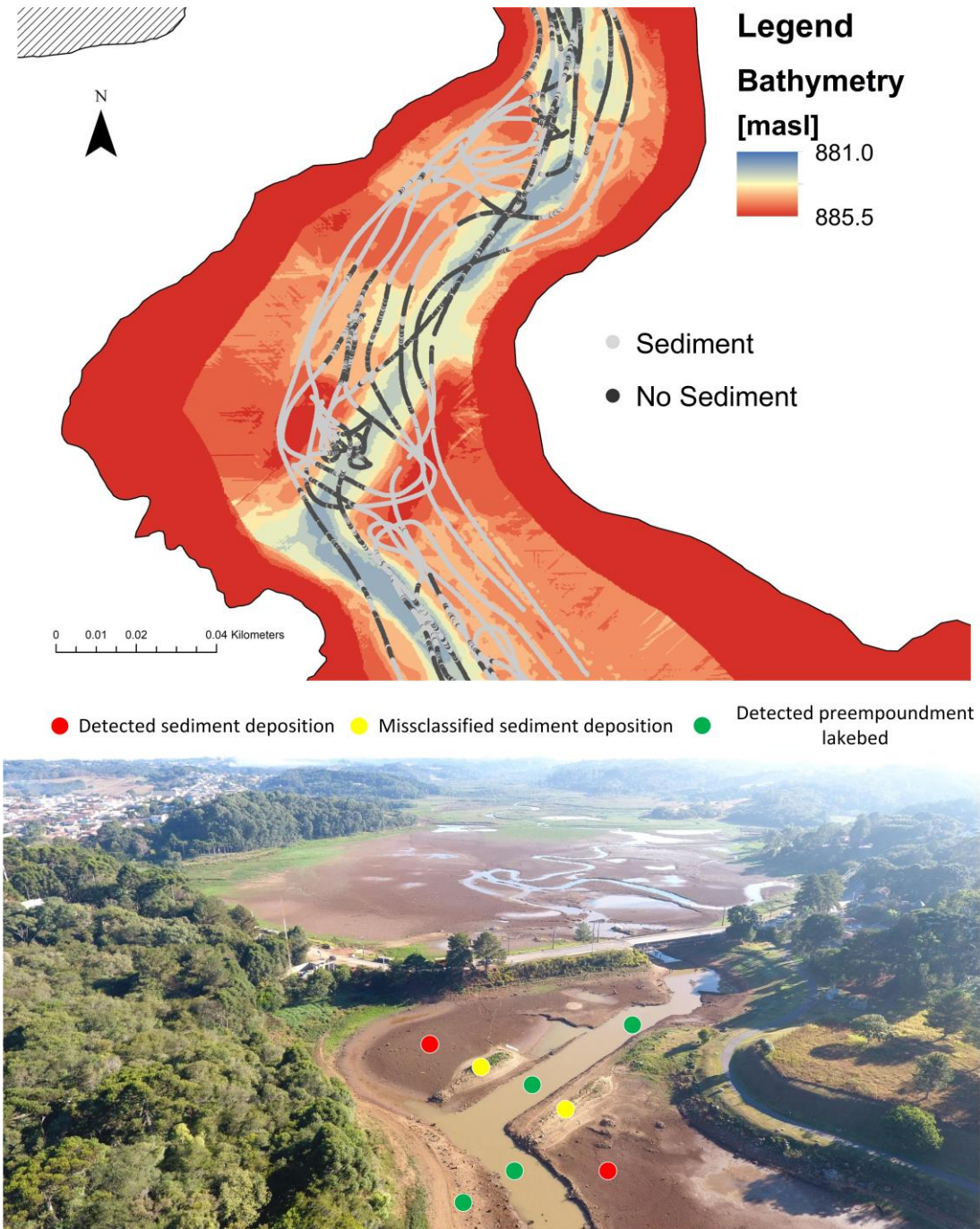


Figure 8—10 Comparison between the hydroacoustic sediment classification with the drone image for the area of the Ferrara Bridge (photo courtesy Tobias Bleninger)

8.2.4. Reservoir lifetime assessment

From the six measurement techniques used for detecting the sediment thickness, four were used to assess the reservoir's lifetime, while the results of multibeam and sub-bottom profiler could not be used for volumetric sediment calculations (Table 8—3). Under the assumption that the sediment input from the catchment will not change in the following years, it will last between 569-909 years for Passaúna Reservoir to entirely fill up with sediment. For the estimation of lifetime, we used both spatial and point information. The reservoir lifetime was calculated by dividing the initial storage capacity by the yearly sediment input. In case of the spatial information (GP and EA400), the interpolated maps were used to calculate the overall sediment volume. The overall sediment volume was transformed in yearly sediment input by dividing the overall sediment volume by the years of reservoir operation under the assumption that the sediment input through the years is constant. For the point information, the overall sediment volume was computed by multiplying the mean measured sediment thickness with the area of the reservoir. The overall lifetime was assessed following the same principle as for the spatial information.

Table 8—3 Summary table of reservoir lifetime assessment based on different measuring techniques

Method	Sediment volume (hm ³)	Mean sedimentation rate (cm a ⁻¹)	Lifetime (years until 887.2 masl)
Topographic differencing via multi-beam	n. a.	n. a.	n. a.
Single beam linear system EA400 - spatial information	2.47	1.2	909
Single beam linear system EA400 - point information at core locations	2.70	1.07	808
Parametric sub-bottom profiler SES2000	n. a.	n. a.	n. a.
Core samples	3.90	1.51	569
DFFP GraviProbe spatial information	3.36	1.9	641

n.a. – not assessable

Based on the classification of Juracek (2015), Passaúna can be classified as a very young reservoir with a slow aging rate. The three measuring techniques used for the lifetime assessment suggest a slow sedimentation rate (0.1–0.2% yearly) and a total storage loss of less than 5% of the overall reservoir volume (Figure 8—11).

		Reservoir age (total storage capacity lost to sedimentation)				
		Very young (VY) (<5%)	Young (Y) (5–10%)	Middle age (M) (10–20%)	Old (O) (20–30%)	Very old (VO) (>30%)
Reservoir aging rate (mean annual sedimentation rate)	Very slow (VS) (<0.1%)	VY/VS	Y/VS	M/VS	O/VS	VO/VS
	Slow (S) (0.1–0.2%)	VY/S	Y/S	M/S	O/S	VO/S
	Moderate (M) (0.2–0.4%)	VY/M	Y/M	M/M	O/M	VO/M
	Fast (F) (0.4–0.6%)	VY/F	Y/F	M/F	O/F	VO/F
	Very fast (VF) (>0.6%)	VY/VF	Y/VF	M/VF	O/VF	VO/VF

(<, less than; %, percent; >, greater than)

Increasing need for sediment management →

↑ **Increasing need for sediment management**

Figure 8—11 Classification of Passaúna reservoir based on Juracek (2015) classification

Despite the findings from Table 8—3, which suggest a reservoir lifetime of at least 569 years, the operation of the reservoir can suffer the problems of sedimentation earlier. By examining the GP profile at the water intake, a mean sedimentation rate of 1.85 cm a⁻¹ was measured in the thalweg. When extrapolating the finding to future scenarios, under the assumptions that the longitudinal deposition pattern in the reservoir and sediment input from the catchment will not

change and no sediment remediation measures will be applied in the reservoir, it is expected that the technical structure of water abstraction will face problems earlier than 300 years (Figure 8—12). However, with the frequency increase of extreme events due to climate change, the increase in internal sediment production and the anthropogenic pressure on the land cover, the Passaúna reservoir may encounter problems even earlier than the predicted time.

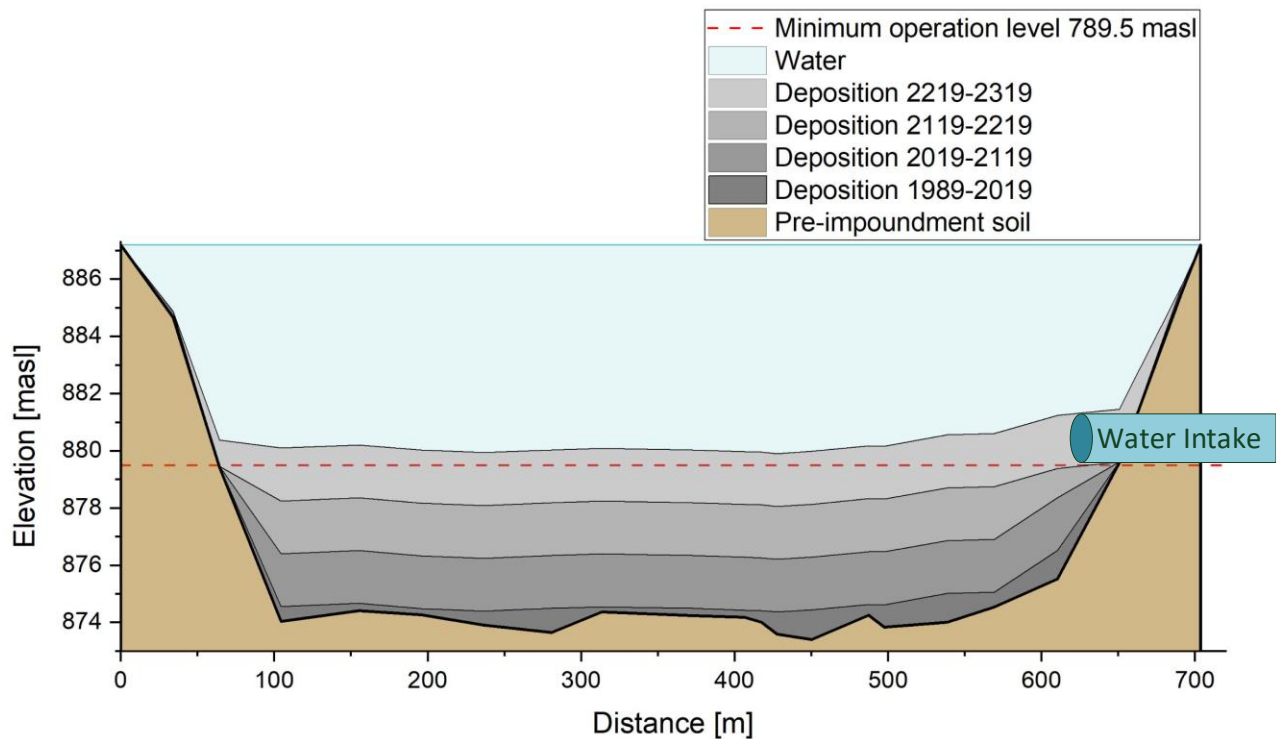


Figure 8—12 Sediment accumulation scenarios in 100, 200 and 300 years based on the actual sedimentation rate measured from GP

In regard to the applicable sediment managing strategies, based on the guiding diagram of Annandale et al. (2016) (Figure 8—13), for Passaúna the best feasible approach is storage operation or density current venting. This approach though does not take in consideration the use of the reservoir. Passaúna is a drinking water reservoir and the water level of the reservoir is rather constant. The operation of the reservoir is dictated from the water security of the region as a lack of water in the reservoir can cause problems for the metropolitan region of Curitiba and the 600,000 inhabitants that the reservoir provides water for. Draught periods as the one during years 2019–2020 can pose a serious risk to the water availability in the region. Therefore, in order to assure the short-term and mid-term water availability, the operators are required to operate the reservoir with minimum water fluctuations, despite the long-term problematic that is created due to sediment accumulation.

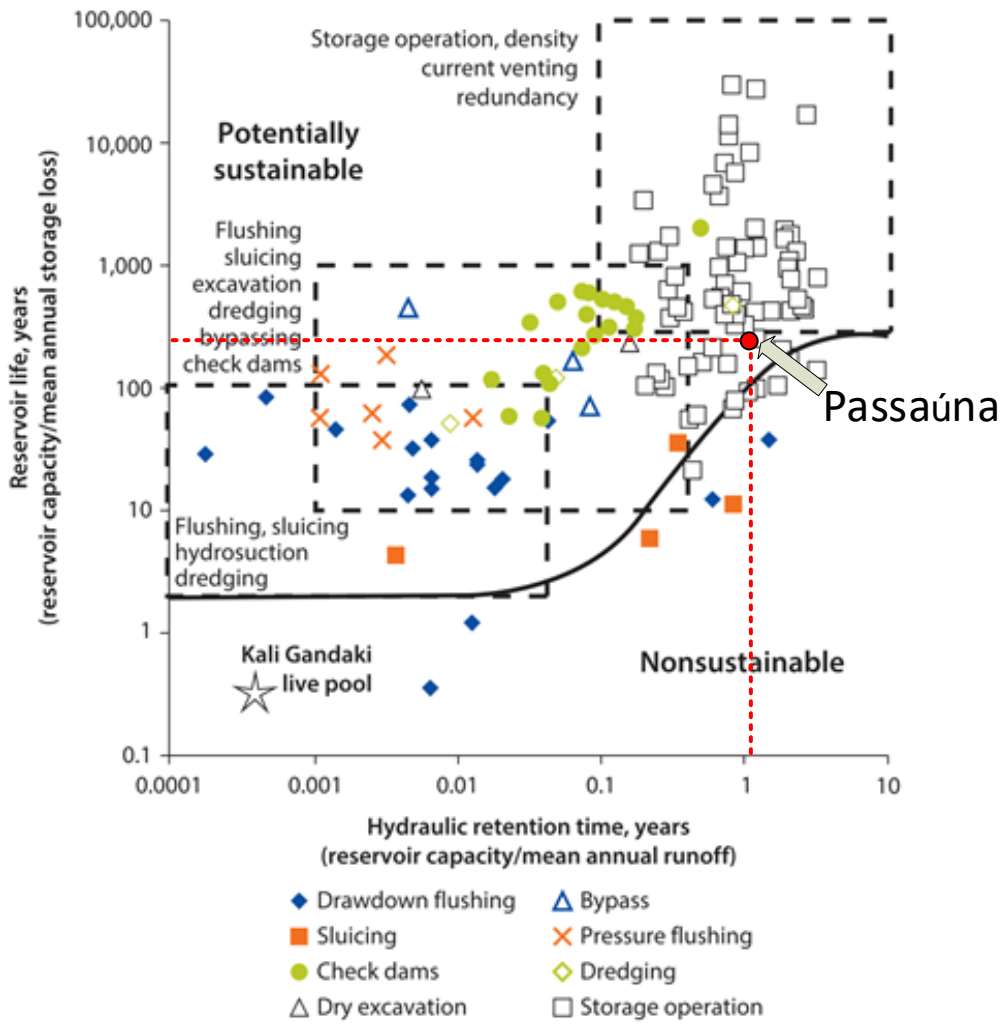


Figure 8—13 Applicability of sediment management techniques for Passaúna based on Annandale et al. (2016)

8.3. Reservoir sediment stock vs. sediment input from catchment

By comparing the results from the two approaches, it is obvious that the sediment stock is 229% higher than the overall sediment input from the catchment as calculated from the model (Figure 8—14). The discrepancies in the results of the modelling are rather high (57% difference between modelled sediment input and measured sediment stock). However when referring to the sediment stock, all the material entering the reservoir (the organic and mineral material that was inside the reservoir before impoundment or was created during the construction phase of the reservoir) is included. On the other hand, based on the definition of Wischmeier and Smith (1978), RUSLE accounts only for the sheet and rill fraction of the soil loss. The previously mentioned are not the only factors causing large differences in the results. The major factors influencing the assessment and their share over the overall sediment stock are listed in Table 8—4 and discussed in more details in the following paragraphs.

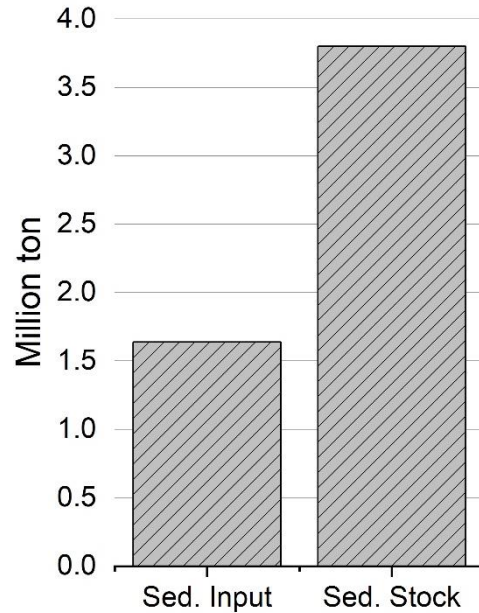


Figure 8—14 comparison between sediment stock in the reservoir and sediment input from the catchment

Table 8—4 Overview of factors creating inconsistencies between measured sediment stock and modelled sediment input

	Factor	Discrepancy
In reservoir	Internal production	2%
	Existing biological stock	<2%
	Errors of the measuring and processing concept	23–36%
	Trapping efficiency of reservoir	0–2%
In catchment	Errors associated with SDR and RUSLE calculations	~50%
	Non-inclusion of gully erosion in RUSLE	
	Non-inclusion of channel erosion in RUSLE	

One of the important factors that affect the sediment balance in the Passaúna reservoir is the contribution of internal production to the sediment stock. Apart from acting as a sink, the reservoir acts also as a source of particles. Due to the climatic conditions and the relatively high nutrient input from the catchment, significant biological activities take place in the water body. Therefore, the autochthonous material created in the reservoir may play an important role in the sediment balance of the system. In other studies it was observed that the autochthonous material can account for up to 75% of the sediment stock (Koszelnik et al. 2017).

In the framework of Mudak-WRM project, sediment traps were installed in the reservoir as described in Ono (2020). Four sediment traps were installed near the intake (INT) and near the dam (DAM) at the surface and at the bottom of the reservoir to quantify the sedimentation rate. Two samples were collected. The first sample was characterized by high rainfall (500 mm) and lasted 157 days, while the second event lasted 47 days and less precipitation was recorded (~130 mm) as shown in Table 8—5. Based on the results of Table 8—5, the sediment from the first sample showed similar results of LOI at the bottom and below the surface. For this event, the material in the traps was a mixture of allochthonous and autochthonous sediment. Therefore, the results could not be used for assessing the sedimentation from the internal production.

Table 8—5 Sampling from the sediment traps

Sediment trap	Mass (g) / LOI (%)		Load (g m ⁻² /d ⁻¹)	
	1	2	1	2
INT bottom	3.9 / 19.2	0.8 / 23.2	4.3	0.9
INT surface	3.0 / 26.2	0.6 / 44.8	3.3	0.7
DAM bottom	3.4 / 21.7	0.7 / 23.6	3.7	0.8
DAM surface	2.0 / 25.2	0.5 / 43.1	2.2	0.6
Sampling Days	157	46		

The second event on the other hand, showed significantly different LOI values at both locations between the near-bottom and the below-surface sediment. The LOI was measured in both cases between 40–45% near the surface, while at the bottom nearly 23%. The decline of the LOI from the surface to the bottom happens due to the mineralization of the organic matter during the settling of the dead algae. It was considered that the values of sediment load at the bottom at both locations had to be attributed to a large part only to the internal production. To estimate the overall sediment deposition due to the internal production, an average load from the values at the bottom of both locations was calculated and was afterwards multiplied with the area of the reservoir and reservoir lifetime in days. This calculation was based on the assumptions that during the total reservoir lifetime and the entire reservoir surface, the internal production and decay of

microorganisms were similar. From this calculation, it was found that 2.2% of the total sediment originates from the internal sediment production. The accuracy of this value needs also to be discussed properly. Passaúna reservoir is a highly dynamic system with 250 stratification days (continuously in summer and spring and episodic in autumn and winter). These variations in the reservoir regime are followed by the variation of the algae bloom regime. Therefore, it is not sure if the measured event is a representative event usable to assess the internal sediment production.

Before flooding, the reservoir area was not cleaned from the existing biomass. Several trees and former vegetation areas are still visible in the reservoir bottom (Figure 8—15). This organic material plays also its role in the bias created when comparing both approaches.

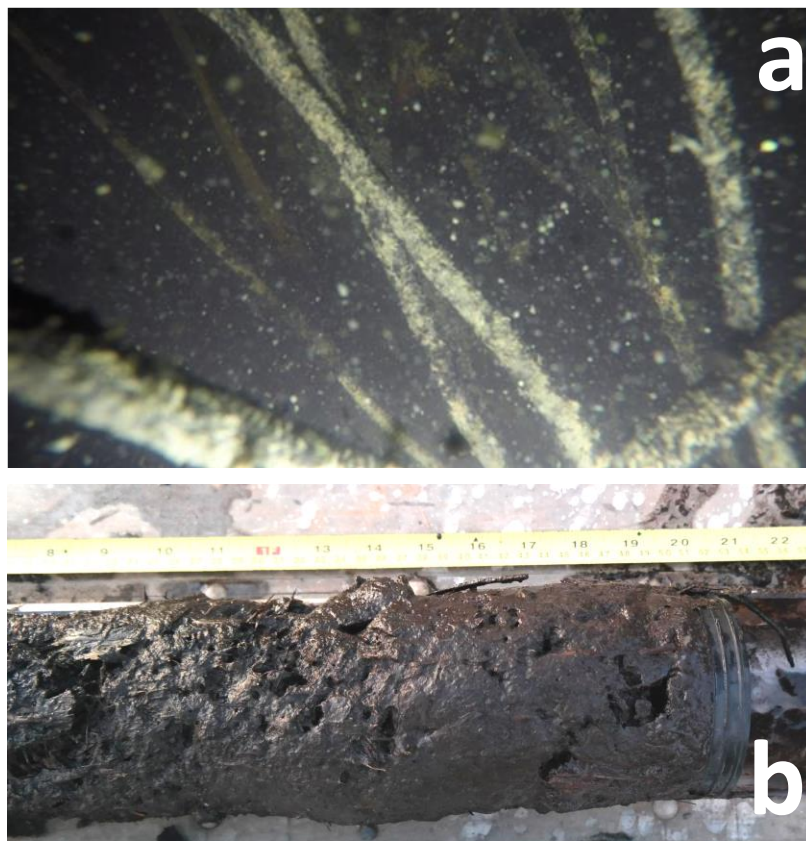


Figure 8—15 a. Image from vegetation in the Passaúna reservoir bottom near the location of core 13 (photo courtesy Lediane Marcon) b. sediment core from Passaúna

In the lacustrine area of the reservoir, the LOI of the sediment was ranging from 15 to 50% while the soil in the Passaúna catchment had LOI up to 16% with an average of 10.3%. The high LOI of the sediment has to be attributed initially to the enrichment of the organic matter during transport (as the organic matter is mostly bounded to the smallest particles which are remobilized at first), and secondly do to the existing stock before pre-impoundment.

A similar phenomena was observed also in the Vossoroca reservoir in the vicinity of Passaúna. As shown in Figure 8—16, after the full drawdown of the Vossoroca reservoir the river eroded the deposited sediment. The sediment is dominated from plant macroremains like leaves, degraded tree branches or roots. The deposition of the organic material was observed in several areas of the reservoir (Stephan Fuchs personal communication on July 2020)



Figure 8—16. Stratigraphy of the sediment after emptying the Vossoroca reservoir (photo courtesy Stephan Fuchs)

Despite the existence of the vegetation macroremains, only one from 31 samples proved their existence in the Passaúna reservoir. In terms of volume, based on the findings and observations in the reservoir, the volume that this deposition type covers in the overall sediment stock is less than three percent. For a more precise estimation, more sediment sampling is needed in the vicinity of Core 18 for defining the area which these plant macroremains cover.

One of the most discussed limitations of RUSLE is the lack of ability to represent also gully and stream bank erosion (Quinton 2004; Belyaev et al. 2005; Alewell et al. 2019). Even with the use of connectivity indexes to calculate the SDR the uncertainties about the prediction of gully

and streambank erosion are still present. In comparison to sheet and rill erosion, gully erosion is less investigated. However, recent studies (Wallbrink et al. 1998; Walling 2005; Wilkinson et al. 2009) showed that gullies contribute substantially in the sediment budget at a catchment scale. They do not only contribute as a sediment source but they also increase the efficiency of sediment transport from uplands to the valley bottom and river channels as most of the sediments generated from rill and inter-rill erosion, that are not connected to gully structures, are deposited at the foot of the hillslopes (Poesen et al. 2003). For the case of Passaúna, this effect is often amplified by the existence of multiple artificial drainage channels near the arable lands, which increase the efficiency of sediment transport.

Poesen et al. 2006 estimate that 47-83% of the sediment occurs from gully erosion. On the other hand, Poesen et al 2003 in a review study indicates that worldwide gullies can represent 10-94% of the total sediment yield from water erosion. When referring to the soil loss calculated from RUSLE it is still unknown to what extent the gully structures contribute to this budget.

For the case of Passaúna reservoir and catchment, the overall discrepancy between the sediment stock and sediment input from the catchment (based on the modelling results) is more than 50%. The 50% deviation is attributed to both the non-inclusion of the channel-gully erosion in the model and the errors in the calculation approach. In order to reduce the errors in the calculation approach, calibration values of measured soil loss at field scale or long term monitoring of suspended sediment in rivers are needed.

Another factor that should be considered is the temporal dimension of the reservoir sedimentation. In case of a rainfall event, a part of the remobilized particles remains in the river stretches. Depending on the size of the catchment and sediment grain size distribution, this amount can be significant for the overall sediment stock assessment as this sediment amount can be stored in the river stretches for days until centuries. Rivers, which have a considerable drainage area and their sediment includes significant part of large grain material are prone to store large amounts of material in the riverbed (Piqué et al. 2014). Passaúna is a (small) mesoscale catchment where sediment is dominated from fine grain material. Therefore, the vast majority of the material during flood is transported directly in the reservoir. For this reason, the overall amount of sediment stored in the river bed was not accounted for in the budget assessment.

Lastly, for the Passaúna reservoir the trapping efficiency, based on the hydrological characteristics of the system, approaches to 1 (0.99). However, for performing such balances with high accuracy, a precise estimate of the trapping efficiency should be performed. Such estimations are cost and time consuming as they require long term measurements of suspended solid loads and bed-load transport in both the inflow and outflow of the reservoir. Using existing mathematical approaches for the calculation often also carries a certain margin of error (Morris

and Fan 2010; Annandale et al. 2016). Therefore, the accurate estimation of trap efficiency, even though to a smaller extent, is as well a limitation and a factor that creates bias in the results.

9. Conclusion

In this final Chapter, the three major research questions presented in the section “2.1. *Research questions and challenges of the thesis*” are answered based on the findings and discussions in the previous chapters.

9.1. How can the developments in free available satellite imagery contribute to improve the sediment input modelling?

With the increased availability of satellite imagery, in the next years a boost in the applications of this freely available datasets in erosion modelling can be expected. The inclusion of additional satellite derived data like grade of soil sealing (imperviousness) and LULC data in combination with NDVI lead to an improved cover and management factor and subsequently in having better modelling outputs. For this study, the use of freely available satellite data, made it possible to reduce the temporal resolution of the model to a month and the spatial resolution to 10 m. It was also possible to model the sediment input in the unsealed areas of the urban settlements, which was found to be around 7% of the overall input. Despite their existence for almost eight years, the full potential of the Sentinel-2 data for erosion modelling is still undiscovered as only a limited number of studies are present. To conclude however, the use of this data can increase the capabilities in terms of spatial and temporal resolution of the model but does not improve their attitude towards the results accuracy without validation measures.

9.2. How can the accuracy of sediment volume assessment and sediment distribution mapping be improved?

During the last decades, significant technological advancements have been recorded in the development of proper tools for the assessment of sediment distribution in the reservoir. In this study, the combination of some of the most advanced systems was investigated in order to increase the sediment detection accuracy.

Hydroacoustics

Topographic differencing can be applied to detect the sediment magnitude in areas where the sediment thickness is higher than the errors of the previous measuring methods and the error of the equipment itself. Linear single beam multifrequency systems show important limitations in gas presence but they can be in detecting the type of lake bottom. Finally, sub-bottom profilers and generally the parametric systems operating at low frequencies (<15 kHz) are powerful tools for sediment detection. When gas is not present, they can achieve sediment mapping in extremely high resolution (up to 1 cm accuracy). As in Passaúna reservoir, for reducing time effort and high surveying costs the use of these systems should be avoided in sediment characterized by high biological activity. The application of these systems should be better confined to reservoirs where sediment is dominated by mineral material and low biochemical activity.

Dynamic freefall penetrometer GraviProbe

The use of GraviProbe enabled the detection of the sediment magnitude with satisfying accuracy. Based on the available data, it cannot be stated with full certainty whether the GP or core samples could derive the most accurate results. There is a mean absolute error of 15.6 cm between the two techniques. This error is considered minimal concerning any engineering applications and the operation of the reservoir. This makes the GraviProbe a useful tool in detecting the sediment layers in reservoirs. In comparison to core sampling, the GP is faster in recording and analyzing the data but also it gives a robust value of the lake bottom characteristics compared to the remote sensing results, which are limited to providing proxy parameters. The limitation of GP is the maximum penetration depth as it operates based on the principle of gravity only. If no pre-impoundment soil is reached than the GP cannot deliver the actual sediment thickness but only the minimum detected thickness. For the Passaúna Reservoir, sediment magnitude measurements up to 1.8 m could be performed. It can therefore be concluded that depending also on the sediment type, the GP can deliver reliable results in reservoirs with no severe sedimentation, where the sediment thickness reaches up to 2 m.

In overall, several techniques can be applied for a precise mapping of sediment deposition in the reservoir. Figure 9—1 presents a guiding diagram on how to choose the most suitable technique for in-reservoir sediment detection and quantification techniques. The accuracy of the measurement depends highly also on the frequency and density of the measured points from each technique. The scientific solutions already exist but they need to be transferred into wide engineering use. One of the main restrictions are the high costs associated with these studies (several hundreds of thousands of Euros including equipment costs and human resources costs).

Therefore, in order to minimize these costs, prior to any sedimentation study or survey, profound knowledge of the geomorphological characteristics of the catchment and of the reservoir are needed to choose the most suitable approach.

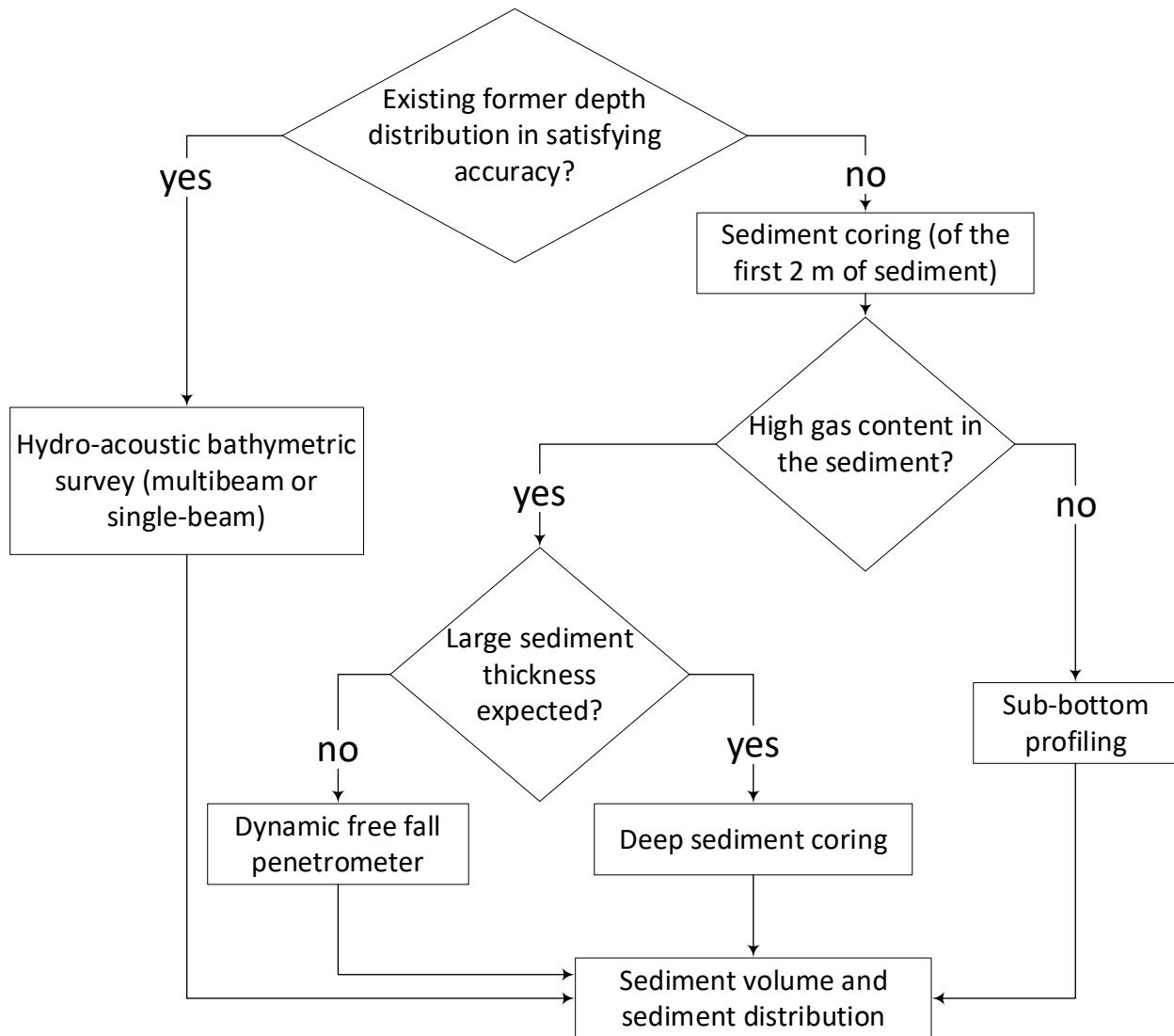


Figure 9—1 Guiding scheme for choosing the most appropriate sediment detection technique

9.3. Can the Passaúna reservoir be used as validation point for the RUSLE based sediment input model?

When using RUSLE the error margins in the results can fluctuate considerably. Therefore, the models have to be coupled with validation measures. The use of reservoirs as validation points represent a real opportunity as they collect almost entirely the incoming sediment. Reservoir sediment stock measurements are often easier to achieve than the conventional

continuous monitoring methods who need high sampling effort and need to deal also with large errors due to the high variability in the river stretches. In case of complex systems however, as shown in this study several other factors can affect the reservoir sediment balance and therefore be misleading to the aim of the research. Reservoirs of lower processes complexity, (e.g. in mountainous areas, low organic material input or low temperatures) can be more easily used as validation points.

To conclude, reservoirs can be used as validation points but there are some limitations. Many uncertainties exist in assessing other factors that contribute in the sediment stock. Sediment input based on RUSLE calculations represents only the sheet-rill part of sediment input and is just one part of the sediment stock. From the findings of this thesis, the modelled sediment input from Passaúna catchment accounts only for 43% of the total sediment stock found in the reservoir. The other 57% include errors of calculation approach, existing organic stock (debris), errors in trap efficiency and autochthonous sediment production. Without information about the actual contribution of other factors no reliable results validation can take place. In every case alternative methods (river suspended solids and bedload monitoring, calibration of models with erosion plots or quantification of gully erosion) have to be taken in consideration as complementary measures for increasing the accuracy of model results.

Publication bibliography

Abdo, Hazem; Salloum, Juliet (2017): Spatial assessment of soil erosion in Alqerdaha basin (Syria). In *Modeling Earth Systems and Environment* 3 (1), p. 26.

Abegg, Friedrich; Anderson, Aubrey L. (1997): The acoustic turbid layer in muddy sediments of Eckernförde Bay, Western Baltic: methane concentration, saturation and bubble characteristics. In *Marine Geology* 137 (1-2), pp. 137–147. DOI: 10.1016/S0025-3227(96)00084-9.

Albatal, Ali; Stark, Nina (2017): Rapid sediment mapping and in situ geotechnical characterization in challenging aquatic areas. In *Limnology and Oceanography: Methods* 15 (8), pp. 690–705. DOI: 10.1002/lom3.10192.

Alewell, Christine; Borrelli, Pasquale; Meusburger, Katrin; Panagos, Panos (2019): Using the USLE: Chances, challenges and limitations of soil erosion modelling. In *International Soil and Water Conservation Research* 7 (3), pp. 203–225. DOI: 10.1016/j.iswcr.2019.05.004.

Almagro, André; Thomé, Thais Caregnatto; Colman, Carina Barbosa; Pereira, Rodrigo Bahia; Marcato Junior, José; Rodrigues, Dulce Buchala Bicca; Oliveira, Paulo Tarso Sanches (2019): Improving cover and management factor (C-factor) estimation using remote sensing approaches for tropical regions. In *International Soil and Water Conservation Research* 7 (4), pp. 325–334. DOI: 10.1016/j.iswcr.2019.08.005.

Anderson, Aubrey L.; Bryant, William R. (1990): Gassy Sediment Occurrence and Properties: Northern Gulf of Mexico. In *Geo-Marine Letters* 10, pp. 209–220.

Anderson, Aubrey L.; Hampton, L. D. (1980): Acoustics of gas bearing sediments. I Background. In *J. Acoust. Soc. Am.* 67, pp. 1865–1889.

Anderson, John T.; van Holliday, D.; Kloser, Rudy; Reid, Dave G.; Simard, Yvan (2008): Acoustic seabed classification. Current practice and future directions. In *ICES Journal of Marine Science* 65 (6), pp. 1004–1011.

Anderson, Michael A.; Pacheco, Porfirio (2011): Characterization of bottom sediments in lakes using hydroacoustic methods and comparison with laboratory measurements. In *Water research* 45 (15), pp. 4399–4408.

Annandale, G. (2014): Sustainable water supply, climate change and reservoir sedimentation management: Technical and economic viability. In *Reservoir Sedimentation*; Schleiss, AJ, Cesare, GD, Franca, MJ, Pfister, M., Eds.

Annandale, G. W.; Morris, G. L.; Karki, P. (2016): Extending the Life of Reservoirs: The World Bank.

Araujo, J. C. de; Knight, D. W. (2005): Assessment of sediment yield of watersheds by reservoir survey and simulation modelling in. In *Geomorphological Processes and Human Impacts in River Basins* (299), p. 124.

Auel, Christian; Berchtold, Th; Boes, Robert (2010): Sediment Management in the Solis Reservoir Using a Bypass Tunnel (8th ICOLD European Club Symposium).

Auel, Christian; Boes, Robert (2011): Sediment bypass tunnel design - review and outlook. In, pp. 403–412.

Bahia, V. G.; Curi, N.; Carmo, D.; Marques, J. (1992): Fundamentos de erosão do solo (tipos, formas, mecanismos, fatores determinantes e controle). In *Informe Agropecuário* 16 (176).

Bakker, Martha M.; Govers, Gerard; van Doorn, Anne; Quetier, Fabien; Chouvardas, Dimitris; Rounsevell, Mark (2008): The response of soil erosion and sediment export to land-use change in four areas of Europe: The importance of landscape pattern. In *Geomorphology* 98 (3), pp. 213–226. DOI: 10.1016/j.geomorph.2006.12.027.

Balk, Helge; Lindem, T. (2014): Sonar4 and Sonar5-Pro Post processing systems. Norway.

Banwart, S. (2011): Save our soils. In *Nature* 474 (7350).

Basson, G. R. (Ed.) (2009): Management of siltation in existing and new reservoirs. General Report. 23rd Congress of the Int. Commission on Large Dams CIGB-ICOLD.

Baumhardt, R. L.; Blanco-Canqui, H. (2014): Soil: Conservation Practices. In : *Encyclopedia of Agriculture and Food Systems*: Elsevier, pp. 153–165.

Baur, Arnold J. (1952): Soil and water conservation glossary. In *Jour. Soil and Water Conserv* 7, pp. 41–52.

BeamworX: AutoClean. Available online at <https://www.beamworx.com/autoclean/>, checked on 11.2020.

Bednarek, A. T. (2001): Undamming Rivers: A Review of the Ecological Impacts of Dam Removal. In *Environmental Management* 27 (6), pp. 803–814. DOI: 10.1007/s002670010189.

Belyaev, V. R.; Wallbrink, P. J.; Golosov, V. N.; Murray, A. S.; Sidorchuk, A.Yu. (2005): A comparison of methods for evaluating soil redistribution in the severely eroded Stavropol region,

southern European Russia. In *Geomorphology* 65 (3), pp. 173–193. DOI: 10.1016/j.geomorph.2004.09.001.

Berhe, Asmeret Asefaw; Barnes, Rebecca T.; Six, Johan; Marín-Spiotta, Erika (2018): Role of Soil Erosion in Biogeochemical Cycling of Essential Elements: Carbon, Nitrogen, and Phosphorus. In *Annu. Rev. Earth Planet. Sci.* 46 (1), pp. 521–548. DOI: 10.1146/annurev-earth-082517-010018.

BioSonics Inc. (2008): User Guide: Visual Bottom Typer 1.10. BioSonics Inc. Seattle.

Boes, Robert; Müller-Hagmann, Michelle (2015): Sedimentation countermeasures – examples from Switzerland. Zurich (International Workshop on Sediment Bypass Tunnels).

Boiffin, J. (1986): Stages and time-dependency of soil crusting in situ. In : Assessment of soil surface sealing and crusting: Flanders Research Center for Soil Erosion and Soil Conservation Ghent, pp. 91–98.

Boiffin, J.; Monnier, G. (Eds.) (1986): Infiltration rate as affected by soil surface crusting caused by rainfall.

Borrelli, P.; van Oost, K.; Meusburger, K.; Alewell, C.; Lugato, E.; Panagos, P. (2018): A step towards a holistic assessment of soil degradation in Europe: Coupling on-site erosion with sediment transfer and carbon fluxes. In *Environmental research* 161, pp. 291–298. DOI: 10.1016/j.envres.2017.11.009.

Borrelli, Pasquale; Robinson, David A.; Fleischer, Larissa R.; Lugato, Emanuele; Ballabio, Cristiano; Alewell, Christine et al. (2017): An assessment of the global impact of 21st century land use change on soil erosion. In *Nat Commun* 8 (1), p. 2013. DOI: 10.1038/s41467-017-02142-7.

Borselli, Lorenzo; Cassi, Paola; Torri, Dino (2008): Prolegomena to sediment and flow connectivity in the landscape: a GIS and field numerical assessment. In *CATENA* 75 (3), pp. 268–277.

Bouyoucos, G. J. (1935): The clay ratio as a criterion of susceptibility of soils to erosion. In *Journal of the American Society of Agronomy* 27, pp. 738–741.

Breiman, L. (2001): Random Forests. In *Machine Learning* 46 (1), 5–32.

Bridges, E. M.; Oldeman, L. R. (1999): Global Assessment of Human-Induced Soil Degradation. In *Arid Soil Research and Rehabilitation* 13 (4), pp. 319–325. DOI: 10.1080/089030699263212.

Brouwer, P.A.I. (2008): Seafloor classification using a single beam echosounder. TU Delft, Department of Earth Observation & Space Systems. Delft, The Netherlands. Available online at http://www.lr.tudelft.nl/fileadmin/Faculteit/LR/Organisatie/Afdelingen_en_Leerstoelen/Afdeling_R

S/Acoustic_Remote_Sensing/Research/Publications/Master_theses/doc/msc_thesis_PB_final.pdf, checked on 15.07.20016.

Brown, L. C.; Foster, G. R. (1987): Storm Erosivity Using Idealized Intensity Distributions. In *Trans. ASAE* 30 (2), p. 379. DOI: 10.13031/2013.31957.

Bruk, Stevan (1985): Methods of computing sedimentation in lakes and reservoirs.

Brune, Gunnar M. (1953): Trap efficiency of reservoirs. In *Eos Trans. AGU* 34 (3), p. 407. DOI: 10.1029/TR034i003p00407.

Bruno, Carmelo; Di Stefano, Costanza; Ferro, Vito (2008): Field investigation on rilling in the experimental Sparacia area, South Italy. In *Earth Surf. Process. Landforms* 33 (2), pp. 263–279. DOI: 10.1002/esp.1544.

Bryan, R. B. (1999): Soil erodibility and processes of water erosion on hillslope. In *Geomorphology* 32, pp. 385–415.

Burczynski, Janusz (1999): Bottom classification. In *BioSonics Inc* 4027.

Caiti A.; Chapmann R.; Hermand J. P.; Jesus S. M. (Eds.) (2006): *Acoustic Sensing Techniques for the Shallow Water Environment*. Dordrecht: Springer.

Carneiro, Charles; Kelderman, Peter; Irvine, Kenneth (2016): Assessment of phosphorus sediment–water exchange through water and mass budget in Passaúna Reservoir (Paraná State, Brazil). In *Environmental Earth Sciences* 75 (7), p. 564.

Carollo, Francesco Giuseppe; Di Stefano, Costanza; Ferro, Vito; Pampalone, Vincenzo (2015): Measuring rill erosion at plot scale by a drone-based technology. In *Hydrological Processes* 29 (17), pp. 3802–3811. DOI: 10.1002/hyp.10479.

Carvalho, N.; Júnior, N. P.; dos Santos, P. M.; Lima, J. E. F. (2000): Reservoir sedimentation assessment guideline. BRAZILIAN ELECTRICITY REGULATORY AGENCY. Brazilia.

Castro Filho, C.; Cataneo, A.; Biscaia, R. (1982): Utilização da metodologia de Wilkinson, para cálculo do potencial erosivo das chuvas em cinco localidades do Paraná. In *Rev. Bras. Ciênc. Solo* 6, pp. 240–241.

Cavalli, Marco; Trevisani, Sebastiano; Comiti, Francesco; Marchi, Lorenzo (2013): Geomorphometric assessment of spatial sediment connectivity in small Alpine catchments. In *Geomorphology* 188, pp. 31–41. DOI: 10.1016/j.geomorph.2012.05.007.

Cebecauer, Tomáš; Hofierka, Jaroslav (2008): The consequences of land-cover changes on soil erosion distribution in Slovakia. In *Geomorphology* 98 (3), pp. 187–198. DOI: 10.1016/j.geomorph.2006.12.035.

Central Water Commission; Central Dam Safety Organisation (2019): Handbook for Assessing and Managing Reservoir Sedimentation. New Delhi.

Cerro, Carlos; Bech, Joan; Codina, Bernat; Lorente, Jeroni (1998): Modeling rain erosivity using disdrometric techniques. In *Soil Science Society of America Journal* 62 (3), pp. 731–735.

Chivers, R. C. (1990): New acoustic processing for underway surveying. In *Hydrogr. J.* 56, pp. 9–17.

Chorley, Richard J.; Kennedy, Barbara A. (1971): Physical geography: a systems approach: Prentice Hall.

Chuenchum, Pavisorn; Xu, Mengzhen; Tang, Wenzhe (2020): Estimation of Soil Erosion and Sediment Yield in the Lancang-Mekong River Using the Modified Revised Universal Soil Loss Equation and GIS Techniques. In *Water* 12, p. 135. DOI: 10.3390/w12010135.

Churchill, M. A. (1948): Discussion of “Analysis and use of reservoir sedimentation data”. In *Proceedings of the Federal Interagency Sedimentation Conference*, pp. 139–140.

Clark, E. V.; Odhiambo, B. K.; Yoon, S.; Pilati, L. (2015): Hydroacoustic and spatial analysis of sediment fluxes and accumulation rates in two Virginia reservoirs, USA. In *Environmental science and pollution research international* 22 (11), pp. 8659–8671. DOI: 10.1007/s11356-014-4050-x.

Clarke, J. Hughes, E; Danforth, B. W.; Valentine, P. (Eds.) (1997): Areal seabed classification using backscatter angular response at 95 kHz.

Clemente, E.; Oliveira, A.; Fontana, A.; Martins, A.; Schuler, A.; Fidalgo, E.; Monteiro, J. (2017): Erodibilidade dos solos da Região Serrana do Rio de Janeiro obtida por diferentes equações de predição indireta. Embrapa Solos. Rio de Janeiro.

Corella, J. P.; Arantegui, A.; Loizeau, J. L.; DelSontro, T.; Le Dantec, N.; Stark, N. et al. (2013): Sediment dynamics in the subaquatic channel of the Rhone delta (Lake Geneva, France/Switzerland). In *Aquat Sci.* DOI: 10.1007/s00027-013-0309-4.

Corella, J. P.; Loizeau, J.-L.; Kremer, K.; Hilbe, M.; Gerard, J.; Le Dantec, N. et al. (2016): The role of mass-transport deposits and turbidites in shaping modern lacustrine deepwater channels. In *Marine and Petroleum Geology* 77, pp. 515–525. DOI: 10.1016/j.marpetgeo.2016.07.004.

Croke, Jacky; Mockler, Simon; Fogarty, Peter; Takken, Ingrid (2005): Sediment concentration changes in runoff pathways from a forest road network and the resultant spatial pattern of catchment connectivity. In *Geomorphology* 68 (3-4), pp. 257–268.

Cross, Benjamin K.; Moore, Barry C. (2014): Lake and reservoir volume: Hydroacoustic survey resolution and accuracy. In *Lake and Reservoir Management* 30 (4), pp. 405–411. DOI: 10.1080/10402381.2014.960115.

da Silva Santos, Leonardo (2019): Sensitivity of sediment budget calculations for an applicable reservoir's lifetime. Master thesis, Karlsruhe, Germany. Institute for Water and River Basin Management.

Dayal, Umesh; Allen, John H. (1973): Instrumented Impact Cone Penetrometer. In *Can. Geotech. J.* 10 (3), pp. 397–409. DOI: 10.1139/t73-034.

Dendy, F. E. (1974): Sediment trap efficiency of small reservoirs. In *Transactions of the American Society of Agricultural Engineers* 17 (5), pp. 899–901.

Desmet, P. J.J.; Govers, Gerard (1997): Modelling topographic potential for erosion and deposition using GIS. In *International Journal of Geographical Information Science* 11 (6), pp. 603–610.

Desmet, P.J.J.; Govers, G. (1996): A GIS procedure for automatically calculating the USLE LS factor on topographically complex landscape units. In *Journal of Soil and Water Conservation* 51 (5), pp. 427–433. Available online at <https://www.scopus.com/inward/record.uri?eid=2-s2.0-0000382819&partnerID=40&md5=8b80a6b35432538b8a5d075a73b86615>.

Diesing, Markus; Green, Sophie L.; Stephens, David; Lark, R. Murray; Stewart, Heather A.; Dove, Dayton (2014): Mapping seabed sediments: Comparison of manual, geostatistical, object-based image analysis and machine learning approaches. In *Continental Shelf Research* 84, pp. 107–119. DOI: 10.1016/j.csr.2014.05.004.

Dorvinen, J. (2016): A Method for Interpreting the In-Situ Consolidation State of Surficial Seabed Sediments using a Free-Fall Penetrometer. Master. Virginia Polytechnic Institute and State University, Blacksburg, Virginia, USA. Available online at https://techworks.lib.vt.edu/bitstream/handle/10919/73216/Dorvinen_JI_T_2016.pdf?sequence=1&isAllowed=y.

Dotterweich, Markus (2013): The history of human-induced soil erosion: Geomorphic legacies, early descriptions and research, and the development of soil conservation—A global synopsis. In *Geomorphology* 201, pp. 1–34. DOI: 10.1016/j.geomorph.2013.07.021.

Draut, Amy E.; Logan, Joshua B.; Mastin, Mark C. (2011): Channel evolution on the dammed Elwha River, Washington, USA. In *Geomorphology* 127 (1-2), pp. 71–87. DOI: 10.1016/j.geomorph.2010.12.008.

Dück, Y.; Lorke, A.; Jokiel, C.; Gierse, J. (2019): Laboratory and field investigations on freeze and gravity core sampling and assessment of coring disturbances with implications on gas bubble

characterization. In *Limnology and Oceanography: Methods* 17 (11), pp. 585–606. DOI: 10.1002/lom3.10335.

Duffaut, P. (2013): The traps behind the failure of Malpasset arch dam, France, in 1959. In *Journal of Rock Mechanics and Geotechnical Engineering* 5 (5), pp. 335–341. DOI: 10.1016/j.jrmge.2013.07.004.

Dunbar, John A.; Allen, Peter M.; Higley, Paul D. (1999): Multifrequency acoustic profiling for water reservoir sedimentation studies. In *Journal of Sedimentary Research* 69 (2), pp. 518–527.

Dunjó, Gemma; Pardini, Giovanni; Gispert, Maria (2004): The role of land use–land cover on runoff generation and sediment yield at a microplot scale, in a small Mediterranean catchment. In *Journal of Arid Environments* 57 (2), pp. 239–256.

Duraes, Matheus; Filho, José; Oliveira, Vinícius (2016a): Water erosion vulnerability and sediment delivery rate in upper Iguazu river basin – Paraná. In *RBRH* 21. DOI: 10.1590/2318-0331.011616029.

Duraes, Matheus Fonseca; Mello, Carlos Rogério de; Beskow, Samuel (2016b): Sediment yield in Paraopeba River Basin – MG, Brazil. In *International Journal of River Basin Management* 14 (4), pp. 367–377. DOI: 10.1080/15715124.2016.1159571.

Durigon, V. L.; Carvalho, D. F.; Antunes, M.A.H.; Oliveira, P.T.S.; Fernandes, M. M. (2014): NDVI time series for monitoring RUSLE cover management factor in a tropical watershed. In *International Journal of Remote Sensing* 35 (2), pp. 441–453. DOI: 10.1080/01431161.2013.871081.

Elçi, Şebnem; Bor, Aslı; Çalışkan, Anıl (2009): Using numerical models and acoustic methods to predict reservoir sedimentation. In *Lake and Reservoir Management* 25 (3), pp. 297–306.

Elzinga, Louwrens (2017): Dredging of Reservoirs. Master Thesis. TU Delft, Delft, The Netherlands.

Embrapa Solos (2007): Mapa de Solos de Estado de Parana. EMBRAPA. Rio de Janeiro.

Ernstsen, Verner; Noormets, Riko; Hebbeln, Dierk; Bartholomä, Alexander; Flemming, Burghard (2006): Precision of high-resolution multibeam echo sounding coupled with high-accuracy positioning in a shallow water coastal environment. In *Geo-Marine Letters* 26, pp. 141–149. DOI: 10.1007/s00367-006-0025-3.

Estrada-Carmona, Natalia; Harper, Elizabeth B.; DeClerck, Fabrice; Fremier, Alexander K. (2017): Quantifying model uncertainty to improve watershed-level ecosystem service quantification: a global sensitivity analysis of the RUSLE. In *International Journal of Biodiversity Science, Ecosystem Services & Management* 13 (1), pp. 40–50. DOI: 10.1080/21513732.2016.1237383.

Favis-Mortlock, David; Boardman, John (1995): Nonlinear responses of soil erosion to climate change: a modelling study on the UK South Downs. In *CATENA* 25 (1-4), pp. 365–387.

Fernández-Raga, María; Campo, Julián; Rodrigo-Comino, Jesús; Keesstra, Saskia D. (2019): Comparative Analysis of Splash Erosion Devices for Rainfall Simulation Experiments: A Laboratory Study. In *Water* 11 (6), p. 1228. DOI: 10.3390/w11061228.

Fernández-Raga, María; Palencia, Covadonga; Keesstra, Saskia; Jordán, Antonio; Fraile, Roberto; Angulo-Martínez, Marta; Cerdà, Artemi (2017): Splash erosion: A review with unanswered questions. In *Earth-Science Reviews* 171, pp. 463–477. DOI: 10.1016/j.earscirev.2017.06.009.

Ferreira, V. A.; Weesies, G. A.; Yoder, D. C.; Foster, G. R.; Renard, K. G. (1995): The site and condition specific nature of sensitivity analysis. In *Journal of Soil and Water Conservation* 50 (5), pp. 493–497.

Fournier, A. J. (2011): *Soil Erosion: Causes, Processes, and Effects*: Nova Science Publishers (Environmental science, engineering and technology series). Available online at <https://books.google.de/books?id=CpygcQAACAAJ>.

Fournier, F. (1972): *Soil conservation (Nature and Environmental Series)*.

Fournier, Frederic (1961): Climat et erosion. In *Soil Science* 92 (2), p. 151.

Fox, Garey; Sheshukov, Aleksey; Cruse, Rick; Kolar, Randall; Guertault, Lucie; Gesch, K.; Dutnell, Russell (2016): Reservoir Sedimentation and Upstream Sediment Sources: Perspectives and Future Research Needs on Streambank and Gully Erosion. In *Environmental Management* 57. DOI: 10.1007/s00267-016-0671-9.

Fredén, Curt; Furuholm, Lars (1978): The Säterberget Gully at Brattforsheden, Värmland, Sweden. In *Geologiska Föreningen i Stockholm Förhandlingar* 100 (2), pp. 231–235. DOI: 10.1080/11035897809454467.

Furnans, Jordan; Austin, Barney (2008): Hydrographic survey methods for determining reservoir volume. In *Environmental Modelling & Software* 23 (2), pp. 139–146. DOI: 10.1016/j.envsoft.2007.05.011.

Gaillot, S.; Piegay, H. (1999): Impact of gravel-mining on stream channel and coastal sediment supply: example of the Calvi Bay in Corsica (France). In *Journal of Coastal Research*, pp. 774–788.

Galdino, Sergio; Sano, Edson E.; Andrade, Ricardo G.; Grego, Celia R.; Nogueira, Sandra F.; Bragantini, Claudio; Flosi, Ana H. G. (2016): Large-scale Modeling of Soil Erosion with RUSLE for Conservationist Planning of Degraded Cultivated Brazilian Pastures. In *Land Degrad. Dev.* 27 (3), pp. 773–784. DOI: 10.1002/ldr.2414.

Ganasri, B. P.; Ramesh, H. (2016): Assessment of soil erosion by RUSLE model using remote sensing and GIS - A case study of Nethravathi Basin. In *Geoscience Frontiers* 7 (6), pp. 953–961. DOI: 10.1016/j.gsf.2015.10.007.

Garg, Vaibhav; Jothiprakash, Vinayakam (2008): Trap efficiency estimation of a large reservoir. In *ISH Journal of Hydraulic Engineering* 14, pp. 88–101. DOI: 10.1080/09715010.2008.10514907.

Gee, Glendon W.; Or, Dani (2002): 2.4 Particle-size analysis. In *Methods of soil analysis: Part 4 physical methods* 5, pp. 255–293.

Gericke, Andreas (2013): Evaluation of empirical approaches to estimate the variability of erosive inputs in river catchments.

Gianinetto, Marco; Aiello, Martina; Polinelli, Francesco; Frassy, Federico; Rulli, Maria Cristina; Ravazzani, Giovanni et al. (2019): D-RUSLE: a dynamic model to estimate potential soil erosion with satellite time series in the Italian Alps. In *European Journal of Remote Sensing* 52 (sup4), pp. 34–53. DOI: 10.1080/22797254.2019.1669491.

Gill, Mohammad Akram (1979): Sedimentation and useful life of reservoirs. In *Journal of hydrology* 44 (1-2), pp. 89–95.

Grauso, Sergio; Pasanisi, Francesco; Tebano, Carlo (2018a): Assessment of a Simplified Connectivity Index and Specific Sediment Potential in River Basins by Means of Geomorphometric Tools. In *Geosciences* 8 (2), p. 48. DOI: 10.3390/geosciences8020048.

Grauso, Sergio; Verrubbi, Vladimiro; Peloso, Alessandro; Zini, Alessandro; Sciortino, Maurizio (2018b): Estimating the C-factor of USLE/RUSLE by means of NDVI time-series in Southern Latium. An improved correlation model. ENEA.

Hakanson, L. (1986): A sediment penetrometer for in situ determination of sediment type and potential bottom dynamic conditions. In *Internationale Revue der gesamten Hydrobiologie* 71 (6), pp. 851–858.

Hamel, Perrine; Chaplin-Kramer, Rebecca; Sim, Sarah; Mueller, Carina (2015): A new approach to modeling the sediment retention service (InVEST 3.0): Case study of the Cape Fear catchment, North Carolina, USA. In *The Science of the total environment* 524-525, pp. 166–177. DOI: 10.1016/j.scitotenv.2015.04.027.

Han, Zhen; Zhong, Shouqin; Ni, Jiupai; Shi, Zhonglin; Wei, Chaofu (2019): Estimation of Soil Erosion to Define the Slope Length of Newly Reconstructed Gentle-Slope Lands in Hilly Mountainous Regions. In *Scientific Reports* 9 (1), p. 4676. DOI: 10.1038/s41598-019-41405-9.

Heald, G. J.; Pace, N. G. (Eds.) (1996): An analysis of 1st and 2nd backscatter for seabed classification (2).

Heinemarm, H. G. (1981): A new sediment trap efficiency curve for small reservoirs 1. In *JAWRA Journal of the American Water Resources Association* 17 (5), pp. 825–830.

Hernani, L. C. (2002): Uma resposta conservacionista—O impacto do Sistema Plantio Direto. MANZATTO, CV, FREITAS JÚNIOR, E. & PERES, JRR (eds.) *Uso agrícola dos solos brasileiros*. In *Rio de Janeiro: Embrapa Solos*, pp. 151–161.

Hilgert, S.; Sotiri, K.; Fuchs, S. (Eds.) (2019a): Advanced assessment of sediment characteristics based on Rheological and hydroacoustic measurements in a Brazilian reservoir. 38th IAHR World Congress. Panama City, Panama. IAHR.

Hilgert, Stephan (2014): Analysis of spatial and temporal heterogenities of methane emissions of reservoir by correlating hydroacoustic with sediment parameters. Doctoral Dissertation. Karlsruhe Institute of Technology. Karlsruhe.

Hilgert, Stephan; Fernandes, Cristovão Vicente Scapulatempo; Fuchs, Stephan (2019b): Redistribution of methane emission hot spots under drawdown conditions. In *Science of The Total Environment* 646, pp. 958–971.

Hilgert, Stephan; Fuchs, Stephan (Eds.) (2015): Static and dynamic hydro-acoustic assessment of sediment magnitudes in a Brazilian reservoir. *RIO Acoustics 2015*. Rio.

Hilgert, Stephan; Sotiri, Klajdi; Marcon, Lediane; Liu, Liu; Bleninger, Tobias; Mannich, Michael; Fuchs, Stephan (2019c): Resolving spatial heterogenities of methane ebullition flux from a Brazilian reservoir by combining hydro-acoustic measurements with methane production potential. In *38th International Association of Hydro Resources World Congress Proceedings*, pp. 3576–3585. Available online at <https://static.iahr.org/34/418.pdf>.

Hilgert, Stephan; Wagner, Adrian; Kiemle, Lisa; Fuchs, Stephan (2016): Investigation of echo sounding parameters for the characterisation of bottom sediments in a sub-tropical reservoir. In *Advances in Oceanography and Limnology*, pp. 93–105.

Hooke, R.B (2000): On the history of humans as geomorphic agents. In *Geology* 28 (9).

Innomar Technologies GmbH: SES-2000 Compact Sub-Bottom Profiler. Available online at www.innomar.com/ses2000compact.php, checked on January 2017.

Innomar Technologies GmbH (2016): User's Guide ISE 2.9.5 Post Processing Software.

Instituto Ambiental do Paraná (2017): QUALIDADE DAS ÁGUAS DOS RESERVATÓRIOS DO ESTADO DO PARANÁ. Curitiba.

Instituto Brasileiro de Geografia e Estatística (2011): Base de informações do Censo Demográfico 2010: Resultados do Universo por setor censitário. Instituto Brasileiro de Geografia e Estatística (IBGE). Rio de Janeiro.

International Commission on Large Dams (2019): General Synthesis. Available online at https://www.icold-cigb.org/GB/world_register/general_synthesis.asp, checked on 5/21/2019.

International Hydrological Programme; UNESCO Office Beijing; The International Research and Training Center on Erosion and Sedimentation (2004): *Warping Dams– Construction and its Effects on Environment, Economy, and Society in Loess Plateau Region of China*. Beijing.

International Hydropower Association (2020): *Hydropower Status Report*. International Hydropower Association.

inVEST- Natural Capital Project. Available online at <http://releases.naturalcapitalproject.org/invest-userguide/latest/sdr.html>, checked on 1/30/2020.

Irudukunda, Parfait; Sang, Joseph K.; Nyadawa, Maurice O.; Maina, Caroline W. (2020): Sedimentation Effect on the Storage Capacity in Lake Nakuru, Kenya. In *JOURNAL OF SUSTAINABLE RESEARCH IN ENGINEERING* 5 (3), pp. 149–158.

Jakubauskas, Mark; deNoyelles, Frank (2008): Methods for assessing sedimentation in reservoirs. In *Sedimentation in Our Reservoirs: Causes and Solutions*, p. 25.

Jamshidi, Reza; Dragovich, Deirdre; Webb, Ashley A. (2014): Distributed empirical algorithms to estimate catchment scale sediment connectivity and yield in a subtropical region. In *Hydrol. Process.* 28 (4), pp. 2671–2684. DOI: 10.1002/hyp.9805.

Janes, V. J. J.; Nicholas, A. P.; Collins, A. L.; Quine, T. A. (2017): Analysis of fundamental physical factors influencing channel bank erosion: results for contrasting catchments in England and Wales. In *Environ Earth Sci* 76 (7), p. 123. DOI: 10.1007/s12665-017-6593-x.

Janowski, Lukasz; Trzcinska, Karolina; Tegowski, Jaroslaw; Kruss, Aleksandra; Rucinska-Zjadacz, Maria; Pocwiardowski, Pawel (2018): Nearshore Benthic Habitat Mapping Based on Multi-Frequency, Multibeam Echosounder Data Using a Combined Object-Based Approach: A Case Study from the Rowy Site in the Southern Baltic Sea. In *Remote Sensing* 10 (12), p. 1983. DOI: 10.3390/rs10121983.

Jayadi, Rachmad; Istiarto; Pradipta, Ansita Gukitapingin (2018): Impact of Sedimentation Counter Measure on the Performance of Flood Control: A Case Study of Wonogiri Reservoir. In *AMM* 881, pp. 78–85. DOI: 10.4028/www.scientific.net/AMM.881.78.

Joel, A.; Messing, I.; Seguel, O.; Casanova, M. (2002): Measurement of surface water runoff from plots of two different sizes. In *Hydrol. Process.* 16 (7), pp. 1467–1478. DOI: 10.1002/hyp.356.

Juracek, Kyle E. (2015): The aging of America's reservoirs: in-reservoir and downstream physical changes and habitat implications. In *JAWRA Journal of the American Water Resources Association* 51 (1), pp. 168–184.

Karydas, Christos; Bouarour, Ouiza; Zdruli, Pandi (2020): Mapping Spatio-Temporal Soil Erosion Patterns in the Candelaro River Basin, Italy, Using the G2 Model With Sentinel2 Imagery. In *Geosciences* 10, p. 89. DOI: 10.3390/geosciences10030089.

Karydas, Christos G.; Sekuloska, Tijana; Silleos, Georgios N. (2009): Quantification and site-specification of the support practice factor when mapping soil erosion risk associated with olive plantations in the Mediterranean island of Crete. In *Environmental Monitoring and Assessment* 149 (1-4), pp. 19–28. DOI: 10.1007/s10661-008-0179-8.

Kaspersen, P.; Fensholt, R.; Drews, M. (2015): Using Landsat Vegetation Indices to Estimate Impervious Surface Fractions for European Cities. In *Remote Sensing* 7 (6), pp. 8224–8249. DOI: 10.3390/rs70608224.

Kilburn, C. R. J.; Petley, D. N. (2003): Forecasting giant, catastrophic slope collapse: lessons from Vajont, Northern Italy. In *Geomorphology* 54 (1), pp. 21–32. DOI: 10.1016/S0169-555X(03)00052-7.

Kirichek, Alex; Rutgers, R. (2019): Water injection dredging and fluid mud trapping in the Port of Rotterdam. Rotterdam, The Netherlands. In *CEDA Dredging Days*.

Kirichek, Alex; Shakeel, Ahmad; Chassagne, Claire (2020): Using in situ density and strength measurements for sediment maintenance in ports and waterways. In *J Soils Sediments*. DOI: 10.1007/s11368-020-02581-8.

Kloser, R. J.; Keith, G.; Ryan, T.; Williams, A.; Penrose, J. (Eds.) (2002): Seabed biotope characterisation in deep water-initial evaluation of single and multi-beam acoustics.

Kondolf, G. Mathias; Gao, Yongxuan; Annandale, George W.; Morris, Gregory L.; Jiang, Enhui; Zhang, Junhua et al. (2014): Sustainable sediment management in reservoirs and regulated rivers: Experiences from five continents. In *Earth's Future* 2 (5), pp. 256–280.

Kongsberg Inc. (2006): EA 400 Single beam hydrographic echo sounder. Available online at [https://www.km.kongsberg.com/ks/web/nokbg0397.nsf/AllWeb/5508DC01B38C35D2C12581B5004514C1/\\$file/160981_ea400_operator_manual.pdf?OpenElement](https://www.km.kongsberg.com/ks/web/nokbg0397.nsf/AllWeb/5508DC01B38C35D2C12581B5004514C1/$file/160981_ea400_operator_manual.pdf?OpenElement).

Koszelnik, Piotr; Gruca-Rokosz, Renata; Bartoszek, Lilianna (2017): An isotopic model for the origin of autochthonous organic matter contained in the bottom sediments of a reservoir. In *International Journal of Sediment Research*. DOI: 10.1016/j.ijsrc.2017.10.002.

Krasa, Josef; Dostal, Tomas; Jachymova, Barbora; Bauer, Miroslav; Devaty, Jan (2019): Soil erosion as a source of sediment and phosphorus in rivers and reservoirs–Watershed analyses using WaTEM/SEDEM. In *Environmental research* 171, pp. 470–483.

Lafren, J. M.; Foster, G. R.; Onstad, C. A. (1985): Simulation of individual-storm soil loss for modeling the impact of soil erosion on crop productivity.

Lamarche, Geoffroy; Lurton, Xavier (2018): Recommendations for improved and coherent acquisition and processing of backscatter data from seafloor-mapping sonars. In *Marine Geophysical Research* 39 (1), pp. 5–22. DOI: 10.1007/s11001-017-9315-6.

Le Gac, Jean-Claude; Steéphan, Yann; Garlan, Thierry; Weber, Nicholas (2006): On the assessment of geoacoustic parameters in shallow water environments. In Andrea Caiti, N. Ross Chapman, Jean-Pierre Hermand, Sérgio M. Jesus (Eds.): *Acoustic Sensing Techniques for the Shallow Water Environment: Inversion Methods and Experiments*. Dordrecht: Springer Netherlands, pp. 1–15. Available online at https://doi.org/10.1007/978-1-4020-4386-4_1.

Lombardi Neto, F.; Moldenhauer, W. C. (1992): Rainfall erosivity: its distribution and relationship with soil loss at Campinas: Brasil (2, 51). In *Bragantia*.

Lu, D.; Li, G.; Valladares, G. S.; Batistella, M. (2004): Mapping soil erosion risk in Rondônia, Brazilian Amazonia: using RUSLE, remote sensing and GIS. In *Land Degrad. Dev.* 15 (5), pp. 499–512. DOI: 10.1002/ldr.634.

Lu, Hua; Moran, C. J.; Sivapalan, Murugesu (2005): A theoretical exploration of catchment-scale sediment delivery. In *Water Resources Research* 41 (9).

Lunne, Tom (2012): The Fourth James K. Mitchell Lecture: The CPT in offshore soil investigations - a historic perspective. In *Geomechanics and Geoengineering* 7 (2), pp. 75–101. DOI: 10.1080/17486025.2011.640712.

Lunne, Tom; Powell, John J. M.; Robertson, Peter K. (2002): *Cone penetration testing in geotechnical practice*: CRC Press.

Lurton X. (2002): *An Introduction to underwater acoustics*. Berlin: Springer.

Ma, Yuanxu; Huang, He Qing; Nanson, Gerald C.; Li, Yong; Yao, Wenyi (2012): Channel adjustments in response to the operation of large dams: The upper reach of the lower Yellow River. In *Geomorphology* 147-148, pp. 35–48. DOI: 10.1016/j.geomorph.2011.07.032.

Maavara, Taylor; Chen, Qiuwen; van Meter, Kimberly; Brown, Lee; Zhang, Jianyun; Ni, Jinren; Zarfl, Christiane (2020): River dam impacts on biogeochemical cycling. In *Nature Reviews Earth & Environment*. DOI: 10.1038/s43017-019-0019-0.

Mannigel, Anny Rosi; Passos, Morel de; Moreti, Dolorice; da Rosa Medeiros, Luciano (2002): Fator erodibilidade e tolerância de perda dos solos do Estado de São Paulo. In *Acta Scientiarum Agronomy* 24, pp. 1335–1340.

Manzatto, C. V.; Junior, Freitas; Peres, J. R.R. (2002): Agricultural use of Brazilian soils. In *Agricultural use of Brazilian soils*.

Marcon, Lediane; Bleninger, Tobias; Mannich, Michael; Hilgert, Stephan (2019): High-frequency measurements of gas ebullition in a Brazilian subtropical reservoir-identification of relevant triggers and seasonal patterns. In *Environmental Monitoring and Assessment* 191. DOI: 10.1007/s10661-019-7498-9.

Marques, Valter; Ceddia, Marcos; Antunes, Mauro; Carvalho, Daniel; Anache, Jamil; Rodrigues, Dulce; Oliveira, Paulo Tarso (2019): USLE K-Factor Method Selection for a Tropical Catchment. In *Sustainability* 11, pp. 1–17. DOI: 10.3390/su11071840.

McCartney, M. P.; Sullivan, C.; Acreman, Michael C. (2001): Ecosystem impacts of large dams. In *Background paper 2*.

McGrane, Scott J. (2016): Impacts of urbanisation on hydrological and water quality dynamics, and urban water management: a review. In *Hydrological Sciences Journal* 61 (13), pp. 2295–2311. DOI: 10.1080/02626667.2015.1128084.

Merritt, Elaine (1984): The identification of four stages during micro-rill development. In *Earth Surf. Process. Landforms* 9 (5), pp. 493–496. DOI: 10.1002/esp.3290090510.

Merritt, W. S.; Letcher, R. A.; Jakeman, A. J. (2003): A review of erosion and sediment transport models. In *Environmental Modelling & Software* 18 (8-9), pp. 761–799. DOI: 10.1016/S1364-8152(03)00078-1.

Merten, Gustavo H.; Minella, Jean P.G. (2013): The expansion of Brazilian agriculture: Soil erosion scenarios. In *International Soil and Water Conservation Research* 1 (3), pp. 37–48. DOI: 10.1016/S2095-6339(15)30029-0.

Miranda, Renato Billia de; Scarpinella, Gustavo D'Almeida; Silva, Ricardo Siloto da; Mauad, Frederico Fábio (2015): Water Erosion in Brazil and in the World: A Brief Review. In *MESE* 1 (1), pp. 17–26. DOI: 10.15341/mese(2333-2581)/01.01.2015/003.

Missiaen, T.; Slob, E.; Donselaar, M. E. (2008): Comparing different shallow geophysical methods in a tidal estuary, Verdrongen Land van Saeftinge, Western Scheldt, the Netherlands. In *Netherlands Journal of Geosciences* 87 (2), pp. 151–164. DOI: 10.1017/S0016774600023192.

Montgomery, David R. (2012): *Dirt: The erosion of civilizations*: Univ of California Press.

Morgan, Royston Philip Charles (1979): *Soil erosion*: Longman.

Morris, Greg; Fan, Jiahua (2010): *Reservoir Sedimentation Handbook* (1.04).

Morris, Gregory (2020): Classification of Management Alternatives to Combat Reservoir Sedimentation. In *Water* 12 (3), p. 861. DOI: 10.3390/w12030861.

Mulu, Arega; Dwarakish, G. S. (2015): Different Approach for Using Trap Efficiency for Estimation of Reservoir Sedimentation. An Overview. In *Aquatic Procedia* 4, pp. 847–852. DOI: 10.1016/j.aqpro.2015.02.106.

Mulukutla, G. K. (2009): Determination of geotechnical properties of seafloor sediment using a freefall penetrometer. Doctoral thesis. University of New Hampshire.

Nearing, M. A.; Jetten, V.; Baffaut, C.; Cerdan, O.; Couturier, A.; Hernandez, M. et al. (2005): Modeling response of soil erosion and runoff to changes in precipitation and cover. In *CATENA* 61 (2-3), pp. 131–154.

Nearing, M. A.; Romkens, M. J.M.; Norton, L. D.; Stott, D. E.; Rhoton, F. E.; Laflen, J. M. et al. (2000): Measurements and models of soil loss rates. In *Science* 290 (5495), pp. 1300–1301.

Odhiambo, Ben K.; Boss, Stephen K. (2004): Integrated echo sounder, GPS, and GIS for reservoir sedimentation studies: Examples from two Arkansas Lakes. In *JAWRA Journal of the American Water Resources Association* 40 (4), pp. 981–997.

Okumura, H.; Sumi, T. (2012): Reservoir Sedimentation Management in Hydropower Plant Regarding Flood Risk and Loss of Power Generation. Kyoto, Japan (International Symposium on Dams for a Changing World).

Onaga, K.; Shirai, K.; Yoshinaga, A.; Rimwanich, S. E. (1988): Rainfall erosion and how to control its effects on farmland in Okinawa. In *Land conservation for future generations. Department of Land Development, Bangkok*, pp. 627–639.

Ono, G. M. (2020): Monitoramento e Análise da Sedimentação no Reservatório Passauna-PR. Master thesis. Universidade Federal do Paraná, Curitiba, Paraná, Brazil.

Orlowski, A. (1984): Application of multiple echoes energy measurement for evaluation of bottom type. *Oceanologia* 19, 61-78. In *Oceanologia* 19.

Osler, John; Furlong, Arnold; Christian, Harold (2006): A sediment probe for the rapid assessment of seabed characteristics. In Andrea Caiti (Ed.): *Acoustic sensing techniques for the shallow water environment. Intervention methods and experiments*. Dordrecht: Springer, pp. 171–181.

Ostrovsky, I.; McGinnis, Daniel Frank; Lapidus, L.; Eckert, W. (2008): Quantifying gas ebullition with echosounder. The role of methane transport by bubbles in a medium-sized lake. In *Limnology and Oceanography: Methods* 6 (2), pp. 105–118.

Ostrovsky, I.; Tęgowski, Jarosław (2010): Hydroacoustic analysis of spatial and temporal variability of bottom sediment characteristics in Lake Kinneret in relation to water level fluctuation. In *Geo-Marine Letters* 30 (3-4), pp. 261–269.

Palmieri, A.; Shah, F.; Dinar, A. (2001): Economics of reservoir sedimentation and sustainable management of dams. In *Journal of Environmental Management* 61 (2), pp. 149–163. DOI: 10.1006/jema.2000.0392.

Panagos, Panos; Borrelli, Pasquale; Meusburger, Katrin; Alewell, Christine; Lugato, Emanuele; Montanarella, Luca (2015a): Estimating the soil erosion cover-management factor at the European scale. In *Land Use Policy* 48, pp. 38–50. DOI: 10.1016/j.landusepol.2015.05.021.

Panagos, Panos; Borrelli, Pasquale; Meusburger, Katrin; van der Zanden, Emma H.; Poesen, Jean; Alewell, Christine (2015b): Modelling the effect of support practices (P-factor) on the reduction of soil erosion by water at European scale. In *Environmental Science & Policy* 51, pp. 23–34. DOI: 10.1016/j.envsci.2015.03.012.

Panagos, Panos; Borrelli, Pasquale; Poesen, Jean; Ballabio, Cristiano; Lugato, Emanuele; Meusburger, Katrin et al. (2015c): The new assessment of soil loss by water erosion in Europe. In *Environmental Science & Policy* 54, pp. 438–447. DOI: 10.1016/j.envsci.2015.08.012.

Patton, J. A. (2016): Sedimentation in the Upper Reaches of Lake Ouachita. In *Journal of the Arkansas Academy of Science* 70 (1), pp. 179–183.

Pham, Tung Gia; Degener, Jan; Kappas, Martin (2018): Integrated universal soil loss equation (USLE) and Geographical Information System (GIS) for soil erosion estimation in A Sap basin: Central Vietnam. In *International Soil and Water Conservation Research* 6 (2), pp. 99–110. DOI: 10.1016/j.iswcr.2018.01.001.

Piest, R. F.; La Kramer; Heinemann, H. G. (1975): Sediment movement from loessial watersheds. In *Present and Prospective Technology for Predicting Sediment Yield and Sources. Publication*, pp. 130–141.

Pimentel, D.; Allen, J.; Beers, A.; Guinand, L.; Linder, R.; McLaughlin, P. et al. (1987): World Agriculture and Soil Erosion. In *BioScience* 37 (4), pp. 277–283. DOI: 10.2307/1310591.

Pimentel, D.; Harvey, C.; Resosudarmo, C.; Sinclair, C.; Kurz, D.; McNair, M. et al. (1995): Environmental and Economic Costs of Soil Erosion and Conservation Benefits. In *Science of The Total Environment* 267 (5201), pp. 1117–1123.

Pimentel, David (2006): Soil Erosion: A Food and Environmental Threat. In *Environ Dev Sustain* 8 (1), pp. 119–137. DOI: 10.1007/s10668-005-1262-8.

Piqué, Gemma; López-Tarazón, José A.; Batalla, Ramon J. (2014): Variability of in-channel sediment storage in a river draining highly erodible areas (the Isábena, Ebro Basin). In *J Soils Sediments* 14 (12), pp. 2031–2044. DOI: 10.1007/s11368-014-0957-6.

Poesen, J.; Nachtergaele, J.; Verstraeten, G.; Valentin, C. (2003): Gully erosion and environmental change: importance and research needs. In *CATENA* 50 (2), pp. 91–133. DOI: 10.1016/S0341-8162(02)00143-1.

Poesen, Jean (1984): The influence of slope angle on infiltration rate and Hortonian overland flow. In *Zeitschrift für Geomorphologie, Supplement Band* 49.

Poesen, Jean; Vanwalleghem, Tom; Vente, Joris de; Knapen, Anke; Verstraeten, Gert; Martínez-Casasnovas, José A. (2006): Gully Erosion in Europe (Wiley Online Books).

Preston, J. M.; Christney, A. C.; Beran, L. S.; Collins, W. T. (Eds.) (2004): Statistical seabed segmentation—from images and echoes to objective clustering.

Quadroni, S.; Brignoli, M. L.; Crosa, G.; Gentili, G.; Salmaso, F.; Zaccara, S.; Espa, P. (2016): Effects of sediment flushing from a small Alpine reservoir on downstream aquatic fauna. In *Ecohydrol.* 9 (7), pp. 1276–1288. DOI: 10.1002/eco.1725.

Quinton, John N. (2004): Erosion and sediment transport. In *Environmental modelling: Finding simplicity in complexity*.

Quinton, John N.; Govers, Gerard; van Oost, Kristof; Bardgett, Richard D. (2010): The impact of agricultural soil erosion on biogeochemical cycling. In *Nature Geoscience* 3, 311 EP -. DOI: 10.1038/ngeo838.

Rejman, Jerzy; Brodowski, Ryszard (2005): Rill characteristics and sediment transport as a function of slope length during a storm event on loess soil. In *Earth Surf. Process. Landforms* 30 (2), pp. 231–239. DOI: 10.1002/esp.1177.

Renard, K. G. (1997): Predicting soil erosion by water. A guide to conservation planning with the revised universal soil loss equation (RUSLE). Washington, D. C. (Agriculture handbook, 703).

Renard, K. G.; Foster, G. R.; Weesies, D. K.; McCool, D. K.; Yoder, D. C. (1997): Predicting soil erosion by water: A guide to conservation planning with the Revised Universal Soil Loss Equation (RUSLE). United States Department of Agriculture.

Reusser, Lucas; Bierman, Paul; Rood, Dylan (2015): Quantifying human impacts on rates of erosion and sediment transport at a landscape scale. In *Geology* 43 (2), pp. 171–174. DOI: 10.1130/G36272.1.

Richter, Gerold; Negendank, Jörg F. W. (1977): Soil erosion processes and their measurement in the German area of the Moselle river. In *Earth Surface Processes* 2 (2-3), pp. 261–278. DOI: 10.1002/esp.3290020217.

Ridd, M. K. (1995): Exploring a V-I-S (vegetation-impervious surface-soil) model for urban ecosystem analysis through remote sensing: comparative anatomy for cities†. In *International Journal of Remote Sensing* 16 (12), pp. 2165–2185. DOI: 10.1080/01431169508954549.

Risse, L. M.; Nearing, M. A.; Lafflen, J. M.; Nicks, A. D. (1993): Error Assessment in the Universal Soil Loss Equation. In *Soil Science Society of America Journal* 57 (3), pp. 825–833. DOI: 10.2136/sssaj1993.03615995005700030032x.

Rosa, Pierluigi de; Cencetti, Corrado; Fredduzzi, Andrea (2016): A GRASS tool for the Sediment Delivery Ratio mapping.

Rufino, R. L.; BISCAIA, R. M. C.; Merten, G. H. (1993): Determinação do potencial erosivo da chuva do estado do Paraná, através de pluviometria: terceira aproximação. In *Rev. Bras. Ciênc. Solo* 17 (3), pp. 439–444.

Saleh, Mohamed; Rabah, Mostafa (2016): Seabed sub-bottom sediment classification using parametric sub-bottom profiler. In *NRIAG Journal of Astronomy and Geophysics* 5 (1), pp. 87–95. DOI: 10.1016/j.nrjag.2016.01.004.

Saunitti, Rosa Maria; Fernandes, Luiz Alberto; Bittencourt, André Virmond Lima (2004): Estudo do assoreamento do reservatório da barragem do rio Passaúna-Curitiba-PR. In *Boletim Paranaense de Geociências* 54.

Schick, J.; Bertol, I.; Cogo, N. P.; González, A. P. (2014): Erodibilidade de um Cambissolo Húmico sob chuva natural. In *Rev. Bras. Ciênc. Solo* 38 (6), pp. 1906–1917. DOI: 10.1590/S0100-06832014000600025.

Schleiss, Anton J.; Franca, Mário J.; Juez, Carmelo; Cesare, Giovanni de (2016): Reservoir sedimentation. In *Journal of Hydraulic Research* 54 (6), pp. 595–614.

Schneider von Deimling, J.; Weinrebe, Willi; Tóth, Zs; Fossing, Henrik; Endler, Rudolf; Rehder, Gregor; Spieß, Volkhard (2013): A low frequency multibeam assessment. Spatial mapping of shallow gas by enhanced penetration and angular response anomaly. In *Marine and Petroleum Geology* 44, pp. 217–222.

Seifert, Annedore; Kopf, Achim (2012): Modified Dynamic CPTU Penetrometer for Fluid Mud Detection. In *J. Geotech. Geoenviron. Eng.* 138 (2), pp. 203–206. DOI: 10.1061/(ASCE)GT.1943-5606.0000563.

Shamshad, A.; Azhari, M. N.; Isa, M. alH; Hussin, W. WanM.A.; Parida, B. P. (2008): Development of an appropriate procedure for estimation of RUSLE EI30 index and preparation of erosivity maps for Pulau Penang in Peninsular Malaysia. In *CATENA* 72 (3), pp. 423–432.

Sharma, Arabinda; Tiwari, Kamlesh N.; Bhadoria, P. B. S. (2011): Effect of land use land cover change on soil erosion potential in an agricultural watershed. In *Environmental Monitoring and Assessment* 173 (1), pp. 789–801. DOI: 10.1007/s10661-010-1423-6.

Shields A. (1936): Anwendung der Aehnlichkeitsmechanik und der Turbulenzforschung auf die Geschiebebewegung. In *Mitteilung der Preussischen Versuchsanstalt fur Wasserbau und Schiffbau* 26.

Shit, Pravat Kumar; Bhunia, Gouri Sankar; Maiti, Ramkrishna (2016): An experimental investigation of rill erosion processes in lateritic upland region: A pilot study. In *EJSS* 5 (2), p. 121. DOI: 10.18393/ejss.2016.2.121-131.

Silva, Antonio; Silva, Marx; Curi, Nilton; Avanzi, Junior; Ferreira, Mozart (2009): Rainfall erosivity and erodibility of Cambisol (Inceptisol) and Latosol (Oxisol) in the region of Lavras, Southern Minas Gerais State, Brazil. In *Rev. Bras. Ciênc. Solo* 33, pp. 1811–1820.

Silva, M.; Freitas, P.; Blancaneaux, P.; Curi, N.; Lima, J. de (1997): Relação entre parâmetros da chuva e perdas de solo e determinação da erodibilidade de um latossolo vermelho-escuro em Goiânia (GO). In *Revista Brasileira de Ciência do Solo* 21 (1), pp. 131–137.

Simon, A.; Rinaldi, Massimo (2006): Disturbance, Stream Incision, and Channel Evolution: The Roles of Excess Transport Capacity and Boundary Materials in Controlling Channel Response. In *Geomorphology* 79, pp. 361–383. DOI: 10.1016/j.geomorph.2006.06.037.

Siwabessy, Justy; Penrose, John; Kloser, R. J.; Fox (Eds.) (1999): Seabed habitat classification.

Smith, Dwight D.; Wischmeier, Walter H. (1957): Factors affecting sheet and rill erosion. In *Eos Trans. AGU* 38 (6), pp. 889–896.

SoCo Project Team (2009): Addressing soil degradation in EU agriculture: relevant processes, practices and policies. Edited by G. Lowagie, S. H. Gay, A. Burell. Joint Research Council (JRC).

Song, Yang; Liu, Lianyou; Yan, Ping; Cao, Tong (2005): A review of soil erodibility in water and wind erosion research. In *J. Geogr. Sci.* 15 (2), pp. 167–176. DOI: 10.1007/BF02872682.

Sotiri, Klajdi; Hilgert, Stephan; Fuchs, Stephan (2019a): Derivation of a hydro-acoustic sediment classification methodology from an extensive dataset of six reservoirs. In *38th International Association of Hydro Resources World Congress Proceedings*, pp. 51–60. Available online at <https://static.iahr.org/34/7.pdf>.

Sotiri, Klajdi; Hilgert, Stephan; Fuchs, Stephan (2019b): Sediment classification in a Brazilian reservoir: Pros and cons of parametric low frequencies. In *Advances in Oceanography and Limnology* 10 (1). DOI: 10.4081/aiol.2019.7953.

Stark, N.; Kopf, A.; Hanff, H.; Stegmann, S.; Wilkens, R. (2009): Geotechnical investigations of sandy seafloors using dynamic penetrometers. In *Oceania*, pp. 1–10.

Stark, Nina; Hay, Alex E.; Trowse, Greg (2014): Cost-effective geotechnical and sedimentological early site assessment for ocean renewable energies. In : Oceans - St. John's, 2014. [conference] ; 14-19 Sept. 2014, St. John's, NL, Canada. OCEANS 2014. St. John's, NL, 9/14/2014 - 9/19/2014. Annual IEEE Computer Conference; Oceans MTS/IEEE Conference. Piscataway, NJ: IEEE, pp. 1–8.

Stark, Nina; Le Dantec, Nicolas; Corella, Juan Pablo; Barry, David Andrew; Lemmin, Ulrich; Girardclos, Stéphanie; Kopf, Achim (2013): Deployment of a dynamic penetrometer from manned submersibles for fine-scale geomorphology studies. In *Limnology and Oceanography: Methods* 11 (10), pp. 529–539. DOI: 10.4319/lom.2013.11.529.

Stark, Nina; Radosavljevic, Boris; Quinn, Brandon; Lantuit, Hugues (2017): Application of portable free-fall penetrometer for geotechnical investigation of Arctic nearshore zone. In *Can. Geotech. J.* 54 (1), pp. 31–46. DOI: 10.1139/cgj-2016-0087.

Stomph, T. J.; Ridder, N. de; Steenhuis, T. S.; Van de Giesen, N. C. (2002): Scale effects of Hortonian overland flow and rainfall-runoff dynamics: laboratory validation of a process-based model. In *Earth Surf. Process. Landforms* 27 (8), pp. 847–855. DOI: 10.1002/esp.356.

Sudmanns, M.; Tiede, D.; Augustin H.; Lang, S. (2019): Assessing global Sentinel-2 coverage dynamics and data availability for operational Earth observation (EO) applications using the EO-Compass. In *International Journal of Digital Earth* 0 (0), pp. 1–17. DOI: 10.1080/17538947.2019.1572799.

Sullivan, P. (2003a): Applying the principles of sustainable farming. National Sustainable Agriculture Information System (ATTRA).

Sullivan, P. (2003b): Overview of cover crops and green manures. National Sustainable Agriculture Information System (ATTRA).

Sumi, Tetsuya (2004): Reservoir sedimentation management with bypass tunnels in Japan.

Sumi, Tetsuya (2008): Evaluation of Efficiency of Reservoir Sediment Flushing in Kurobe River. Fourth International Conference on Scour and Erosion. Tokyo, Japan.

Sun, Liying; Fang, Haiyan; Qi, Deli; Li, Junlan; Cai, Qiangguo (2013): A review on rill erosion process and its influencing factors. In *Chinese Geographical Science* 23 (4), pp. 389–402. DOI: 10.1007/s11769-013-0612-y.

Tęgowski, Jarosław (2005): Acoustical classification of the bottom sediments in the southern Baltic Sea. In *Quaternary International* 130 (1), pp. 153–161.

Tęgowski, Jarosław; Łubniewski, Zbigniew (2000): The use of fractal properties of echo signals for acoustical classification of bottom sediments. In *Acta Acustica united with Acustica* 86 (2), pp. 276–282.

Tęgowski, Jarosław; Łubniewski, Zbigniew (2002): Seabed characterisation using spectral moments of the echo signal. In *Acta Acustica united with Acustica* 88 (5), pp. 623–626.

Tóth, Zsuzsanna; Spiess, Volkhard; Keil, Hanno (2015): Frequency dependence in seismoacoustic imaging of shallow free gas due to gas bubble resonance. In *Journal of Geophysical Research: Solid Earth* 120 (12), pp. 8056–8072.

Tóth, Zsuzsanna; Spiess, Volkhard; Mogollón, José M.; Jensen, Jørn Bo (2014): Estimating the free gas content in Baltic Sea sediments using compressional wave velocity from marine seismic data. In *Journal of Geophysical Research: Solid Earth* 119 (12), pp. 8577–8593.

Trimble, Stanley W. (1975): A volumetric estimate of man-induced soil erosion on the southern Piedmont Plateau. In *Prospective technology for predicting sediment yields and sources*, pp. 142–152.

Tucker, C. J.; P. J. Sellers. (1986): Satellite Remote Sensing of Primary Production. In *International Journal of Remote Sensing* 7 (11), pp. 1395–1416.

U.S. Department of the Interior, Bureau of Reclamation (2006): Erosion and Sedimentation Manual. U.S. Department of the Interior, Bureau of Reclamation, Technical Service Center, Sedimentation and River Hydraulics Group. Denver, Colorado.

United Nations (2015): Global sustainable development report.

Uri, N. D.; Lewis, J. A. (1998): The dynamics of soil erosion in US agriculture. In *The Science of the total environment* 218, pp. 45–48.

Urlick, Robert J. (1982): Sound propagation in the sea: Peninsula Publishing Los Altos, CA.

USDA (1954): A manual on conservation of soil and water. 61st ed. Beltsville.

Uwitec (2014): Lake Barombi Mbo coring campaign. Available online at Lake Barombi Mbo coring campaign, checked on 5/12/2020.

van de Giesen, Nick; Stomph, Tjeerd Jan; Ridder, Nico de (2005): Surface runoff scale effects in West African watersheds: modeling and management options. In *Agricultural water management* 72 (2), pp. 109–130. DOI: 10.1016/j.agwat.2004.09.007.

van der Knijff, J. M.F.; Jones, R. J.A.; Montanarella, L. (1999): Soil erosion risk assessment in Italy: Citeseer.

Vaoligao, Baiyin; Xu, F.-R; Chen, X.-R; Chen, W.-X (2012): Impact of sediment flushing of Xiaolangdi Reservoir on downstream fish. In *Journal of Hydraulic Engineering* 43, pp. 1146–1153.

Vaoligao, Baiyin; Xu, Fengran; Chen, Xingru; Wang, Xiuying; Chen, Wenxue (2016): Acute impacts of reservoir sediment flushing on fishes in the Yellow River. In *Journal of Hydro-environment Research* 13, pp. 26–35. DOI: 10.1016/j.jher.2015.11.003.

Vente, Joris de; Poesen, Jean; Arabkhedri, Mahmood; Verstraeten, Gert (2007): The sediment delivery problem revisited. In *Progress in Physical Geography* 31 (2), pp. 155–178.

Verstraeten, Gert; Poesen, Jean (2001): Factors controlling sediment yield from small intensively cultivated catchments in a temperate humid climate. In *Geomorphology* 40 (1-2), pp. 123–144.

Vigiak, O.; Borselli, L.; Newham, L.T.H.; McInnes, J.; Roberts, A. M. (2012): Comparison of conceptual landscape metrics to define hillslope-scale sediment delivery ratio. In *Geomorphology* 138 (1), pp. 74–88. DOI: 10.1016/j.geomorph.2011.08.026.

Vörösmarty, Charles J.; Meybeck, Michel; Fekete, Balázs; Sharma, Keshav; Green, Pamela; Syvitski, James P.M (2003): Anthropogenic sediment retention: major global impact from registered river impoundments. In *Global and Planetary Change* 39 (1-2), pp. 169–190. DOI: 10.1016/S0921-8181(03)00023-7.

Wagner, A.; Hilgert, S.; Kishi T., R.; Drummond's.; Kiemle, L.; Nickel, J. P. et al. (Eds.) (2019): Flow-proportional large volume composite sampling to assess substance fluxes. EGU2019. Vienna. EGU. 21 volumes.

Wagner, Adrian (2019): Event-Based Measurement and Mean Annual Flux Assessment of Suspended Sediment in Meso Scale Catchments. Doctoral Thesis. Karlsruhe Institute of Technology, Karlsruhe, Germany.

Wallbrink, P. J.; Murray, A. S.; Olley, J. M.; Olive, L. J. (1998): Determining sources and transit times of suspended sediment in the Murrumbidgee River, New South Wales, Australia, using fallout ¹³⁷Cs and ²¹⁰Pb. In *Water Resources Research* 34 (4), pp. 879–887.

Walling, D. E. (1983): The sediment delivery problem. In *Journal of hydrology* 65 (1-3), pp. 209–237.

Walling, D. E. (2005): Tracing suspended sediment sources in catchments and river systems. In *Science of The Total Environment* 344 (1-3), pp. 159–184. DOI: 10.1016/j.scitotenv.2005.02.011.

Walling, D. E.; he, Qili; Quine, Timothy (1996): Use of fallout radionuclide measurements in sediment budget investigations/La mesure des retombées de radionucléides : un outil pour

l'évaluation des bilans sédimentaires. In *Geomorphologie-relief Processus Environnement - GEOMORPHOLOGIE 2*, pp. 17–27. DOI: 10.3406/morfo.1996.882.

Walling, D. E.; Porto, P.; Zhang, Y.; Du, P. (2014): Upscaling the Use of Fallout Radionuclides in Soil Erosion and Sediment Budget Investigations: Addressing the Challenge. In *International Soil and Water Conservation Research 2* (3), pp. 1–21. DOI: 10.1016/S2095-6339(15)30019-8.

Waltrick, Paulo Cesar; Machado, Marco Aurélio de Mello; Dieckow, Jeferson; Oliveira, Dalziza de (2015): ESTIMATIVA DA EROSIVIDADE DE CHUVAS NO ESTADO DO PARANÁ PELO MÉTODO DA PLUVIOMETRIA: ATUALIZAÇÃO COM DADOS DE 1986 A 2008. In *Rev. Bras. Ciênc. Solo* 39 (1), pp. 256–267. DOI: 10.1590/01000683rbcscs20150147.

Wang, G.; Wentz, S.; Gertner, G. Z.; Anderson, A. (2002): Improvement in mapping vegetation cover factor for the universal soil loss equation by geostatistical methods with Landsat Thematic Mapper images. In *International Journal of Remote Sensing* 23 (18), pp. 3649–3667. DOI: 10.1080/01431160110114538.

Wang, Guiping (1998): Summary of rill erosion study. In *Soil and Water Conservation in China* 8, pp. 23–26.

Weltz, M. A.; Renard, K. G.; Simanton, JR (1987): Revised Universal Soil Loss Equation for Western. In *General Technical Report RM (150-154)*, p. 104.

Werner, C. G. (1980): Soil Conservation in Kenia.

Wilkinson, Scott N.; Prosser, Ian P.; Rustomji, Paul; Read, Arthur M. (2009): Modelling and testing spatially distributed sediment budgets to relate erosion processes to sediment yields. In *Environmental Modelling & Software* 24 (4), pp. 489–501.

Wilson, Margaret F. J.; O'Connell, Brian; Brown, Colin; Guinan, Janine C.; Grehan, Anthony J. (2007): Multiscale Terrain Analysis of Multibeam Bathymetry Data for Habitat Mapping on the Continental Slope. In *Marine Geodesy* 30 (1-2), pp. 3–35. DOI: 10.1080/01490410701295962.

Wischmeier, Walter H.; Smith, Dwight D. (1958): Rainfall energy and its relationship to soil loss. In *Eos Trans. AGU* 39 (2), pp. 285–291.

Wischmeier, Walter H.; Smith, Dwight David (1978): Predicting rainfall erosion losses-a guide to conservation planning. In *Predicting rainfall erosion losses-a guide to conservation planning*.

Wu, Lei; Liu, Xia; Ma, Xiao-yi (2018): Research progress on the watershed sediment delivery ratio. In *International Journal of Environmental Studies* 75 (4), pp. 565–579.

Wunderlich, Jens; Müller, Sabine (2003): High-resolution sub-bottom profiling using parametric acoustics. In *International Ocean Systems* (4), pp. 6–11.

Wunderlich, Jens; Wendt, Gert; Müller, Sabine (2005): High-resolution echo-sounding and detection of embedded archaeological objects with nonlinear sub-bottom profilers. In *Marine Geophysical Research* 26 (2), pp. 123–133.

Yan, Zhong-Luan; Qin, Lei-Lei; Wang, Rui; Li, Jia; Wang, Xiao-Ming; Tang, Xi-Liang; An, Rui-Dong (2018): The Application of a Multi-Beam Echo-Sounder in the Analysis of the Sedimentation Situation of a Large Reservoir after an Earthquake. In *Water* 10 (5), p. 557. DOI: 10.3390/w10050557.

Yariv, Shmuel (1976): Comments on the mechanism of soil detachment by rainfall. In *Geoderma* 15 (5), pp. 393–399. DOI: 10.1016/0016-7061(76)90043-4.

Young, Anthony (1989): Agroforestry for soil conservation.

Yu, C.; Cheng, J. J.; Jones, L. G.; Wang, Y. Y.; Faillace, E.; Loureiro, C.; Chia, Y. P. (1993): Data collection handbook to support modeling the impacts of radioactive material in soil.

Yu, D.; Shi, X.; Lü, X. (1998): C Value of Different Land Use Patterns and Its Assessment on Sustainability in Low Hill Red Soil Area. In *Journal of Soil Erosion and Soil and Water Conservation* 4 (1), pp. 71–76.

Yutsis, Vsevolod; Krivosheya, Konstantin; Levchenko, Oleg; Lowag, Jens; León Gómez, Héctor de; Tamez Ponce, Antonio (2014): Bottom topography, recent sedimentation and water volume of the Cerro Prieto Dam, NE Mexico. In *Geofísica Internacional* 53 (1), pp. 27–38. DOI: 10.1016/S0016-7169(14)71488-6.

Zalles, Viviana; Hansen, Matthew C.; Potapov, Peter V.; Stehman, Stephen V.; Tyukavina, Alexandra; Pickens, Amy et al. (2019): Near doubling of Brazil's intensive row crop area since 2000. In *Proceedings of the National Academy of Sciences of the United States of America* 116 (2), pp. 428–435. DOI: 10.1073/pnas.1810301115.

Zanchi, C.; Torri, D. (1980): Evaluation of rainfall energy in central Italy. In *Evaluation of rainfall energy in central Italy*, pp. 133–142.

Zdruli, Pandi; Karydas, Christos G.; Dedaj, Klarent; Salillari, Ilir; Cela, Florjana; Lushaj, Sherif; Panagos, Panos (2016): High resolution spatiotemporal analysis of erosion risk per land cover category in Korçe region, Albania. In *Earth Sci Inform* 9 (4), pp. 481–495. DOI: 10.1007/s12145-016-0269-z.

Zhang, Weiwei; Zhang, Zengxiang; Liu, Fang; Qiao, Zhuping; Hu, Shunguang (2011): Estimation of the USLE cover and management factor C using satellite remote sensing: A review.

Zhang, Xiankui; Xu, J.; Lu, Xiuqin (1992): Research on Soil Loss Equation in Prediction of Soil Erosion in Heilongjiang Province. In *Bulletin of Soil and Water Conservation* 12 (4), pp. 1–9.

Zhang, Yan; Yuan, Jianping; Liu, Baoyuan (2002): Advance in researches on vegetation cover and management factor in the soil erosion prediction model. In *Ying yong sheng tai xue bao= The journal of applied ecology* 13 (8), pp. 1033–1036.

Zhu, T. X. (2003): Tunnel development over a 12 year period in a semi-arid catchment of the Loess Plateau, China. In *Earth Surf. Process. Landforms* 28 (5), pp. 507–525.

Zingg, A. W. (1940): Degree and length of land slope as it affects soil loss in runoff. In *Agricultural Engineering* 21 (2), pp. 59–64.

Appendix

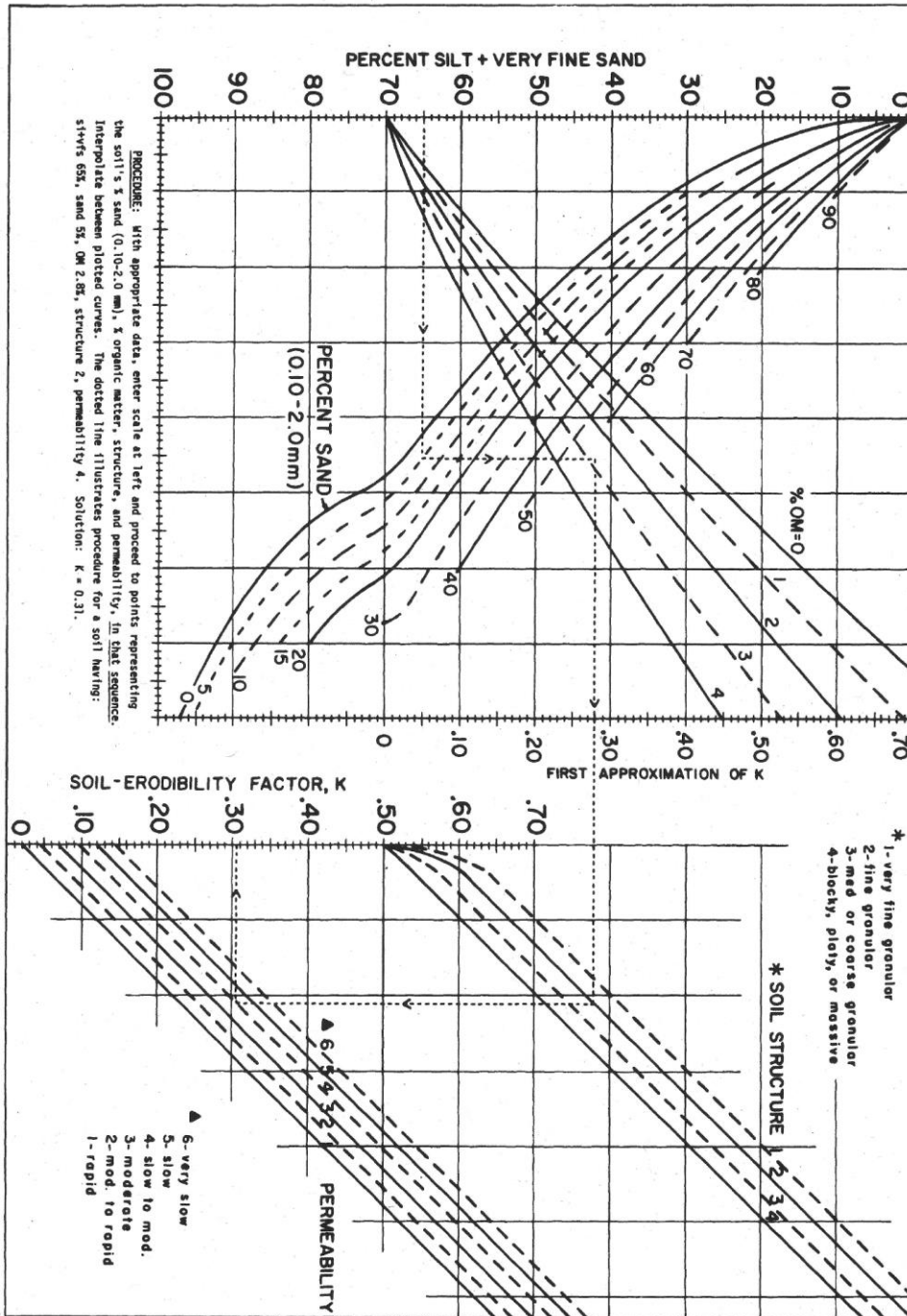


Figure A—1 Nomograph for calculating the K-Factor based on Wischmeier and Smith (1978)

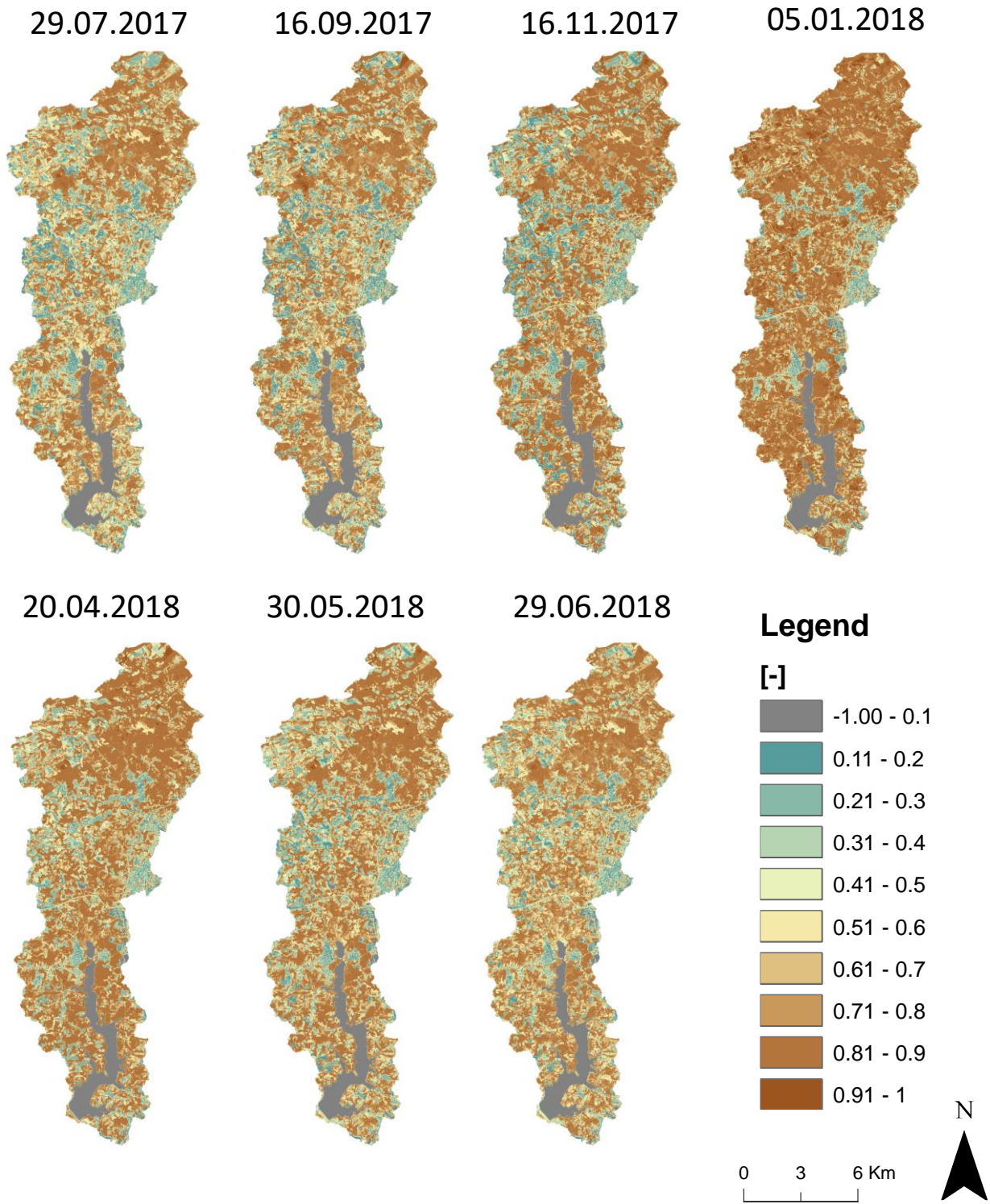


Figure A—2 NDVI scenes from July 2017-June 2018 calculated from Sentinel-2 data. Delivered from EFTAS Fernerkundung Technologietransfer GmbH

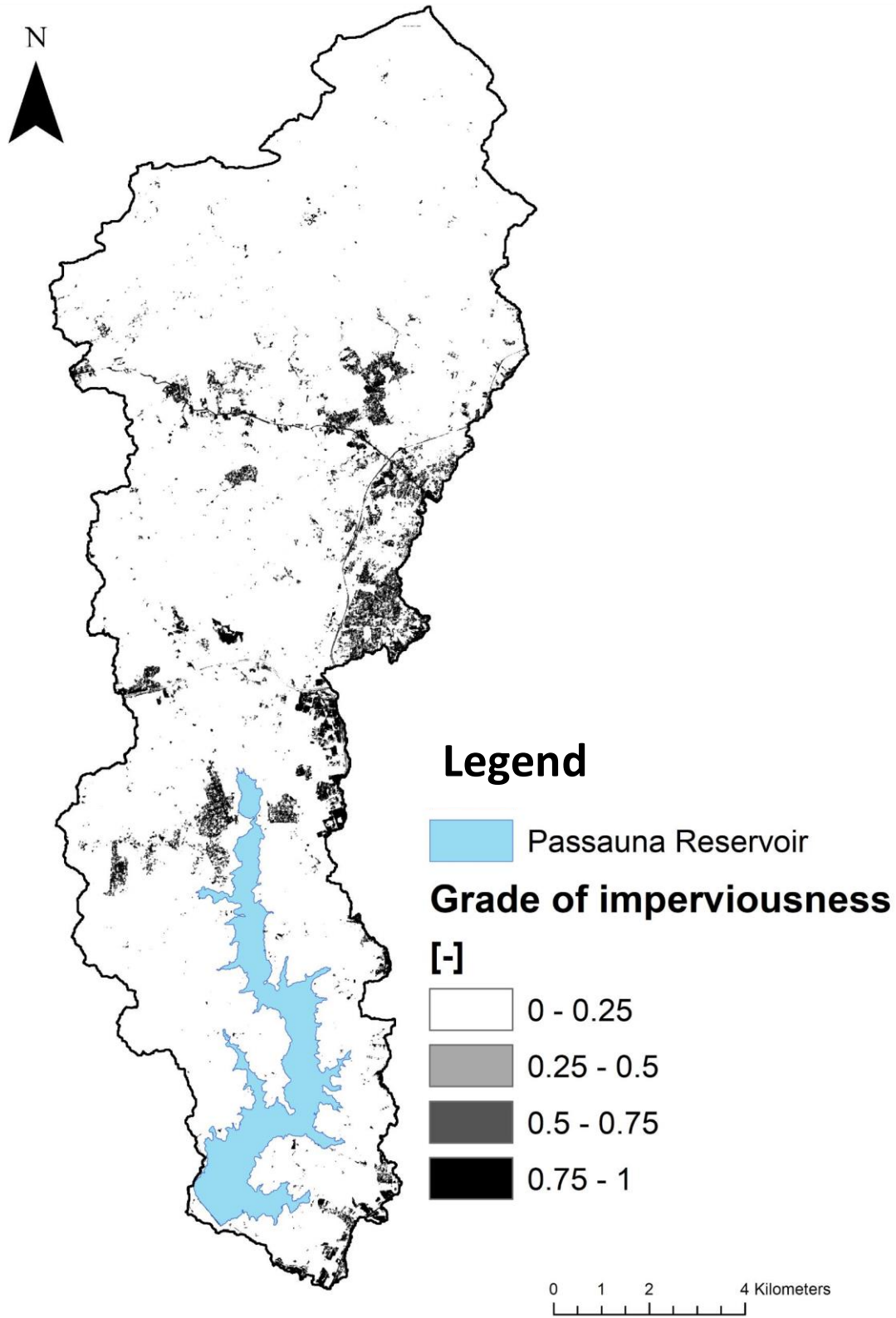


Figure A—3 Degree of soil sealing calculated from Sentinel-2 data. Delivered from EFTAS Fernerkundung Technologietransfer GmbH

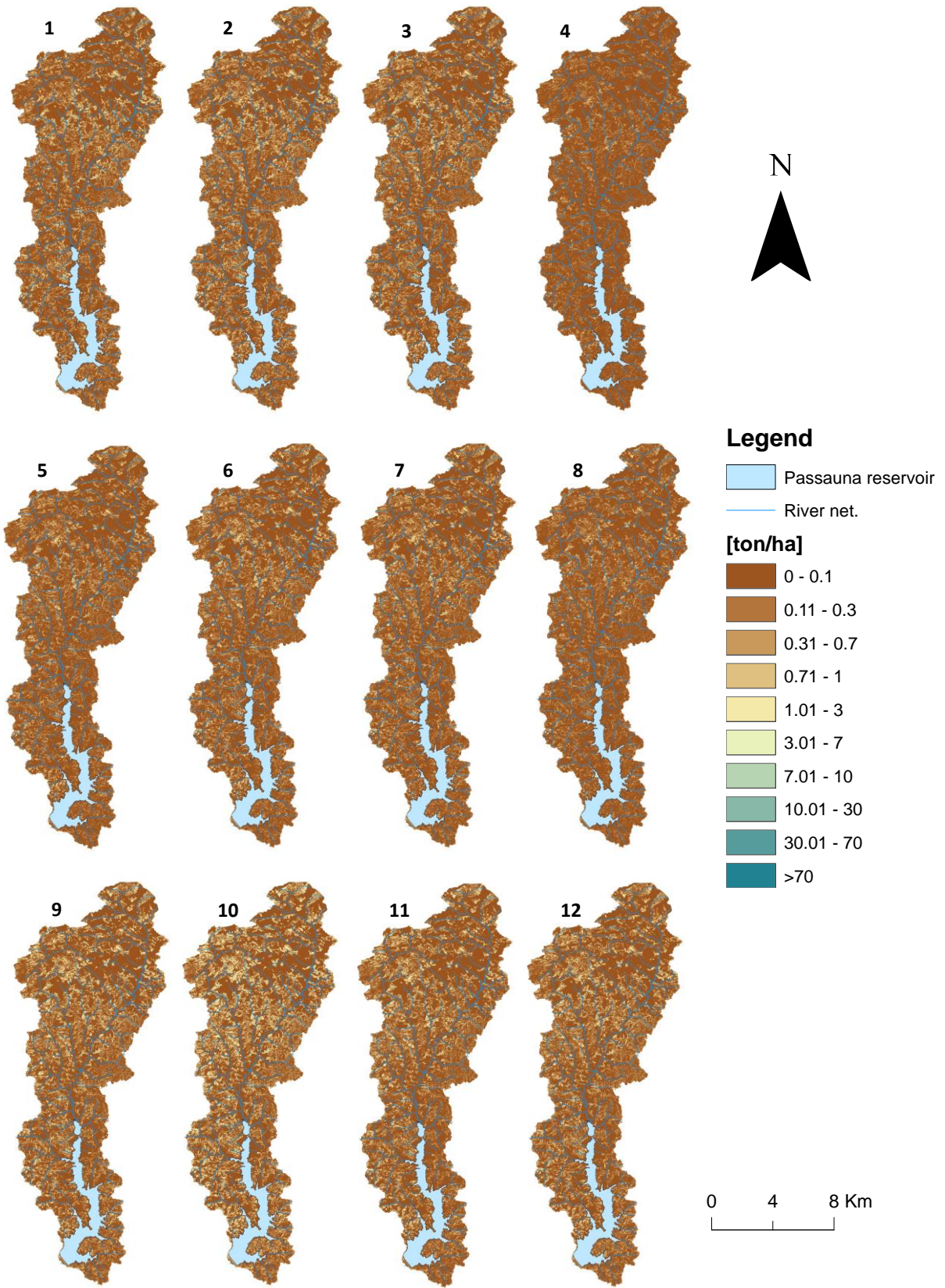


Figure A—4 Sediment input from Passaúna catchment on a monthly timestep

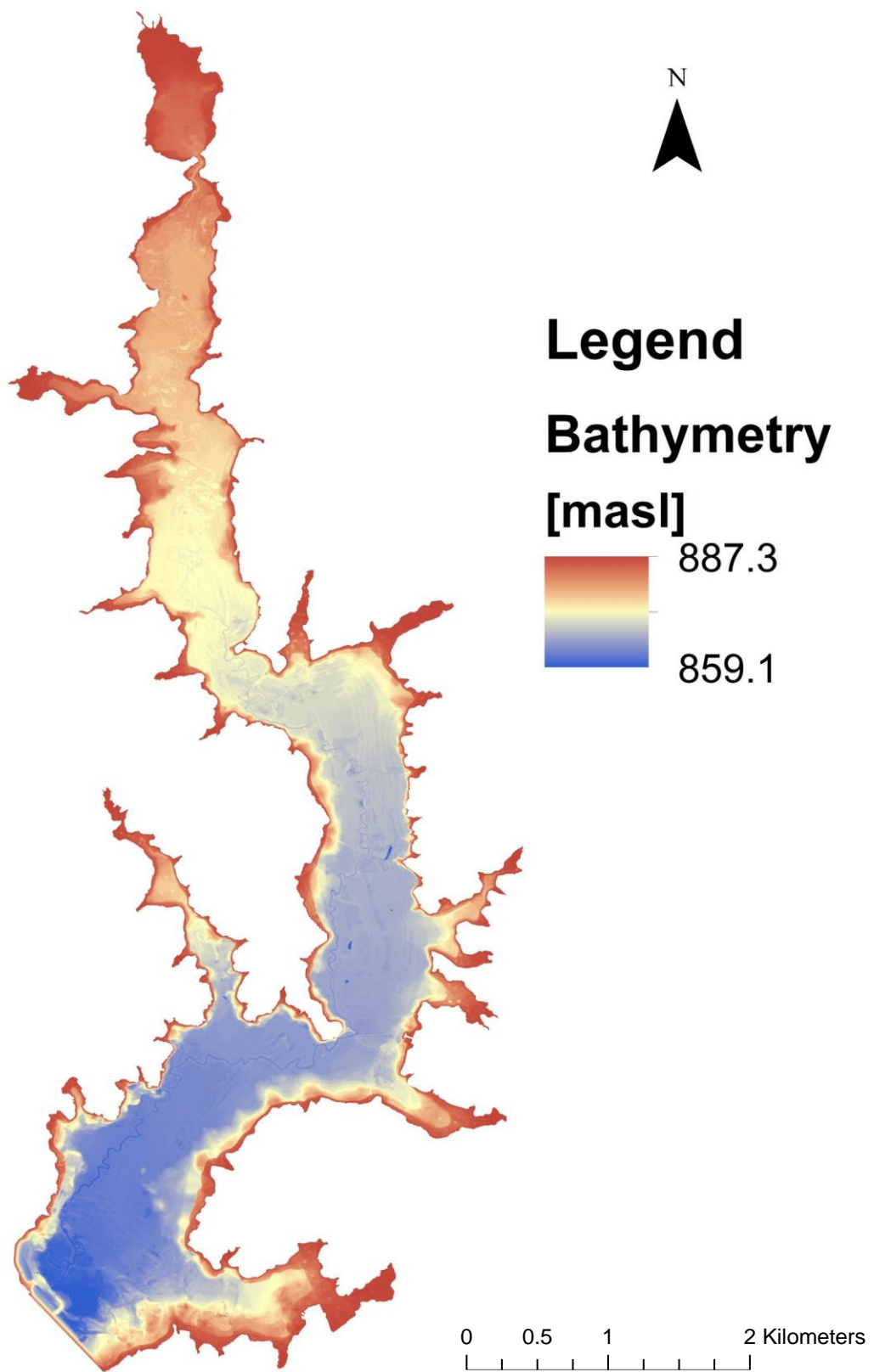


Figure A—5 Bathymetry in 20 cm horizontal resolution

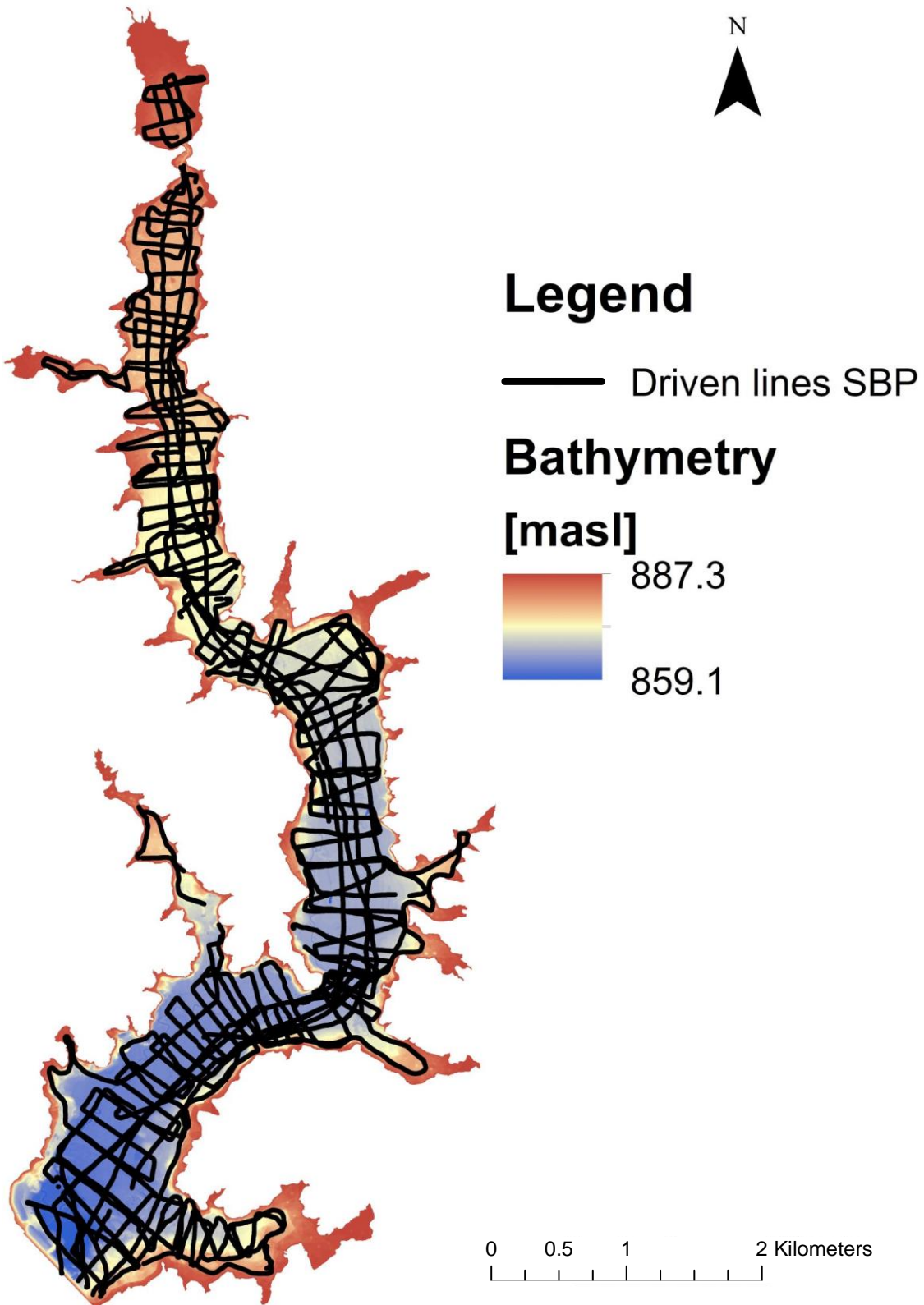


Figure A—6 Dynamic profiles with the SES2000 Compact sub-bottom profiler

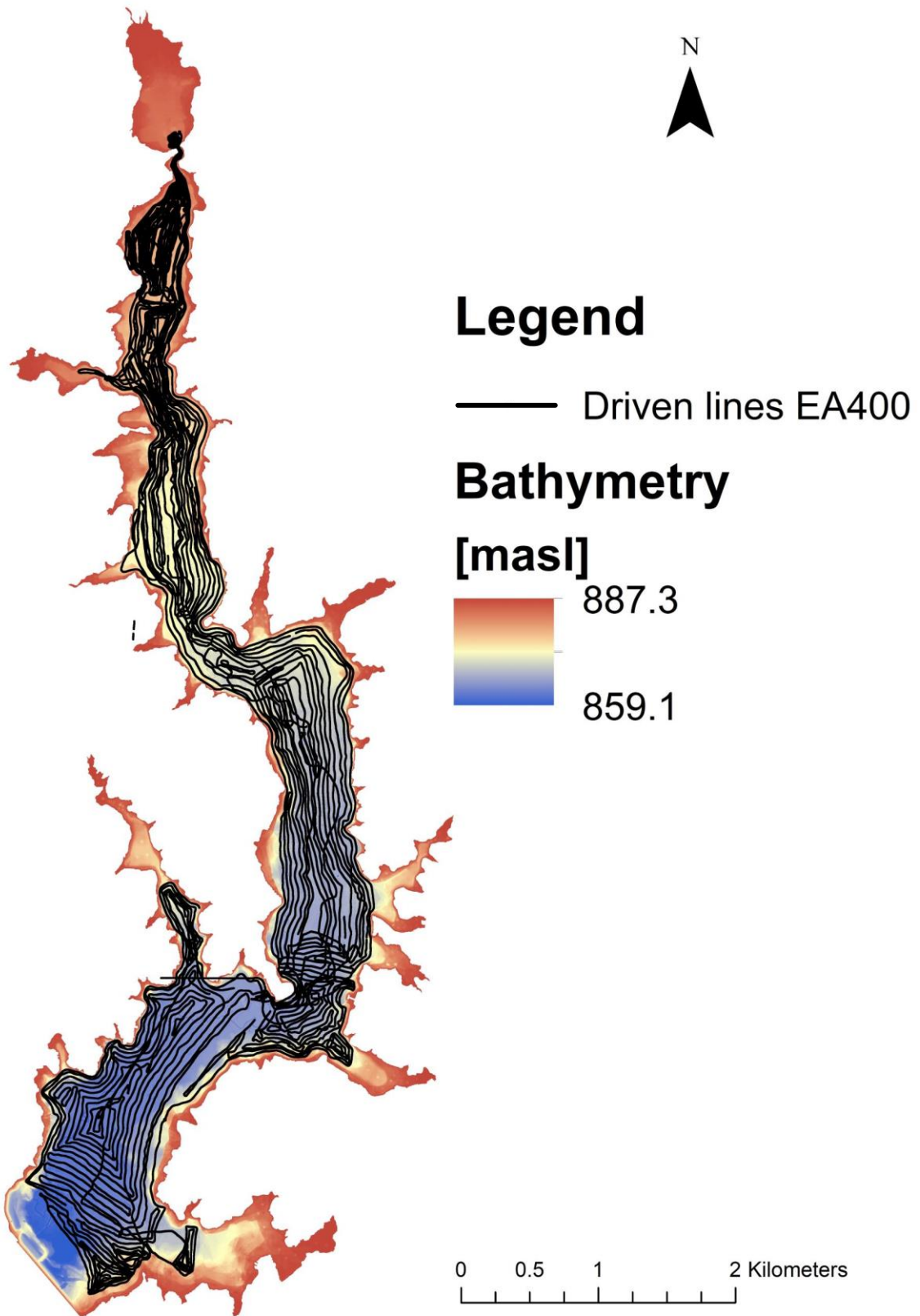


Figure A—7 Dynamic profiles with the linear system EA400

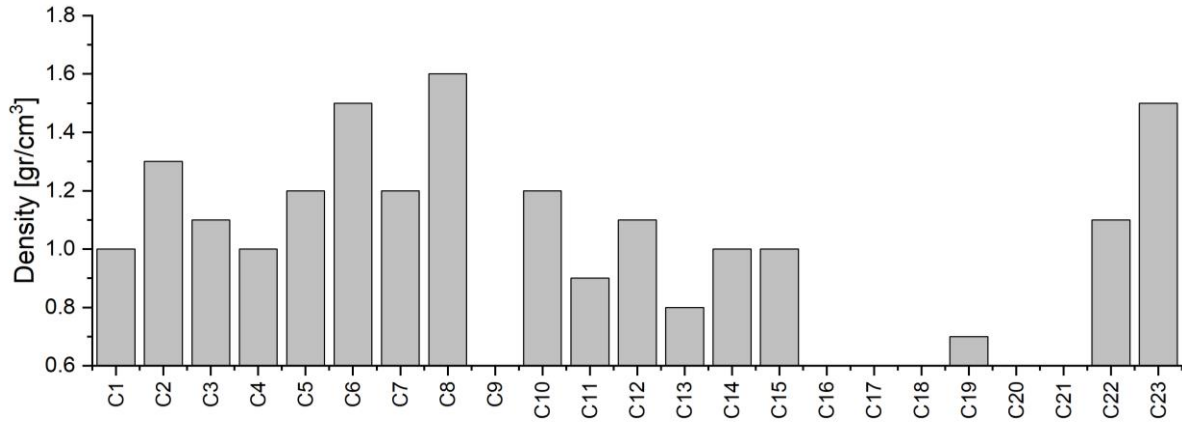


Figure A—8 Density of core samples

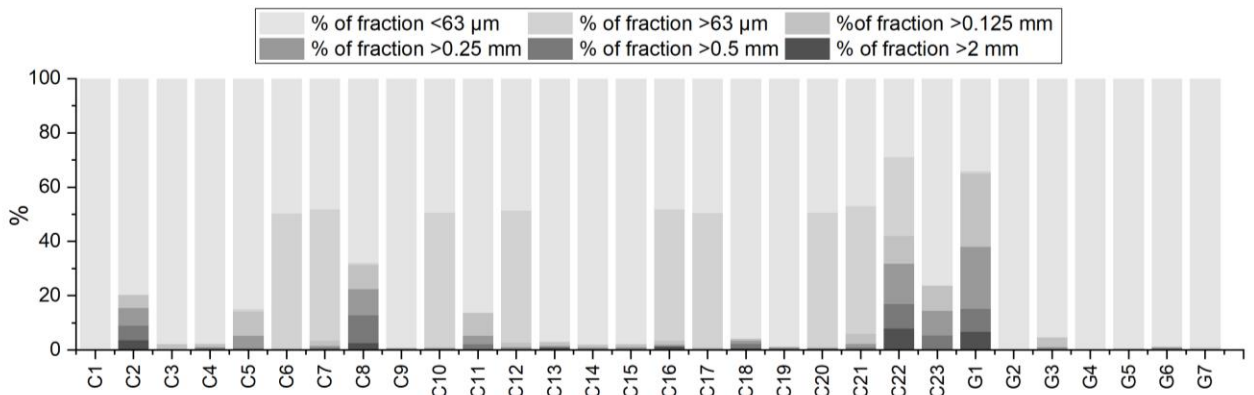


Figure A—9 Granulometry of all sediment samples

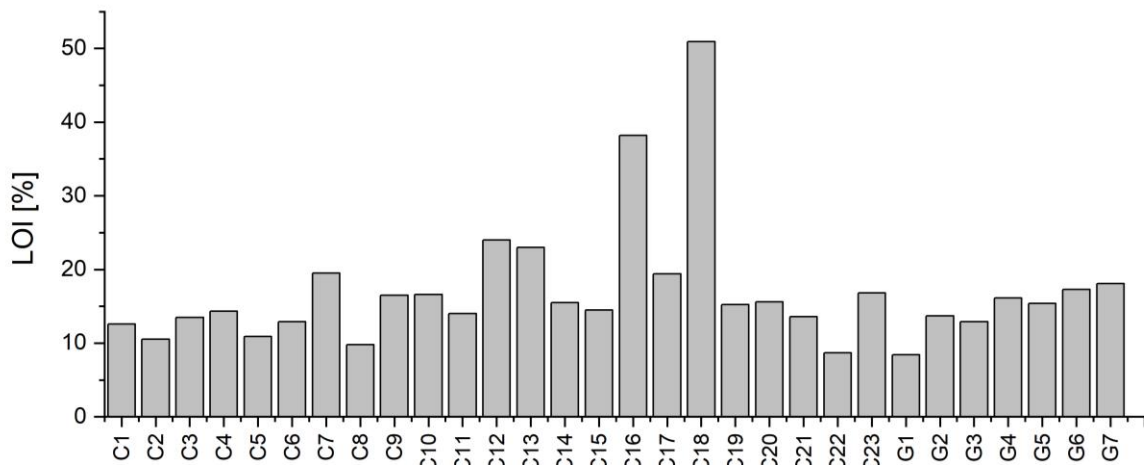


Figure A—10 LOI of all sediment samples

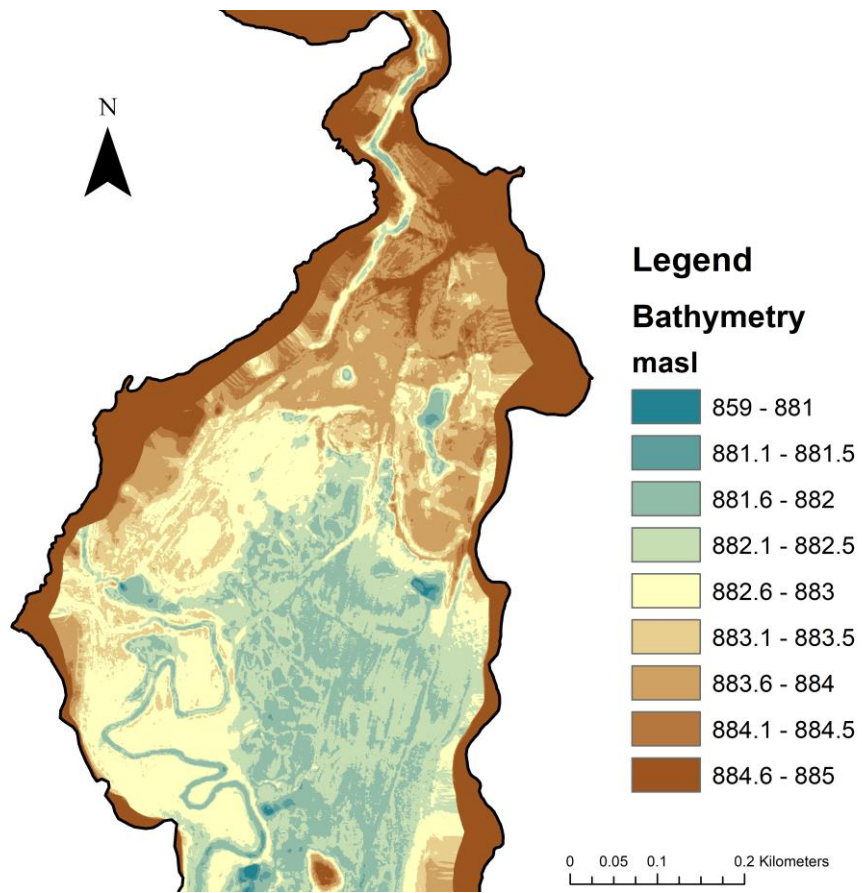
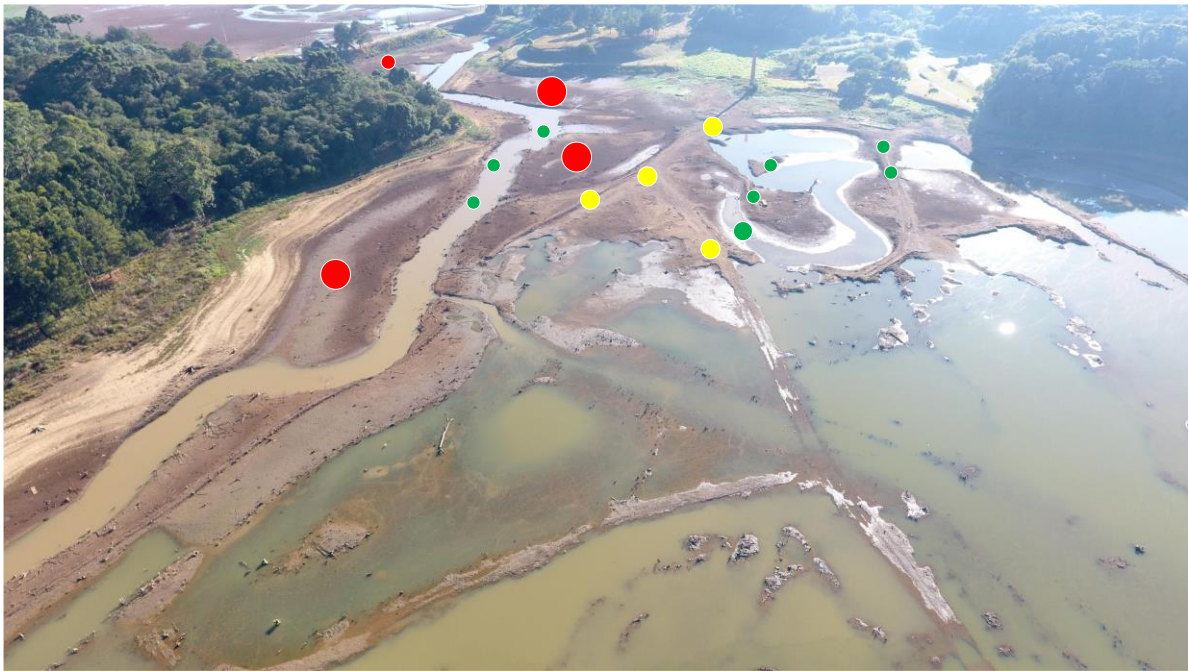
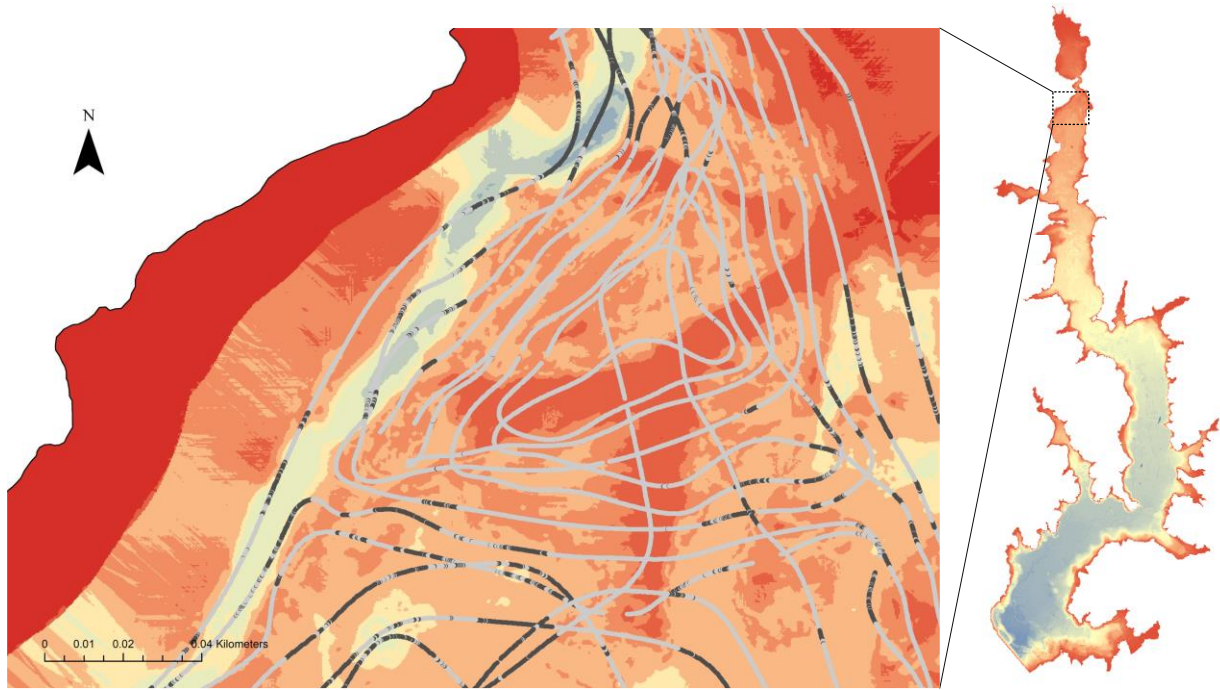


Figure A—11 Terrain in the northern part of the reservoir



- Detected sediment deposition
- Misclassified sediment deposition
- Detected preimpoundment lakebed

Figure A—12 Comparison between the sediment classification and the drone image

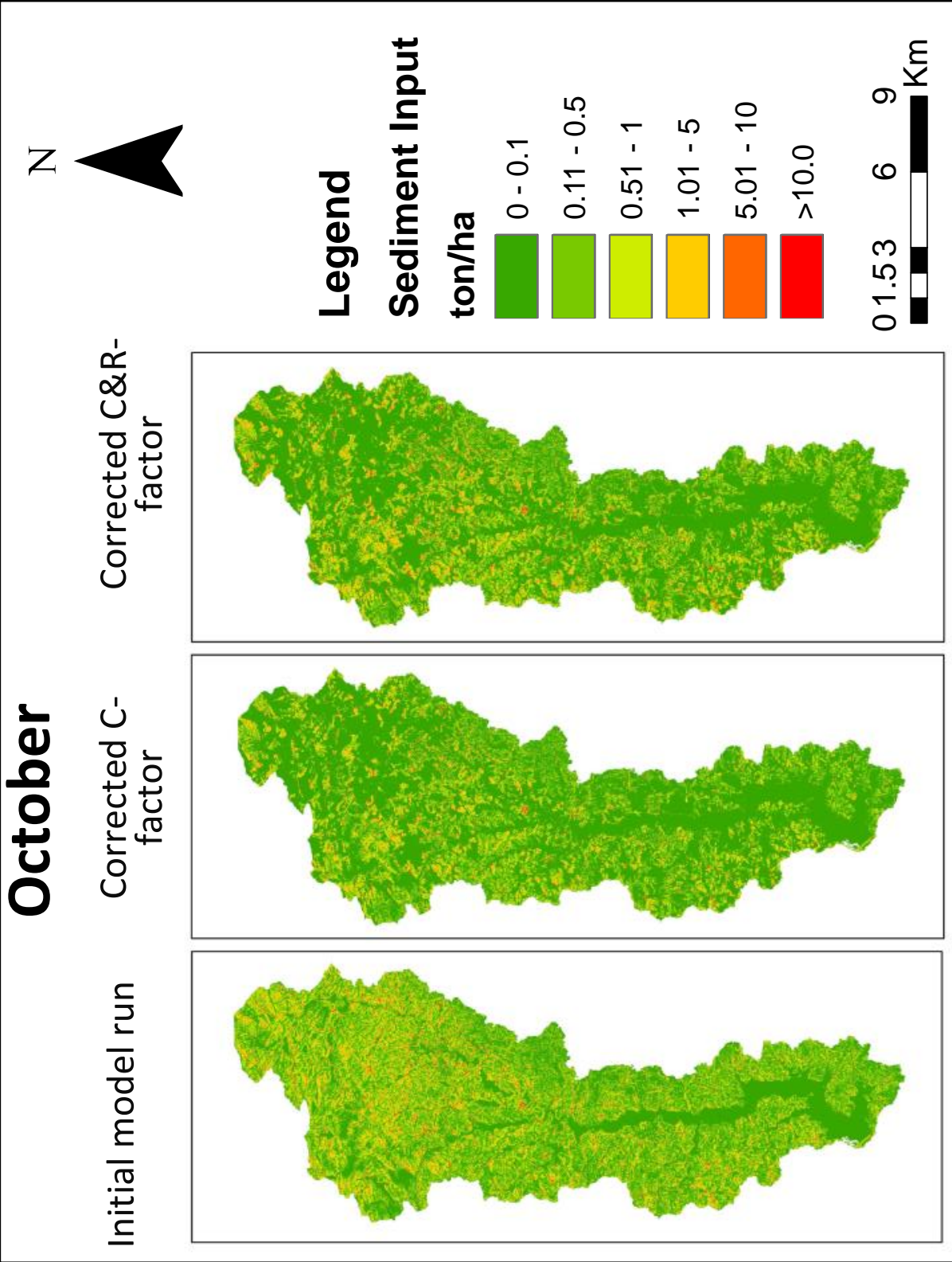


Figure A— 13 Final distribution of sediment input after C and R-Factor correction

Table A—1. Acoustic parameters for all configurations of the 200 kHz

Type	#	Frequency	Config	Depth	AttSv1	DecSv1	AttDecSv1	Att/DecSv1
Core	1	200 kHz	A	6.72	-11.40	-17.20	-14.40	0.68
			B	6.75	-16.00	-21.50	-18.70	0.77
			C	6.77	-15.90	-37.90	-21.60	0.42
			D	6.77	-18.60	-52.00	-24.50	0.36
Core	2	200 kHz	A	14.10	-8.42	-7.37	-7.20	1.25
			B	13.90	-31.30	-15.10	-16.40	2.10
			C	14.00	-17.80	-21.60	-19.60	0.85
			D	14.10	-19.80	-52.40	-25.70	0.38
Core	3	200 kHz	A	4.18	-19.40	-17.80	-17.90	1.11
			B	4.20	-17.30	-27.30	-21.70	0.64
			C	4.22	-19.40	-41.40	-25.10	0.47
			D	4.30	-24.80	-55.20	-30.70	0.45
Core	4	200 kHz	A	13.50	-24.80	-16.10	-17.20	1.56
			B	13.70	-16.30	-32.50	-21.60	0.52
			C	13.60	-18.70	-36.20	-24.20	0.52
			D	13.60	-23.30	-55.10	-29.20	0.42
Core	5	200 kHz	A	7.72	-17.20	-10.90	-11.70	1.62
			B	7.72	-14.10	-16.20	-15.30	0.89
			C	7.88	-13.00	-30.00	-18.60	0.44
			D	7.84	-15.40	-41.00	-21.20	0.38
Core	6	200 kHz	A	4.84	-14.60	-19.70	-16.90	0.77
			B	4.85	-16.10	-32.60	-21.50	0.50
			C	4.92	-18.20	-50.40	-24.10	0.36
			D	4.93	-19.30	-53.90	-25.20	0.36
Core	7	200 kHz	A	2.73	-19.20	-17.20	-17.20	1.14
			B	2.73	-19.20	-17.20	-17.20	1.14
			C	2.77	-19.50	-43.50	-25.30	0.45
			D	2.80	-20.70	-54.40	-26.60	0.38
Core	8	200 kHz	A	3.62	-19.80	-15.10	-15.20	1.36
			B	3.16	-12.80	-21.80	-16.50	0.62
			C	3.53	-14.80	-40.60	-20.50	0.38
			D	3.73	-19.90	-52.20	-25.80	0.38
Core	9	200 kHz	A	9.56	-17.90	-14.50	-15.00	1.24
			B	9.59	-16.60	-20.30	-18.60	0.83
			C	9.63	-16.00	-29.70	-21.20	0.54
			D	9.69	-18.80	-46.30	-24.70	0.41
Core	10	200 kHz	A	3.66	-25.00	-22.40	-22.70	1.13
			B	3.66	-26.50	-27.90	-27.10	0.96
			C	3.75	-24.60	-49.00	-30.40	0.51
			D	3.84	-29.50	-61.80	-35.30	0.48

Core	11	200 kHz	A	11.80	-29.60	-17.90	-19.10	1.68
			B	11.90	-27.00	-15.90	-17.10	1.72
			C	12.00	-20.10	-20.40	-19.90	1.00
			D	12.20	-17.90	-41.90	-23.60	0.43
Core	12	200 kHz	A	2.54	-16.50	-12.30	-12.80	1.38
			B	2.57	-13.90	-19.30	-16.70	0.74
			C	2.62	-14.60	-33.10	-20.20	0.45
			D	2.67	-15.80	-46.60	-21.60	0.34
Core	13	200 kHz	A	4.84	-20.70	-10.80	-11.80	2.01
			B	4.88	-12.60	-20.80	-16.40	0.62
			C	4.91	-17.00	-39.40	-22.50	0.45
			D	4.88	-18.70	-46.10	-24.40	0.42
Core	14	200 kHz	A	10.50	-20.00	-10.40	-11.50	1.98
			B	10.50	-19.00	-17.00	-17.20	1.15
			C	10.50	-15.10	-29.70	-20.40	0.51
			D	10.60	-17.90	-45.10	-23.80	0.40
Core	15	200 kHz	A	13.89	-32.96	-20.61	-21.76	1.63
			B	14.54	-26.95	-19.69	-20.57	1.39
			C	14.55	-18.43	-25.80	-22.08	0.72
			D	14.41	-20.32	-41.19	-25.96	0.50
Core	16	200 kHz	A	13.57	-29.33	-16.82	-17.99	1.77
			B	13.59	-22.20	-18.39	-18.81	1.24
			C	13.65	-17.37	-33.45	-22.76	0.52
			D	12.14	-22.83	-52.67	-27.72	0.47
Core	17	200 kHz	A	9.77	-23.40	-18.17	-18.46	1.31
			B	7.23	-15.16	-24.46	-19.48	0.63
			C	7.23	-15.16	-24.46	-19.48	0.63
			D	7.23	-15.16	-24.46	-19.48	0.63
Core	18	200 kHz	A	12.34	-32.90	-15.82	-17.06	2.15
			B	12.51	-20.52	-17.59	-18.00	1.18
			C	12.49	-15.03	-23.70	-18.86	0.65
			D	12.58	-17.17	-45.97	-23.02	0.38
Core	19	200 kHz	A	11.57	-30.03	-15.54	-16.77	1.96
			B	11.42	-25.94	-19.51	-20.32	1.36
			C	10.89	-18.65	-29.87	-23.34	0.63
			D	10.92	-18.43	-52.13	-24.30	0.35
Core	20	200 kHz	A	11.07	-27.20	-13.34	-14.54	2.12
			B	11.02	-24.22	-15.29	-16.20	1.67
			C	11.02	-24.22	-15.29	-16.20	1.67
			D	11.02	-24.22	-15.29	-16.20	1.67
Core	21	200 kHz	A	9.22	-30.22	-18.81	-19.91	1.73
			B	9.29	-25.05	-17.31	-17.91	1.49

			C	9.29	-19.19	-20.48	-19.38	0.97
			D	9.36	-17.29	-35.00	-22.62	0.51
Core	22	200 kHz	A	6.45	-20.39	-18.88	-17.75	1.20
			B	6.60	-20.74	-18.07	-18.12	1.19
			C	6.60	-20.74	-18.07	-18.12	1.19
			D	6.60	-20.74	-18.07	-18.12	1.19
Core	23	200 kHz	A	4.97	-20.98	-11.91	-12.96	1.79
			B	4.99	-14.17	-16.90	-15.63	0.86
			C	5.01	-12.84	-26.01	-17.93	0.50
			D	5.08	-14.53	-41.82	-20.37	0.35
Grab	1	200 kHz	A	4.47	-24.30	-10.40	-11.60	2.44
			B	4.40	-12.10	-16.40	-14.50	0.75
			C	4.46	-13.30	-31.20	-18.90	0.43
			D	4.51	-13.20	-44.40	-19.10	0.30
Grab	2	200 kHz	A	10.40	-26.10	-13.90	-15.00	1.92
			B	10.40	-16.00	-18.50	-17.30	0.88
			C	10.30	-17.00	-24.60	-20.40	0.71
			D	10.40	-16.00	-41.10	-21.80	0.39
Grab	3	200 kHz	A	13.00	-22.80	-18.10	-18.80	1.27
			B	13.00	-20.30	-20.80	-20.40	0.99
			C	13.00	-17.60	-30.20	-22.60	0.59
			D	13.10	-19.60	-48.60	-25.50	0.41
Grab	4	200 kHz	A	7.98	-16.40	-10.50	-11.10	1.57
			B	8.01	-13.00	-16.20	-14.50	0.83
			C	8.04	-12.70	-26.90	-18.00	0.47
			D	8.08	-17.20	-40.10	-23.00	0.43
Grab	5	200 kHz	A	2.08	-17.20	-40.10	-23.00	0.43
			B	2.07	-17.90	-29.60	-22.40	0.62
			C	2.07	-17.90	-29.60	-22.40	0.62
			D	2.21	-23.70	-54.00	-29.50	0.44
Grab	6	200 kHz	A	8.87	-15.50	-11.70	-12.30	1.36
			B	8.85	-12.80	-16.80	-15.10	0.77
			C	8.90	-14.70	-25.20	-19.30	0.59
			D	8.97	-16.20	-38.40	-22.00	0.42
Grab	7	200 kHz	A	3.99	-21.90	-15.70	-16.30	1.44
			B	3.84	-17.10	-22.80	-19.80	0.77
			C	4.11	-18.10	-42.60	-23.90	0.43
			D	4.40	-19.40	-53.50	-25.10	0.37

Table A—2. Acoustic parameters for all configurations of the 38 kHz

Type	#	Frequency	Config.	Depth	AttSv1	DecSv1	AttDecSv1	Att/DecSv1
Core	1	38 kHz	A	6.72	-4.07	-11.70	-7.91	0.36
			B	6.86	-6.77	-28.00	-12.50	0.25
			C	6.90	-10.40	-44.40	-16.30	0.24
			D	6.93	-15.90	-28.10	-20.50	0.58
Core	2	38 kHz	A	14.10	-8.42	-7.37	-7.20	1.25
			B	14.10	-10.50	-19.70	-14.70	0.54
			C	14.20	-10.80	-33.20	-16.60	0.33
			D	4.27	-5.84	-13.20	-9.41	0.46
Core	3	38 kHz	B	4.32	-9.58	-25.30	-15.00	0.38
			C	4.42	-14.40	-29.60	-19.80	0.49
			D	4.61	-18.70	-33.20	-24.00	0.56
Core	4	38 kHz	A	13.60	-7.68	-8.53	-7.92	0.94
			B	13.70	-8.28	-21.50	-13.30	0.39
			C	13.60	-22.20	-20.60	-20.70	1.10
			D	13.80	-14.00	-48.00	-19.90	0.29
Core	5	38 kHz	A	7.80	-3.28	-8.20	-5.99	0.40
			B	7.82	-6.85	-19.30	-11.80	0.36
			C	7.88	-10.60	-29.40	-16.20	0.36
			D	8.05	-13.90	-44.50	-19.70	0.31
Core	6	38 kHz	A	4.92	-3.47	-17.40	-8.73	0.20
			B	4.96	-10.80	-37.70	-16.70	0.29
			C	5.10	-15.10	-33.50	-20.60	0.45
			D	5.30	-17.40	-33.90	-22.70	0.52
Core	7	38 kHz	A	2.83	-5.95	-14.50	-10.00	0.43
			B	2.73	-19.20	-17.20	-17.20	1.14
			C	2.73	-19.20	-17.20	-17.20	1.14
			D	3.07	-18.70	-30.10	-23.60	0.63
Core	8	38 kHz	A	2.80	-20.70	-54.40	-26.60	0.38
			B	3.08	-17.90	-33.00	-23.30	0.54
			C	3.61	-18.60	-41.30	-24.40	0.45
			D	3.99	-23.20	-44.30	-28.80	0.52
Core	9	38 kHz	A	9.65	-4.01	-7.73	-6.29	0.50
			B	9.70	-7.77	-17.10	-12.10	0.46
			C	9.79	-11.40	-27.90	-16.80	0.42
			D	9.84	-12.60	-41.00	-18.40	0.31
Core	10	38 kHz	A	3.73	-9.81	-12.40	-11.10	0.81
			B	3.82	-13.60	-35.00	-19.30	0.39
			C	3.92	-16.90	-37.20	-22.50	0.45
			D	4.23	-20.90	-39.60	-26.40	0.53
Core	11	38 kHz	A	12.00	-14.50	-7.90	-8.73	2.13
			B	12.10	-11.40	-16.00	-14.00	0.73
			C	12.30	-11.10	-31.00	-16.80	0.36
			D	12.50	-13.40	-48.30	-19.20	0.28
Core	12	38 kHz	A	2.60	-3.05	-9.96	-6.75	0.32

			B	2.68	-9.15	-20.40	-14.10	0.45
			C	2.69	-13.40	-17.90	-16.00	0.77
			D	2.69	-17.10	-20.60	-19.20	0.85
Core	13	38 kHz	A	4.90	-5.09	-9.33	-6.97	0.66
			B	4.92	-7.67	-25.20	-13.20	0.31
			C	4.81	-13.20	-35.20	-18.90	0.38
			D	5.03	-16.20	-30.60	-21.30	0.53
Core	14	38 kHz	A	10.60	-2.27	-6.55	-4.65	0.41
			B	10.70	-7.36	-19.00	-12.10	0.40
			C	10.70	-8.17	-34.50	-14.00	0.24
			D	10.80	-11.70	-47.60	-17.60	0.25
Core	15	38 kHz	A	13.83	-13.37	-8.79	-9.36	1.59
			B	14.48	-11.92	-17.12	-14.15	0.74
			C	14.51	-11.72	-34.52	-17.49	0.34
			D	14.31	-16.23	-44.87	-22.09	0.36
Core	16	38 kHz	A	13.63	-12.11	-10.46	-10.38	1.18
			B	13.73	-11.84	-25.42	-16.83	0.47
			C	13.82	-15.84	-34.28	-21.45	0.47
			D	13.78	-14.05	-52.36	-19.93	0.27
Core	17	38 kHz	A	9.77	-18.86	-9.20	-10.23	2.20
			B	7.38	-15.92	-27.41	-20.75	0.59
			C	7.23	-15.16	-24.46	-19.48	0.63
			D	7.23	-15.16	-24.46	-19.48	0.63
Core	18	38 kHz	A	12.54	-7.22	-7.61	-7.01	1.33
			B	12.62	-9.87	-20.75	-14.63	0.48
			C	12.64	-11.95	-34.02	-17.72	0.35
			D	12.59	-14.83	-43.28	-20.68	0.34
Core	19	38 kHz	A	11.63	-10.24	-6.64	-6.95	1.75
			B	11.50	-9.85	-19.18	-14.08	0.52
			C	10.98	-12.66	-34.07	-18.40	0.37
			D	11.01	-13.68	-40.73	-19.51	0.34
Core	20	38 kHz	A	11.07	-14.93	-7.22	-7.98	2.68
			B	11.18	-7.08	-20.69	-12.21	0.35
			C	11.02	-24.22	-15.29	-16.20	1.67
			D	11.02	-24.22	-15.29	-16.20	1.67
Core	21	38 kHz	A	9.14	-26.96	-7.00	-8.19	4.08
			B	9.41	-10.40	-17.13	-13.61	0.63
			C	9.50	-13.33	-29.91	-18.80	0.45
			D	9.61	-16.11	-34.48	-21.61	0.47
Core	22	38 kHz	A	6.45	-7.17	-11.52	-9.36	0.63
			B	6.77	-7.74	-24.11	-13.15	0.32
			C	6.60	-20.74	-18.07	-18.12	1.19
			D	6.60	-20.74	-18.07	-18.12	1.19
Core	23	38 kHz	A	5.01	-3.23	-7.29	-5.38	0.50
			B	5.06	-7.14	-22.68	-12.59	0.32
			C	5.02	-11.14	-30.79	-16.82	0.37
			D	5.02	-14.54	-26.17	-19.31	0.56

Grab	1	38 kHz	A	4.60	-17.90	-45.10	-23.80	0.40
			B	4.50	-7.77	-30.30	-13.60	0.26
			C	4.60	-12.40	-24.70	-17.20	0.52
			D	4.64	-14.50	-22.30	-18.40	0.66
Grab	2	38 kHz	A	10.40	-17.80	-6.28	-6.96	3.64
			B	10.50	-9.71	-20.20	-14.30	0.48
			C	10.40	-12.40	-28.80	-17.80	0.44
			D	10.50	-13.70	-36.20	-19.40	0.38
Grab	3	38 kHz	A	13.10	-9.35	-7.03	-7.35	1.43
			B	13.20	-7.40	-18.00	-12.10	0.42
			C	13.20	-11.30	-31.30	-17.00	0.37
			D	13.40	-13.00	-47.10	-18.90	0.28
Grab	4	38 kHz	A	7.99	-5.23	-7.62	-5.34	1.17
			B	8.07	-6.25	-18.90	-11.30	0.34
			C	8.09	-9.48	-30.10	-15.20	0.32
			D	8.11	-13.20	-44.40	-19.10	0.30
Grab	5	38 kHz	A	2.08	-17.20	-40.10	-23.00	0.43
			B	2.03	-12.20	-25.40	-17.50	0.49
			C	2.07	-17.90	-29.60	-22.40	0.62
			D	2.21	-20.00	-26.90	-23.70	0.75
Grab	6	38 kHz	A	8.91	-3.96	-8.28	-6.35	0.49
			B	8.92	-7.71	-15.80	-11.60	0.49
			C	9.00	-10.10	-24.00	-15.30	0.43
			D	9.09	-12.60	-34.70	-18.20	0.37

Table A—3. Correlation matrix between the sediment physical properties and acoustic parameters from configuration A of the 38 kHz

		AttSv1	DecSv1	AttDecSv1	Att/DecSv1	LOI 550°C	<63 μm	Density	Relative depth
AttSv1	Pearson Corr.	1.00	0.41	0.57	-0.67	0.07	0.17	-0.05	-0.07
	p-value	--	0.03	0.00	0.00	0.72	0.38	0.85	0.72
DecSv1	Pearson Corr.		1.00	0.97	0.35	0.25	0.02	-0.17	0.56
	p-value		--	0.00	0.07	0.20	0.91	0.52	0.00
AttDecSv1	Pearson Corr.			1.00	0.21	0.24	0.09	-0.17	0.46
	p-value			--	0.29	0.22	0.65	0.54	0.01
Att/DecSv1	Pearson Corr.				1.00	0.18	-0.05	-0.05	0.48
	p-value				--	0.37	0.81	0.84	0.01
LOI 550°C	Pearson Corr.					1.00	0.23	-0.35	0.36
	p-value					--	0.25	0.19	0.06
<63 μm	Pearson Corr.						1.00	-0.72	0.06
	p-value							0.00	0.78
Density	Pearson Corr.							1.00	-0.20
	p-value							--	0.45
Relative depth	Pearson Corr.								1.00
	p-value								--

Table A—4. Correlation matrix between the sediment physical properties and acoustic parameters from configuration B of the 38 kHz

		AttSv1	DecSv1	AttDecSv1	Att/DecSv1	LOI 550°C	<63 µm	Density	Relative depth
AttSv1	Pearson Corr.	1.00	0.27	0.88	-0.72	0.18	0.47	-0.07	0.27
	p-value	--	0.16	0.00	0.00	0.35	0.01	0.78	0.15
DecSv1	Pearson Corr.		1.00	0.61	0.43	0.33	0.44	-0.48	0.53
	p-value		--	0.00	0.02	0.08	0.02	0.05	0.00
AttDecSv1	Pearson Corr.			1.00	-0.32	0.24	0.56	-0.16	0.38
	p-value			--	0.09	0.21	0.00	0.53	0.04
Att/DecSv1	Pearson Corr.				1.00	0.05	-0.11	-0.17	0.09
	p-value				--	0.81	0.57	0.51	0.63
LOI 550°C	Pearson Corr.					1.00	0.23	-0.32	0.51
	p-value					--	0.23	0.21	0.00
<63 µm	Pearson Corr.						1.00	-0.67	0.15
	p-value						--	0.00	0.43
Density	Pearson Corr.							1.00	-0.48
	p-value							--	0.05
Relative depth	Pearson Corr.								1.00
	p-value								--

Table A—5. Correlation matrix between the sediment physical properties and acoustic parameters from configuration C of the 38 kHz

		AttSv1	DecSv1	AttDecSv1	Att/DecSv1	LOI 550°C	<63 μm	Density	Relative depth
AttSv1	Pearson Corr.	1.00	-0.48	0.55	-0.86	0.15	0.15	0.04	0.21
	p-value	--	0.01	0.00	0.00	0.45	0.43	0.87	0.29
DecSv1	Pearson Corr.		1.00	0.27	0.80	-0.08	0.10	-0.25	-0.09
	p-value		--	0.15	0.00	0.67	0.59	0.32	0.62
AttDecSv1	Pearson Corr.			1.00	-0.06	0.25	0.24	-0.07	0.29
	p-value			--	0.74	0.19	0.21	0.80	0.13
Att/DecSv1	Pearson Corr.				1.00	-0.06	-0.04	-0.10	-0.12
	p-value				--	0.77	0.83	0.71	0.54
LOI 550°C	Pearson Corr.					1.00	0.23	-0.32	0.50
	p-value					--	0.23	0.21	0.01
<63 μm	Pearson Corr.						1.00	-0.67	0.16
	p-value						--	0.00	0.42
Density	Pearson Corr.							1.00	-0.48
	p-value							--	0.05
Relative depth	Pearson Corr.								1.00
	p-value								--

Table A—6. Correlation matrix between the sediment physical properties and acoustic parameters from configuration D of the 38 kHz

		AttSv1	DecSv1	AttDecSv1	Att/DecSv1	LOI 550°C	<63 μm	Density	Relative depth
AttSv1	Pearson Corr.	1.00	-0.20	0.67	-0.67	0.45	0.14	-0.30	0.32
	p-value	--	0.29	0.00	0.00	0.01	0.46	0.24	0.09
DecSv1	Pearson Corr.		1.00	0.35	0.76	0.23	-0.14	0.48	-0.62
	p-value		--	0.06	0.00	0.23	0.46	0.05	0.00
AttDecSv1	Pearson Corr.			1.00	0.08	0.65	0.14	-0.19	0.24
	p-value			--	0.67	0.00	0.46	0.46	0.20
Att/DecSv1	Pearson Corr.				1.00	0.00	-0.10	0.26	-0.35
	p-value				--	0.99	0.59	0.31	0.06
LOI 550°C	Pearson Corr.					1.00	0.23	-0.32	0.14
	p-value					--	0.23	0.21	0.47
<63 μm	Pearson Corr.						1.00	-0.67	0.13
	p-value						--	0.00	0.49
Density	Pearson Corr.							1.00	-0.49
	p-value							--	0.04
Relative depth	Pearson Corr.								1.00
	p-value								--

Table A—7. Correlation matrix between the sediment physical properties and acoustic parameters from configuration A of the 200 kHz

		AttSv1	DecSv1	AttDecSv1	Att/DecSv1	LOI 550°C	<63 μm	Density	Relative depth
AttSv1	Pearson Corr.	1.00	0.15	0.54	-0.60	0.05	-0.09	0.47	-0.42
	p-value	--	0.42	0.00	0.00	0.79	0.64	0.05	0.02
DecSv1	Pearson Corr.		1.00	0.84	0.59	0.27	0.10	-0.16	0.24
	p-value		--	0.00	0.00	0.15	0.60	0.55	0.20
AttDecSv1	Pearson Corr.			1.00	0.33	0.32	0.12	0.12	0.03
	p-value			--	0.07	0.09	0.53	0.64	0.89
Att/DecSv1	Pearson Corr.				1.00	0.16	0.24	-0.43	0.38
	p-value				--	0.40	0.20	0.08	0.04
LOI 550°C	Pearson Corr.					1.00	0.30	-0.32	0.52
	p-value					--	0.11	0.21	0.00
<63 μm	Pearson Corr.						1.00	-0.67	0.17
	p-value						--	0.00	0.37
Density	Pearson Corr.							1.00	-0.48
	p-value							--	0.05
Relative depth	Pearson Corr.								1.00
	p-value								--

Table A—8. Correlation matrix between the sediment physical properties and acoustic parameters from configuration B of the 200 kHz

		AttSv1	DecSv1	AttDecSv1	Att/DecSv1	LOI 550°C	<63 μm	Density	Relative depth
AttSv1	Pearson Corr.	1.00	-0.15	0.35	-0.86	-0.65	-0.13	0.27	-0.54
	p-value	--	0.41	0.06	0.00	0.00	0.49	0.29	0.00
DecSv1	Pearson Corr.		1.00	0.78	0.61	0.37	0.28	0.00	0.29
	p-value		--	0.00	0.00	0.05	0.13	1.00	0.11
AttDecSv1	Pearson Corr.			1.00	0.17	0.13	0.18	0.14	0.06
	p-value			--	0.36	0.51	0.35	0.59	0.75
Att/DecSv1	Pearson Corr.				1.00	0.74	0.23	-0.18	0.59
	p-value				--	0.00	0.22	0.48	0.00
LOI 550°C	Pearson Corr.					1.00	0.30	-0.32	0.53
	p-value					--	0.11	0.21	0.00
<63 μm	Pearson Corr.						1.00	-0.67	0.25
	p-value						--	0.00	0.19
Density	Pearson Corr.							1.00	-0.48
	p-value							--	0.05
Relative depth	Pearson Corr.								1.00
	p-value								--

Table A—9. Correlation matrix between the sediment physical properties and acoustic parameters from configuration C of the 200 kHz

		AttSv1	DecSv1	AttDecSv1	Att/DecSv1	LOI 550°C	<63 μm	Density	Relative depth
AttSv1	Pearson Corr.	1.00	0.07	0.46	-0.57	-0.21	0.00	0.20	-0.09
	p-value	--	0.71	0.01	0.00	0.27	0.98	0.44	0.63
DecSv1	Pearson Corr.		1.00	0.80	0.73	0.44	0.29	-0.18	0.54
	p-value		--	0.00	0.00	0.01	0.12	0.48	0.00
AttDecSv1	Pearson Corr.			1.00	0.46	0.19	0.13	0.15	0.24
	p-value			--	0.01	0.31	0.48	0.57	0.21
Att/DecSv1	Pearson Corr.				1.00	0.43	0.17	-0.12	0.39
	p-value				--	0.02	0.38	0.65	0.03
LOI 550°C	Pearson Corr.					1.00	0.30	-0.32	0.52
	p-value					--	0.11	0.21	0.00
<63 μm	Pearson Corr.						1.00	-0.67	0.24
	p-value						--	0.00	0.20
Density	Pearson Corr.							1.00	-0.48
	p-value							--	0.05
Relative depth	Pearson Corr.								1.00
	p-value								--

Table A—10. Correlation matrix between the sediment physical properties and acoustic parameters from configuration D of the 200 kHz

		AttSv1	DecSv1	AttDecSv1	Att/DecSv1	LOI 550°C	<63 µm	Density	Relative depth
AttSv1	Pearson Corr.	1.00	0.31	0.70	-0.33	-0.03	-0.07	0.24	0.03
	p-value	--	0.10	0.00	0.07	0.87	0.71	0.34	0.86
DecSv1	Pearson Corr.		1.00	0.83	0.75	0.04	-0.03	0.08	0.19
	p-value		--	0.00	0.00	0.85	0.89	0.77	0.31
AttDecSv1	Pearson Corr.			1.00	0.44	0.08	-0.07	0.27	0.10
	p-value			--	0.02	0.69	0.71	0.30	0.59
Att/DecSv1	Pearson Corr.				1.00	0.12	-0.01	0.03	0.13
	p-value				--	0.53	0.96	0.91	0.51
LOI 550°C	Pearson Corr.					1.00	0.30	-0.32	0.54
	p-value					--	0.11	0.21	0.00
<63 µm	Pearson Corr.						1.00	-0.67	0.24
	p-value						--	0.00	0.20
Density	Pearson Corr.							1.00	-0.49
	p-value							--	0.05
Relative depth	Pearson Corr.								1.00
	p-value								--